FINAL REPORT

SITE-SPECIFIC SEISMIC HAZARD ANALYSES FOR THE RESOLUTION MINING COMPANY TAILINGS STORAGE FACILITIES OPTIONS, SOUTHERN ARIZONA

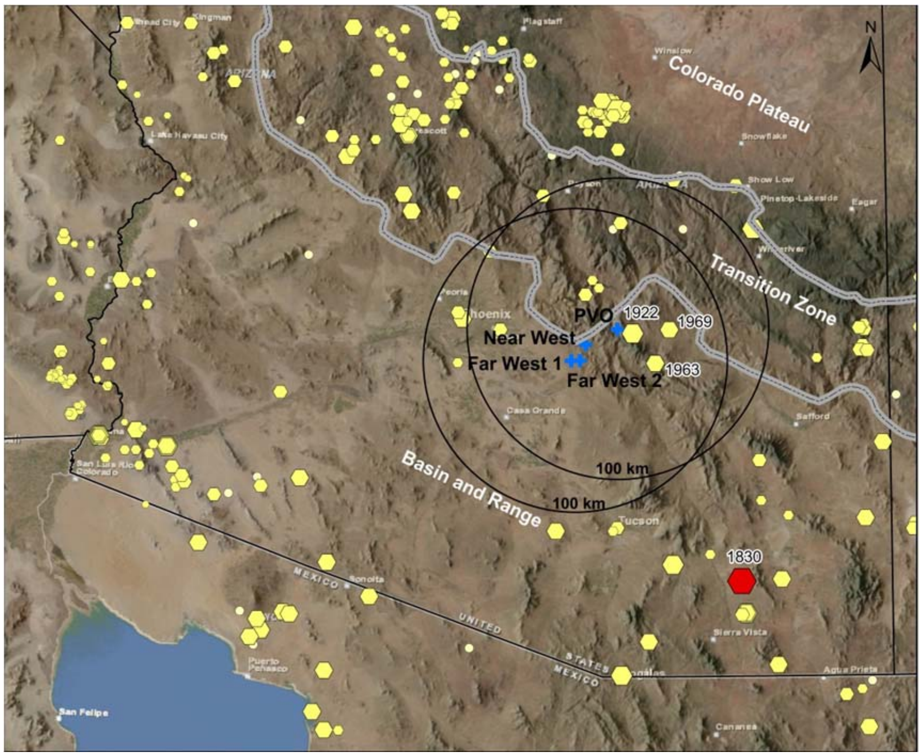

Prepared for

Resolution Copper Mining

3 June 2013

Prepared by

URS

Ivan Wong, Eliza Nemser, Mark Dober, Susan Olig, Jacqueline Bott, and Fabia Terra
Seismic Hazards Group, URS Corporation
1333 Broadway, Suite 800, Oakland, California 94612
and
Robert Darragh and Walter Silva
Pacific Engineering & Analysis
856 Seaview Drive, El Cerrito, California 94530

TABLE OF CONTENTS

TABLE OF CONTENTS

Tables

Figures

TABLE OF CONTENTS

At the request of Resolution Mining Company (RMC), this report presents the results of site-specific probabilistic seismic hazard analyses (PSHA) and deterministic seismic hazard analyses (DSHA) of four sites for the RMC tailings storage facilities options in southern Arizona. The four sites include two sites within the proposed Far West Tailings Management Area: Far West 1 (on alluvium) (33.216° N latitude and -111.296° W longitude) and Far West 2 (on hard rock) (33.217°N latitude and -111.234°W longitude); one site in the proposed Near West Tailings Management Area (33.313°N latitude and -111.195°W longitude); and one site in the proposed Pinto Valley Operations (PVO) Tailings Management Area (33.405°N latitude and -110.968°W longitude) (Figure 1). Far West sites 1 and 2 are located in northern Pinal County, 80 and 86 km southeast of Phoenix and 117 km and 115 km north of Tucson, respectively (Figures 1 and 2). The Near West site, 14 km northeast of Far West 1 and also in northern Pinal County, is located 85 km southeast of Phoenix and 125 km north of Tucson. The PVO site is located in southwestern Gila County, 23 km northeast of the Near West site, 104 km east of Phoenix and 132 km north of Tucson (Figures 1 and 2).

1.1 PURPOSE

The objective of this study is to estimate the levels of ground motions that could be exceeded at specified annual frequencies (or return periods) at the sites and to compare the probabilistic hazard results with the results of a DSHA. The Resolution Copper Project is located in the Basin and Range Province of southern Arizona, near (within 12 km of) the southern boundary of the Transition Zone (Figure 2). Southern Arizona has a low level of seismicity (Figure 2). The four sites at which we computed the hazard are located 49 to 56 km southeast of the Sugarloaf fault zone, the nearest Quaternary fault source (Figure 3).

In this study, geologic and seismologic data were used to evaluate and characterize potential seismic sources, the likelihood of earthquakes of various magnitudes occurring on those sources, and the likelihood of the earthquakes producing ground motions over a specified level. This study incorporates data from seismotectonic and ground motion studies in the region, which were previously performed by URS Corporation for: Phelps Dodge Sierrita Inc. for the Sierrita Tailing Dam in Green Valley, Arizona (Wong *et al*., 2008b); Freeport-McMoran Copper and Gold Miami Operations for the Miami Tailing Dams in Claypool, Arizona (Wong *et al.*, 2008a); Freeport-McMoran Copper & Gold Inc. for the Morenci Mine Tailing Dams (Wong *et al*., 2011); the U.S. Bureau of Reclamation for Granite Reef Diversion Dam and Theodore Roosevelt Dam, Salt River Project, southern Arizona (URS Corporation, 2002), and the U.S. Fish and Wildlife Service for Lake Roberts Dam, New Mexico (URS Corporation, 2011). This evaluation was limited in scope with respect to input data; we relied solely on available data and information and no field investigations were performed for this analysis.

The PSHA methodology used in this study for assessing ground motion hazard allows for the explicit inclusion of the range of possible interpretations of components in the seismic hazard model, including seismic source characterization and ground motion estimation. Uncertainties in models and parameters are incorporated into the PSHA through the use of logic trees (Figure 4). The following report presents the seismic source characterization, the ground motion prediction models used in the PSHA and DSHA, the probabilistic and deterministic ground motion hazard results, site response analysis, selection of the design earthquake, and development of time histories.

1.2 DESIGN GUIDANCE

As stated in Appendix E "Engineering Design Guidance" of the Arizona Mining BADCT Guidance Manual:

The minimum design earthquake is the maximum probable earthquake (MPE). The MPE is defined as the maximum earthquake that is likely to occur during a 100-year intervals (80% probability of not being exceeded in 100 years) and shall not be less than the maximum historical event. The design earthquake may apply to structures with a relatively short design life (e.g., 10 years) and minimum potential threat to human life or the environment.

Where human life is potentially threatened, the maximum credible earthquake (MCE) should be used. MCE is the maximum earthquake that appears capable of occurring under the presently known tectonic framework.

- *Potential threat to human life or the environment*
- *Facility life*
- *Potential future property development downstream of the embankment or earth structure*
- *Seismic history in the area*

The MPE 80% probability of not being exceeded in 100 years has an equivalent return period of about 450 years.

1.3 SCOPE OF WORK

The following scope of work was performed.

Task 1 – Review of Previous Seismic Hazard Studies

Any previous geologic and seismic hazard studies performed for the project sites will be reviewed.

Task 2 – Seismic Source Characterization

All local and regional active faults surrounding the site that may be significant in terms of ground shaking hazard will be included in the site-specific PSHA. Fault parameters that will be characterized include geometry and rupture dimensions, maximum earthquake, nature and amount of slip for the maximum earthquake, and rate and nature of earthquake recurrence. URS has developed a seismic source model for southern Arizona as a result of numerous analyses. The model will be reviewed and updated for the sites. In particular, we will contact scientists who may be working in the region to determine whether our model needs to be updated. The hazard from crustal background seismicity will be included in the analysis using regional seismic source zones and Gaussian smoothing.

Task 3 – Evaluation of Historical and Contemporary Seismicity

The historical and contemporary seismicity will be evaluated in the site region based on an updated seismicity catalog. Historical ground shaking at the project site from past events will be evaluated. Recurrence rates of the historical seismicity for defined regional seismic source zones may be updated, if necessary, for input into the PSHA.

Task 4 – Site Characterization

All available geological, geophysical, and geotechnical information on each site will be reviewed. Of particular importance is shear-wave velocity (V_S) data so that a V_S30 (time averaged V_S in the top 30 m) for the project sites can be computed. V_S30 is an input parameter into several of the ground motion prediction models. If V_S data are not available, a V_S30 will be estimated based on the foundation geology. The epistemic uncertainty in V_S30 will be addressed in the hazard analyses.

Task 5– Probabilistic Seismic Hazard Analysis

Based on our seismic source model for the region and ground motion prediction models, site-specific probabilistic hazard will be calculated at the three project sites. State-of-the-art ground motion prediction models will be used in the PSHA and DSHA including the recent Pacific Earthquake Engineering Research (PEER) Center's Next Generation of Attenuation (NGA) models.

Hazard curves and Uniform Hazard Spectra (UHS) at 5% damping will be calculated. The hazard will be deaggregated at selected periods to characterize the controlling earthquakes. The probabilistic hazard will be compared with the 2008 U.S. Geological Survey National Hazard Maps, which are for a firm rock site condition (V_S30 of 760 m/sec).

Task 6 – Deterministic Seismic Hazard Analysis

A DSHA will be performed for the most significant seismic sources to the project sites using the NGA ground motion prediction models. The ground motions from the controlling deterministic earthquakes will be compared to the UHS from the PSHA.

Task 7 – Conditional Mean Spectra

Based on the UHS, deaggregation, and the structural periods of interest Conditional Mean Spectra (CMS) were computed at the selected design return period.

Task 8 – Design Earthquakes

In accordance with the Arizona Mining Guidance Manual BADCT and existing U.S. practice, operation and design earthquake ground motions will be selected for each project site based on the results of the PSHA.

Task 9 – Development of Time Histories

Five horizontal-component time histories were developed for each site by spectral matching of the CMS.

Task 10 – Final Report

The approach and results of all tasks will be described and summarized in a draft report. The draft report will be submitted to RMC for their review and their comments will be addressed in the final report.

1.4 ACKNOWLEDGMENTS

The analyses of the Far West, Near West and PVO sites were performed by the following personnel of URS Corporation:

Seismic Source Characterization	Susan Olig and Jacqueline Bott
Ground Motion Analyses	Mark Dober and Ivan Wong
Time History Development	Jacqueline Bott and Mark Dober
Report Preparation	Eliza Nemser, Susan Olig, Ivan Wong, Jacqueline Bott, and Fabia Terra

Ivan Wong was the Project Manager. Our thanks to Sergio Gonzalez and Frank Deal of RCM and Howard Plewes and Kate Patterson of Klohn Crippen Berger for their support and assistance. Our appreciation to Melinda Lee for her assistance in the preparation of this report and to Phil Pearthree of the Arizona Geological Survey for providing information.

The PSHA approach used in this study is based on the model developed principally by Cornell (1968). The occurrence of earthquakes on a fault is assumed to be a Poisson process. The Poisson model is widely used and is a reasonable assumption in regions where data are sufficient to provide only an estimate of average recurrence rate (Cornell, 1968). When there are sufficient data to permit a real-time estimate of the occurrence of earthquakes, the probability of exceeding a given value can be modeled as an equivalent Poisson process in which a variable average recurrence rate is assumed. The occurrence of ground motions at the site in excess of a specified level is also a Poisson process, if (1) the occurrence of earthquakes is a Poisson process, and (2) the probability that any one event will result in ground motions at the site in excess of a specified level is independent of the occurrence of other events.

The probability that a ground motion parameter "Z" exceeds a specified value "z" in a time period "t" is given by:

$$p(Z > z) = 1 - e^{-\nu(z) \cdot t} \tag{1}$$

where $\nu(z)$ is the annual mean number (or rate) of events in which Z exceeds z. It should be noted that the assumption of a Poisson process for the number of events is not critical. This is because the mean number of events in time t, $\nu(z) \cdot t$, can be shown to be a close upper bound on the probability $p(Z > z)$ for small probabilities (less than 0.10) that generally are of interest for engineering applications. The annual mean number of events is obtained by summing the contributions from all sources, that is:

$$\nu(z) = \sum_n \nu_n(z) \tag{2}$$

where $\nu_n(z)$ is the annual mean number (or rate) of events on source n for which Z exceeds z at the site. The parameter $\nu_n(z)$ is given by the expression:

$$\nu_n(z) = \sum_i \sum_j \beta_n(m_i) \cdot p(R=r_j|m_i) \cdot p(Z>z|m_i,r_j) \tag{3}$$

where:

$\beta_n(m_i)$ = annual mean rate of recurrence of earthquakes of magnitude increment m_i on source n;

$p(R=r_j|m_i)$ = probability that given the occurrence of an earthquake of magnitude m_i on source n, r_j is the closest distance increment from the rupture surface to the site;

$p(Z > z|m_i,r_j)$ = probability that given an earthquake of magnitude m_i at a distance of r_j, the ground motion exceeds the specified level z.

The calculations were made using the computer program HAZ38 developed by N. Abrahamson. This program has been validated in the Pacific Earthquake Engineering Research (PEER) Center-sponsored "Validation of PSHA Computer Programs" Project (Thomas *et al.*, 2010).

2.1 SEISMIC SOURCE CHARACTERIZATION

Two types of earthquake sources are characterized in this PSHA: (1) fault sources; and (2) areal source zones (Section 4.1). Fault sources are modeled as three-dimensional fault surfaces and details of their behavior are incorporated into the source characterization. Areal source zones are regions where earthquakes are assumed to occur randomly. Seismic sources are modeled in the hazard analysis in terms of geometry and earthquake recurrence.

The geometric source parameters for faults include fault location, segmentation model, dip, and thickness of the seismogenic zone. The recurrence parameters include recurrence model, recurrence rate (slip rate or average recurrence interval for the maximum event), slope of the recurrence curve (*b*-value), and maximum magnitude. Clearly, the geometry and recurrence are not totally independent. For example, if a fault is modeled with several small segments instead of large segments, the maximum magnitude is lower, and a given slip rate requires many more small earthquakes to accommodate a cumulative seismic moment. For areal source zones, only the areas, maximum magnitude, and recurrence parameters (based on the historical earthquake record) need to be defined.

Uncertainties in the seismic source parameters as described below, which were sometimes large, were incorporated into the PSHA using a logic tree approach (Figure 4). In this procedure, values of the source parameters are represented by the branches of logic trees with weights that define the distribution of values. A sample logic tree for a fault is shown on Figure 4. In general, three values for each parameter were weighted and used in the analysis. Statistical analyses by Keefer and Bodily (1983) indicate that a three-point distribution of 5th, 50th, and 95th percentiles weighted 0.185, 0.63, and 0.185 (rounded to 0.2, 0.6, and 0.2), respectively, is the best discrete approximation of a continuous distribution. Alternatively, they found that the 10th, 50th, and 90th percentiles weighted 0.3, 0.4, and 0.3, respectively, can be used when limited available data make it difficult to determine the extreme tails (i.e., the 5th and 95th percentiles) of a distribution. Note that the weights associated with the percentiles are not equivalent to probabilities for these values, but rather are weights assigned to define the distribution. We generally applied these guidelines in developing distributions for seismic source parameters with continuous distributions (e.g., M_{max}, fault dip, slip rate or recurrence) unless the available data suggested otherwise. Estimating the 5th, 95th, or even 50th percentiles is typically challenging and involves subjective judgment given limited available data.

Source Geometry

In the PSHA, it is assumed that earthquakes of a certain magnitude may occur randomly along the length of a given fault or segment. The distance from an earthquake to the site is dependent on the source geometry, the size and shape of the rupture on the fault plane, and the likelihood of the earthquake occurring at different points along the fault length. The distance to the fault is defined to be consistent with the specific ground motion prediction model used to calculate the ground motions. The distance, therefore, is dependent on both the dip and depth of the fault plane, and a separate distance function is calculated for each geometry and each ground motion model. The size and shape of the rupture on the fault plane are dependent on the magnitude of the earthquake; larger events rupture longer and wider portions of the fault plane. We modeled the rupture dimensions following the magnitude-rupture length relationship of Wells and Coppersmith (1994).

Recurrence

The recurrence relationships for the seismic sources are modeled using the truncated-exponentially Gutenberg-Richter, characteristic earthquake, and the maximum magnitude recurrence models (Section 4.1). These models are weighted (Figure 4) to represent our judgment on their applicability to the sources. For the areal source zones, only a truncated exponential recurrence relationship is assumed to be appropriate.

We have used the general approach of Molnar (1979) and Anderson (1979) to arrive at the recurrence for the truncated exponential model. The number of events exceeding a given magnitude, N(m), for the truncated exponential relationship is

$$N(m) = \alpha(m^o)\frac{10^{-b(m-m^o)} - 10^{-b(m^u-m^o)}}{1 - 10^{-b(m^u-m^o)}} \qquad (4)$$

where $\alpha(m^o)$ is the annual frequency of occurrence of earthquakes greater than the minimum magnitude, m^o; b is the Gutenberg-Richter parameter defining the slope of the recurrence curve; and m^u is the upper-bound magnitude event that can occur on the source. A m^o of **M** 5.0 was used for the hazard calculations because smaller events are not considered likely to produce ground motions with sufficient energy to damage well-designed structures.

We have included the model where faults rupture with a "characteristic" magnitude on specific segments; this model is described by Aki (1983) and Schwartz and Coppersmith (1984). For the characteristic model, we have used the numerical model of Youngs and Coppersmith (1985). In the characteristic model, the number of events exceeding a given magnitude is the sum of the characteristic events and the non-characteristic events. The characteristic events are distributed uniformly over a $\pm$ 0.3 magnitude unit around the characteristic magnitude, and the remainder of the moment rate is distributed exponentially using the above equation with a maximum magnitude one unit lower than the characteristic magnitude (Youngs and Coppersmith, 1985).

The maximum magnitude model can be regarded as an extreme version of the characteristic model. We adopted the model proposed by Wesnousky (1986). In the maximum magnitude model, there is no exponential portion of the recurrence curve, i.e., no events can occur between the minimum magnitude of **M** 5.0 and the distribution about the maximum magnitude.

The recurrence rates for the fault sources are defined by either the slip rate or the average return time for the maximum or characteristic event and the recurrence *b*-value. The slip rate is used to calculate the moment rate on the fault using the following equation defining the seismic moment:

$$M_o = \mu \, A \, D \qquad (5)$$

where M_o is the seismic moment, μ is the shear modulus, A is the area of the rupture plane, and D is the slip on the plane. Dividing both sides of the equation by time results in the moment rate as a function of slip rate:

$$\dot{M}_o = \mu \, A \, S \qquad (6)$$

where $\dot{M}_o$ is the moment rate and S is the slip rate. M_o has been related to moment magnitude, **M**, by Hanks and Kanamori (1979):

$$\mathbf{M} = 2/3 \log M_o - 10.7 \qquad (7)$$

Using this relationship and the relative frequency of different magnitude events from the recurrence model, the slip rate can be used to estimate the absolute frequency of different magnitude events.

The average return time for the characteristic or maximum magnitude event defines the high magnitude (low likelihood) end of the recurrence curve. When combined with the relative frequency of different magnitude events from the recurrence model, the recurrence curve is established.

2.2 GROUND MOTION PREDICTION

To characterize the ground motions at a specified site as a result of the seismic sources considered in the PSHA and DSHA, we used empirical ground motion prediction equations (models) for spectral accelerations. The models used in this study were selected on the basis of the appropriateness of the site conditions and tectonic environment for which they were developed (Figure 4; Section 4.3).

The uncertainty in ground motion prediction models was included in the PSHA by using the lognormal distribution about the median values as defined by the standard error associated with each model. Three standard deviations about the median value were included in the analysis.

The seismotectonic setting and historical seismicity of the Resolution Copper Project region is discussed below.

3.1 SEISMOTECTONIC SETTING

The Resolution Copper Project is located in south-central Arizona; we computed the hazard at four sites that are located between 80 to 104 km east-southeast of Phoenix, and 115 to 132 km north of Tucson (Figure 2). Arizona is divided into three physiographic and seismotectonic provinces: the Colorado Plateau in the northeast, the Basin and Range in the southwest, and the intervening Transition Zone that is roughly 40 to 100-km-wide and northwest-southeast trending (Figures 2 and 5). All three provinces are characterized by relatively few late Quaternary faults and low rates of seismicity. These regions are bounded to the east by the Rio Grande Rift, and to the west by the Salton Trough Province (Figure 5). The Far West, Near West and PVO sites are located in the Basin and Range Province, near (within 12 km of) the southern boundary of the Transition Zone (Figures 2, 3 and 5).

The southern Basin and Range Province is a block-faulted terrain of alternating mountain ranges and intervening valleys, bounded by moderately to steeply dipping normal faults. The mountains comprise igneous, metamorphic, and indurated sedimentary rocks of Precambrian through Tertiary age; the valleys are filled with undeformed sequences of fluvial and lacustrine sediments of Oligocene to Pleistocene age. There are differing estimates on the timing of initiation of Basin and Range extension; McQuarrie and Wernicke (2005) suggest that deformation began at 25 Ma, whereas Menges and Pearthree (1989) indicate that deformation may have commenced during the Miocene at 15 Ma. However, there is general consensus that major extension ceased at some time in the late Miocene or Pliocene, and the modern landscape is dominated by geomorphological landforms that indicate tectonic inactivity (Menges and McFadden, 1981). Relative tectonic quiescence in southern Arizona is also reflected by the low levels of historical seismicity and sparse evidence for Quaternary faulting. The southern Basin and Range Province is dominated by northwest-southeast-striking normal faults; however, the study area encompasses the transition from this northwest-southeast structural grain to a more north-south orientation as the province extends into northern Mexico.

The Transition Zone represents a tectonic transition from the relatively thin (~15 to 20 km) extended crust of the Basin and Range to the thick (~40 km) crust of the Colorado Plateau. Bedrock in the region consists primarily of Precambrian metamorphic and granitic plutonic rocks and Paleozoic sediments. The composition of late Cenozoic basin-fill sediments reflects widespread Tertiary volcanism in the region. The Transition Zone is characterized by north- to northwest-trending mountain ranges and intervening basins related mainly to Miocene and younger normal faulting (Menges and McFadden, 1981; Mack *et al.*, 2003). The topography of the Transition Zone is more subdued than that of the southern Basin and Range Province to the south: the ranges are less pronounced and the basins are smaller and less well-defined. The relatively subdued landforms, low to moderate levels of seismicity (Brumbaugh, 1987; Bausch and Brumbaugh, 1997), and relative lack of significant late Quaternary faulting (Pearthree *et al.*, 1983) have been interpreted to indicate geologically recent tectonic cessation of major extension in the region (Menges and McFadden, 1981). The few Quaternary normal faults that are mapped in the region generally trend northwest-southeast and are likely reactivated faults that originated during Basin and Range extension (Lockridge et al., 2012). Based on reconnaissance mapping and limited paleoseismic studies, these faults have average recurrence intervals of tens to hundreds of thousands of years (Pearthree, 1998; Piety and Anderson, 1991).

Similar tectonic processes that characterize the Transition Zone dominate the southern Rio Grande rift that lies to the east of the Transition Zone, though Mack *et al*., (2003) suggest that the two provinces can be differentiated using Plio-Pleistocene sedimentation records. Several major fault-bounded basins resulted from the late Miocene-Holocene deformation phase along the Rio Grande rift; these basins are filled with up to 150 m of sediment. In contrast, in the Transition Zone there is some evidence of post-Miocene faulting, but little evidence for Plio-Pleistocene sedimentation. On the basis of the fault-controlled sedimentation record, the boundary between the Transition Zone and the Rio Grande rift in southwestern New Mexico may be delineated along the western margin of the Palomas Basin. However, Machette (1998) places the western boundary of the southern Rio Grande rift further west to encompass the extent of north-trending Quaternary normal faults as far west as the Arizona/New Mexico border. According to this assessment, the sites would still be located in the Transition Zone though somewhat closer to the boundary with the Rio Grande rift (Figure 5).

The Colorado Plateau in northern Arizona is part of a large region that extends across southeastern Utah, northwestern New Mexico, and western Colorado. Physiographically and geologically distinct from the highly deformed Rocky Mountains to the north and east and the Basin and Range region to the south and west, the Colorado Plateau is characterized by relative tectonic stability and elevated topography dissected by rivers. Whereas major crustal deformation of the Colorado Plateau ceased at the end of Laramide orogeny (40 Ma), the region has been subject to about 2 km of epeirogenic uplift during the Cenozoic (Morgan and Swanberg, 1985). During uplift, the plateau acted as a coherent block, with only minor differential movements creating northerly-trending monoclines and associated structural basins. Contemporary seismicity in the Colorado Plateau Province is low to moderate, with widespread, generally small events that cannot be correlated with surface geological features (Wong and Humphrey, 1989).

The Salton Trough to the west of the Basin and Range marks the transition between ocean-floor spreading in the Gulf of California and right-lateral strike-slip faulting along the San Andreas fault zone. This region is one of the most seismically active areas in the western United States, characterized by right-lateral strike-slip faulting and elevated levels of contemporary seismicity with repeated events of **M** 6 to 7 during historical time. Slip rates on faults in this region are as high as 30 mm/yr (Working Group on California Earthquake Probabilities, 2008).

3.2 HISTORICAL SEISMICITY

A project catalog was compiled for an area encompassing southern Arizona and parts of neighboring states as shown in Figure 2. The principal earthquake data sources were catalogs from the Northern Arizona University regional catalog for 1830 through 2005 and the Advanced National Seismic Service (ANSS) for 1931 through the end of 2012. DuBois *et al*. (1982) also provided a valuable resource for Arizona earthquakes. As in most of the western U.S., the historical record extends back less than 200 years, which is a relatively short period compared to the recurrence intervals of most active crustal faults.

Only 7 earthquakes of **M** 5 or greater have occurred within 200 km of the Far West, Near West and PVO sites (Figure 2). The largest of these events is the supposed 1830's (?) intensity-based magnitude (M_I) 7.0 (Modified Mercalli [MM] VII-IX) event whose location is estimated to be about 185 km southeast of the sites. This event is the first listed in the catalog and its location, size and date are based on the interpretation of second-hand information reported by an Apache medicine man to an Arizona pioneer in the 1850's (DuBois, *et al.* 1982). Descriptions of this earthquake include: "A loud rumbling noise was heard coming from the southwest"; "The whole earth split open from one side of the valley to the other sending forth a blue smoke heavenward for a mile"; and "A Great Spirit became very angry and knocked the people around for a few moments, making them feel as if they were drunk". Though this event is still listed in some catalogs, the Arizona Geological Survey (and the USGS) have removed this event from their catalog, stating that the account of the event is dubious, poorly dated and that the reported effects are rather extreme for a relatively young event for which no physical evidence has been found (Phil Pearthree, Arizona Geological Survey written communication, 2013). We have included this event in this report because of its presence in DuBois *et al.* (1982), but it has been removed from the earthquake recurrence calculations.

Historical seismicity in the site region is sparse with only 17 events within 100 km of the sites (Figure 2). The largest and closest event within 100 km of the sites is the MM VI event that occurred on 17 June 1922 and was located in the vicinity of the town of Miami, 44 km northeast of the Far West 1 site, 39 km northeast of the Far West 2 site, 32 km northeast of the Near West site and about 10.5 km east of the PVO site (Figures 2 and 6). DuBois *et al.* (1982) report the following for the event in Miami: "No damage was incurred in any instance. Caused considerable commotion in both the downtown and residential sections of this community. Inhabitants of the larger dwellings and business houses in and about Miami summarily lost interest in their various undertakings and took to the streets and open spaces. The temblor is said to have been particularly felt in the large structures of the town, in which the brunt of the shock was effectively borne up through the deep foundations." The earthquake was recorded on the seismograph in Tucson. The location and size of this event, however, are highly uncertain.

Two other moderate events of M_L 4.1 and M_L 4.4 occurred to the east of the sites in 1963 and 1969, respectively (Figures 2, 7 and 8). The 1963 Globe earthquake was not likely felt at the site locations (Figure 7), though the 1969 San Carlos event was likely felt, particularly PVO (Figure 8). The maximum intensity of these two events was MM VI with little to no damage reported. The felt area of the 1963 event is estimated at about 6,500 km^2 (DuBois, 1982) (Figures 7 and 8).

Although quite distant (about 285 km southeast of the sites), a notable earthquake of **M** 7.4 occurred on 5 May 1887 in northern Sonora, Mexico (DuBois *et al.*, 1982; Suter and Contreras, 2002; Figure 9). This earthquake ruptured the Pitaycachi, Teras, and Otates faults (Suter, 2008) and was felt throughout the region and as far away as Albuquerque, New Mexico and El Paso, Texas. In Phoenix, hanging chandeliers swung in every building (DuBois *et al.*, 1982). A MM VI is estimated for the sites (Figure 9).

The following section discusses the characterization of the seismic sources and the ground motion prediction models selected and used in the PSHA and DSHA. The seismic source model used in this study was based on previous URS studies in the region (Wong *et al*., 2008a, 2008b, 2011; URS Corporation, 2011) and review of existing maps and reports as discussed in this section. No new geological or geophysical investigations were conducted for this study.

4.1 SEISMIC SOURCES

Seismic source characterization is concerned with three fundamental elements: (1) the identification, location and geometry of significant sources of earthquakes; (2) the maximum size of the earthquakes associated with these sources; and (3) the rate at which the earthquakes occur. The seismic source model includes crustal faults capable of generating larger, surface-faulting earthquakes (Section 4.1.1), and areal source zones, which account for background crustal seismicity that cannot be attributed to identified structures explicitly included in the seismic source model (Section 4.1.2).

4.1.1 Crustal Fault Sources

Fault parameters required in the PSHA include: (1) rupture model (including independent single plane and potentially linked models); (2) probability of activity; (3) fault geometry including rupture length, rupture width, fault orientation, and sense of slip; (4) maximum magnitude [M_{max}]; and (5) earthquake recurrence including both recurrence model and rates. These parameters are generally discussed further below. Selected faults that contribute the most to the hazard are specifically discussed in subsequent sections. We have explicitly incorporated the uncertainties in each parameter through the use of logic trees, as exemplified in Figure 4.

Faults were included in the analyses that were judged to potentially contribute to the probabilistic hazard at the site because of their activity, length, or proximity to the site region. We included known faults within 100 km of the sites (referred to herein as local faults) showing evidence for late Quaternary (≤ 130,000 years) activity or repeated Quaternary (≤ 1.6 million years) activity (Figure 3). We also included longer, more active faults in southern California and Baja California, such as the southern San Andreas fault, because from previous analyses in the region (e.g., Wong *et al*., 2008a; 2011), we know that these major fault sources can be significant contributors to the hazard at longer periods, despite their great distances.

The Pitaycachi fault, source of the 1887 Sonora earthquake, was not included in the hazard analysis because it is too distant (> 250 km away) and the slip rate is too slow (< ~0.1 mm/ yr) to potentially contribute to the hazard at the site. Additionally, previous geotechnical and hydrological studies (Klohn Crippen Berger, 2012; Montgomery and Associates, 2012) for the proposed tailings storage facilities have identified several faults near the sites, including the Elephant Butte fault near the Far West sites (Figures 10 and 11), the Concentrator and Conley Spring faults near the Near West site (Figure 12), and the West End, Gold Gulch, Dome and Jewel Hill faults near the PVO site (Figures 13 and 14). We considered, but did not include these nearby faults in our analysis because they appear to be old (> 1.6 million years old) and show negligible rates of activity based on our review of published and unpublished information, and consultation with Phil Pearthree at the Arizona Geological Survey. Several of these normal faults offset Tertiary rocks down-to-the-west and are compatible with the current extensional stress regime. However, they were not included in Quaternary fault compilations for Arizona (Pearthree *et al*., 1983; Pearthree, 1998) or the USGS Quaternary fault database because their geomorphic expression is moderate to poor, they do not appear to displace Quaternary deposits (including middle Pleistocene alluvium), and indeed some traces are even buried by Tertiary volcanic and sedimentary rocks in some locations.

Specifically, the Elephant Butte fault was mapped by Ferguson and Skotnicki (1995) as extending from the Superstition Mountains south to about Comet Peak, and then continuing southward to Dromedary Peak as a buried structure. They note that although the Elephant Butte fault offsets the ~24-Ma Siphon Draw member of the Superstition Tuff, the fault is buried by Coffee Creek Mountain lavas, which are correlated to be slightly younger, but still middle Tertiary in age (Ferguson and Skotnicki, 1995). Montgomery and Associates (2012a) projected the Elephant Butte fault farther south of Dromedary Peak, roughly bisecting the Far West proposed site as two, northwest-striking, left-stepping en echelon faults, based on mapping of Bouger gravity anomalies (Figure 11). However, mapping of surficial deposits in the area (Huckleberry, 1993; Spencer *et al*., 1998) shows the faults are buried by late and middle Pleistocene alluvium as well as Tertiary conglomerate (Figure 15), consistent with a pre-Quaternary age.

The north-south striking Concentrator fault (Figure 12) bounds the eastern side of the Superior Basin (Peterson, 1969), and includes multiple branches as mapped by Richard and Spencer (1998). None of the traces appear to offset Quaternary deposits (Spencer *et al*., 1998). The northern 5 km of the western branch, closest to Superior, has the best geomorphic expression with a moderate topographic escarpment, and this branch appears to be the main basin-bounding splay. However, this branch is buried by Miocene rhyolitic and basaltic rocks (units Tr and Tb of Richard and Spencer, 1998), and thus appears to be pre-Quaternary (Figure 16).

The west-northwest striking Conley Spring fault is located a few kilometers east of the Concentrator fault (Figure 12) and was mapped by Richard and Spencer (1998), but not referred to by name. Montgomery and Associates (2012a) show this fault cutting Quaternary alluvium (unit Qal, Figure 12). However, this Qal unit appears to be erroneously labeled because both Richard and Spencer (1998) and Spencer *et al*. (1998) label this unit as Tta, the 18.6-Ma Apache Leap Tuff, and they do not show the Conley Spring fault offsetting any Quaternary deposits. Indeed, the fault has poor geomorphic expression overall and in some locations north of Highway 66, they show the fault buried by older alluvium, suggesting it is an older structure as well.

The seismic source model used in this study includes characterization of four local faults or fault zones: Carefree, Horseshoe, Sugarloaf and Whitlock Wash (Figure 3). Faults are generally modeled as single, independent, planar sources, simplified from the complex zones shown on Figure 3. Table 1 shows the parameters for local faults. Our characterization of local faults herein is revised and updated from our previous probabilistic seismic hazard analysis for a tailings dam near Miami, AZ (Wong *et al*., 2008a), based on data compiled in the USGS Quaternary Fault and Fold Database (http://earthquake.usgs.gov/hazards/qfaults/) and sources listed in Table 1.

Maximum magnitudes were estimated for local faults using the empirical relationships of Wells and Coppersmith (1994) for all types of faults, as noted in the footnotes of Table 1. None of the local faults are blind, and minimum seismogenic depths were assumed to be 0 km. We assumed maximum seismogenic depths of 12 km (weighted 0.3), 15 km (weighted 0.5), and 17 km (weighted 0.2), primarily based on the maximum depth of historical seismicity in the region.

Fault dips were averages over the entire seismogenic crust. Although near-surface fault dip data are available for many of the faults, crustal dip data are lacking. We assumed default dips of 50° (weighted 0.6) ±15° (weighted 0.2) for all the local faults, which all show dominantly normal slip. This default fault dip distribution is after recommendations made by the Basin and Range Province Earthquake Working Group II (BRPEWGII; Lund, 2012; see Issue G4) to the U.S. Geological Survey (USGS) regarding crustal-scale dips for typical range-bounding normal faults in the Basin and Range province to be used in the next update of the National Hazard Maps. This distribution was based on focal plane and aftershock data for historical surface-rupturing earthquakes in the Basin and Range Province, as well as normal faults worldwide (see presentation by Crone at: http://geology.utah. gov/ghp/workgroups /pdf/brpewg/BRPEWGII _Presentations.pdf).

Recurrence models can significantly impact hazard calculations and we considered truncated exponential, maximum magnitude, and characteristic recurrence models for this analysis. Observations of historical seismicity and paleoseismic investigations suggest that characteristic behavior is more likely for individual faults, whereas seismicity in areal zones best fits a truncated exponential model (Schwartz and Coppersmith, 1984; Youngs and Coppersmith, 1985). The maximum magnitude model is an extreme version of the characteristic model (Wesnousky, 1986). We favored (weighted 0.6) the characteristic model for all local fault sources and assigned equal weights of 0.2 to the exponential and maximum magnitude models.

In assigning probabilities of activity for local fault sources, we considered both the likelihood that the fault is structurally capable of independently generating earthquakes, and the likelihood that it is still active within the modern stress field. We incorporated many factors in assessing these likelihoods, such as: orientation in the modern stress field, fault geometry (length, continuity, and dip), relation to other faults, age of youngest movement, rates of activity, geomorphic expression, amount of cumulative offset, and any evidence for a non-tectonic origin. Faults with definitive evidence for repeated Quaternary activity were generally assigned probabilities of being active (seismogenic) of 1.0 (Table 1). The probability of activity for faults that do not show definitive evidence for repeated Quaternary activity was individually judged based on available data and the criteria explained above. Resulting values range from 0.9 to 1.0 (Table 1) and the specific reasons for assigning probabilities less than 1.0 to a particular fault are generally given in the comments column of Table 1.

As recurrence interval data are generally lacking for local faults, we used slip rates to characterize rates of fault activity (Table 1). We considered all available long- (≤ 1.6 Ma) and short-term (≤ 130 ka) data in developing slip rate distributions, but we preferred short-term data whenever possible. In addition to the time period, we also considered the type and quality of data in determining rates. Preferred slip rates (generally weighted 0.6) are primarily based on data in the USGS Quaternary fault database and as noted in the comments column of Table 1. Maximum and minimum values (each generally weighted 0.2) are typically selected to represent 95th and 5th percentile values as previously discussed in Section 2, unless the available data suggest otherwise as noted in the comments column of Table 1 (see also local fault summaries in Wong *et al*., 2008a). Note that from our previous hazard analysis in the area (Wong *et al*., 2008a) we found that none of the local faults contributed significantly to the hazard so we do not include detailed local fault specific discussions herein.

Our characterization of southern California faults was modified from our recent hazard analysis in the region (Wong *et al*., 2011a). We included the five most significant fault or shear zones:

the San Andreas, San Jacinto-Imperial, Elsinore, Garlock, and Eastern California. These plate-boundary structures are all long, complex, and highly-active fault zones or systems that have been extensively studied. The source characterization of these faults used in this study is from the 2007 CGS/USGS Uniform California Earthquake Rupture Forecast (UCERF) model (Working Group on California Earthquake Probabilities [WGCEP], 2008). Tables 2a through 2e show the parameters used for the southern California faults. The UCERF seismic source model was used in the development of the California portion of the 2008 National Hazard Maps (Petersen *et al.*, 2008). One of the most significant changes in the 2008 UCERF model from the previous 2002 model (Cao *et al.*, 2003) is in the method of characterization of some of the major faults including the San Andreas, San Jacinto, Elsinore, and Garlock faults. Specifically, instead of defining rupture segments with slip rates to define the rate of earthquake recurrence, WGCEP (2008) divided the faults into sections, which may or may not be rupture segments, based on variations in geometry, slip rate, and other physical characteristics. WGCEP used paleoseismic data to develop a model of the rate of earthquake ruptures per section, independent of the rupture history of adjacent sections (i.e., excluding *a priori* models of rupture segmentation). From that, and again using paleoseismic data, they compiled a list of all possible rupture scenarios involving rupture of one or more sections, and developed a rate of recurrence of ruptures for each scenario based on the initial “a priori” or “geologic insight” model moment balanced by slip rate. WGCEP used two different magnitude-area relationships, weighted equally, to calculate the rate of events. This approach depends more heavily on paleoseismic observations and geologic constraints and less on models of rupture segmentation. We have adopted the method and rupture rates of the WGCEP (2008) for the San Andreas and other southern California faults and have incorporated them into our analysis (Tables 2b and 2e).

The southern San Andreas fault system is the most significant fault source to the hazard at all the sites, and so it is discussed further below. The Sugarloaf fault zone is the closest Quaternary fault to the sites so it is also discussed (Figure 3).

Southern San Andreas Fault System

The right-lateral strike-slip San Andreas fault zone is the most significant structure accommodating North American-Pacific plate motion, accounting for up to 70% of the relative plate motion along most of its length. The southern San Andreas fault zone includes the section of the fault south of the creeping segment in central California. This part of the fault has generated two large historical earthquakes, the 1857 **M** 7.8 to 8 Ft. Tejon that ruptured the Parkfield through Mojave South sections, and an **M** ~7½ earthquake in 1812 that ruptured the North San Bernardino and Mojave South and possibly Mojave North sections. In addition, the northernmost Parkfield section has experienced numerous moderate earthquakes (**M** ~6) in the historical period, the most recent of which occurred in 2004.

The 2007 WGCEP (2008) has developed a new characterization of the San Andreas fault that differs considerably from that of previous working groups (e.g., WGCEP, 1988; 1995; Cao *et al.*, 2003). We use a simplified version of their fault characterization and earthquake recurrence models to model the southern San Andreas fault. They include three alternative deformation models to describe how slip is distributed between the southern San Andreas and other faults in the area including the San Jacinto fault; we use only their preferred model.

Changes in the 2007 UCERF model (WGCEP, 2008) from the 2002 model of Cao *et al.* (2003) include modification to the sectioning, geometry, recurrence and slip rates on the fault. WGCEP

(2008) divide the southern San Andreas fault zone into ten sections, a departure from earlier working groups who divided it into six rupture segments (e.g., WGCEP, 1988, 1995; Cao *et al.*, 2003). The sections of the 2007 Working Group are not necessarily rupture segments and do not imply a specific earthquake model; rather, they are defined based on distinct geological characteristics that may or may not relate to earthquake rupture characteristics. We have adopted the divisions of the 2007 Working Group, with the following sections: Parkfield (PK), a 36-km-long section extending from Parkfield to the town of Cholame; Cholame (CH), extending southeast 62 km from Cholame; Carrizo (CC), a 59-km-long segment extending to the southern end of the Carrizo Plain; Big Bend (BB), a 50-km-long stretch ending at the intersection with the east-west-striking Garlock fault; Mojave North (NM), which extends 40 km from the Garlock fault to Elizabeth Lake, the northern end of the “Mojave segment” used by previous working groups; Mojave South (SM), a 100-km-long section similar to the former “Mojave segment”, that traverses the southeastern edge of the Mojave desert from Elizabeth Lake to near Cajon Pass, about halfway between Wrightwood and Lost Lake; San Bernardino Mountains North (NSB), which extends about 35 km southeast from Cajon Pass to the intersection with the Mill Creek fault and the northern end of an region of structural complexity called the San Gorgonio Pass knot (WGCEP, 2008); San Bernardino South (SSB) and San Gorgonio Pass-Garnet Hill, also referred to as Banning-Garnet Hill (BG), which pass through the complex San Gorgonio Pass region and are northwest-striking strike-slip and slightly more west-striking reverse oblique-slip faults, respectively; and last, Coachella Valley (CO), which starts at the junction with the Mission Creek fault where the SAF again regains its northwest strike, and ends at the Salton Sea (WGCEP, 2008).

Slip rates on several of the newly defined sections also have changed in the UCERF model, reflecting both the new sectioning and more recent geologic and geodetic data. The San Andreas fault zone has the highest slip rate of any fault in California. On the Parkfield, Cholame, Carrizo and Big Bend sections, the average late Holocene slip rate is about 34-35 mm/yr, consistent with previous estimates (Sieh and Jahns, 1984; Sims, 1994). The slip rate decreases southward as more slip is transferred to other structures of the San Andreas fault system, especially the San Jacinto fault. As a consequence, the average slip rate on the southern sections of the fault decreases from about 27±7 mm/yr in the Mojave North section to about 20±6 mm/yr on the southernmost Coachella Valley section.

WGCEP (2008) account for new paleoseismic data obtained at several sites along the fault, and use a new approach to incorporating those data. Paleoseismic data and recurrence information for the fault sections nearest the sites are summarized below.

The northernmost Parkfield section ruptured with about 1.5 m of slip during the 1857 earthquake. It has also had repeated independent ruptures (WGCEP, 2008). Independent rupture is probably the most common mode of failure for this section, but it clearly can also rupture during large events on sections to the south. WGCEP (2008) assign an average recurrence interval of about 25 years, with the bulk of events occurring as independent ruptures and few with one or more other sections.

Investigations of the Las Yeguas site on the Cholame section have identified 2 to 4 surface rupturing events since 1058 AD, with the penultimate event occurring between 1030 and 1460 AD, suggesting an average recurrence interval of about 240 years, although this is poorly constrained (Stone *et al.*, 2002; Young *et al.*, 2002). Single-event displacement data from the Cholame section come largely from studies of the 1857 rupture, but these yield highly variable results. Sieh (1978) and Lienkamper (2001) both measured offset geomorphic features but found that average slip in 1857 was about 3.5 m and 6 m respectively. Runnerstrom *et al.* (2002) analyzed pre- and post-earthquake wide-aperture survey data and determined that displacement as large as 16 ± 6 m occurred in 1857, indicating that more than half of the total slip might occur off the main fault. WGCEP (2008) consider it likely that the Cholame section sometimes ruptures in large events like that of 1857 and sometimes in smaller independent ruptures or with Parkfield. They assign it a recurrence interval of 150 years because it may include events recorded at Carrizo paleoseismic sites.

WGCEP (2008) has subdivided the Carrizo segment, as defined by previous working groups, into three sections, based on changes in fault strike and amount of slip in the 1857 event. The Carrizo section is the northernmost and extends to the sharp change in fault strike at the south end of the Carrizo Plain and had about 8 m of slip on average in 1857. Sims (1994) found a record of 5 to 6 earthquakes at Phelan Creek in the Carrizo section with an average recurrence interval of 150 to 300 years. Grant and Sieh (1994) found evidence of five earthquakes at Bidart Fan since 1218 AD, yielding an average recurrence interval of about 160 years. However, they concluded that the timing has been irregular, and 350-400 years of quiescence preceded the 1857 earthquake, with about 100 years between earlier events. More recent investigations at Bidart Fan support a short recurrence interval of about 88±14 years over the last six events (Akciz *et al.*, 2010), but that the preceding events were separated by more than 200 years, consistent with a model of clustered ruptures (Grant Ludwig and Akciz, 2012). Estimates of single-event displacement vary widely for this section. Sieh and Jahns (1984) argued for ca. 10 to 12 m offsets in the last three earthquakes, whereas Grant and Sieh (1993) observed displacements of 6.5 to 7 m in 1857. Another surveying study found wide-aperture displacement of about 11 m in 1857 (Grant and Donnellan, 1994). A study by Liu *et al.* (2004) found that the last six displacements ranged from 1.4 to 8.0 m, with three events between 7.5 and 8.0 m. The inconsistency between the short intervals, large displacements, and well-supported slip rate has not been resolved for the Carrizo section. More recent work suggests that the earlier inferences of large displacements may be incorrect and that most displacements, including that in 1857, were closer to 5 m (Grant Ludwig *et al.*, 2010; Zielke *et al.*, 2010.) The WGCEP (2008) decreased the average recurrence interval to acknowledge the new work but recognize unresolved discrepancies with older studies and use 150 years.

The Big Bend section was included in the former Carrizo segment, includes the more westerly striking section of the fault and extends through a region of transpression, with associated thrust faulting, to the junction with the Garlock fault. Slip in 1857 decreased from about 8 to about 6 m from the Carrizo to Big Bend sections. Two paleoseismic sites yield a possibly incomplete record suggesting 2 to 3 events in 500 years, longer than that of the Carrizo section (Lindvall *et al.*, 2002). WGCEP (2008) assign a recurrence interval for Big Bend of 175 years, based on correlation modeling and the inference that some events might be missing from the record. They suggest it could be the source of the relocated 12/21/1812 earthquake of Toppozada *et al.* (2002). Recent paleoseismic data from the Frazier Mountain site suggests the average recurrence interval on this section over the last 1,000 years about 122 years (Scharer *et al.*, 2011). The earthquake rate may, therefore be modified in the next UCERF iteration, but we retain the values in the published WGCEP (2008) model.

WGCEP (2008) use the recurrence interval data determined from paleoseismic studies and a method of assessing the probability that a specific rupture scenario is consistent with the paleoseismic record to determine a rupture recurrence rate for each of the ten sections. They use slip rates to moment balance the *a priori* recurrence rates to develop final moment-balanced rupture rates for all possible rupture scenarios. We have adopted these rates for use in our model. The table of rupture rates appears in Table 2b.

Sugarloaf Fault Zone

The Sugarloaf fault zone is expressed as a low, fairly continuous east-facing fault scarp as much as 5 m high at the contact between Precambrian granite and Tertiary basin fill sediments along the western margin of the small sedimentary basin on the flank of the Mazatzal Mountains (Pearthree *et al*., 1995) (Figure 1). The relief across the fault is minimal, indicating relatively little Quaternary activity (Pearthree, 1998). Stream bank exposures show down-to-the-east displacement on a northwest-striking fault plane dipping 70° to 80° to the northeast. Fault scarps on alluvium are rare and are poorly preserved. Paleoseismic trenching shows that the fault offsets late to latest Pleistocene deposits, but middle to upper Holocene deposits are not displaced (Pearthree *et al*., 1995). There is evidence for multiple Quaternary events, yet, the timing of individual events cannot be constrained (Pearthree *et al*., 1995; Pearthree, 1998). A preferred slip rate of 0.02 ± 0.01 mm/yr is calculated from ~ 1 m of vertical displacement in late Pleistocene (ca. 50 to 100 ka) deposits. A preferred maximum magnitude of **M** 6.5, the minimum magnitude for surface-faulting, was assumed for this 8-km long short fault in the PSHA. A slightly larger magnitude, **M** 6.6, was assumed for the DSHA.

4.1.2 Crustal Background Earthquakes

The hazard from crustal background (floating or random) earthquakes that are not associated with the known or mapped faults must be incorporated into the PSHA. Earthquake recurrence estimates in the site region and maximum magnitudes are required to assess the hazard from background earthquakes. In this study, we have adopted the zonation model for background earthquakes based on the physiographic zone boundaries of Peirce (1984). The site is located close to the boundary of two seismotectonic zones: the southern Arizona Basin and Range and the Transition Zone between the Colorado Plateau and the Basin and Range (Figures 2 and 5). However, in the PSHA model we combined the two zones because there were not enough earthquakes in each zone to determine earthquake recurrence for the two separate zones. The recurrence parameters were developed using the historical seismicity catalog for the period 1830 to 2012.

The earthquake recurrence of the site region assumes the truncated exponential form of the Gutenberg-Richter relationship of $\log N = a - bM$. Dependent events were removed using the approach of Youngs *et al.* (2000). Additional earthquakes associated with known faults, in this case aftershocks of the 1887 Pitaycachi earthquake, were also removed as these events were not removed using the approach described above as the main shock was outside of our catalog area. The catalog was then divided by the seismotectonic province boundaries, in this case the combined southern Arizona Basin and Range and Transition Zone.

Completeness intervals were estimated based on previous studies in the region and Stepp plot analysis of the catalog (Stepp, 1972). The Stepp plot (Figure 17) was developed by calculating the average annual number of independently occurring events in each half magnitude increment for both of the combined source zone. These values are plotted as a function of time before present. If the rate of earthquake occurrence is relatively uniform over time (horizontal line), it indicates that the catalog is complete for this period of time. When the catalog is not complete, the curves begin to diverge downwards from a relatively horizontal line on the log-log plots. After adjusting the earthquake catalog for dependent events and completeness, 34 events remained in the range **M** 3.5 to 6.5 for the combined southern Arizona Basin and Range and Transition Zone from which to estimate the recurrence for the study region. The recurrence was calculated using the maximum likelihood technique of Weichert (1980) for each province (Figure 18). The normalized *a*-value (by area) and the *b*-value computed for the combined source zone are -2.27 and 0.90 respectively. Included are the mean plus and minus one standard deviation curves. A maximum magnitude of **M** 6½ ± 0.3 was used for the seismic source zone.

Felzer (2008) used California seismicity for the U.S. National Hazard Maps to indicate that corrections should be made for both magnitude rounding and errors, before calculating seismicity rates (*a*-values). Felzer (2008) reports that *a*-values can also be overestimated as a result of magnitude errors in historical seismicity catalogs. The Gaussian distribution for magnitude errors is symmetrical but that of earthquake occurrence is asymmetrical. Thus magnitudes above a specific magnitude (e.g., **M** 5.2) have equal probabilities as magnitudes below a specific magnitude (e.g., **M** 4.8) because of the symmetrical Gaussian distribution, which does not reflect the reality that larger earthquakes are less frequent than smaller earthquakes. This results in an apparent increase in earthquakes for a particular magnitude (e.g., **M** 5.0), which is then carried into the recurrence calculations, thus increasing the seismicity rate. Again, if magnitude error is uniform throughout the catalog, then it is easy to fix, but when it varies throughout the catalog a correction can be made for each magnitude based on its error and the Gutenberg-Richter relationship and substituted for the reported magnitude. Then the actual seismicity rate (*a*-value) can be estimated. Again Felzer (2008) has tested this methodology using simulated catalogs and was able to recover the correct *a*-value with this method.

Both the corrections for magnitude error and magnitude rounding are incorporated into the recurrence estimates reported here for the combined seismic source zone. We were able to determine rounding by observing the magnitudes reported in the catalogs over time and estimated magnitude errors based on the work of Felzer (2008). For those earthquakes whose errors have been reported in the literature, these errors are included. Otherwise a standard error of 0.333 was assigned to pre-1960 earthquake magnitudes computed from MM intensity, 0.222 for instrumental magnitudes during 1940-1982, and 0.111 for all earthquakes occurring after 1982. These are similar to errors calculated during these periods for California (Felzer, 2008). First the recurrence was calculated from the seismic source zone catalog as described above. Then recurrence was re-calculated for each zone 200 times, first fixing the *b*-value obtained initially (0.90), and applying the two magnitude corrections discussed above for each iteration (first the rounding error, then the magnitude error for each magnitude in the catalog) to obtain an average corrected *a*-value (-2.35). This average corrected *a*-value is used in the PSHA.

Because of the limited duration of the historical catalog, we incorporated uncertainties in the recurrence parameters for the background seismicity into the hazard analysis. We used three b-values. This uncertainty of ± 0.13 includes the uncertainty in the b-value but also additional uncertainty due to the possibility that the historical record may not be a robust representation of the next 50 to 100 years.

The use of seismic source zones assumes that background earthquakes are uniformly (randomly) distributed throughout the seismogenic crust. However, some seismicity may be stationary through time (at least over the next few decades of interest) and can be smoothed using a

Gaussian filter. In the Gaussian smoothing approach, we smoothed the historical seismicity on a grid at 0.1 degree intervals to incorporate a degree of stationarity. The version of Gaussian smoothing adopted in this study (Frankel, 1995) is the same as that used in the National Hazard Maps (Petersen *et al.*, 2008). This scheme addresses both the spatial stationarity of seismicity and its randomness. We smoothed the historical background seismicity for the combined seismotectonic zones within 100 km of the site, using a spatial window of 25 km. Thus the hazard from seismicity that clusters in a specific seismic zone is retained spatially rather than being smoothed to a uniform distribution as in a seismic source zone.

4.2 SITE CHARACTERISTICS

Four locations in the three areas were selected to compute the seismic hazard: one site each in the Near West area and PVO, and two sites in the Far East area (Figure 1). We computed the hazard at a site in the PVO open pit shown on Figure 19. The PVO open pit is in ore-grade Precambrian quartz monzonite porphyry (Figures 13 and 14). For the Near West area, we computed the hazard at a site that sits on the Miocene Gila conglomerate (Tcu, Figure 16). For the Far West area, we considered two sites: Far West 1, on alluvium (Qal), near the western edge of the area, and Far West 2, which rests on the Early Proterozoic Pinal Schist at the eastern edge (pCpl, Figures 10 and 15). There are no site-specific shear-wave velocity (V_S) data for these sites. The NGA ground motion prediction models (Section 4.3) require V_S30, the time averaged V_S in the top 30 m (100 ft) as input. We conducted a site response analysis for the Far West 1 site because of the presence of alluvium, which tends to amplify ground motions at moderate to high frequencies. (Section 6).

A V_S30 of 1200 m/sec, appropriate for firm to hard rock, was used for the sites that rest on Precambrian quartz monzonite and schist. The V_S30 may be higher than this value but the NGA ground motion prediction models are capped at about 1,200 m/sec. We selected a best estimate V_S30 value of 500 m/sec for the Near West site based on *in situ* shear-wave measurements performed on Gila Conglomerate at another mine site in the region. To incorporate the epistemic uncertainty in the V_S30 and variability beneath the site, we included an uncertainty of 100 m/sec so values of 400 and 600 m/sec were also used in the hazard calculations for the Near West site.

To develop a V_S profile for the Far West 1 site, we examined the log from borehole FW15-R and an interpreted geologic cross-section based on gravity modeling (Montgomery & Associates, 2012) (Figure 10). Figure 66 shows our V_S profile based on the limited data. The thickness of the alluvium and basalt fill deposits were accurately known from the borehole log but the extent of the basalt below 170 m and the lithology beneath the basalt are unknown. The depth to the Precambrian basement (Pinal schist) is 900 m based on the gravity modeling but a decrease in the density of the Apache Leap Tuff could bring the modeled depth to basement to 600 m (Mark Cross, Montgomery & Associates, written communication, January 2013).

The V_S for each layer in Figure 66 was estimated based on data from other areas. The V_S for the alluvium is based on numerous measurements of alluvium in the Salt Lake Valley (McDonald and Ashland, 2008). We could not find any information on basaltic fill deposits so the value of 400 ± 100 m/sec is estimated from fill deposits in Utah basins. The V_S for basalt is adopted from V_S measurements made in the eastern Snake River Plain (Woodward-Clyde Federal Services *et al.*, 1996). The Pinal schist V_S assumes hard rock at depth.

4.3 GROUND MOTION PREDICTION MODELS

To estimate the ground motions in the PSHA and DSHA, we have used recently developed empirical ground motion prediction models appropriate for tectonically active crustal regions such as the western U.S. and subduction zones. The crustal relationships, developed as part of the NGA Project sponsored by PEER Center Lifelines Program, have been published and are available on the PEER website. The NGA models have a substantially better scientific basis than current relationships (e.g., Abrahamson and Silva, 1997) because they are developed through the efforts of five selected ground motion prediction developer teams working in a highly interactive process with other researchers who have: (a) developed an expanded and improved database of strong ground motion recordings and supporting information on the causative earthquakes, the source-to-site travel path characteristics, and the site and structure conditions at ground motion recording stations; (b) conducted research to provide improved understanding of the effects of various parameters and effects on ground motions that are used to constrain models; and (c) developed improved statistical methods to develop ground motion relationships including uncertainty quantification. The models have benefited greatly from a large amount of new strong motion data from large earthquakes (**M** > 7) at close distances (< 25 km). Data include records from the 1999 **M** 7.6 Chi Chi, Taiwan, 1999 **M** 7.4 Kocaeli, Turkey, and 2002 **M** 7.9 Denali, Alaska earthquakes. Review of the NGA relationships indicate that, in general, ground motions are significantly reduced particularly for very large magnitudes (**M** ≥ 7.5) compared to current relationships.

The models by Chiou and Youngs (2008), Campbell and Bozorgnia (2008), Abrahamson and Silva (2008), and Boore and Atkinson (2008) were used in the PSHA and DSHA. The models were weighted equally in the hazard analyses.

Other NGA input parameters include $Z_{1.0}$, the depth of a V_S of 1.0 km/sec, and $Z_{2.5}$, the depth to a V_S of 2.5 km/sec. Both parameters were used by some of the developers as proxies for basin effects. $Z_{1.0}$ is used by Chiou and Youngs (2008) and Abrahamson and Silva (2008) and $Z_{2.5}$ is only used in one model, Campbell and Bozorgnia (2008). Due to the lack of site-specific data, the default values of $Z_{1.0}$ and $Z_{2.5}$, based on the V_S30 from equations provided by the developers, were used in the PSHA. Other parameters such as depth to the top of rupture (zero for all faults that intersect the surface unless specified otherwise), dip angle, rupture width, and aspect ratio were specified for each fault or calculated within the PSHA code.

The hazard results for ground motions are described below and shown in Figures 20 to 63. For the PVO and Far West sites, the results are for a V_S30 of 1200 m/sec. For the Near West site, the results are for a V_S30 of 400 m/sec; the results for 500 and 600 m/sec are very similar. The embankments are the most critical elements of the planned operations and they have natural periods between 0.7 and 2 sec (H. Plewes, Klohn Crippen Berger, personal communication, January 2013).

5.1 PSHA RESULTS

The results of the PSHA for the four sites are presented in terms of ground motion as a function of annual exceedance probability. The annual exceedance probability is the reciprocal of the average return period. Figures 20 to 23 show the mean, median (50th percentile), 5th, 15th, 85th, and 95th percentile hazard curves for PGA at the four sites. The range of uncertainty between the 5th and 95th percentile fractiles is a factor of four at a return period of 5,000 years. These fractiles indicate the range of epistemic uncertainty about the mean hazard. The 1.0 sec horizontal spectral acceleration (Sa) hazard is shown on Figures 24 to 27. At the return periods of 100, 450, 5,000, and 10,000 years, the mean spectral values are listed in Table 3. The hazard can be characterized as low to moderate even at a long return period of 10,000 years.

The contributions of the various seismic sources to the mean PGA and 1.0 sec Sa hazard are shown on Figures 28 to 35. At PGA, the contribution from the background earthquakes in the combined southern Basin and Range/Transition Zone Province dominates the hazard; the distant San Andreas contributes more than the local faults at all return periods (Figures 28 to 31). At 1.0 sec Sa, the San Andreas fault controls the hazard, with the San Jacinto fault and the background earthquakes contributing more than the other faults in southern California and the local faults. (Figures 32 to 35). Although quite distant, the San Andreas fault controls the long-period hazard at the site due to the absence of any nearby active faults with high slip rates and the ability of the fault to generate large earthquakes (**M** ~8) at short recurrence intervals of hundreds of years.

We deaggregated the PGA and 1.0 sec Sa hazard by magnitude and distance bins. Figures 36 to 51 illustrate the contributions by events for return periods of 100 and 5,000 years. At PGA, for the 100-year return period, the contributions from the San Andreas and San Jacinto faults in southern California and the local background earthquakes are apparent in the bimodal peaks centered at **M** 5.5 at 50 km and **M** 7.5 at 400 km, respectively; the contribution from the local earthquakes is dominant (Figures 36 to 39). For the 5,000 year return period, the contribution is only from the background earthquakes from **M** 5 to **M** 7 at 0 to 75 km (Figures 40 to 43). At 1.0 sec Sa, for the 100-year return period there is a bimodal distribution, though the contribution from the distant southern California faults dominate, and the contribution from the nearby crustal sources is relatively small (Figures 44 to 47). For the 5,000-year return period, the contributions from the faults in southern California and the local background earthquakes are apparent in the bimodal peaks centered at **M** 6.25 at 25 km and **M** 8 at 400 km, respectively; the contribution from the local earthquakes is somewhat larger (Figures 48 to 51).

Figures 52 to 59 illustrate the sensitivity of the mean PGA and 1.0 sec horizontal Sa hazard to the choice of ground motion models. Each hazard curve is labeled with one of the models calculated using only that model. At PGA, for return periods less than about 500 years, Abrahamson and Silva (2008) gives the highest hazard (Figures 52 to 55). At all return periods, the 1.0 sec Sa hazard is significantly higher than the total mean hazard using the Abrahamson and Silva (2008) model (Figures 56 to 59).

Based on the magnitude and distance bins (Figures 36 to 51), the controlling earthquakes as defined by the modal magnitude M* and modal distance D* can be calculated. Epsilon is the difference between the logarithm of the ground motion amplitude and the modal logarithm of ground motion (for that M and R) measured in units of standard deviation (σ). Table 4 lists the M*, D*, and ε* for the four return periods (100, 450, 5,000, and 10,000 years) and for PGA and 1.0 sec horizontal Sa.

UHS for the four return periods are shown for the four sites on Figures 60 to 63. A UHS depicts the ground motions at all spectral periods at the same return period. The UHS for Near West at a V_S30 of 400 m/sec envelopes the UHS for 500 and 600 m/sec. Thus to capture the uncertainty in V_S30 and the random variability beneath the site, the enveloped spectra are used in future seismic safety evaluations of the site.

5.2 DSHA RESULTS

The most significant seismic source to the sites in a deterministic sense is the Sugarloaf fault. The maximum event that was modeled in the DSHA is a **M** 6.6 on the Sugarloaf fault at a rupture distance of 48.6 km from the Near West site, 54.6 km from Far West 1, 56.5 km from Far West 2, and 54.8 km from the PVO site. Figure 64 shows the median and 84th percentile 5%-damped horizontal acceleration response spectra. The same NGA models used in the PSHA were used in the DSHA. A V_S30 of 1200 m/sec was used for all sites except for Near West, for which a V_S30 of 400 m/sec was used.

Figure 65 shows a comparison of the horizontal deterministic spectra with UHS for a range of return periods for PVO. The 84th percentile spectrum has an equivalent return period of significantly less than 5,000 years.

5.3 COMPARISON WITH NATIONAL SEISMIC HAZARD MAPS

In the 2008 version of the U.S. Geological Survey's National Hazard Maps, which are the basis for the U.S. building code, the International Building Code, Petersen *et al.* (2008) have estimated probabilistic ground motions for the U.S. for the annual exceedance frequency of 2% in 50 years (2,475-year return period). The 2,475-year return period PGA values for a firm rock (NEHRP B/C; 760 m/sec) site condition at the PVO, Far West 1, Far West 2 and Near West sites are 0.13 g, 0.11 g, 0.12 g and 0.12 g, respectively. Our site-specific values for a 2,475-year return period using a V_S30 of 1200 m/sec are significantly lower at 0.07 g, 0.05 g and 0.05 g for the PVO, Far West 1 and Far West 2 sites, respectively (Table 3). Our site-specific value for a 2,475-year return period using a V_S30 of 400 m/sec for Near West is also significantly lower at 0.08 g (Table 3). The difference between our site-specific values and the National Hazard Maps can be partly attributed to our higher V_S30 at least for the hard rock sites. It should also be noted that the hazard from background earthquakes is distributed more widely in the National Hazard Maps due to their use of a large spatial window of 50 km in the Gaussian smoothing (Section 4.1.2).

The Far West 1 site is located on alluvium (Qal) and Quaternary and Tertiary basaltic fill deposits to a depth of 170 m (Figure 66). Beneath these deposits is hard rock, i.e., basalt. We performed a site-specific site response analysis to account for the expected site effects on ground motions at the site. Traditionally in the estimation of site-specific probabilistic ground motions for a soil site, a rock ground motion is calculated and modified by deterministic site response analyses derived for the soil column to arrive at the ground motions at the soil surface. In doing so, the annual exceedance probability of that soil motion is generally unknown, varies with period, and may be of a higher probability than the control (rock) motion. If a risk analysis is desired, the surface motions must be hazard consistent, i.e., the annual exceedance probability of the soil ground motion should be the same as the rock ground motion. In NUREG/CR-6728 (McGuire *et al.*, 2001), several site response approaches are recommended to produce soil motions consistent with the rock outcrop hazard. The approaches also incorporate the aleatory variabilities in the soil properties into the soil motions. McGuire *et al.* (2001) identified four basic approaches for determining the ground motions at a soil site. The approaches range from a PSHA using ground motion prediction models for the specific site (or location) of interest (Approach 4) to scaling the rock motion on the basis of a site response analysis using a broadband input motion (Approach 1). Conceptually, Approach 4 is the ideal approach and other approaches are approximations to it.

To compute the ground motions for Far West 1, we implemented Approach 3 as it is called (McGuire *et al.*, 2001; Bazzurro and Cornell, 2004). Approach 3 is a fully probabilistic analysis procedure which moves the site response, in an approximate way, into the hazard integral. The approach is described by Bazzurro and Cornell (2004) and NUREG/CR-6769 (McGuire *et al.*, 2002). In this approach, the hazard at the soil surface is computed by integrating the site-specific hazard curve at generic rock or soil level with the probability distribution of the amplification factors (Lee *et al.*, 1998; 1999). The site-specific amplification, relative to hard rock, is characterized by a suite of frequency-dependent amplification factors that can account for nonlinearity in soil response. Approach 3 involves approximations to the hazard integration using suites of transfer functions, which result in complete hazard curves at the ground surface for specific ground motion parameters (e.g., spectral accelerations) and a range of frequencies.

The basis for Approach 3 is a modification of the standard PSHA integration:

$$P[A_S>z] = \iiint P\left[AF > \frac{z}{a}\middle| m,r,a\right] f_{M,R|A}\ (m,r;a) f_A(a)\,dm\,dr\,da \qquad (6\text{-}1)$$

where A_S is the random ground-motion amplitude on soil at a certain natural frequency; z is a specific level of A_S; m is earthquake magnitude; r is distance; a is an amplitude level of the random rock ground motion, A, at the same frequency as A_S; $f_A(a)$ is derived from the rock hazard curve for this same frequency (namely it is the absolute value of its derivative); and $f_{M,R|A}$ is the deaggregated hazard (i.e., the joint distribution of M and R, given that the rock amplitude is level a). AF is an amplification factor defined as:

$$AF = A_S/a \qquad (6\text{-}2)$$

where AF is a random variable with a distribution that can be a function of m, r, and a. To accommodate epistemic uncertainties in site dynamic material properties, multiple suites of AF may be used and the resulting hazard curves combined with weights to properly reflect mean hazard and fractiles.

Soil response is controlled primarily by the level of rock motion and m, so Equation 6-1 can be approximated by:

$$P[A_S>z] = \int\int P[AF > \frac{z}{a}(m,a)] f_{M|A}(m;a) f_A(a) dm da \qquad (6\text{-}3)$$

where r is dropped because it has an insignificant effect in most applications (McGuire *et al.*, 2001). To implement Equation 6-3, only the conditional magnitude distribution for relevant amplitudes of a is needed. $f_{M|A}(m;a)$ can be represented (with successively less accuracy) by a continuous function, with three discrete values or with a single point, (e.g., $m^1(a)$, the mean magnitude given a). With the latter, Equation 6-3 can be simplified to:

$$P[A>z] = \int\int P[AF > \frac{z}{a} | a, m^1(a)] f_A(a) da \qquad (6\text{-}4)$$

where, $f_{M|A}(m;a)$ has been replaced with m^1 derived from deaggregation. With this equation, one can integrate over the rock acceleration, a, to calculate $P[A_S>z]$ for a range of soil amplitudes, z.

6.1 IMPLEMENTATION OF APPROACH 3

In Approach 3, the following steps were performed:

- Randomization of base case site-dynamic material properties to produce a suite of velocity profiles as well as G/Gmax and hysteretic damping curves that incorporate site randomness.
- Computation of transfer functions (hereafter termed amplification factors) as characterized by a mean and distribution for each set of base case site properties using the RVT-based equivalent-linear site response model.
- Full integration of the fractile and mean hazard curves for the generic site condition in this case hard rock and amplification factors to arrive at a distribution of site-specific hazard curves.

Specifically, the suites of rock hazard curves are first combined into a single suite and site-specific amplification factors applied using Approach 3. Combining the empirical hazard curves, rather than applying Approach 3 to each suite independently, results in the same mean hazard—the desired product—but does not properly preserve the full epistemic variability in the fractile estimates. As a result, the range in probability reflected in the resulting fractiles is likely somewhat underestimated. Although the fractiles are likely not significantly in error since the differences in hazard fractiles between the empirical relations are not large, the site-specific hazard fractiles should not be used for hazard or risk assessment.

Approach 3 is implemented through a number of computer programs, which are described below. The computation of the amplification factors is the first phase of the calculations and is similar to what is done in other site-response approaches.

6.1.1 RVT-Based Equivalent-Linear Site Response Approach

To compute the ground motions at the ground surface, the results of the PSHA are modified using a site-response model. The conventional site response approach in quantifying the effects of soil and other unconsolidated sediments on strong ground motions involves the use of time histories compatible with the specified outcrop response spectra to serve as control (input) motions. The control motions are then used to drive a nonlinear computational formulation to transmit the motions through the profile.

The computational formulation that has been most widely employed to evaluate 1D site response assumes vertically-propagating plane S-waves. Departures of soil response from a linear constitutive relation are treated in an approximate manner through the use of the equivalent-linear formulation. The equivalent-linear formulation, in its present form, was introduced by Idriss and Seed (1968). A stepwise analysis approach was formalized into a 1D, vertically propagating S-wave code called SHAKE (Schnabel *et al*., 1972). Subsequently, this code has become the most widely used and validated analysis package for 1D site response calculations.

The computational scheme employed to compute the amplification factors in this study uses an alternative approach employing random vibration theory (RVT) (Silva and Lee, 1987). In this approach, as embodied in the computer program RASCALS, the control motion power spectrum is propagated through the 1D soil profile using the plane-wave propagators of Silva (1976). The power spectrum is derived from the uniform hazard spectrum by spectral matching assuming the controlling earthquake. In this formulation only SH waves are considered. Arbitrary angles of incidence may be specified. In this case, vertical incidence was assumed.

Inputs to RASCALS are as follows:

- Location of input and output motions within the site profile.
- Input (control) motions characterized by earthquake power spectra.
- Incidence angles of input motion.
- A representation of the rock and soil at the site, consisting of homogeneous layers with specified thickness, seismic velocity, and density.
- A representation of the dynamic material properties of the rock and soil at the site, consisting of strain-dependent shear modulus and damping curves for each layer.

Control motions (power spectral density) must be calculated for input into the site response analysis that are representative of the earthquake magnitude and distance dominating the hazard at the desired rate of exceedance. The basis for the control motions are the magnitude and distances specified by the hazard deaggregation. Control motions may be specified by a response spectrum, which is then followed by an RVT spectral match to generate a power spectral density. This is then input to the site column as an outcrop motion at the control point. Evaluation of site-response using the equivalent-linear site response model is based on convolution of appropriate control motions through randomized velocity profiles combined with randomized G/Gmax and hysteretic damping curves. The randomized profiles and curves are generated from base case velocity and nonlinear dynamic properties. The convolutions yield transfer functions for 5%-damped response spectra and peak particle velocity.

For the computation of spectra for a site with uncertain properties and exhibiting a degree of lateral variability, a best-estimate (mean) base case velocity profile is developed and used to simulate a number of V_S profiles. Additionally, strain-dependent shear modulus and hysteretic damping are also randomized about best-estimate base cases. A large number of simulations can be required to achieve stable statistics on the response. To achieve statistical stability, 30 randomizations were produced using the velocity correlation models for each base case velocity profile and each base case nonlinear dynamic property curve. In order to randomly vary the V_S profile, a profile randomization scheme has been developed which varies both layer velocity and thickness. The randomization is based on a correlation model developed from an analysis of variance on about 500 measured V_S velocity profiles (EPRI, 1993; Silva *et al.*, 1996). Profile depth (depth to competent material) is also varied on a site specific basis using a uniform distribution. The depth range is generally selected to reflect expected variability over the structural foundation as well as uncertainty in the estimation of depth to competent material.

6.1.2 Inputs and Analysis

Representative V_S profiles of the site and shear modulus (G/Gmax) reduction and damping curves are required for the analysis. To perform the site response analysis, the PSHA calculations were rerun for a V_S30 of 270 m/sec. The NGA models have a sounder basis at around this V_S30 value as compared to hard rock because most of the PEER strong motion database is for soil. A generic V_S profile with a V_S30 of 270 m/sec is used in the site response analysis in addition to the site-specific profile. The shallow V_S profile described in Section 4.2 is the base case profile for the Far West 1 site (Figure 66). The top 750 m of the site-specific profile is appended to a standard western U.S. velocity profile at a V_S of 1,800 m/sec. Thus the amplification factors are relative to a generic soil profile and not rock, which is the traditional approach used in site response analysis. Thirty randomized V_S profiles were generated for each of three site-specific base case V_S profiles using a soil correlation model developed by Silva *et al.* (1996). In addition to the best estimate profile, upper and lower base case profiles were calculated using a factor of 1.57 times the mean profile and divided by 1.57, respectively. This factor of 1.57 is used in the site response analysis for nuclear power plants (W. Silva, written communication, 2012).

Associated with each of the 30 randomized profiles was also a set of randomized dynamic material property curves. For the dynamic material properties, the EPRI (1993) and Peninsular Range curves for cohesionless soils (Silva *et al.*, 1996) were used to approximate a nonlinear response over the top 152 m (500 ft), with linear response below (Silva *et al.*, 1996). To accommodate the large uncertainty in nonlinear dynamic material properties, two sets of curves were used in the site-specific analyses. A subset of the EPRI (1993) curves was used for each profile to account for the possibility that the site may behave more linearly. The second set, termed Peninsular Range curves, use the EPRI (1993) 51 to 120 ft curves for 0 to 50 ft and the 501 to 1,000 ft curves for deeper materials and reflect much more linear response than the EPRI curves. The two sets of curves were given equal weights and are considered to cover the range in nonlinear dynamic material properties.

Based on the RASCALS runs for the 30 V_S profiles for each base case profile, a probability distribution of amplification factors was calculated. Input control motions are computed using RASCALS for each set of 30 V_S profiles and dynamic property curves. RASCALS is used for horizontal spectra using normally-incident and inclined SH-waves. For each control motion, mean and standard deviation are computed from the 30 response spectra (from 30 randomized profiles). Thirty realizations result in stable estimates. The mean response spectrum from the 30 convolutions is divided by the mean (log) spectrum for hard rock spectrum to produce the amplification factors. The amplification factors include the effects of the inherent aleatory variability (randomness) of the site properties about each base case and any possible effects of magnitude of the control motions. Epistemic variability (uncertainty) is captured in consideration of alternate base case (mean) profiles and properties.

RASCALS was used to generate control motions and acceleration power response spectra for two earthquakes, **M** 5.5 and 7.5, which are approximately the controlling earthquakes at the site at short- and long-period ground motions (Table 4). The events were placed at a suite of distances to produce expected median rock peak accelerations of 0.01, 0.05, 0.10, 0.20, 0.30, 0.40, 0.50, 0.75, 1.00, 1.25 and 1.50 g. The amplification factors (the ratios of the response spectra at the top of the site-specific profile to the generic soil profile [270 m/sec] profile) are a function of the reference peak acceleration (or SA), spectral frequency, and nonlinear soil response.

6.2 SITE-SPECIFIC HORIZONTAL RESULTS

The hazard curves derived from the PSHA and the amplification factors were multiplied to arrive at site-specific amplified hazard curves. The hazard curves calculated using the amplification factors from the **M** 5.5 and 7.5 earthquakes were weighted based on their contributions to the hazard at each spectral frequency. The uncertainty or epistemic variability in seismic hazard is typically represented by a set of weighted hazard curves. Using these sets of curves as discrete probability distributions, they can be sorted by the frequency of exceedance at each ground-motion level and summed into a cumulative probability mass function. When the cumulative probability mass function for a particular exceedance frequency equals or exceeds fractile y, then the exceedance frequency represents the y^{th} fractile. The weighted-mean hazard curve is the weighted average of the exceedance frequency values. This approach is a standard practice in PSHA.

Figure 67 shows the ground surface spectra for several return periods resulting from the site response analysis. Also shown are the input hard rock UHS for the same return periods. The amplification is broadband in nature and is most significant at the long return periods (Figure 67). A factor of 2 to 2½ appears to be the largest amplification.

The following describes the CMS approach and CMS calculated for the four sites.

7.1 APPROACH

The UHS represents the spectral accelerations at each period based on the rates of occurrence of all nearby sources, the ground motion prediction models and the uncertainties in these models. It is a broader spectrum than is expected for any single event. This uniform hazard can be represented by a suite of spectra that individually more closely represent the spectral shape of expected events contributing to the UHS. At a given period, a spectrum can be computed based on the deaggregated magnitude, distance and epsilon at that period. Depending on the epsilon required to match the spectrum to the UHS, the expected shape of this spectrum is not necessarily the median predicted spectral shape. Given the epsilon at a target period, epsilon at all other periods can be determined using a correlation function. Thus, a CMS represents a more realistic shape of an event likely to cause the target spectral acceleration at the target period.

The CMS approach was developed for the purpose of using the results of a PSHA to develop input to the seismic evaluation of structures (i.e., performing dynamic response calculations). The approach provides a method for defining the ground motion response spectrum input to a structural response analysis, where the estimated response is linked to the PSHA result (the hazard curve for a spectral acceleration at a given period), and where the estimate of structural response is mean-centered (i.e., non-conservative). The CMS response spectrum is associated with a Sa level for a single-structure period or narrow period range (e.g. the fundamental period of the structure to be analyzed), at a specified annual frequency of exceedance or return period. By linking a response spectrum suited to input to structure response analyses to the PSHA results, it is possible to make statements about the likelihood of observing levels of structural response and potential damage.

The procedure to implement the CMS approach is described in Baker (2011) and is summarized here. The steps in the process as defined by Baker (2011) are:

Step 1: Determine the Target Sa at a Given Period, and the Associated M, R and ε

For a specified annual frequency of exceedance (AFE) or return period, determine the target Sa from the mean hazard curve for Sa for the fundamental period of the structure to be analyzed. This period is denoted *T**. For this ground motion, obtain the mean magnitude (*M)*, distance (R), and ε from the PSHA deaggregation results. Depending upon the response characteristics of the structure or structures to be analyzed, CMS may need to be developed for several values of *T**.

Step 2: Compute the Mean and Standard Deviation of the Response Spectrum, Given M and R

For the mean M and R determined in Step 1, compute the mean and standard deviation of logarithmic spectral acceleration at all periods for a the mean magnitude and distance. These are provided by standard ground motion prediction (attenuation) models. The predicted mean and standard deviation, given magnitude, distance, period, etc., are denoted $\overline{\ln Sa}(M,R,T)$ and $\sigma_{\ln Sa}(T)$, respectively. The mean and standard deviation of the log spectral acceleration can be computed using the ground motion prediction models that were used in the PSHA itself. Since multiple ground motion models were used in the PSHA, a weighted estimate of the mean log Sa and the standard deviation can be used. Alternatively, a CMS can be developed for each ground motion prediction model and a weighted average taken to produce the final CMS.

Step 3: Compute ε at Other Periods, Given ε(T*)

Compute the "conditional mean" ε at other periods. The conditional mean ε at ε (T^*) was determined in Step 1. The conditional mean at other periods, T_i, is determined by,

$$\mu_{\varepsilon(Ti)|\varepsilon(T*)} \tag{7-1}$$

where $\rho(T_i,T^*)$ is the correlation coefficient between ε for periods T_i and T^*. This correlation coefficient, which is applicable to periods in the range 0.05 – 5 sec, is (Baker and Cornell 2006),

$$\rho(T_{\min},T_{\max}) = 1-\cos\left[\frac{\Pi}{2}-\left(0.359+0.163 I_{(T_{\min}<0.189)}\ln\left(\frac{T_{\min}}{0.189}\right)\ln\left(\frac{T_{\min}}{T_{\max}}\right)\right)\right] \tag{7-2}$$

where $I_{(T_{\min}<0.189)}$ is an indicator function equal to 1 if $T_{\min} < 0.189$ and 0 otherwise. $T_{\min}$ and $T_{\max}$ are the smaller and larger of the periods of interest, respectively.

Step 4: Compute the Conditional Mean Spectrum

The CMS is computed using the estimated log mean and standard deviation from Step 2 and the conditional mean $\varepsilon(T_i)$ values determined in Step 3. The CMS is estimated according to:

$$\mu_{\ln S_a(T_i)|\ln(S_a(T^*)} = \mu_{\ln S_a}(M,R,T_i) + \rho(T_i,T^*)\varepsilon(T^*)\sigma_{\ln S_a}(T_i) \tag{7-3}$$

The CMS is,

$$S_{a,CMS}(T) = \exp(\mu_{\ln(S_a(T_i)|\ln(S_a(T^*)}) \tag{7-4}$$

7.2 CMS

Short-period (0.20 sec) and long-period (1.0 sec) CMS have been computed for 5,000-year return period for the four sites (Figures 68 to 71). As discussed in Section 5.1, the hazard at the four sites at a 5,000-year return period is controlled by **M** 5.4 to 5.5 events at 1 to 2 km at short-periods and **M** 6.9 to 7.7 at 228 to 373 km at long-periods (Table 4). The 5,000-year return period CMS are tabulated in Table 6.

The hazard is very bimodal. Examination of the CMS shows how broad-banded the UHS is compared to more realistically shaped CMS (Figures 68 to 71).

Based on the BADCT Guidance Manual, Appendix E “Earthquake design parameters are usually selected based on professional judgment considering both probabilistic and deterministic analysis. Recent trends in dam safety have resulted in a probabilistic approach for defining seismic design ground motions. The U.S. Bureau of Reclamation uses a PSHA approach and return periods generally ranging from 10,000 to 50,000 years. The U.S. Committee on Large Dams (USCOLD) (now U.S. Society of Dams) and the International Committee on Large Dams (ICOLD) state that when using a probabilistic approach, an annual probability of 1 in 3,000 to 1 in 10,000 should be used (return periods of 3,000 to 10,000 years). The Federal Energy Regulatory Commission is currently adopting a risk-informed approach to dam safety, which requires the use of PSHA.

The difficulty with using DSHA for the basis for seismic design particularly in a region like southern Arizona is that the hazard is usually controlled by background earthquakes whose hazard cannot be explicitly addressed in a DSHA. Background earthquakes can occur anywhere in the site region at some probability and since DSHA does not consider the probability of occurrence, it cannot be used to compute the hazard at a site unless some arbitrary distance is selected. Hence we use PSHA to address the hazard from background earthquakes and as the basis for our recommendation for design earthquake ground motions.

Based on considerations of the downstream risk and consequences of failure of any of the potential tailings embankments in the four proposed locations, we recommend that the ground motions associated with a return period of 5,000 years be adopted for use in seismic design analysis. The recommended 5,000-year return period design UHS and CMS are shown on Figures 68 to 71 and tabulated in Tables 3 and 6. Figure 72 compares the recommended Design CMS for the four sites.

We developed 7 horizontal-component time histories for the design earthquake return period of 5,000 years. Because the response spectrum of a time history has peaks and valleys that deviate from the design response spectrum (target spectrum), it is necessary to modify the motion to improve its response spectrum compatibility. The procedure proposed by Lilhanand and Tseng (1988), as modified by Norm Abrahamson (written communication, 1999), was used to develop the acceleration time histories through spectral matching to the target (seed) spectrum. This time-domain procedure has been shown to be superior to previous frequency-domain approaches because the adjustments to the time history are only done at the time at which the spectral response occurs resulting in only localized perturbations on both the time history and the spectra (Lilhanand and Tseng, 1988).

To match the target spectrum, seed time histories should be from events of similar magnitude, distance (for duration), to a lesser extent site condition, and most importantly, spectral shape as the earthquake dominating the spectrum. The seed time-histories selected are based on the controlling earthquakes (Table 4). Table 5 lists the seed time histories and they are shown on Figures 73 to 75. Because of the bimodal nature of the hazard at the RMC sites, we developed two histories for a spectral period of 0.2 sec for use in the analysis of any short-period structures and 5 time histories for the embankments that are long period (0.7 to 2 sec). The CMS at 0.2 and 1.0 sec were used as the target spectra.

The spectral matches and the resulting time histories are shown on Figures 76 to 131 with the response spectra calculated from the matched time histories. Shown with each set of time histories is the normalized Arias intensity or Husid plot, which provides an appropriate duration measure independent of the absolute amplitude level of the acceleration time history.

Abrahamson, N.A. and Silva, W.J., 1997, Empirical response spectral attenuation relations for shallow crustal earthquakes: Seismological Research Letters, v. 68, p. 94-127.

Abrahamson, N.A. and Silva, W.J., 2008, Summary of the Abrahamson and Silva NGA ground motion relations. Earthquake Spectra, v. 24, p. 67-97.

Akciz, S.O., Grant Ludwig, L., Arrowsmith, J R., and Zielke, O., 2010, Century-long average time intervals between earthquake ruptures of the San Andreas fault in the Carrizo Plain, California: Geology, v. 38, p. 787-790.

Aki, K., 1983, Seismological evidence in support of the existence of "Characteristic Earthquakes": Earthquake Notes, v. 54, p. 60-61.

Anderson, J.G., 1979, Estimating the seismicity from geological structure for seismic risk studies: Bulletin of the Seismological Society of America, v. 69, p. 135-158.

Anderson, L.W., Piety, L.A., and Hansen, R.A., 1986, Seismotectonic investigations, Stewart Mountain Dam, Salt River Project, Arizona: U. S. Bureau of Reclamation Seismotectonic Report 86-2, 41 p.

Baker, J.W., 2011, The conditional mean spectrum: A tool for ground motion selection," American Society of Civil Engineers, Journal of Structural Engineering, v. 137, p. 322-331.

Baker J.W. and Cornell C.A., 2006, Correlation of response spectral values for multi-component ground motions: Bulletin of the Seismological Society of America, v. 96, p. 215-227.

Bausch, D. and Brumbaugh, D.A., 1997, Relocation study of early Arizona earthquakes: Events of 1906, 1910, and 1912: unpublished report prepared for Arizona Division of Emergency Management, Earthquake Program, 65 p. + Appendices.

Bazzurro, P. and Cornell, C.A., 2004, Nonlinear soil-site effects in probabilistic seismic-hazard analysis: Bulletin of the Seismological Society of America, v. 94, p. 2110-2123.

Boore, D.M., and Atkinson, G.M., 2008, Ground motion predictive equations for the average horizontal component of PGA, PGV, and 5% damped PSA at spectral periods between 0.01s to 10.0s: Earthquake Spectra, v. 24, p. 99-138.

Brumbaugh, D. S., 1987, A tectonic boundary for the Southern Colorado Plateau: Tectonophysics, v. 136, p. 125-136.

Campbell, K.W. and Bozorgnia, Y., 2008, NGA ground motion model for the geometric mean horizontal component of PGA, PGV, PGD, and 5% damped linear elastic response spectra for periods ranging from 0.01 to 10s: Earthquake Spectra, v. 24, p. 139-171.

Cao, T.C., Bryant, W.A., Rowshandel, B., Branum, D., and Wills, C.J., 2003, The revised 2002 California probabilistic seismic hazard maps, June 2003: California Geological Survey website.

Chiou, B.S.J. and Youngs, R.R., 2008, An NGA model for the average horizontal component of peak ground motion and response spectra: Earthquake Spectra, v. 24, p. 173-215.

Cornell, C.A., 1968, Engineering seismic risk analysis: Bulletin of the Seismological Society of America, v. 58, p. 1583-1606.

dePolo, C.M., 1994, The maximum background earthquake for the Basin and Range Province, western North America: Bulletin of the Seismological Society of America, v. 84, p. 466-472.

DuBois, S.M., Smith, A.W., Nye, N.K., and Nowak, T.A., 1982, Arizona earthquakes, 1776-1980: Arizona Bureau of Geology and Mineral Technology Bulletin, v. 192, 456 p.

Electric Power Research Institute (EPRI), 1993, Guidelines for determining design basic ground motions, v. 1: Method and guidelines for estimating earthquakes ground motion in eastern North America: EPRI Report TR-102293.

Felzer, K.R., 2008, Calculating California seismicity rates, Appendix I in the Uniform California Earthquake Rupture Forecast, version 2: U.S. Geological Survey Open-File Report 2007-1437I.

Ferguson, C.A. and Skotnicki, S.J., 1995, Geology of the Florence Junction and southern portion of the Weavers Needle 7.5' Quadrangles, Pinal County, Arizona: Arizona Geological Survey Open-File Report 95-10, includes 1:24,000 scale geologic map, cross-sections, 27 p.

Frankel, A., 1995, Mapping seismic hazard in the central and eastern United States: Seismological Research Letters, v. 66, p. 8-21.

Fugro National, Inc., 1981, Seismotectonic study, Stewart Mountain Dam, Arizona: Report prepared for Water and Power Services, U.S. Bureau of Reclamation, Denver, Colorado, 39 p.

Grant, L.B. and Donnellan, A., 1994, 1855 and 1991 surveys of the San Andreas Fault; implications for fault mechanics: Bulletin of the Seismological Society of America, v. 84, p. 241-246.

Grant, L. and Sieh, K., 1993, Stratigraphic evidence for 7 meters of dextral slip on the San Andreas fault during the great 1857 earthquake in the Carrizo Plain: Bulletin of the Seismological Society, v 83, 619-635.

Grant, L.B. and Sieh, K., 1994, Paleoseismic evidence of clustered earthquakes on the San Andreas fault in the Carrizo Plain, CA.: Journal of Geophysical Research, v. 99, p. 6819-6842.

Grant Ludwig, L. and Akciz, S., 2012, Rupture History of the San Andreas Fault in the Carrizo Plain prior to 1300 A.D., Final Technical Report, U.S. Geological Survey National Earthquake Hazard Reduction Program Award No. G10AP00073.

Grant Ludwig, L., Akciz, S.O., Noriega, G. R., Zielka, O., and Arrowsmith, J R., 2010. Climate-modulated channel incision and rupture history of the San Andreas fault in the Carrizo Plain: Science, v. 327, p. 1117-111.

Hanks, T.C. and Bakun, W.H., 2002, A bilinear source-caling model for M-log A observations of continental earthquakes: Bulletin of the Seismological Society of America, v. 92, p. 1841-1846.

Hanks, T.C. and Kanamori, H. 1979, A moment magnitude scale: Journal of Geophysical Research, v. 84, p. 2348-2350.

Huckleberry, G., 1993, Surficial Geology of the Supersition Mountain Piedmont Area, Northern Pinal and Eastern Maricopa Counties, Arizona: OFR-93-15, scale 1:24,000, 6 sheets, 33 p.

Idriss, I.M. and Seed, H.B., 1968, Seismic response of horizontal soil layers: Journal of the Soil Mechanics and Foundations Division, v. 94, p. 1003-1031.

Keefer, D.I. and Bodily, S.E., 1983, Three-point approximations for continuous random variables: Management Science, v. 26, p. 595-609.

Klohn Crippen Berger, 2012 Far West Tailings Management Site, Geotechnical Site Investigation Data Report: draft report prepared for Resolution Copper Mining.

Lee, R., Maryak, M.E., and Kimball, J., 1999, A methodology to estimate site-specific seismic hazard for critical facilities on soil or soft-rock sites (abs.): Seismological Research Letters, v. 70, p. 230.

Lee, R., Silva, W.J., and Cornell, C.A., 1998, Alternatives in evaluating soil- and rock-site seismic hazard (abs.): Seismological Research Letters, v. 69, p. 81.

Lienkaemper, J.J., 2001, 1857 slip on the San Andreas fault southeast of Cholame, California: Bulletin of the Seismological Society of America, v. 91, p. 1659-1672.

Lilhanand, K. and Tseng, W.S., 1988, Development and application of realistic earthquake time histories compatible with multiple-damping design spectra: Proceeding of the 9th World Conference on Earthquake Engineering, Tokyo-Kyoto, Japan.

Lindvall, S.C., Rockwell, T.K., Dawson, T.E., Helms, J.G., and Bowman, K.W., 2002, Evidence for two surface ruptures in the past 500 years on the San Andreas fault at Frazier Mountain, California: Bulletin of the Seismological Society of America, v. 92, p. 2689-2703.

Liu, J., Klinger, K., Sieh, K., and Rubin, C., 2004, Six similar sequential ruptures of the San Andreas fault, Carrizo Plain, California: Geology, v. 32, p. 649-652.

Lockridge, J.S., Fouch, M.J., Arrowsmith, J.R., and Linkimer, L., 2012, Analysis of seismic activity near Theodore Roosevelt Dam, Arizona, during the Occupation of the EarthScope/USArray Transportable Array: Bulletin of the Seismological Society of America, v. 83, p. 1014-1022.

Lund, W.R., 2012, Basin and Range Province Earthquake Working Group II Recommendations to the U.S. Geological Survey National Seismic Hazard Mapping Program for the 2014 Update of the National Seismic Hazard Maps: Utah Geological Survey Open-File Report 591, 17 p.

Machette, M.N., 1998, Contrasts between short- and long-term records of seismicity in the Rio Grande rift – Important implications for seismic hazard assessments in areas of slow extension, *in* W.R. Lund (ed.), Western States Seismic Policy Council Proceedings Volume, Basin and Range Province Seismic Hazards Summit, Utah Geological Survey Miscellaneous Publication 98-2, p. 84-95.

Mack, G.H., Seager, W.R., and Leeder, M.R., 2003, Synclinal-horst basins: examples from the southern Rio Grande rift and southern transition zone of southwestern New Mexico: Basin Research, v. 15, p. 365-377.

McDonald, G.N. and Ashland, F.X., 2008, Earthquake site conditions in the Wasatch Front urban corridor, Utah: Utah Geological Special Study 125, 41 p., 1 plate, scale 1:150,000.

McGuire, R.K., Silva, W.J., and Costantino, C.J., 2001, Technical basis for revision of regulatory guidance on design ground motions: Hazard- and risk-consistent ground motion spectra guidelines: U.S. Nuclear Regulatory Commission NUREG/CR-6728.

McGuire, R.K., Silva, W.J., and Costantino, C.J., 2002, Technical basis for revision of regulatory Guidance on design ground motions, report prepared for U.S. Nuclear Regulatory Commission.

McQuarrie, N., and Wernicke, B.P., 2005, An animated tectonic reconstruction of southwestern North America since 36 Ma: Geosphere, v. 1, p. 147–172.

Menges, C.M. and McFadden, L.D., 1981, Evidence for the latest-Miocene to Pliocene transition from Basin-Range tectonic to post-tectonic landscape evolution in southeastern Arizona: Arizona Geological Society Digest, v. 13, p. 151-160.

Menges, C.M. and Pearthree, P.A., 1983, Map of neotectonic (latest Pliocene-Quaternary) deformation in Arizona: Arizona Bureau of Geology Mineral Technology Open-File Report 83-22, 48 p., scale 1:500,000.

Menges, C.M. and Pearthree, P.A., 1989, Late Cenozoic tectonism in Arizona and its impact on regional landscape evolution: *in* Geologic Evolution of Arizona, Arizona Geological Society, Digest No. 17, p. 649–680.

Molnar, P., 1979, Earthquake recurrence intervals and plate tectonics: Bulletin of the Seismological Society of America, v. 69, p. 115-133.

Montgomery and Associates, 2012, Hydrogeologic data submittal, Tailings Prefeasibility Study, Whitford, Silver King and Happy Camp sites, draft technical memorandum.

Morgan, P., and Swanberg, C.A., 1985, on the Cenozoic uplift and tectonic stability of the Colorado Plateau: Journal of Geodynamics, v. 3, p. 39-63.

Pearthree, P.A., 1998, Quaternary fault data and map of Arizona: Arizona Geological Survey Open-File Report 98-24, 122 p.

Pearthree, P.A., McKittrick, M.A., Jackson, G.A., and Demsey, K.A., 1988, Geologic map of Quaternary and upper Tertiary deposits, Tucson 1° x 2° quadrangle, Arizona: Arizona Geological Survey Open-File Report 88-21, scale 1:250,000.

Pearthree, P.A., Menges, C.M., and Mayer, L., 1983, Distribution, recurrence, and possible tectonic implications of late Quaternary faulting in Arizona: Arizona Bureau of Geologic Mineral Technical Open-File Report 83-20, 51 p.

Pearthree, P.A., and Scarborough, R.B., 1984, Reconnaissance analysis of possible Quaternary faulting in central Arizona: Arizona Bureau of Geology and Mineral Technology Open-File Report 85-4, 75 p., scale 1:250,000.

Pearthree, P.A., Vincent, K.R., Brazier, R., Fellows, L.D., and Davis, O.K., 1995, Seismic hazard posed by the Sugarloaf fault, central Arizona: Arizona Geological Survey Open-File Report 95-7, 41, p.

Peirce, H.W., 1984, The Mogollon escarpment: Arizona Bureau of Geology and Mineral Technology Fieldnotes, v. 4, p. 8-11.

Peterson, D.W., 1969, Geologic map of the Superior Quadrangle, Pinal county, Arizona: U.S. Geological Survey Quadrangle Map GQ 818, scale 1:24,000.

Petersen, M.D., Frankel, A.D., Harmsen, S.C., Mueller, C.S., Haller, K.M., Wheeler, R.L., Wesson, R.L., Zeng, Y., Boyd, O.S., Perkins, D.M., Luco, N., Field, E.H., Wills, C.J., and Rukstales, K.S., 2008, Documentation for the 2008 update of the United States National Seismic Hazard Maps: U.S. Geological Survey Open-File Report 2008-1128, 61 p.

Piety, L.A. and Anderson, L.W., 1990, Seismotectonic investigation for Horseshoe and Bartlett Dams, Salt River Project, Arizona: Bureau of Reclamation Seismotectonic Report 90-7, 59 p.

Piety, L.A. and Anderson, L.W., 1991, The Horseshoe fault--Evidence for prehistoric surface-rupturing earthquakes in central Arizona: Arizona Geology, v. 21, no. 3, p. 1, 4-8.

Richard, S.M. and Spencer, J.E., 1998, Compilation Geologic Map of the Ray-Superior area, Central Arizona: Arizona Geological Survey Open-file Report 98-13, 47 p.

Runnerstrom, E.E., Grant, L.B., Arrowsmith, J.R., Rhodes, D.D., and Stone, E.M., 2002, Displacement across the Cholame segment of the San Andreas Fault between 1855 and 1896 from cadastral surveys: Bulletin of the Seismological Society of America: v. 92, p. 2,659-2,669.

Scharer, K.M., Weldon, R.J., Gibson, B.C., and Streig, A.R., 2011, Earthquake ages and displacements, Frazier Mountain paleoseismic site, Abstract T51B-2324 presented at 2011 Fall Meeting, AGU, San Francisco, Calif., 5-9 Dec.

Schnabel, P.B., Lysmer, J. and Seed, H.B., 1972, SHAKE - A computer program for earthquake analysis of horizontally layered sites, Earthquake Engineering Research Center, University of California, Berkeley, Report No. EERC 72-12.

Schwartz, D.P. and Coppersmith, K.J., 1984, Fault behavior and characteristic earthquakes--examples from the Wasatch and San Andreas fault zones: Journal of Geophysical Research, v. 89, p. 5681-5698.

Shenk, J.D., 1990, Economic geology of the White Cliffs diatomite deposit, Mammoth, Arizona: Tucson, University of Arizona, unpublished M.S. thesis, 157 p.

Sieh, K.E., 1978, Slip along the San Andreas fault associated with the great 1857 earthquake: Bulletin of the Seismological Society of America, v. 68, p. 1421-1448.

Sieh, K.E. and Jahns, R.H., 1984, Holocene activity of the San Andreas fault at Wallace Creek, California: Geological Society of America Bulletin, v. 95, p. 883-896.

Silva, W.J., 1976, Body waves in a layered anelastic solid, Bulletin of the Seismological Society of America, v. 66, p. 1539-1554.

Silva, W.J. and Lee, K., 1987, WES RASCAL code for synthesizing earthquake ground motions: State-of-the-art for Assessing Earthquake Hazards in the United States, Report 24: U.S. Army Engineer Waterways Experiment Station Miscellaneous Paper S-73-1, 120 p.

Silva, W.J., Abrahamson, N., Toro, G., and Costantino, C, 1996, Description and Validation of the Stochastic Ground Motion Model. El Cerrito, CA: Pacific Engineering and Analysis.

Sims, J.D., 1994, Stream channel offset and abandonment and a 200-year average recurrence interval of earthquakes on the San Andreas fault at Phelan Creek, Carrizo Plain, California, *in*

Prentice, C.S., Schwartz, D.P., and Yeats, R.S. (eds.), Proceedings of the workshop on paleoseismology: U.S. Geological Survey Open-File Report 94-568, p. 170-172.

Skotnicki, S.J., Leighty, R.S., and Pearthree, P.A., 1997, Geologic map of the Wildcat Hill quadrangle, Maricopa County, Arizona: Arizona Geological Survey Open-File Report 97-2, 17 p., 1 pl., scale 1:24,000.

Spencer, J.E., Richard, S.M., and Pearthree, P.A., 1998, Geologic map of the Mesa 30'x60' quadrangle, east-central Arizona: Arizona Geological Survey Open-File Report 96-23, scale 1:100,000.

Stepp, J.C., 1972, Analysis of completeness of the earthquake sample in the Puget Sound area and its effect on statistical estimates of earthquake hazard: Proceedings of the International Conference on Microzonation, v. 2, 897-910.

Stone, E.M., Grant, L., and Arrowsmith, J.R., 2002, Recent rupture history of the San Andreas Fault southeast of Cholame in the northern Carrizo Plain, California: Bulletin of the Seismological Society of America, v. 92, p. 983-997.

Suter, M., 2008, Structural configuration of the Otates fault (Southern Basin and Range Province) and its rupture in the 3 May 1887 M 7.5 Sonora, Mexico, earthquake: Bulletin of the Seismological Society of America, v. 98, p. 2879-2893.

Suter, M. and Contreras, J., 2002, Active tectonics of northeastern Sonora, Mexico (southern Basin and Range Province) and the 3 May 1887 M_W 7.4 earthquake: Bulletin of the Seismological Society of America, v. 92, p. 581-589.

Thomas, P.A., Wong, I.G., and Abrahamson, N., 2010, Verification of probabilistic seismic hazard analysis software programs: PEER Report 2010/106, Pacific Earthquake Engineering Research Center, College of Engineering, University of California, Berkeley, 173 p.

Toppozada, T.R., Branum, D.M., Reichle, M.S., and Hallstrom, C.L., 2002, San Andreas fault zone, California: M>5.5 earthquake history: Bulletin of the Seismological Society of America, v. 92, p. 2555-2601.

URS Corporation, 2002, Screening/scoping level probabilistic seismic hazard analyses for Granite Reef Diversion and Theodore Roosevelt Dams, Salt River Project: unpublished report prepared for the U.S. Bureau of Reclamation.

URS Corporation, 2011, Site-specific seismic hazard evaluation of the Lake Roberts Dam, New Mexico: unpublished report prepared for U.S. Fish and Wildlife Service.

Weichert, D.H., 1980, Estimation of the earthquake recurrence parameters for unequal observation periods for different magnitudes: Bulletin of the Seismological Society of America, v. 70, p. 1337-1346.

Wells, D.L. and Coppersmith, K.J., 1994, New empirical relationships among magnitude, rupture length, rupture width, rupture area, and surface displacement: Bulletin of the Seismological Society of America, v. 84, p. 974-1002.

Wesnousky, S.G., 1986, Earthquakes, Quaternary faults, and seismic hazard in California: Journal Geophysical Research, v. 91, p. 12,587-12,631.

WGCEP (Working Group on California Earthquake Probabilities), 1988, Probabilities of large earthquakes occurring in California on the San Andreas fault: U.S. Geological Survey Open-File Report 88-398, 62 p.

WGCEP (Working Group on California Earthquake Predictions), 1995, Seismic hazards in southern California: probable earthquakes, 1994 to 2024: Bulletin of the Seismological Society of America, v. 95, p. 379-439.

WGCEP (Working Group on California Earthquake Probabilities), 2008, The Uniform California Earthquake Rupture Forecast, Version 2 (UCERF 2), USGS Open-File Report 2007-1437/CGS Special Report 203/SCEC Contribution #1138, Version 1.0.

Wong, I.G. and Humphrey, J.R., 1989, Contemporary seismicity, faulting, and the state of stress in the Colorado Plateau: Geological Society of America Bulletin, v. 101, p. 1127-1146.

Wong, I., Pezzopane, S., and Dober, M., 2008, Site-specific seismic hazard analyses for Miami Tailing Dams, Claypool, Arizona: unpublished report prepared for Freeport-McMoran Copper and Gold Miami Operations.

Wong, I., Terra, F., Olig, S., and Dober, M., 2011, Site-specific seismic hazard evaluation of the Morenci Mine Tailing Dam, Arizona: unpublished report prepared for Freeport-McMoran Copper and Gold Inc.

Wong, I., Thomas, P., Olig, S., and Terra, F., 2008, Site-specific probabilistic and deterministic seismic hazard analyses for Sierrita Tailing Dam, Green Valley, Arizona: unpublished report prepared for Phelps Dodge Sierrita Inc.

Woodward-Clyde Federal Services, Geomatrix Consultants, and Pacific Engineering and Analysis, 1996, Site specific probabilistic seismic hazard analysis for the Idaho National Engineering Laboratory: Final Report prepared for Lockheed Martin Idaho Technologies and U.S. Department of Energy, INEL-95/0536, Volumes 1 and 2.

Young, J.J., Arrowsmith, JR., Colini, L., Grant, L.B., and Gootee, B., 2002, 3-D excavation and measurement of recent rupture history along the Cholame segment of the San Andreas Fault: Bulletin of the Seismological Society of America, v. 92, p. 2,670-2,688.

Youngs, R.R., Swan, F.H., Power, M.S., Schwartz, D.P., and Green, R.K., 2000, Probabilistic analysis of earthquake ground shaking hazard along the Wasatch Front, Utah, *in* P.L. Gori and W.W. Hays (eds.), Assessment of Regional Earthquake Hazards and Risk Along the Wasatch Front, Utah: U.S. Geological Survey Professional Paper 1500-K-R, p. M1-M74.

Youngs, R.R. and Coppersmith, K.J., 1985, Implications of fault slip rates and earthquake recurrence models to probabilistic seismic hazard estimates: Bulletin of the Seismological Society of America, v. 75, p. 939-964.

Zielke, O., Arrowsmith, J R., Ludwig L G., Akciz, S.O., 2010, Slip in the 1857 and Earlier Large Earthquakes Along the Carrizo Plain, San Andreas Fault: Science, v. 327, 5969, p. 1119-1122.

Table 1. Local Fault Parameters for Proposed Resolution Copper Tailings Sites

FAULT NAME[1]	RUPTURE MODEL	MAXIMUM RUPTURE LENGTH[2] (km)	MAXIMUM MAGNITUDE[3] (Mw)	FAULT DIP[4] (degrees)	KNOWN OR SUSPECTED AGE OF YOUNGEST OFFSET	PROBABILITY OF ACTIVITY[5]	FAULT SLIP RATE[6] (mm/yr)	COMMENTS	REFERENCES
Carefree Fault Zone #947	Independent (1.0)	11	6.2 (0.3) 6.5 (0.5) 6.8 (0.2)	35º W (0.2) 50º W (0.6) 65º W (0.2)	Middle Pleistocene to Late Quaternary (< 750 ka)	1.0	0.002 (0.2) 0.01 (0.6) 0.02 (0.2)	NW-striking, W-down normal faults that divide a Precambrian granite pediment from tilted Tertiary volcanic rocks to the W in the McDowell Mountains. Scarps < 3 m high along a contact between the granite bedrock and middle Pleistocene alluvium. Skotnicki *et al.* (1997) interpret middle Pleistocene deposits are faulted; but Holocene and late Pleistocene deposits are not displaced. Slip rate is based on < 3 m offset in middle Pleistocene (~300 kyr) and older deposits (Pearthree, 1998).	Pearthree (1998) Pearthree and Scarborough (1984) Skotnicki *et al.* (1997)
Horseshoe Fault Zone #946	Independent (1.0)	21	6.3 (0.2) 6.6 (0.6) 6.9 (0.2)	35º NE (0.2) 50º NE (0.6) 65º NE (0.2)	Holocene (<15 ka)	1.0	0.01 (0.3) 0.04 (0.6) 0.1 (0.1)	Nearly perpendicular normal faults along the western and southern margins of the Horseshoe Basin, an asymmetric graben in the upland region between the Mazatzal Mountains and Humboldt Mountain. Trenches, scarp analyses and mapping indicate latest Pleistocene and Holocene faulting along the entire zone and two or more episodes of faulting since ~300 kyr. Scarp analyses, soil development, topographic relations, and fault trench results indicate a slip rate of about 0.04 ± 0.03 mm/yr; displacements of about 1.5 to 2 m, and recurrence intervals of approximately 100 kyr (Pearthree, 1998). Piety and Anderson (1991) estimate the paleoearthquakes were magnitude 6.5 to 7. Fault dip is generalized as NE, a combination of E on the northern section and N on southern section. Slip rate is based on < 5 ± 2.5 m of vertical displacement in the past 150 kyr (northern section) and < 2 m vertical displacement in the past 200 to 300 kyr on the southern section (Pearthree 1998). (~2 to 7.5m/150yr = 0.03 ± 0.02 mm/yr) (2m/200 to 300 kyr = 0.04 ± 0.03 mm/yr).	Menges and Pearthree (1983) Pearthree (1998) Pearthree *et al.* (1988) Pearthree and Scarborough (1984) Piety and Anderson (1990) Piety and Anderson (1991)
Sugarloaf Fault Zone #945	Independent (1.0)	8	6.2 (0.3) 6.5 (0.5) 6.8 (0.2)	35º NE (0.2) 50º NE (0.6) 65º NE (0.2)	Late to latest Pleistocene (< 130 ka)	1.0	0.005 (0.3) 0.02 (0.6) 0.05 (0.1)	NW-striking normal fault that forms an asymmetric graben along the western flank of the Mazatzal Mountains. E-facing scarps are low but sharp and as much as 5 m high between granite bedrock and basin-fill deposits. Natural exposures and two trenches revealed late and latest Pleistocene deposits are offset, but middle to Holocene deposits are not faulted. Slip rate is based on < 1 m vertical displacement in the past 50 to 100 kyr Pearthree (1998).	Anderson *et al.* (1986) Fugro National (1981) Menges and Pearthree (1983) Pearthree (1998) Pearthree *et al.* (1995)
Whitlock Wash Fault #940	Independent (1.0)	23	6.4 (0.2) 6.7 (0.6) 7.0 (0.2)	35º W (0.2) 50º W (0.6) 65º W (0.2)	Quaternary (< 1.6 Ma)	0.9	0.005 (0.2) 0.01 (0.6) 0.02 (0.2)	Discontinuous N- to NW-striking, W-down normal faults along the eastern side of San Pedro Valley. Quaternary activity is suspected based on a prominent escarpment and faulting in Pliocene basin-fill deposits. No evidence of Quaternary movement has been found. Mapping on the southern zone revealed lower to middle Quaternary deposits that are not faulted. Probability of activity is assumed to be 0.9, as evidence for Quaternary activity is equivocal (Pearthree, 1998). The slip rate is unknown, but probably < 0.02 mm/yr (Pearthree1998).	Menges and Pearthree (1983) Pearthree (1998) Pearthree *et al.* (1988) Shenk (1990)

1 Known and suspected Quaternary faults within 100 km of the site, listed in order of closest distance. Fault name and number from Pearthree (1998) and USGS online Quaternary fault and fold database. Note that southern San Andreas fault source parameters are not included in this table due to their complexity.

2 Measured along strike and rounded to the nearest km.

3 Estimated using the empirical relation of Wells and Coppersmith (1994) for all fault types based on maximum surface rupture length. Fault lengths ≤ 10 km are too short to use for an accurate magnitude estimate. Rather, the maximum magnitude distribution is taken to be M= 6.5 ± 0.3, which is based on the minimum magnitude threshold for surface rupture in the Basin and Range Province (dePolo, 1994).

4 Dips are assumed averages for the seismogenic crust after Lund (2012)-see discussion in text.

5 Probability of activity considers the likelihood that a fault is an independent seismogenic structure capable of generating earthquakes within the modern stress field.

6 Rates are average net slip rates. All faults assumed to be pure normal slip (100% dip slip), so net slip was calculated from vertical slip by assuming the preferred fault dip. See also individual summaries in Wong et al. (2008a) for more discussion on the basis for slip rates. Recurrence models used in the analysis were: characteristic (weighted 0.6), maximum magnitude (weighted 0.2), and truncated exponential (weighted 0.2).

Table 2a. Southern California and Baja California Fault Source Parameters Included in the Analyses[1]

Fault Name fm2.1 (0.5) [7] fm 2.2 (0.5)	P(a)[2]	Rupture Length (km)	Slip Rate (mm/yr)	SR unc.[3]	Aseismic Slip Factor[4]	Paleoseismic Recurrence Interval (yrs)	Sense of Slip[5]	Downdip Width (km)	Width unc.	Rupture Top (km)	Rupture Bottom (km)	Dip (degrees)	Dip Direction	Preferred Mmax ± 0.3[6]
San Andreas Fault Zone [segmented (0.9)]														
San Andreas-1906 rupture	1.0	473.0	24.0	3.0	0.0	300	rl-ss	13.0	2	0	13.0	90		7.9
San Andreas Parkfield	1.0	36.4	34.0	5.0	0.8	24.5	rl-ss	10.2	2	0	10.2	90		6.7
San Andreas-Cholame	1.0	62.5	34.0	5.0	0.0	155	rl-ss	12.0	2	0	12.0	90		7.0
San Andreas-Carrizo	1.0	59.0	34.0	3.0	0.0	175	rl-ss	15.1	2	0	15.1	90		7.1
San Andreas-Big Bend	1.0	49.7	34.0	3.0	0.0	175	rl-ss	15.1	2	0	15.1	90		7.0
San Andreas-Mojave N	1.0	36.9	27.0	7.0	0.0	155	rl-ss	15.1	2	0	15.1	90		6.8
San Andreas-Mojave S	1.0	97.6	29.0	7.0	0.0	130	rl-ss	13.1	2	0	13.1	90		7.3
San Andreas-San Bernardino N	1.0	35.3	22.0	6.0	0.0	175	rl-ss	12.8	2	0	12.8	90		6.8
San Andreas-San Bernardino S	1.0	43.4	16.0	6.0	0.0	200	rl-ss	12.8	2	0	12.8	90		6.9
San Andreas-San Gorgonio Pass/Garnet Hill	1.0	55.9	10.0	6.0	0.0	225	rl-ss	19.3	2	0	16.4	58	N	7.0
San Andreas-Coachella	1.0	69.4	20.0	5.0	0.1	212	rl-ss	11.1	2	0	11.1	90		7.1
Rupture Scenarios (see SoSAF Table 2b)														
San Jacinto - Imperial Fault Zone [segmented (0.9)]														
Imperial	1.0	45.8	20.0	5.0	0.1	—	rl-ss	14.7	2	0	14.6	82	N	6.9
Superstition Hills	1.0	36.2	4.0	2.0	0.1	—	rl-ss	12.6	2	0	12.6	90		6.8
Superstition Mountain	1.0	26.3	5.0	3.0	0.1	395	rl-ss	12.4	2	0	12.4	90		6.6
San Jacinto-Borrego	1.0	34.2	4.0	2.0	0.1	130	rl-ss	13.1	2	0	13.1	90		6.7
San Jacinto-Coyote Creek	1.0	42.9	4.0	2.0	0.0	375	rl-ss	15.9	2	0	15.9	90		6.9
San Jacinto-Clark	1.0	46.8	14.0	6.0	0.0	240	rl-ss	16.8	2	0	16.8	90		7.0
San Jacinto-Anza	1.0	46.1	18.0	6.0	0.0	240	rl-ss	16.8	2	0	16.8	90		7.0
San Jacinto-Anza stepover	1.0	24.2	9.0	4.0	0.0	—	rl-ss	16.8	2	0	16.8	90		6.6
San Jacinto-SJV stepover	1.0	24.2	9.0	4.0	0.0	—	rl-ss	16.8	2	0	16.8	90		6.6
San Jacinto- San Jacinto Valley	1.0	18.5	18.0	6.0	0.0	—	rl-ss	18.5	2	0	18.5	90		6.5
San Jacinto-San Bernardino	1.0	45.1	6.0	4.0	0.0	200	rl-ss	16.1	2	0	16.1	90		6.9
Rupture Scenarios (see Table 2c)														
Elsinore Fault Zone [segmented (0.9)]														
Elsinore-Coyote Mountain	1.0	38.8	3.0	1.0	0.0	933	rl-ss	13.3	2	0	13.2	82	NE	6.8
Elsinore-Julian	1.0	75.4	3.0	1.0	0.0	2000	rl-ss	18.9	2	0	18.8	84	NE	7.3
Elsinore-Temecula	1.0	40.0	5.0	2.0	0.0	600	rl-ss	14.2	2	0	14.2	88	NE	6.8
Elsinore-Temecula stepover	1.0	11.8	2.5	2.0	0.0		rl-ss	13.5	2	0	13.3	80	NE	6.3
Elsinore-Glen Ivy stepover	1.0	11.8	2.5	2.0	0.0		rl-ss	13.5	2	0	13.3	80	SW	6.3
Elsinore-Glen Ivy	1.0	25.8	5.0	2.0	0.0	271	rl-ss	13.5	2	0	13.3	80	SW	6.6
Elsinore-Whittier (fm2.1) (0.5)	1.0	46.2	2.5	1.0	0.0	—	rl-ss	14.6	2	0	14.1	75	NE	6.9
Elsinore-Whittier (fm2.2) (0.5)	1.0	46.2	2.5	1.0	0.0	—	rl-ss	13.2	2	0	12.4	70	NE	6.9
Rupture Scenarios (see Elsinore Table 2d)						—								

Table 2a. Southern California and Baja California Fault Source Parameters Included in the Analyses[1]

Fault Name fm2.1 (0.5) [7] fm 2.2 (0.5)	P(a)[2]	Rupture Length (km)	Slip Rate (mm/yr)	SR unc.[3]	Aseismic Slip Factor[4]	Paleoseismic Recurrence Interval (yrs)	Sense of Slip[5]	Downdip Width (km)	Width unc.	Rupture Top (km)	Rupture Bottom (km)	Dip (degrees)	Dip Direction	Preferred Mmax ± 0.3[6]
Earthquake Valley[7]	1.0	20.4	2.0	1.0	0.0	—	rl-ss	18.8	2	0	18.8	90		6.6
Laguna Salada	1.0	99.5	3.5	1.5	0.0	—	rl-ss	13.3	2	0	13.3	90		7.3
Garlock Fault Zone [segmented (0.9)]														
Garlock-West	1.0	97.6	6.0	3.0	0.0	1159	ll-ss	14.7	2	0	14.7	90		7.3
Garlock-Central	1.0	110.7	7.0	2.0	0.0	1276	ll-ss	11.5	2	0	11.5	90		7.3
Garlock-East	1.0	45.1	3.0	2.0	0.0	—	ll-ss	11.5	2	0	11.5	90		6.8
Rupture Scenarios (see Table 2e)														
SHEAR ZONES														
Eastern CA Shear zone	0.5	219.0	4.0	2.0	0.0	—	rl-ss	14.0	2	0	14.0	90		7.6

[1] Parameters are largely after the 2007 California Geological Survey/U.S. Geological Survey Uniform California Earthquake Rupture Forecast (UCERF) model (WGCEP, 2008).
[2] Probability of activity
[3] Uncertainty in slip rate value. Single number implies slip rates are modeled with slip rate value in "Slip Rate" column ± value in "SR unc.", with weightings of 0.2, 0.6, 0.2.
[4] Aseismic slip factor (ASF) is used to account for some fraction of aseismic slip due to fault creep by decreasing the effective coseismic rupture area (multiply fault area by 1-ASF to determine effective rupture area). A totally locked fault will have an ASF of 0 and a fully creeping fault will have an ASF of 1.0.
[5] (ss) strike slip, (r) reverse, (n) normal, (rl) rt. lateral, (ll) left lateral, (o) oblique
[6] Mmax obtained either from historical data or calculated from empirical magnitude-area (M-A) and/or magnitude-length (M-L) relationships. For strike-slip faults we used the average of Wells and Coppersmith (1994) M-L and Hanks and Bakun (2002) M-A relationships; for others, we used the average of Wells and Coppersmith (1994) M-L and M-A relationships.
[7] "fm2.1" and "fm2.2" refer to two alternative fault models used in the calculations, weighted equally. Refer to WGCEP (2008) for discussion.
[8] Earthquake Valley fault: not modeled as separate source for sites far from fault. Rather it is included in Elsinore calculations (Julian and Coyote Mtn segments).
[9] Values shown in this cell are not uncertainties in slip rate as described in note 2, but weights on the corresponding slip rates in the "Slip Rate" column.

Table 2b. Maximum Magnitudes and Rupture Rates for the Southern San Andreas Fault*

	Rupture Name (segments involved)	Area (km^2)	Ells-B Mag	H&B Mag	A-Priori Rate	Ells-B Rate	H&B Rate	Comments
	Weight				**0.5**	**0.25**	**0.25**	
1	PK	78	6.09	5.87	3.46E-02	2.49E-02	5.26E-02	Rupture area is reduced from fault by 0.79 aseismic factor
2	CH	750.2	7.08	6.9	5.00E-05	5.21E-05	5.46E-05	
3	CC	891.2	7.15	7	3.00E-04	1.60E-04	5.74E-05	
4	BB	751	7.08	6.9	3.00E-04	5.68E-04	5.26E-04	
5	NM	556.5	6.95	6.73	2.00E-04	1.05E-04	1.44E-04	
6	SM	1279	7.31	7.21	5.00E-04	6.45E-04	6.78E-04	
7	NSB	451.9	6.86	6.64	7.00E-04	7.12E-04	6.64E-04	
8	SSB	555.5	6.94	6.73	5.00E-05	5.10E-05	5.17E-05	
9	BG	843	7.13	6.97	5.00E-04	1.88E-04	1.35E-05	
10	CO	693.4	7.04	6.86	2.50E-03	6.70E-03	1.21E-02	Rupture area is reduced from fault by 0.1 aseismic factor
11	PK+CH	828.2	7.12	6.96	1.60E-03	4.36E-03	7.01E-03	
12	CH+CC	1641.4	7.42	7.36	3.00E-04	2.39E-04	2.15E-04	
13	CC+BB	1642.2	7.42	7.36	0	5.02E-06	5.07E-06	
14	BB+NM	1307.5	7.32	7.23	0	1.01E-06	1.01E-06	
15	NM+SM	1835.4	7.46	7.42	7.00E-04	4.95E-06	5.04E-06	
16	SM+NSB	1730.9	7.44	7.39	6.00E-04	8.79E-04	8.90E-04	
17	NSB+SSB	1007.4	7.2	7.07	8.00E-04	1.05E-03	1.22E-03	
18	SSB+BG	1398.5	7.35	7.26	9.00E-04	5.03E-06	4.95E-06	
19	BG+CO	1536.4	7.39	7.32	7.00E-04	2.83E-04	4.10E-04	
20	PK+CH+CC	1719.4	7.44	7.38	7.00E-04	4.26E-04	4.19E-04	
21	CH+CC+BB	2392.4	7.58	7.58	0	9.94E-07	9.93E-07	
22	CC+BB+NM	2198.7	7.54	7.53	0	1.00E-06	1.01E-06	
23	BB+NM+SM	2586.4	7.61	7.62	2.50E-04	1.88E-04	2.67E-04	
24	NM+SM+NSB	2287.4	7.56	7.55	1.00E-04	7.24E-05	6.69E-05	
25	SM+NSB+SSB	2286.4	7.56	7.55	4.00E-04	6.05E-04	7.55E-04	
26	NSB+SSB+BG	1850.4	7.47	7.43	4.00E-04	2.22E-04	3.05E-05	
27	SSB+BG+CO	2091.9	7.52	7.5	4.00E-04	2.23E-04	2.48E-04	
28	PK+CH+CC+BB	2470.4	7.59	7.59	4.00E-04	8.20E-04	8.34E-04	
29	CH+CC+BB+NM	2948.8	7.67	7.7	0	9.91E-07	9.99E-07	
30	CC+BB+NM+SM	3477.7	7.74	7.79	4.00E-04	1.95E-04	4.99E-06	
31	BB+NM+SM+NSB	3038.4	7.68	7.71	0	9.95E-07	1.00E-06	
32	NM+SM+NSB+SSB	2842.9	7.65	7.68	2.00E-04	1.04E-04	1.02E-04	
33	SM+NSB+SSB+BG	3129.4	7.7	7.73	3.00E-04	2.92E-04	1.97E-04	
34	NSB+SSB+BG+CO	2543.8	7.61	7.61	4.00E-04	2.23E-04	2.17E-04	
35	PK+CH+CC+BB+NM	3026.9	7.68	7.71	7.00E-04	1.54E-03	1.66E-03	
36	CH+CC+BB+NM+SM	4227.8	7.83	7.9	5.00E-04	4.16E-04	2.67E-04	
37	CC+BB+NM+SM+NSB	3929.6	7.79	7.86	1.00E-04	8.64E-05	5.55E-05	

*** From Table 3, Appendix G, WGCEP (2008)**

Table 2b. Maximum Magnitudes and Rupture Rates for the Southern San Andreas Fault*

	Rupture Name (segments involved)	Area (km^2)	Ells-B Mag	H&B Mag	A-Priori Rate	Ells-B Rate	H&B Rate	Comments
	Weight				**0.5**	**0.25**	**0.25**	
38	BB+NM+SM+NSB+SSB	3593.9	7.76	7.81	5.00E-05	4.92E-05	5.42E-05	
39	NM+SM+NSB+SSB+BG	3685.9	7.77	7.83	1.00E-04	6.19E-05	3.29E-05	
40	SM+NSB+SSB+BG+CO	3822.8	7.78	7.85	4.00E-04	3.58E-04	4.16E-04	
41	PK+CH+CC+BB+NM+SM	4305.9	7.83	7.92	2.00E-03	1.04E-03	6.43E-04	
42	CH+CC+BB+NM+SM+NSB	4679.8	7.87	7.96	0	9.91E-07	9.89E-07	
43	CC+BB+NM+SM+NSB+SSB	4485.1	7.85	7.94	1.00E-04	9.04E-05	6.76E-05	
44	BB+NM+SM+NSB+SSB+BG	4436.9	7.85	7.93	0	1.01E-06	1.01E-06	
45	NM+SM+NSB+SSB+BG+CO	4379.2	7.84	7.93	1.00E-04	6.01E-05	3.90E-05	
46	PK+CH+CC+BB+NM+SM+NSB	4757.8	7.88	7.97	5.00E-04	4.21E-04	3.49E-04	
47	CH+CC+BB+NM+SM+NSB+SSB	5235.3	7.92	8.03	5.00E-05	5.00E-05	5.09E-05	
48	CC+BB+NM+SM+NSB+SSB+BG	5328.1	7.93	8.04	5.00E-05	4.44E-05	3.00E-05	
49	BB+NM+SM+NSB+SSB+BG+CO	5130.2	7.91	8.02	5.00E-05	4.50E-05	4.70E-05	
50	PK+CH+CC+BB+NM+SM+NSB+SSB	5313.3	7.93	8.04	1.00E-04	1.00E-04	1.09E-04	
51	CH+CC+BB+NM+SM+NSB+SSB+BG	6078.2	7.98	8.12	0	9.95E-07	1.01E-06	
52	CC+BB+NM+SM+NSB+SSB+BG+CO	6021.5	7.98	8.11	1.00E-05	9.66E-06	9.24E-06	
53	PK+CH+CC+BB+NM+SM+NSB+SSB+BG	6156.3	7.99	8.12	5.00E-05	4.65E-05	4.09E-05	
54	CH+CC+BB+NM+SM+NSB+SSB+BG+CO	6771.6	8.03	8.18	0	1.01E-06	9.93E-07	
55	PK+CH+CC+BB+NM+SM+NSB+SSB+BG+CO	6849.7	8.04	8.18	1.00E-04	8.29E-05	6.59E-05	
Total					*5.42E-02*	*4.88E-02*	*8.37E-02*	

PK Parkfield
CH Cholame
CC Carrizo
BB Big Bend
NM Mojave North
SM Mojave South
NSB San Bernardino North
SSB San Bernardino South
BG San Gorgonio Pass-Garnet Hill (aka Banning-Garnet Hill)
CO Coachella

*** From Table 3, Appendix G, WGCEP (2008)**

Table 2c. Maximum Magnitudes and Rupture Rates for the San Jacinto Fault*

	Rupture Name (segments involved)	Area (km^2)	Ells-B Mag	H&B Mag	A-Priori Rate	Ells-B Rate	H&B Rate	Comments
	Weight				**0.5**	**0.25**	**0.25**	
1	SBV	725.7	7.06	6.88	2.31E-03	4.39E-04	4.42E-04	
2	SJV (SJV+SJV stepover sections)	686.7	7.04	6.85	2.43E-03	4.50E-04	4.49E-04	
3	A (A+A stepover sections)	1193.9	7.28	7.17	0	8.83E-05	8.82E-05	
4	C	786.1	7.1	6.93	0	8.87E-05	8.98E-05	
5	CC	681.5	7.03	6.85	8.89E-04	4.50E-04	4.48E-04	
6	B	403.6	6.81	6.59	4.82E-03	4.45E-04	4.43E-04	Rupture area is reduced from fault by 0.1 aseismic factor
7	SM	325.8	6.71	6.49	1.09E-03	1.50E-03	4.01E-03	Rupture area is reduced from fault by 0.1 aseismic factor
8	SBV+SJV	1412.4	7.35	7.27	1.32E-03	4.49E-04	4.41E-04	
9	SJV+A	1880.6	7.47	7.44	0	4.41E-04	4.50E-04	
10	A+C	1980.1	7.5	7.47	3.15E-03	1.21E-03	1.16E-03	
11	A+CC	1875.4	7.47	7.43	0	8.82E-05	9.00E-05	
12	CC+B	1085.1	7.24	7.12	8.89E-04	4.50E-04	4.47E-04	
13	B+SM	729.4	7.06	6.89	1.09E-03	4.40E-04	4.43E-04	
14	SBV+SJV+A	2606.4	7.62	7.62	0	4.47E-04	4.48E-04	
15	SJV+A+C	2666.8	7.63	7.64	0	4.48E-04	4.51E-04	
16	SJV+A+CC	2562.2	7.61	7.61	0	8.91E-05	8.93E-05	
17	A+CC+B	2279.1	7.56	7.55	0	9.02E-05	8.95E-05	
18	CC+B+SM	1411	7.35	7.27	8.89E-04	4.48E-04	4.40E-04	
19	SBV+SJV+A+C	3392.5	7.73	7.78	1.05E-03	4.49E-04	4.41E-04	
20	SBV+SJV+A+CC	3287.9	7.72	7.76	0	8.94E-05	9.03E-05	
21	SJV+A+CC+B	2965.8	7.67	7.7	0	8.82E-05	8.89E-05	
22	A+CC+B+SM	2604.9	7.62	7.62	0	8.93E-05	8.96E-05	
23	SBV+SJV+A+CC+B	3691.5	7.77	7.83	0	8.80E-05	8.97E-05	
24	SJV+A+CC+B+SM	3291.6	7.72	7.76	0	8.94E-05	9.03E-05	
25	SBV+SJV+A+CC+B+SM	4017.3	7.8	7.88	0	8.90E-05	8.82E-05	
Total					*1.99E-02*	*9.04E-03*	*1.15E-02*	

SBV San Bernardino Valley
SJV San Jacinto Valley
A Anza
C Clark
CC Coyote Creek
B Borrego Mountain
SM Superstition Mountain
Note: Does not include Imperial or Superstition Hills faults

*** From Table 3, Appendix G, WGCEP (2008)**

Table 2d. Maximum Magnitudes and Rupture Rates for the Elsinore Fault*

	Rupture Name (segments involved)	**Area (km^2)**	**Ells-B Mag**	**H&B Mag**	**A-Priori Rate**	**Ells-B Rate**	**H&B Rate**	**E/HB ave Mag**	**Comments**
	Weight				**0.5**	**0.25**	**0.25**		
1	W	674.8	7.03	6.84	7.14E-04	9.27E-04	1.37E-03	6.94	
2	GI (GI+GI stepover sections)	488.6	6.89	6.67	2.55E-03	1.19E-03	2.19E-03	6.78	
3	T (T+T stepover sections)	734.9	7.07	6.89	6.10E-04	1.24E-04	3.46E-04	6.98	
4	J	1426.1	7.35	7.28	0	3.85E-05	2.48E-05	7.32	
5	CM	517.3	6.91	6.69	5.71E-04	1.04E-03	2.11E-03	6.80	
6	W+GI	1163.4	7.27	7.16	0	2.48E-05	1.42E-04	7.22	
7	GI+T	1223.5	7.29	7.19	8.90E-04	1.25E-04	1.25E-04	7.24	
8	T+J	2161	7.53	7.52	0	1.27E-04	1.26E-04	7.53	
9	J+CM	1943.3	7.49	7.45	0	1.74E-04	2.92E-04	7.47	
10	W+GI+T	1898.3	7.48	7.44	0	2.48E-05	9.07E-05	7.46	
11	GI+T+J	2649.6	7.62	7.63	0	1.26E-04	1.27E-04	7.63	
12	T+J+CM	2678.2	7.63	7.64	2.50E-04	2.83E-04	2.54E-04	7.64	
13	W+GI+T+J	3324.4	7.72	7.77	0	2.52E-05	2.48E-05	7.75	
14	GI+T+J+CM	3166.9	7.7	7.74	2.50E-04	1.83E-04	1.27E-04	7.72	
15	W+GI+T+J+CM	3841.7	7.78	7.85	0	2.49E-05	2.52E-05	7.82	
Total					*5.84E-03*	*4.44E-03*	*7.37E-03*		

W Whittier
GI Glen Ivy
T Temecula
J Julian
CM Coyote Mountain

Note: Does not include Laguna Salada fault

*** From Table 3, Appendix G, WGCEP (2008)**

Table 2e. Rupture Rates for the Garkock Fault*

	Rupture Name (segments involved)	Area (km^2)	Ells-B Mag	H&B Mag	A-Priori Rate	Ells-B Rate	H&B Rate	Comments
	Weight				**0.5**	**0.25**	**0.25**	
1	GE	519.3	6.92	6.7	6.80E-04	3.61E-04	6.21E-04	None.
2	GC	1276.1	7.31	7.21	7.84E-05	9.26E-05	8.32E-05	
3	GW	1290.9	7.31	7.22	2.36E-04	2.19E-04	2.61E-04	
4	GE+GC	1795.4	7.45	7.41	7.84E-05	9.05E-05	8.32E-05	
5	GC+GW	2567.1	7.61	7.62	3.13E-04	5.99E-04	5.50E-04	
6	GE+GC+GW	3086.3	7.69	7.72	3.13E-04	5.83E-04	5.78E-04	
Total					*1.70E-03*	*1.95E-03*	*2.18E-03*	

GE Garlock East
GC Garlock Central
GW Garlock West

*** From Table 3, Appendix G, WGCEP (2008)**

Table 3
UHS

Period (sec)	Far West 2 (rock)				Near West (Tcu)				Pinto Valley (rock)			
	100-yr UHS	450-yr UHS	5,000-yr UHS	10,000-yr UHS	100-yr UHS	450-yr UHS	5,000-yr UHS	10,000-yr UHS	100-yr UHS	450-yr UHS	5,000-yr UHS	10,000-yr UHS
0.010	0.011	0.022	0.069	0.093	0.015	0.034	0.107	0.142	0.010	0.026	0.094	0.125
0.030	0.011	0.024	0.075	0.101	0.015	0.036	0.114	0.152	0.011	0.028	0.103	0.137
0.050	0.012	0.028	0.091	0.125	0.016	0.040	0.135	0.181	0.012	0.033	0.128	0.171
0.100	0.015	0.039	0.140	0.193	0.020	0.056	0.206	0.276	0.015	0.047	0.199	0.267
0.150	0.017	0.046	0.165	0.225	0.026	0.070	0.253	0.338	0.017	0.055	0.230	0.308
0.200	0.020	0.049	0.162	0.219	0.032	0.078	0.263	0.350	0.020	0.057	0.219	0.293
0.300	0.021	0.047	0.130	0.174	0.038	0.082	0.236	0.312	0.021	0.051	0.168	0.225
0.400	0.019	0.042	0.106	0.137	0.037	0.078	0.201	0.261	0.019	0.044	0.130	0.173
0.500	0.018	0.039	0.093	0.116	0.038	0.077	0.183	0.230	0.018	0.041	0.106	0.136
0.600	0.017	0.038	0.088	0.108	0.037	0.076	0.178	0.219	0.017	0.038	0.094	0.117
0.750	0.017	0.039	0.094	0.115	0.037	0.078	0.187	0.228	0.017	0.039	0.096	0.118
1.000	0.015	0.034	0.087	0.107	0.031	0.064	0.154	0.188	0.014	0.034	0.087	0.107
1.500	0.011	0.024	0.062	0.077	0.021	0.046	0.108	0.131	0.010	0.023	0.061	0.076
2.000	0.008	0.017	0.046	0.056	0.016	0.035	0.080	0.098	0.008	0.017	0.045	0.055
3.000	0.005	0.011	0.028	0.035	0.011	0.022	0.052	0.062	0.005	0.011	0.028	0.034
4.000	0.004	0.008	0.019	0.024	0.007	0.015	0.037	0.045	0.004	0.008	0.018	0.023
5.000	0.003	0.006	0.015	0.018	0.006	0.012	0.031	0.036	0.003	0.006	0.015	0.018
7.500	0.002	0.004	0.010	0.012	0.004	0.008	0.019	0.024	0.002	0.004	0.010	0.012
10.000	0.002	0.003	0.007	0.009	0.002	0.005	0.013	0.016	0.002	0.003	0.007	0.009

Table 4
Controlling Earthquakes

	100-yr UHS	475-yr UHS	5,000-yr UHS	10,000-yr UHS
Far West 2 (east)				
PGA				
M*	5.1	5.1	5.4	5.1
D* (km)	58	58	35	18
ε*	0.5	1.5	1.3	1.2
1.0 Sec SA				
M*	7.4	7.9	7.6	7.0
D*	438	468	325	260
ε*	1.2	1.7	2.3	2.1
Far West 1 (west)				
PGA				
M*	5.1	5.1	5.4	5.4
D* (km)	58	58	40	29
ε*	0.5	1.5	16	1.5
1.0 Sec SA				
M*	7.4	7.9	6.9	7.0
D*	445	435	228	260
ε*	1.4	1.8	2.1	2.1
Near West				
PGA				
M*	5.1	5.1	5.4	5.4
D* (km)	58	58	38	26
ε*	0.4	1.6	1.7	1.5
1.0 Sec SA				
M*	7.3	7.9	7.7	7.7
D*	435	435	373	370
ε*	1.2	1.6	2.2	2.2
Pinto Valley				
PGA				
M*	5.1	5.1	5.5	5.6
D* (km)	33	33	33	30
ε*	-0.1	0.8	2.0	2.0
1.0 Sec SA				
M*	7.1	7.3	7.1	7.2
D*	405	358	248	280
ε*	1.4	1.7	2.1	2.1

Table 5
Far West 1 Soil UHS

Period (sec)	Far West 1			
	100-yr UHS SA (g)	**450-yr UHS SA (g)**	**5,000-yr UHS SA (g)**	**10,000-yr UHS SA (g)**
0.010	0.011	0.022	0.067	0.090
0.030	0.011	0.023	0.072	0.099
0.050	0.012	0.027	0.088	0.121
0.100	0.014	0.038	0.135	0.187
0.150	0.017	0.045	0.159	0.219
0.200	0.020	0.049	0.157	0.213
0.300	0.021	0.046	0.127	0.169
0.400	0.019	0.042	0.104	0.135
0.500	0.018	0.039	0.093	0.115
0.600	0.017	0.038	0.088	0.108
0.750	0.017	0.039	0.095	0.116
1.000	0.015	0.035	0.087	0.107
1.500	0.011	0.024	0.063	0.078
2.000	0.008	0.017	0.046	0.057
3.000	0.005	0.011	0.029	0.035
4.000	0.004	0.008	0.019	0.024
5.000	0.003	0.006	0.015	0.018
7.500	0.002	0.004	0.010	0.012
10.000	0.002	0.003	0.007	0.009

Table 6
5,000-Year Return Period CMS

Period (s)	Far West 1		Far West 2		Near West		Pinto Valley	
	0.2 Sec SA	**1.0 Sec SA**	**0.2 Sec SA**	**1.0 Sec SA**	**0.2 Sec SA**	**1.0 Sec SA**	**0.2 Sec SA**	**1.0 Sec SA**
0.010	0.090	0.017	0.057	0.010	0.087	0.014	0.078	0.010
0.020	0.090	0.017	0.058	0.010	0.088	0.014	0.080	0.010
0.030	0.095	0.016	0.062	0.010	0.093	0.013	0.085	0.010
0.050	0.111	0.015	0.075	0.009	0.110	0.012	0.101	0.009
0.075	0.136	0.013	0.095	0.008	0.135	0.011	0.126	0.008
0.100	0.163	0.014	0.111	0.008	0.161	0.011	0.147	0.008
0.150	0.231	0.021	0.148	0.012	0.227	0.017	0.196	0.012
0.200	0.269	0.034	0.162	0.018	0.263	0.027	0.219	0.018
0.250	0.231	0.051	0.126	0.025	0.221	0.040	0.180	0.025
0.300	0.199	0.068	0.101	0.032	0.188	0.052	0.151	0.032
0.400	0.143	0.097	0.067	0.043	0.134	0.073	0.109	0.043
0.500	0.109	0.127	0.048	0.053	0.100	0.095	0.081	0.053
0.750	0.060	0.189	0.024	0.075	0.054	0.138	0.045	0.075
1.000	0.038	0.213	0.015	0.087	0.034	0.154	0.030	0.087
1.500	0.019	0.155	0.007	0.057	0.017	0.107	0.016	0.057
2.000	0.011	0.115	0.004	0.040	0.010	0.076	0.010	0.040
3.000	0.004	0.068	0.002	0.022	0.004	0.043	0.005	0.022
4.000	0.002	0.044	0.001	0.013	0.002	0.027	0.003	0.013
5.000	0.001	0.030	0.001	0.009	0.001	0.018	0.002	0.009
7.500	0.001	0.016	0.000	0.005	0.001	0.010	0.001	0.005
10.000	0.000	0.009	0.000	0.003	0.000	0.005	0.000	0.003

Table 7
Seed Time Histories

Year	Earthquake	M	Station	Comp.	Closest Distance (km)	V_S30 (m/s)	PGA (g)
1999	Chi-Chi, Taiwan	7.6	KAU046	E	162	204	0.023
1999	Chi-Chi, Taiwan	7.6	KAU081	E	161	272	0.027
2002	Denali, Alaska	7.9	Anchorage - New Fire Station #1	090	267	275	0.018
2002	Denali, Alaska	7.9	Valdez City Hall	090	239	275	0.027
1999	Kocaeli, Turkey	7.5	Afyon Bay	000	208	–	0.013
1979	Imperial Valley, California	6.5	Cerro Prieto	147	15	660	0.169
1995	Kozani, Greece	6.4	Kozani	L	20	660	0.215

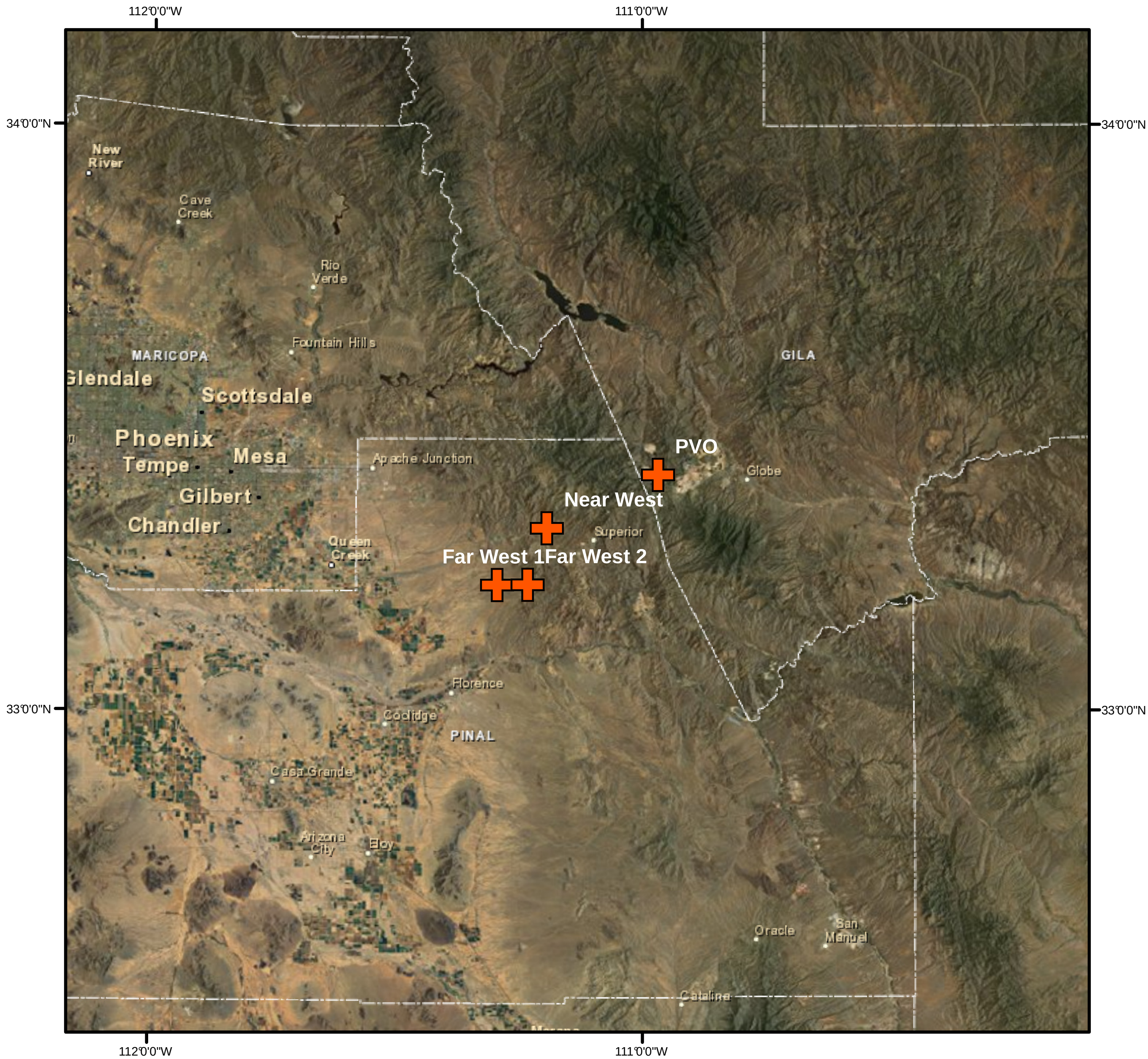

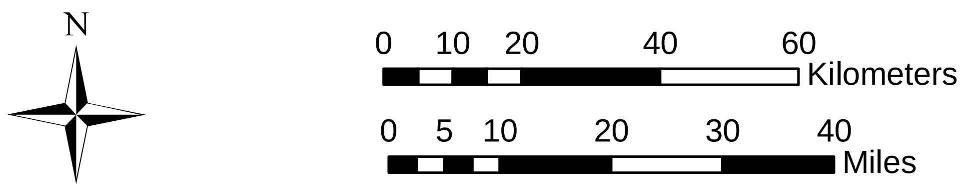

URS	Project No. 26818581 Resolution Copper Mining, Arizona	SITE LOCATIONS	Figure 1

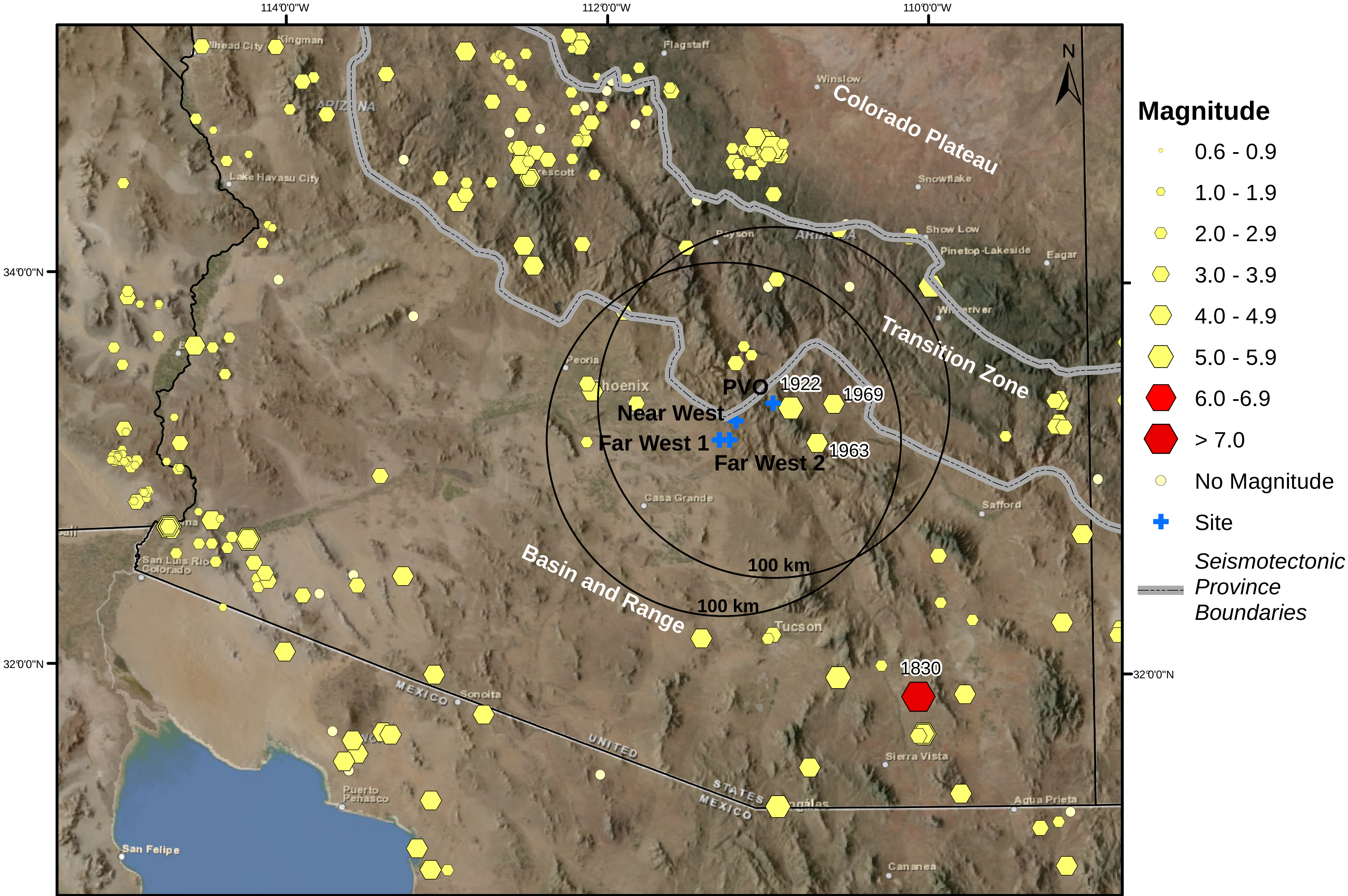

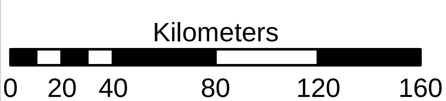

URS

Project No. 26818581	HISTORICAL SEISMICITY IN THE SITE REGION, 1830-2012	Figure 2
Resolution Copper Mining, Arizona		

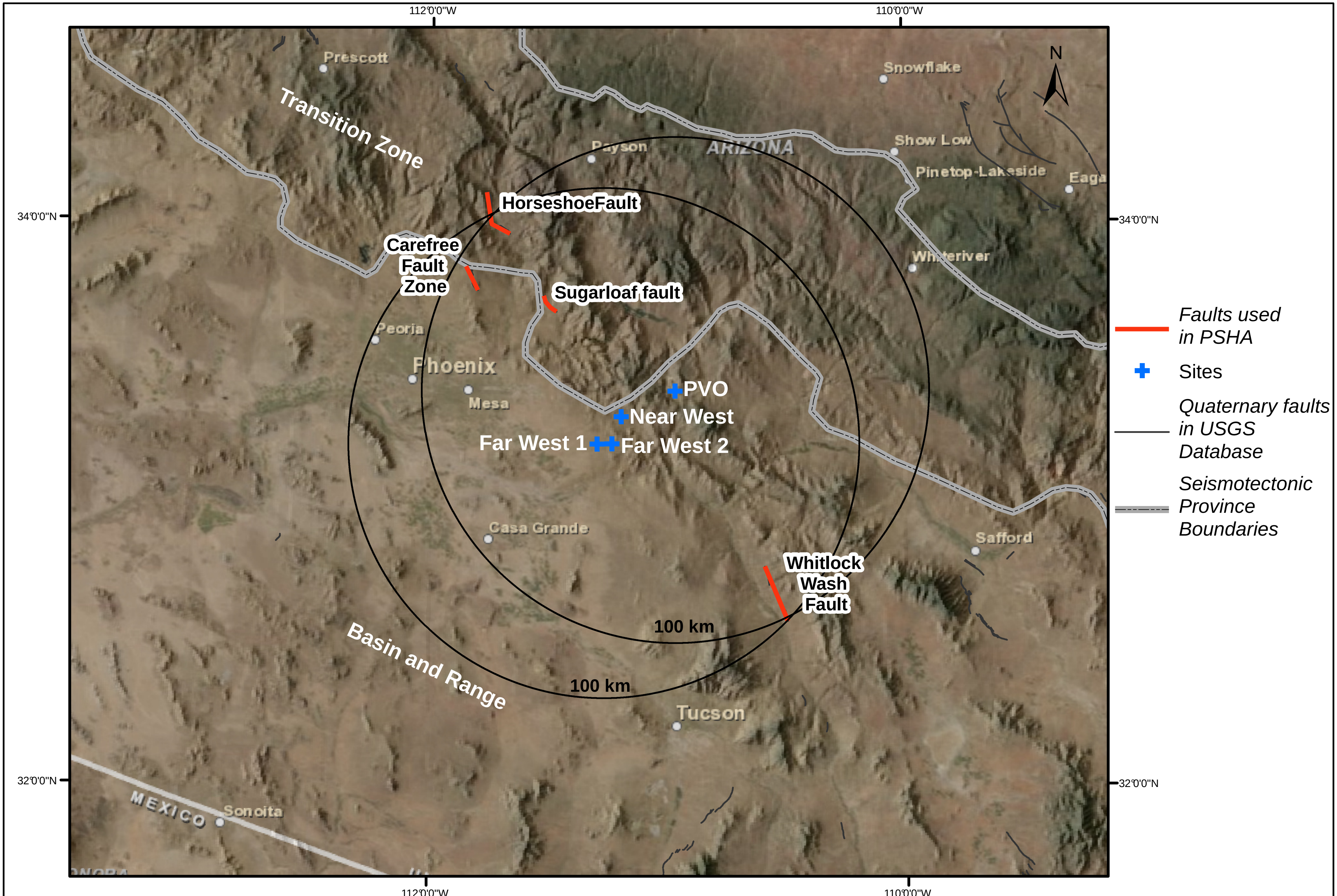

URS	Project No. 26818581 Resolution Copper Mining, Arizona	SEISMIC SOURCES INCLUDED IN THE PSHA	Figure 3

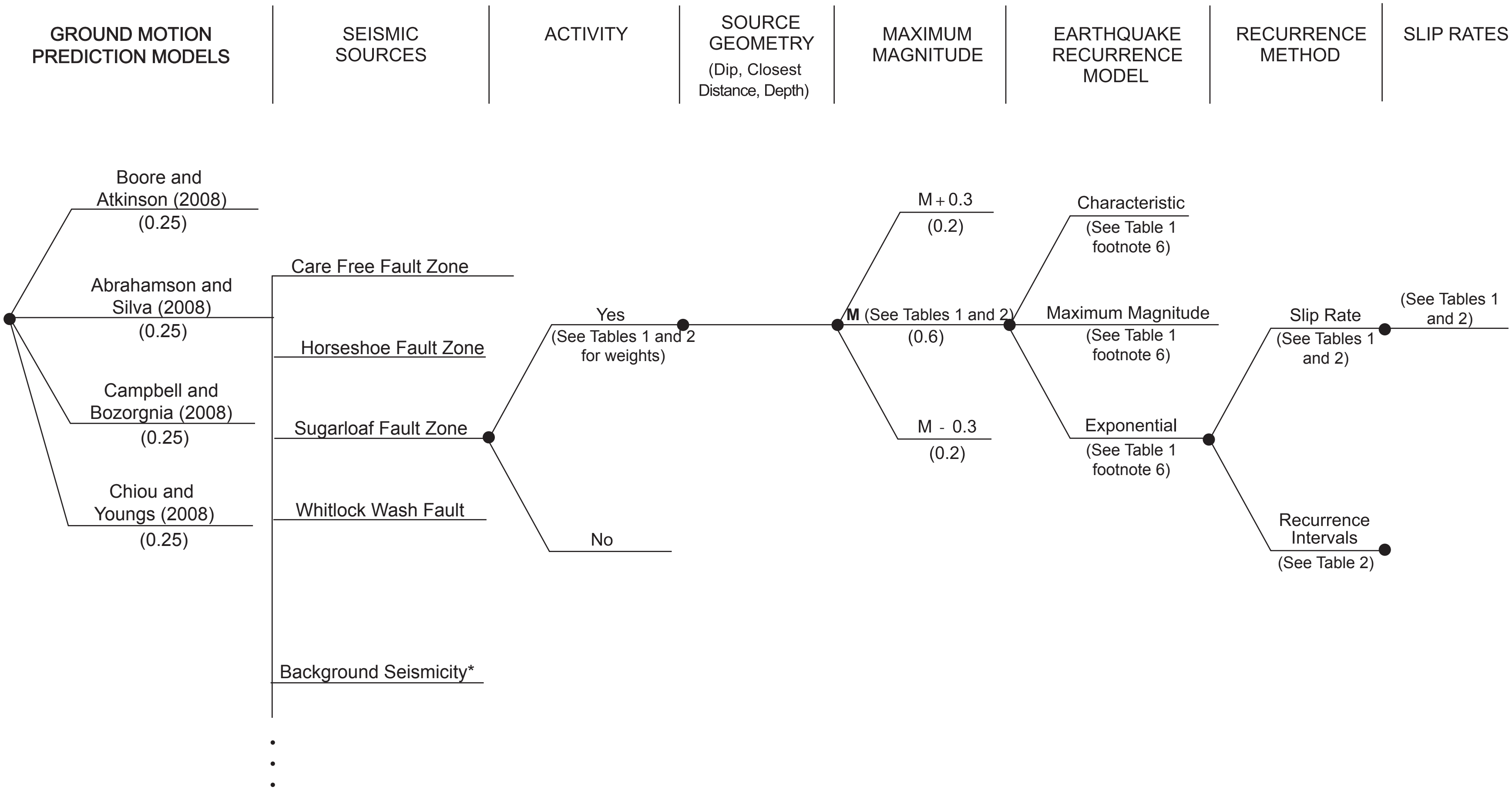

*Treated as areal source zone and with Gaussian Smoothing, each weighted 50 percent.

URS

Project No. 26818581

Resolution Copper Mining, Arizona

SEISMIC HAZARD MODEL LOGIC TREE

Figure 4

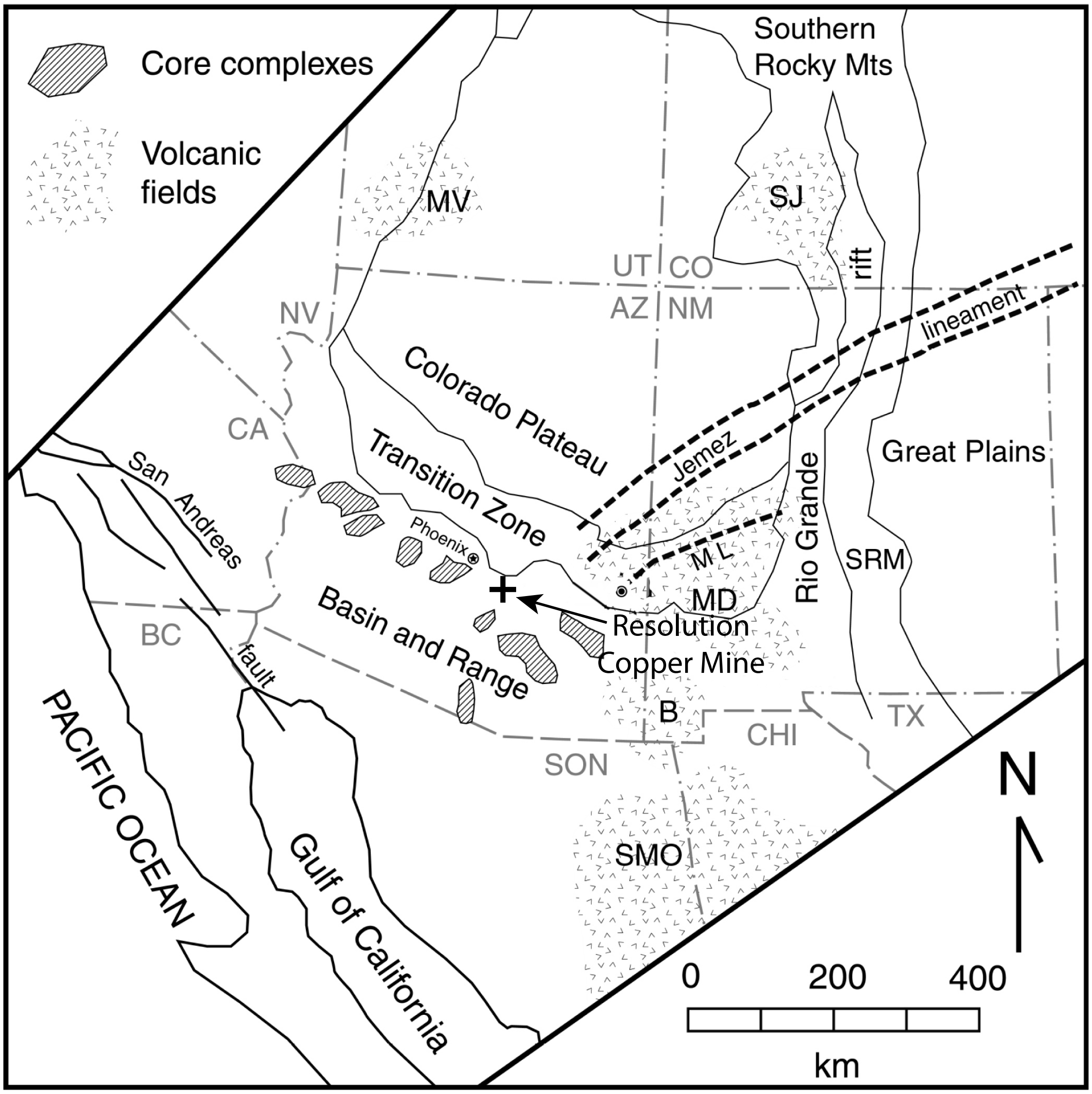

Modified from: Drewes *et al.* (1985)

URS	Project No. 26818581	SEISMOTECTONIC SETTING	Figure 5
	Resolution Copper Mining, Arizona		

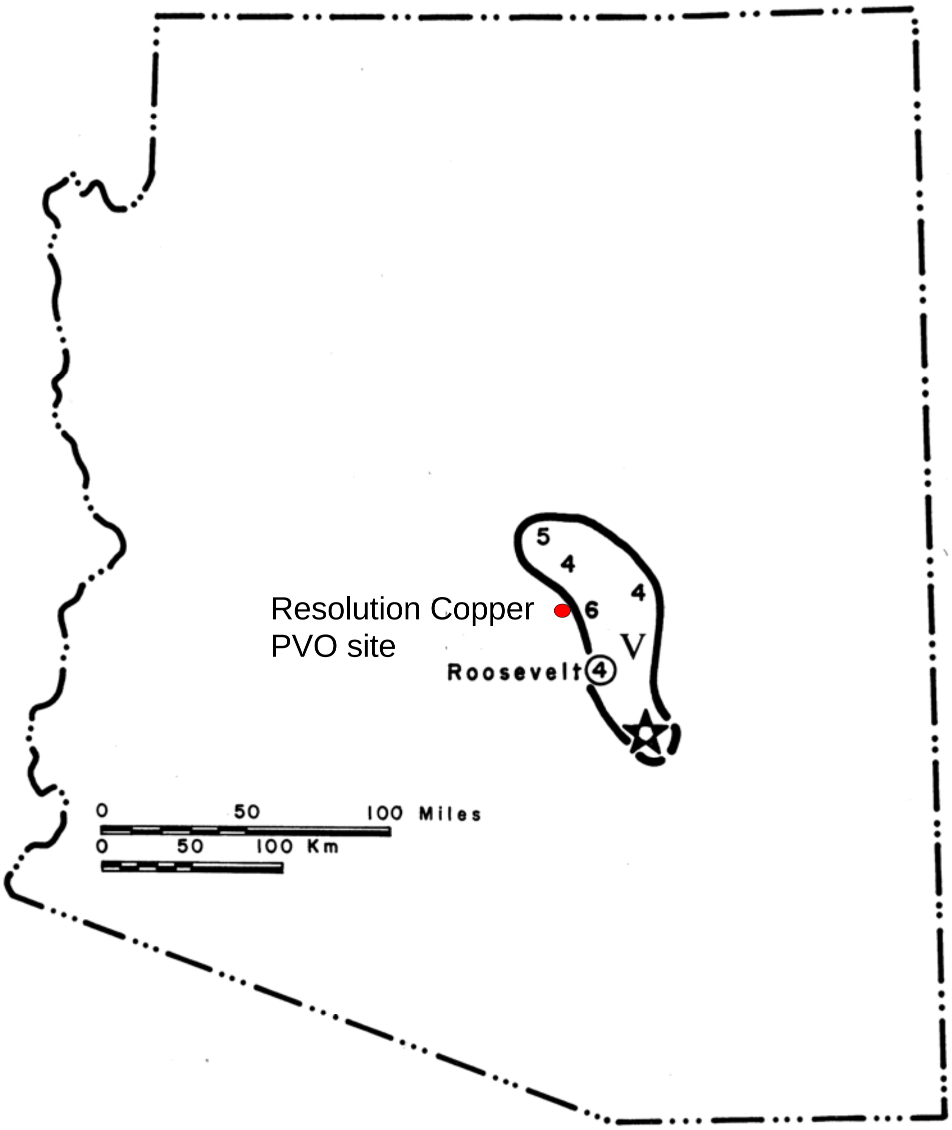

From DuBois (1982)

URS	Project No. 26818581	ISOSEISMAL MAP FOR THE 1922 MM VI (M_I 5) MIAMI EARTHQUAKE	Figure 6
	Resolution Copper Arizona		

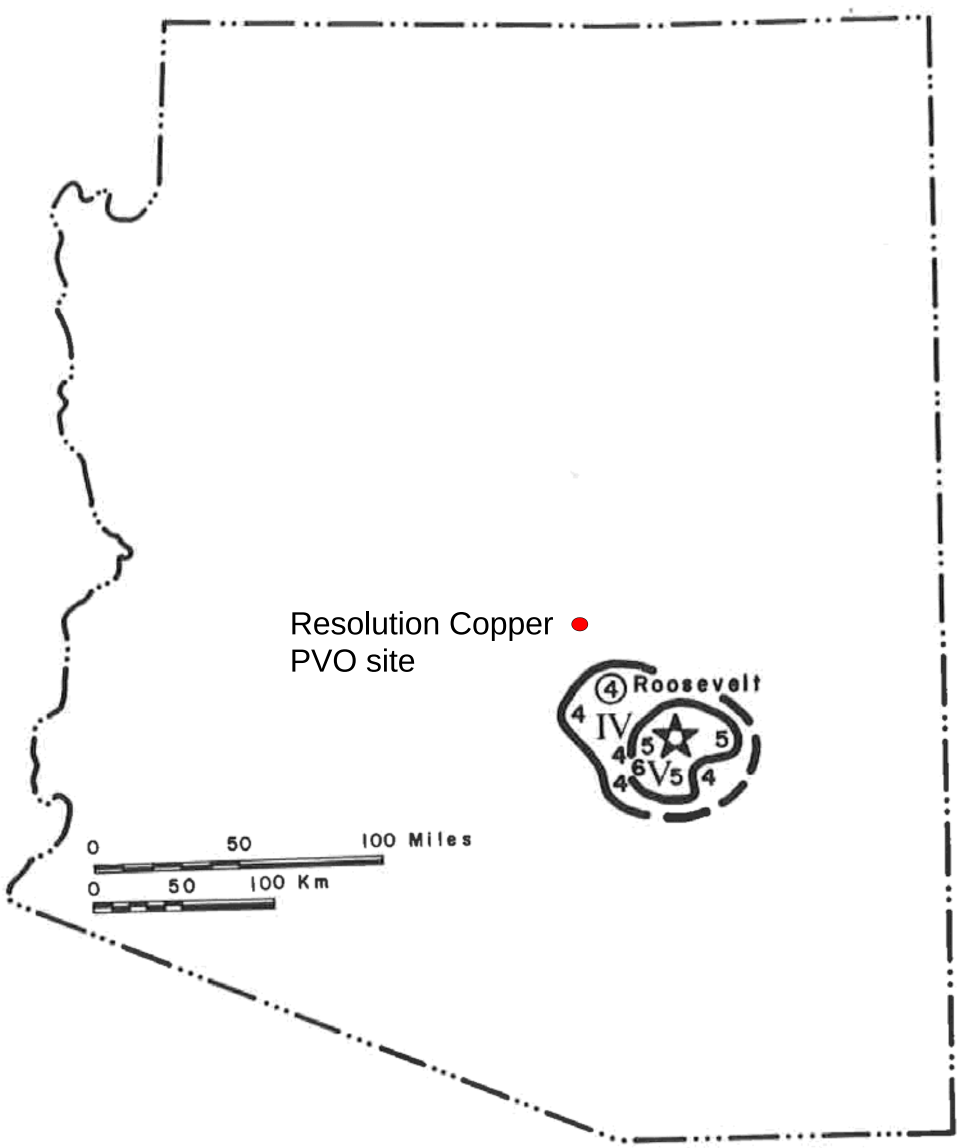

From DuBois (1982)

URS	Project No. 26818581	ISOSEISMAL MAP FOR THE 1963 M_L 4.1 GLOBE EARTHQUAKE	Figure 7
	Resolution Copper Mining, Arizona		

W:\x_wcfs\PROJECTS\Resolution Copper Mine\Figures\Isoseismal maps\1963 isoseismal.grf

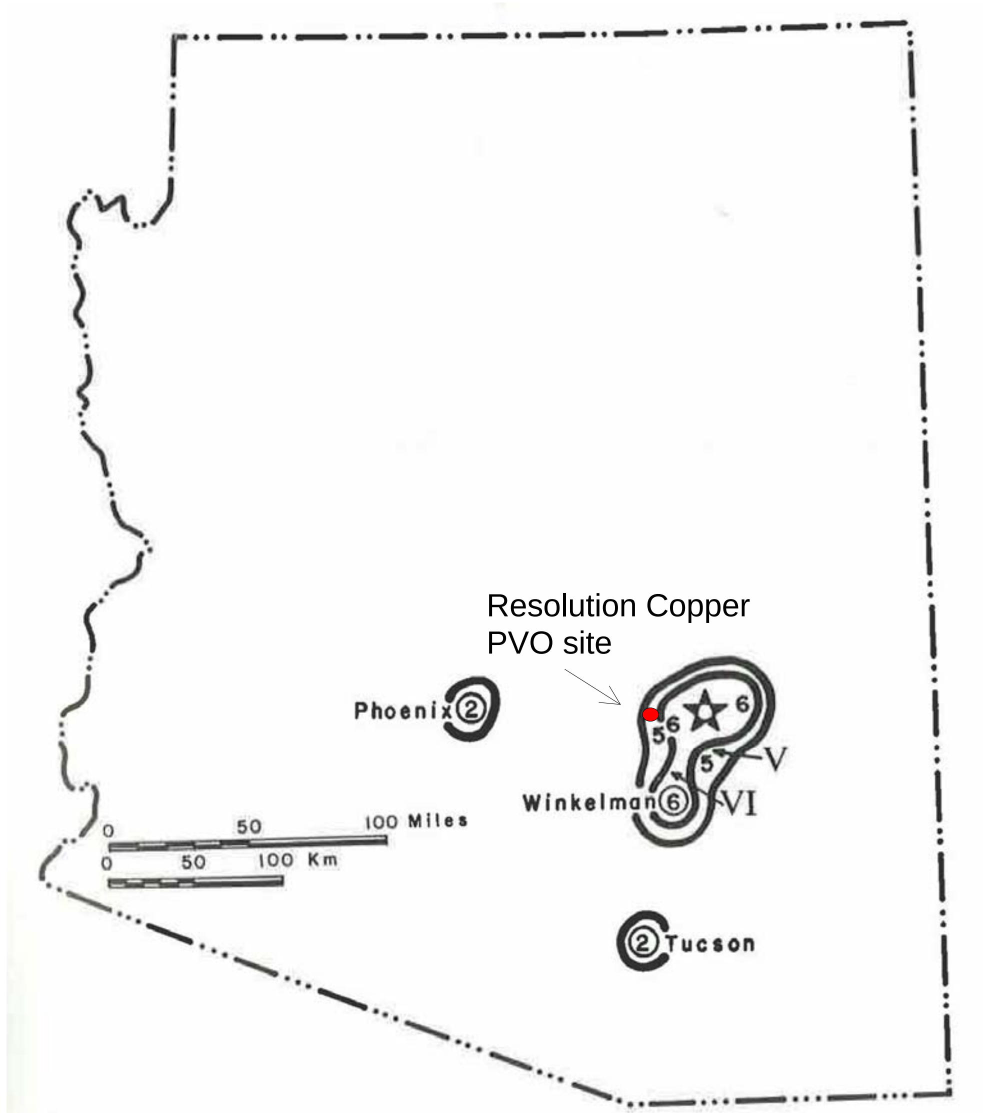

From DuBois (1982)

URS	Project No. 26818581 Resolution Copper Mining, Arizona	ISOSEISMAL MAP FOR THE 1969 M_L 4.4 SAN CARLOS EARTHQUAKE	Figure 8

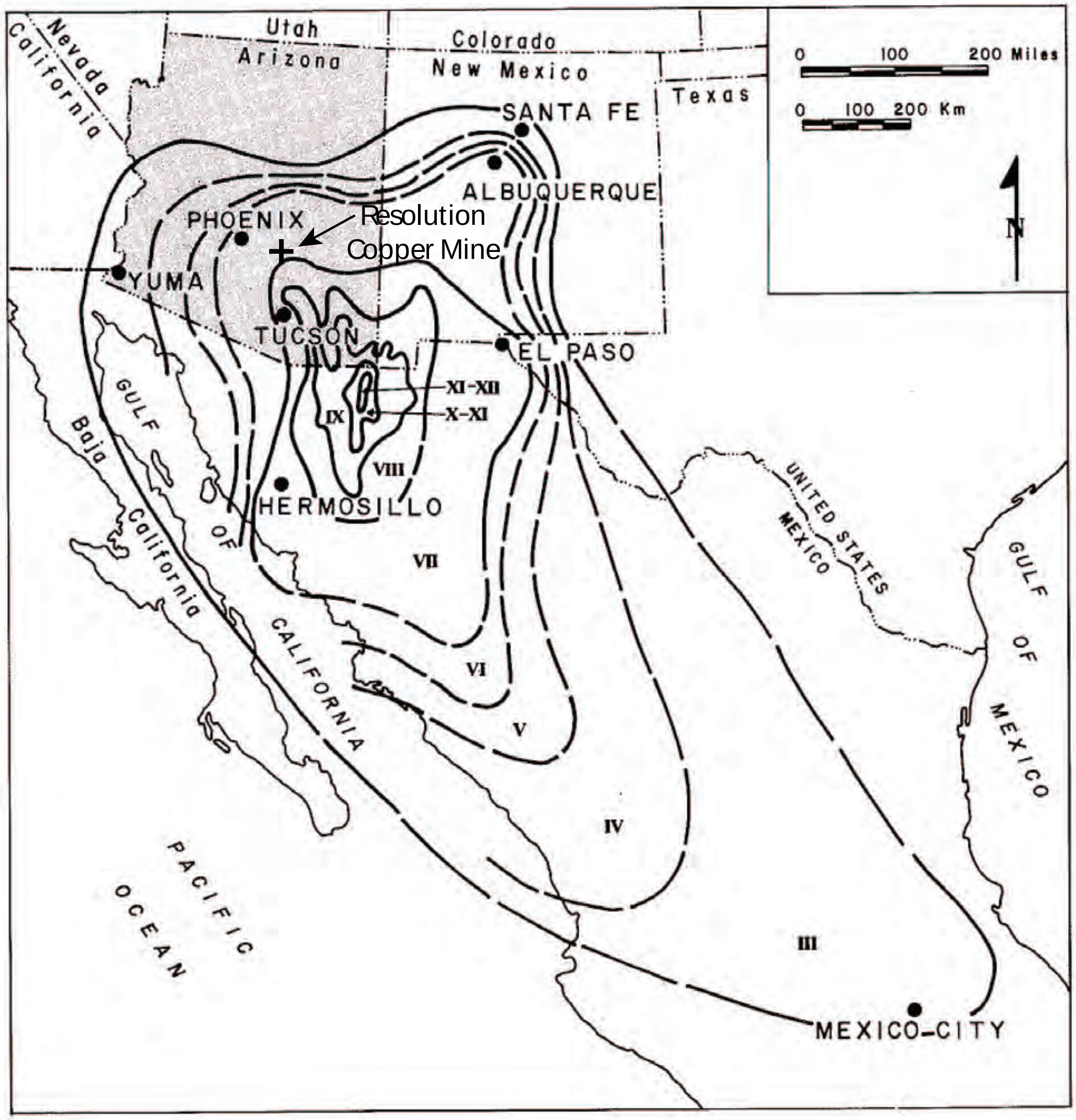

Modified From DuBois et al., 1982

URS	Project No. 26818581	ISOSEISMAL MAP OF THE 3 MAY 1887 M 7.4 SONORA, MEXICO EARTHQUAKE	Figure 9
	Resolution Copper Mining, Arizona		

KEY PLAN
SCALE: NTS

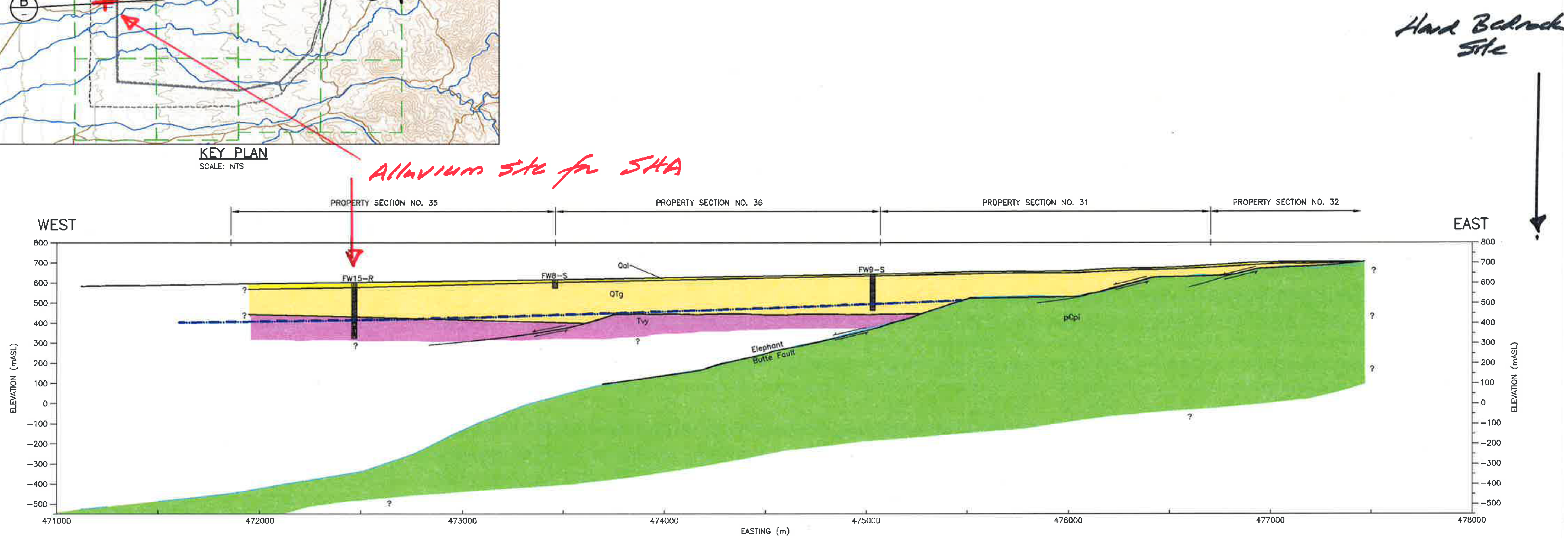

SECTION B 3.1
SCALE A

LEGEND

- QUATERNARY ALLUVIUM (Qal)
- QUATERNARY AND TERTIARY BASIN-FILL DEPOSITS (QTg)
- TERTIARY YOUNGER VOLCANICS (Tvy)
- PRECAMBRIAN PINAL SCHIST (pCpl)
- FAULT
- INTERPRETED TOP OF BEDROCK FROM HGI GRAVITY MODELING (APPENDIX G)
- GROUNDWATER LEVEL ELEVATION (MAY 22, 2012)

NOT FOR CONSTRUCTION

To be read with Klohn Crippen Berger report dated

DRAFT

URS	Project No. 26818581 Resolution Copper Mining, Arizona	FAR WEST GEOLOGIC CROSS SECTION SHOWING ALLUVIUM AND ROCK SITE LOCATIONS	Figure 10

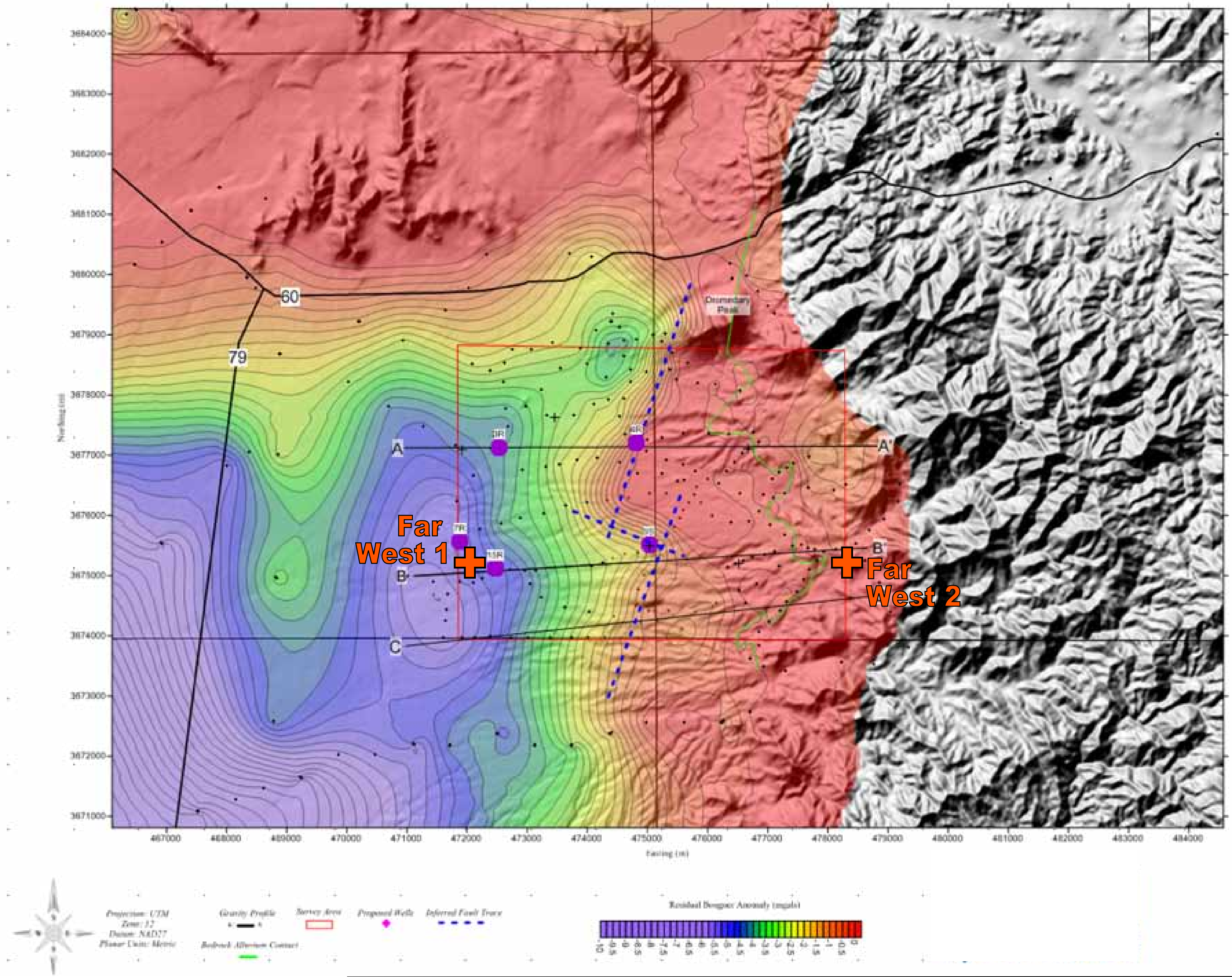

Source: Hydro Geophysics (2012)

URS

Project No. 26818581

Resoultion Copper Mining, Arizona

FAR WEST FOCUSED RESIDUAL BOUGER ANOMALY MAP

Figure 11

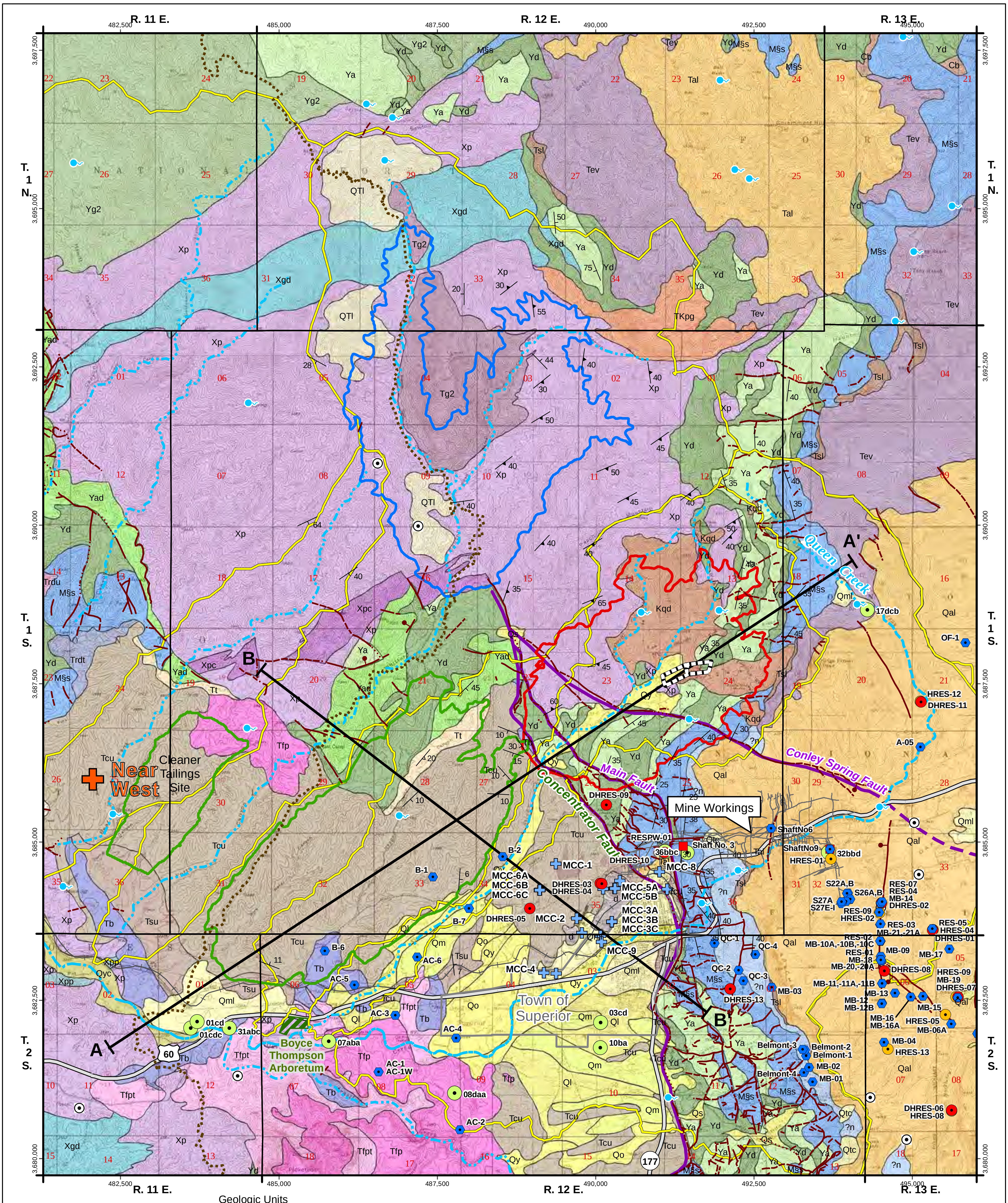

EXPLANATION

- Apache Leap Tuff Aquifer Monitor Well
- Deep Groundwater System Monitor Well
- West Plant Monitor Well
- Shaft
- Historic/Current Point of Groundwater Withdrawal
- Exploration Borehole
- Spring
- Watershed Boundary
- Silver King Canyon Site
- Whitford Canyon Site
- Happy Camp Site
- Arizona Trail
- Resolution Claims

Geologic Structural Features

- Fault; dashed where approximately located; dotted where concealed. Bar and Ball on Downthrown Side.
- 40 Strike and Dip of Beds
- 30 Strike and Dip of Metamorphic Foliation
- 15 Strike and Dip of Igneous Foliation

Geologic Units

- d-Holocene Disturbed Surficial Deposits
- Qyc- Holocene Active Alluvium
- Qtc-Holocene & Pleistocene Tallus & Colluvium
- Qy-Holocene Low Terrace & Alluvial Fan Deposits
- Qml-Late Pleistocene to Middle Pleistocene Alluvium Undifferentiated
- Qm-Mid Pleistocene Dissected Alluvial Fan & Terrace Deposits
- Ql-Late Pleistocene Moderately Dissected Alluvial Fan & Terrace Deposits
- Qo-Early Pleistocene Deeply Dissected Alluvium Undifferentiated
- Qs-Quaternary Surficial Deposits
- Qtc-Holocene & PleistoceneTalus & Colluvium
- Qal-Quaternary Alluvium
- QTl-Holocene or Pliocene Landslide Deposits
- Tcu-Miocene Conglomerate
- Tsu-Miocene Sandstone
- Tt-Miocene Tuff (poorly welded)
- Tfp-Mid Miocene to Early Miocene Felsic Lava Flows Picketpost Mountain
- Tfpt-Mid Miocene to Early Miocene Tuffs Picketpost Mountain
- Tb-Mid Miocene to Early Miocene Basalt Picket Post Mountain
- Tg2-Miocene Granitoid Stock of Wood Camp Canyon
- Trdu-Middle Miocene Undifferentiated Felsic Lava
- Tal-Early Miocene Apache Leap Tuff
- Trdt-Early Miocene Undifferentiated Felsic Tuffs
- Tev-Early Miocene Volcanic Rocks
- Tsl-Miocene to Late Oligocene Clastic Rocks
- TKpg-Late Cretaceous or Paleocene Porphyry of Government Hill
- Kqd-Late Cretaceous Quartz Diorite of Peachville Wash
- ?n-Naco Formation
- M§s-Mississipian/Devonian/Cambrian Undifferentiated Escabrosa, Martin & Bolsa
- Cb-Bolsa Quartzite
- Yad-Mid Proterozoic Apache Group, Troy Quartzite & Diabase
- Yd-Mid Proterozoic Diabase
- Ya-Mid Proterozoic Apache Group
- Yg2-Mid Proterozoic Porphyritic Biotite Granite
- Xgd-Early Proterozoic Granodiorite to Granite
- Xp-Early Proterozoic Pinal Schist
- Xpc-Pinal Schist Calc - Silicate & Amphibolite Facies
- Xpp-Pinal Schist - Phyllite Facies

(Geology from Spencer and others, 1998; Faults from Peterson, 1969, and Spencer and Richard, 1995)

DRAFT

0 1,000 2,000
Meters

0 2,000 4,000 6,000 8,000
Feet

A A' Location of Hydrogeologic Section

URS	Project No. 26818581 Resolution Copper Mining, Arizona	NEAR WEST GEOLOGIC MAP SHOWING MAPPED LOCAL FAULTS	Figure 12

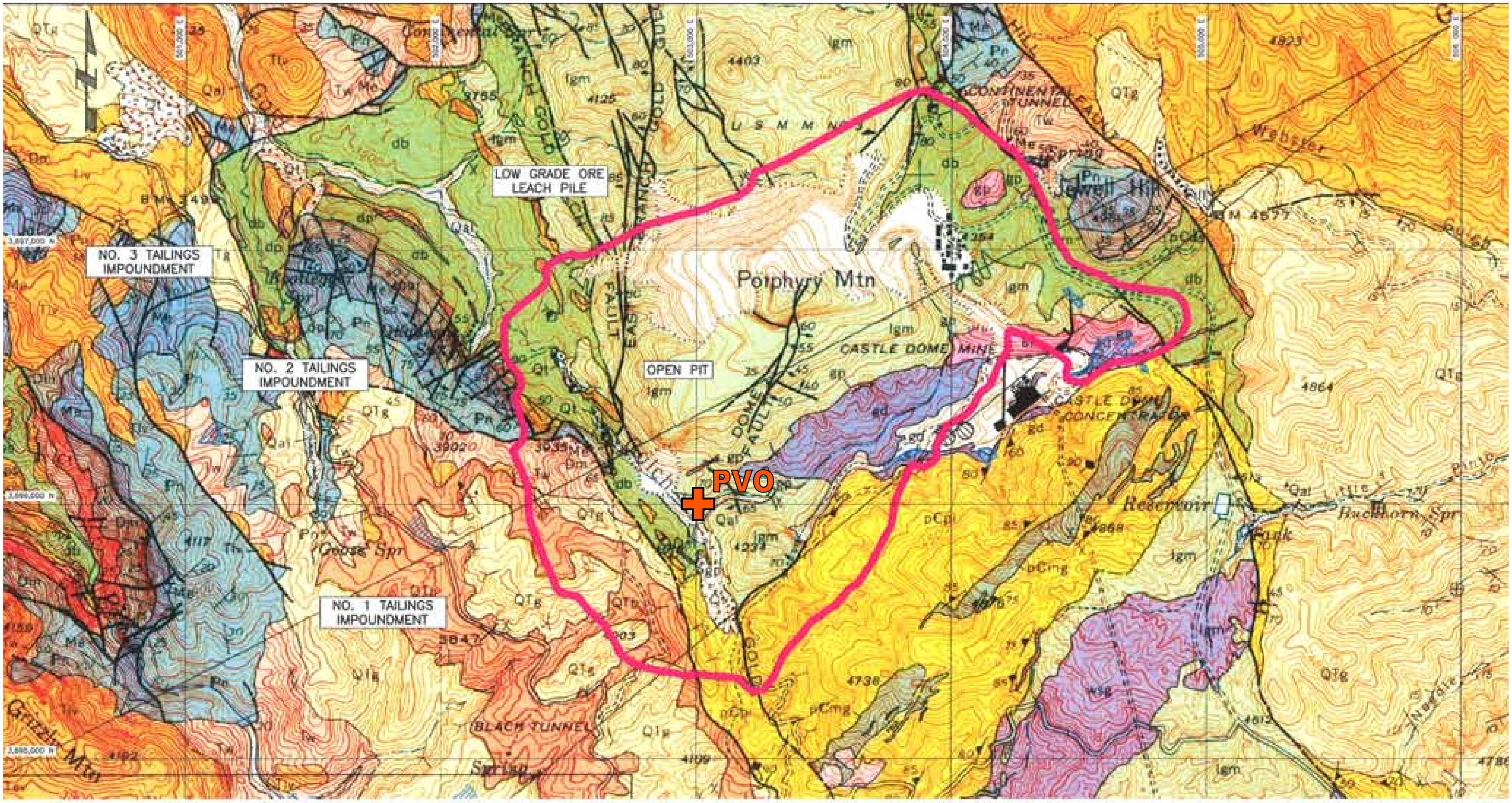

LEGEND

OUTLINE OF CURRENT OPEN PIT

NOTES:

1. GEOLOGY EXCERPT FROM PETERSON, N.P. (1962). GEOLOGY AND ORE DEPOSITS OF THE GLOBE – MIAMI DISTRICT, ARIZONA. U.S.G.S. PROFESSIONAL PAPER 342, PLATE 1
2. SEE APPENDIX FIGURE V-17 FOR GEOLOGY LEGEND.

NOT FOR CONSTRUCTION

OCT. 2012

0 500 m

URS	Project No. 26818581	PVO GEOLOGIC MAP	Figure 13
	Resolution Copper Mining, Arizona		

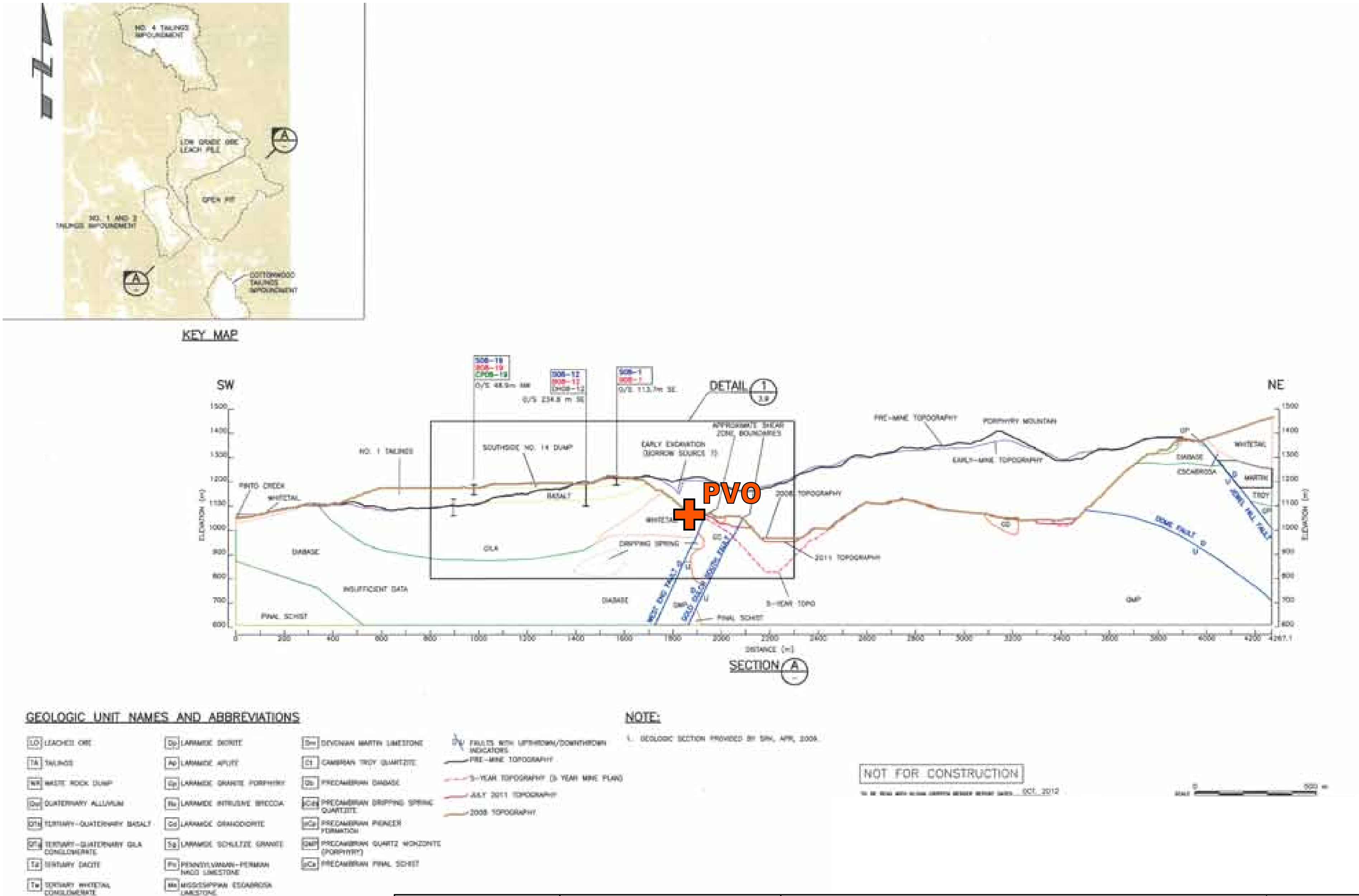

URS	Project No. 26818581	PVO GEOLOGIC CROSS SECTION	Figure 14
	Resolution Copper Mining, Arizona		

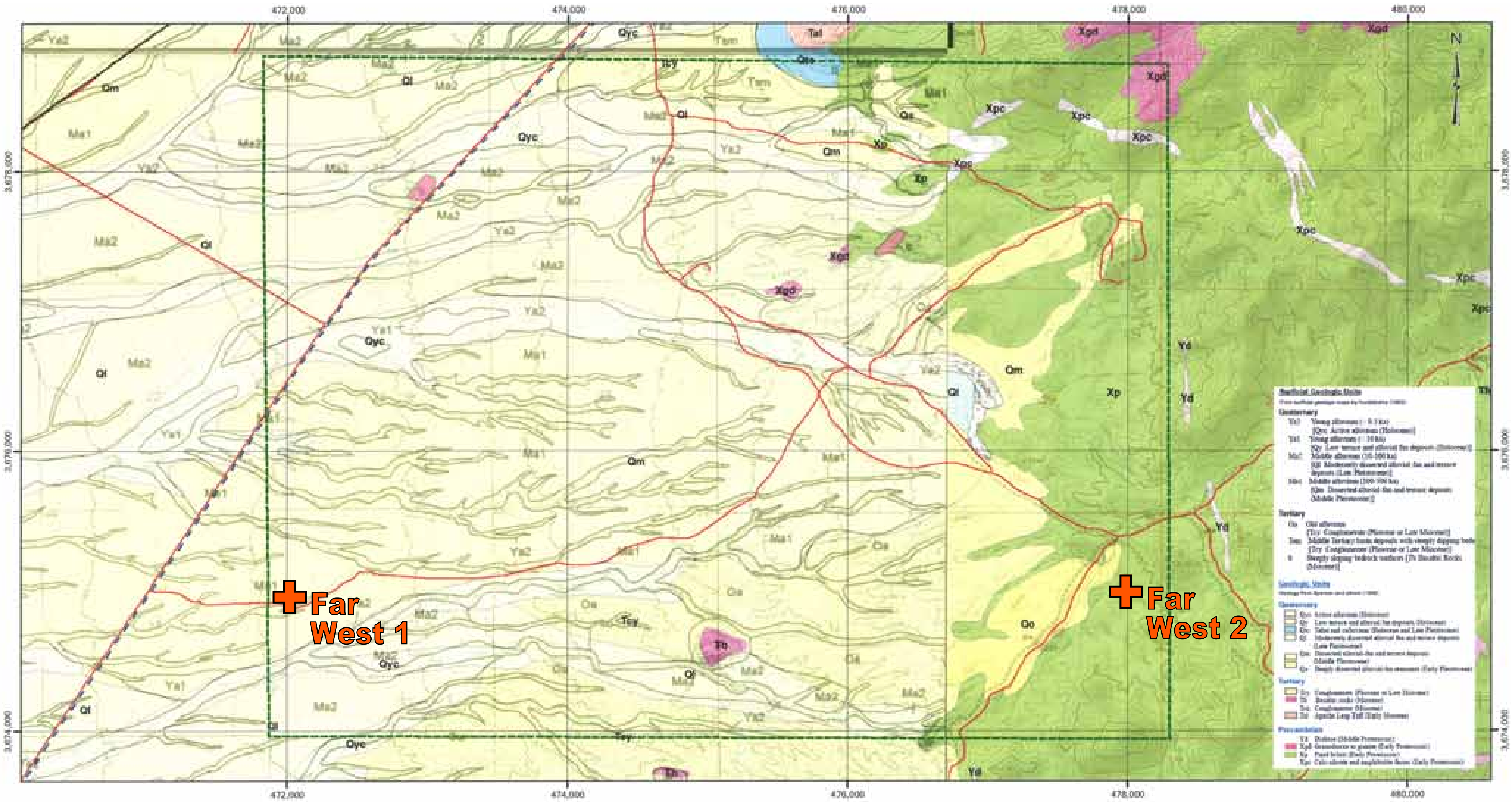

LEGEND

- RAIL
- PIPELINE
- ROAD
- FAR WEST STUDY AREA

NOT FOR CONSTRUCTION

DRAFT

Notes:
1. NAD27 UTM12
2. Regional geological map based on Huckleberry (1993) and Spencer and others (1996). Provided by Montgomery and Associates.
3. Additional topographic data from USGS and National Geographic Society topographic maps, accessed via ESRI ArcGIS Online.

URS	Project No. 26818581 Resolution Copper Mining, Arizona	FAR WEST MAP OF SURFICIAL GEOLOGY	Figure 15

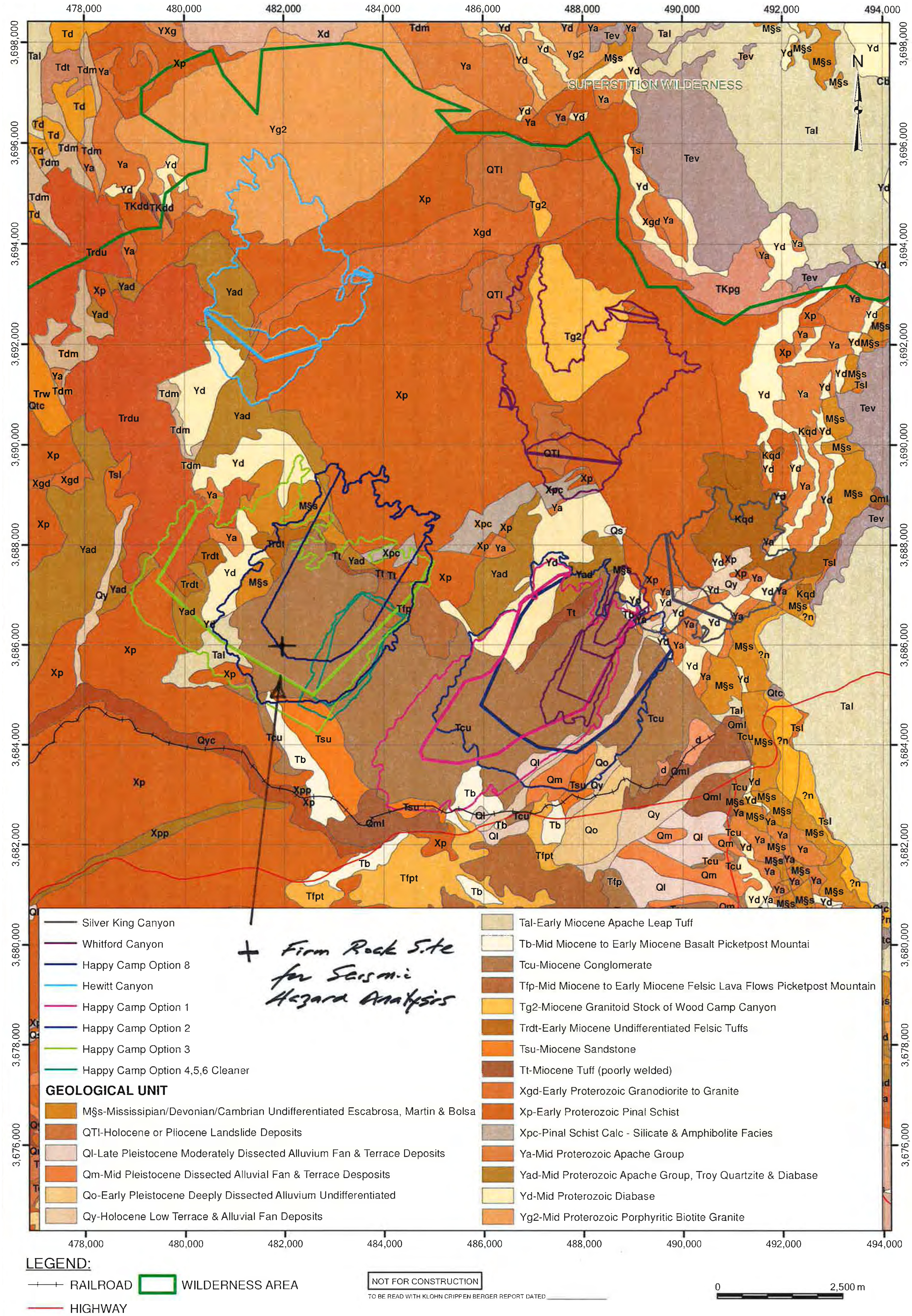

NOT FOR CONSTRUCTION

TO BE READ WITH KLOHN CRIPPEN BERGER REPORT DATED ______

NOTES:

1. PROJECTION AND DATUM: UTM12N NAD27
2. GEOLOGY DATA FROM SPENCE ET AL., 1998; FAULTS AND PETERSON, 1969 AND SPENCER AND RICHARDS, 1995.

URS	Project No. 26818581	NEAR WEST MAP OF SURFICIAL GEOLOGY	Figure 16
	Resolution Copper Mining, Arizona		

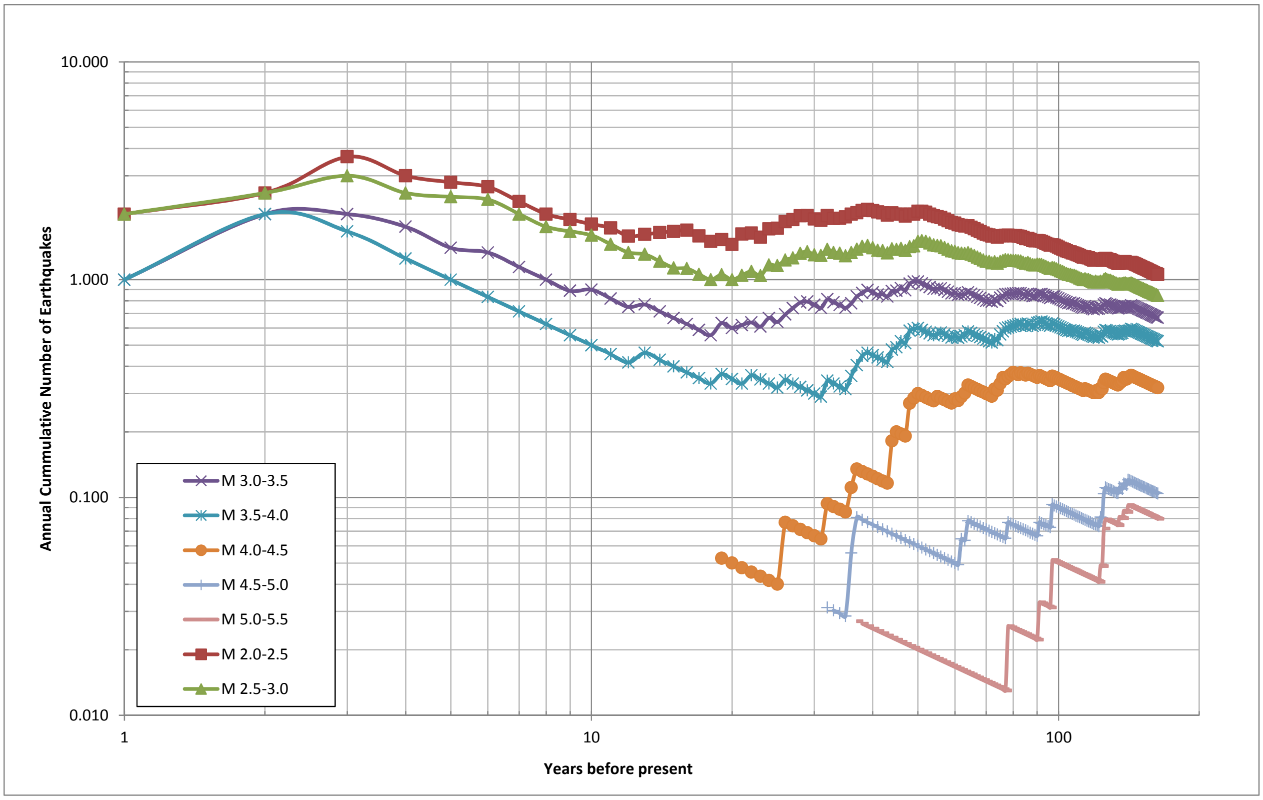

URS	Project No. 26818581	STEPP PLOT FOR THE COMBINED BASIN AND RANGE AND TRANSTION ZONE PROVINCES	Figure 17
	Resolution Copper Arizona		

W:\x_wcfs\PROJECTS\Resolution Copper Mine\Seismicity\Stepp Plot Fig17.grf

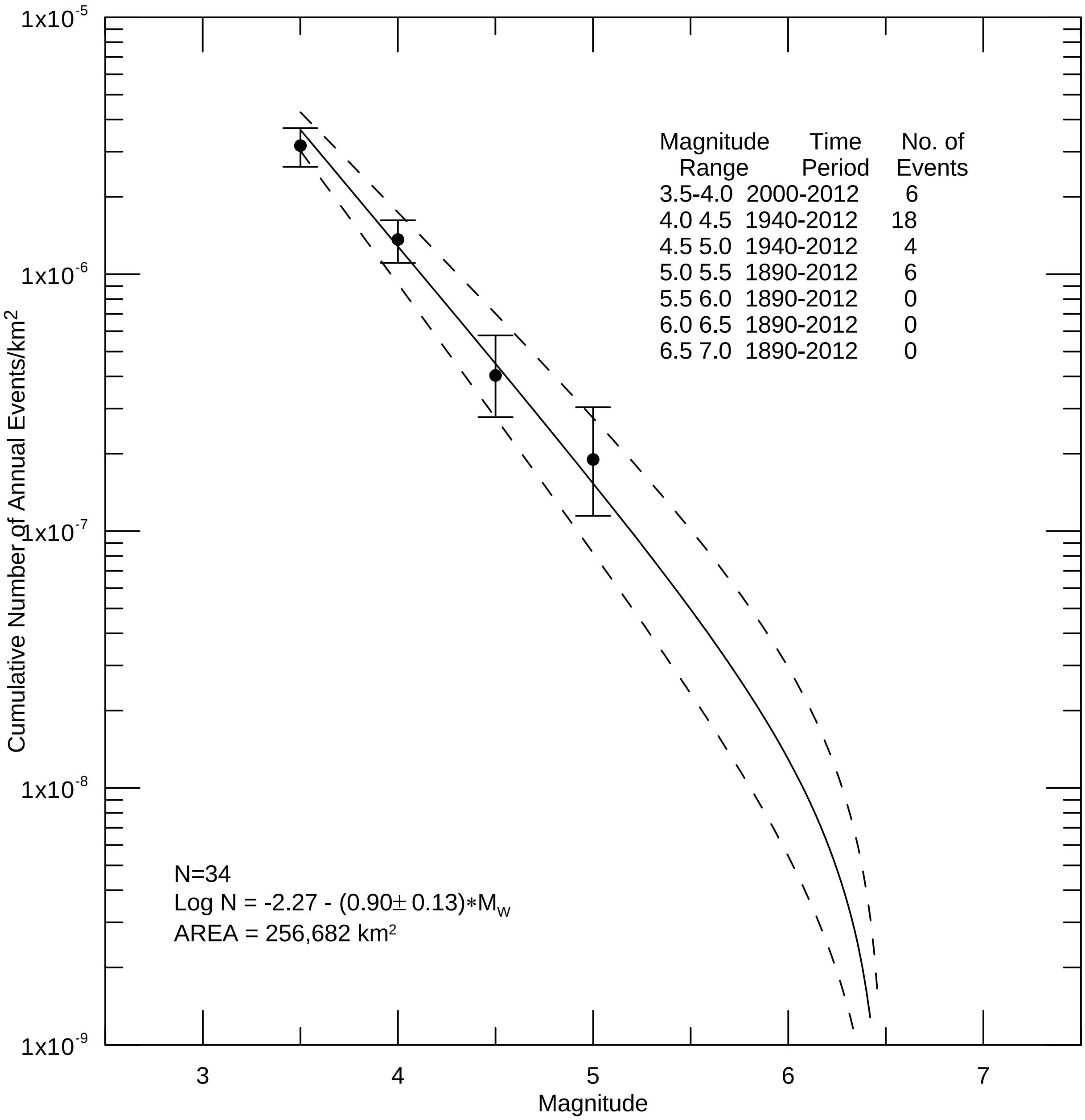

Return Periods
for zone

M5.0	24 yr
M6.0	195 yr
M6.5	554 yr

URS	Project No. 26818581 Resolution Copper Arizona	EARTHQUAKE RECURRENCE FOR THE COMBINED SOUTHERN ARIZONA BASIN AND RANGE AND TRANSITION ZONE	Figure 18

W:\x_wcfs\PROJECTS\Resolution Copper Mine\Seismicity\recurrence\CombinedZones\rec-CB_6_Final_Figure.grf

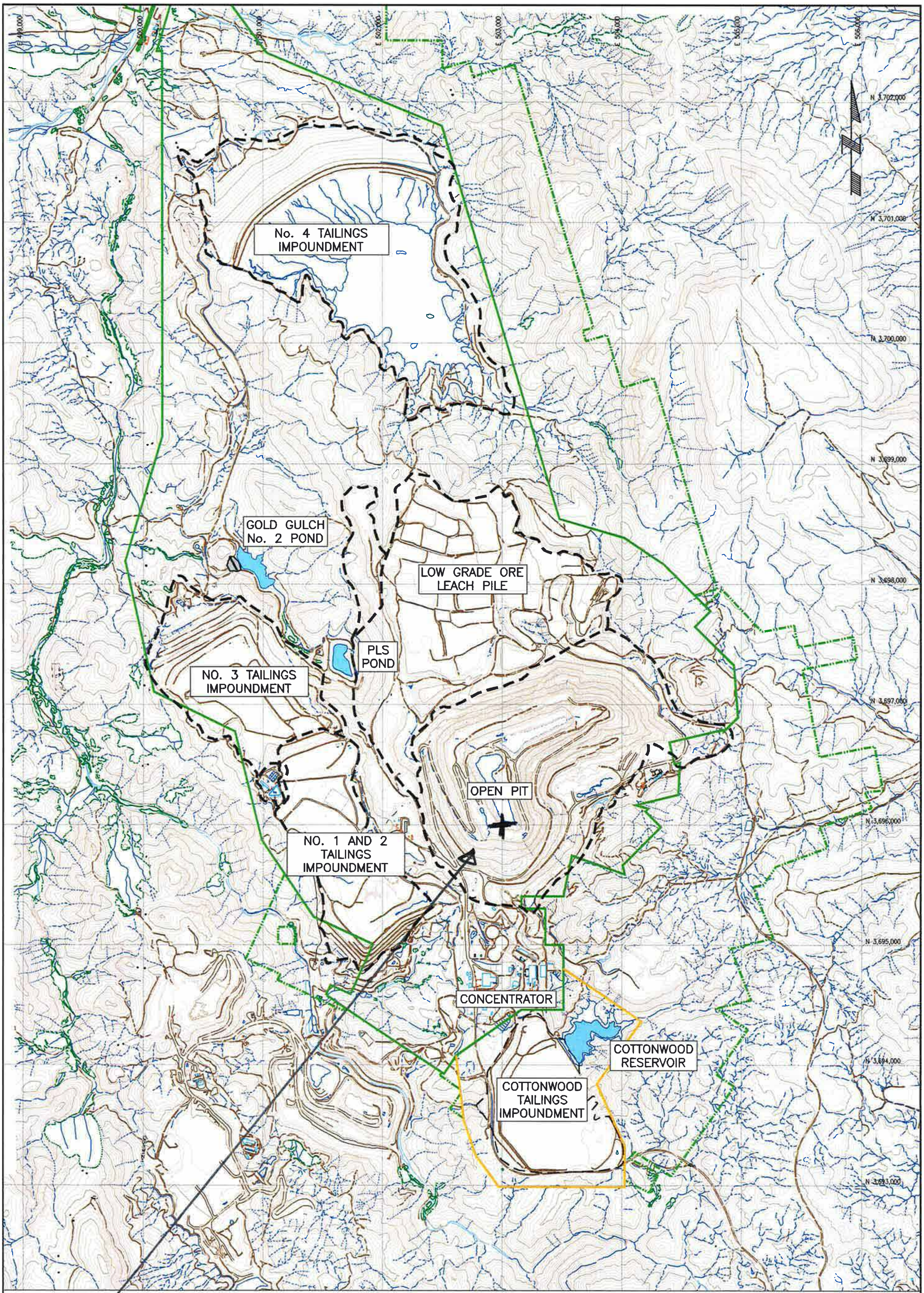

LEGEND

- CREEK
- PATENTED PROPERTY BOUNDARY
- UNPATENTED PROPERTY BOUNDARY
- PERMITTED BOUNDARY

+ Hard rock site Seismic Hazard Ana

NOT FOR CONSTRUCTION

TO BE READ WITH KLOHN CRIPPEN BERGER REPORT DATED OCT. 2012

SCALE 0 750 m

NOTE:

1. DIGITAL TOPOGRAPHY PROVIDED BY RESOLUTION – JULY, 2011. DATUM: UTM NAD27 ZONE 12

URS	Project No. 26818581	PVO GENERAL SITE ARRANGEMENT SHOWING SITE LOCATION	Figure 19
	Resolution Copper Mining, Arizona		

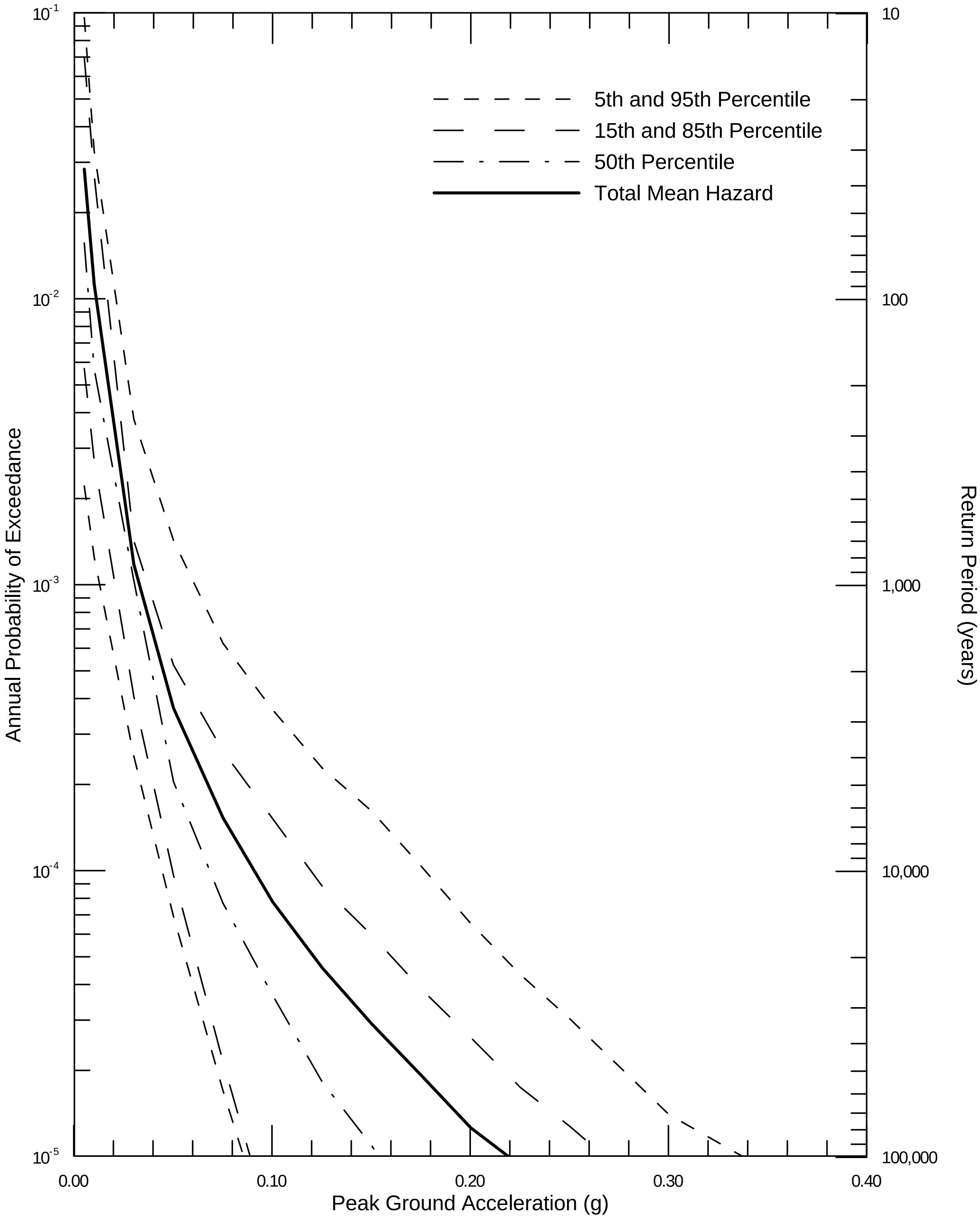

URS	Project No. 26818581 Resolution Copper Mining Arizona	SEISMIC HAZARD CURVES FOR PEAK HORIZONTAL ACCELERATION AT FAR WEST 1 SITE	Figure 20

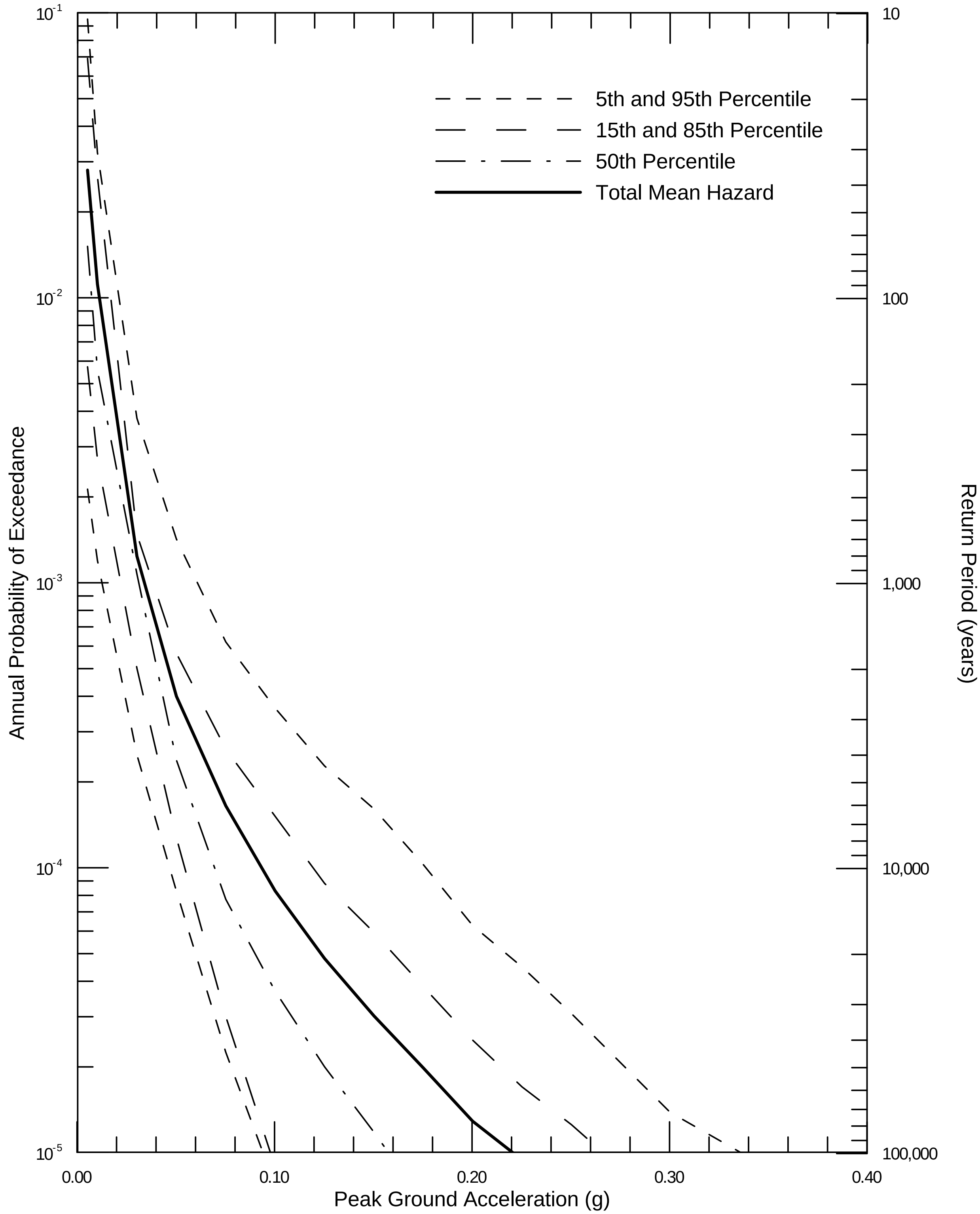

URS	Project No. 26818581 Resolution Copper Mining Arizona	SEISMIC HAZARD CURVES FOR PEAK HORIZONTAL ACCELERATION AT FAR WEST 2 SITE	Figure 21

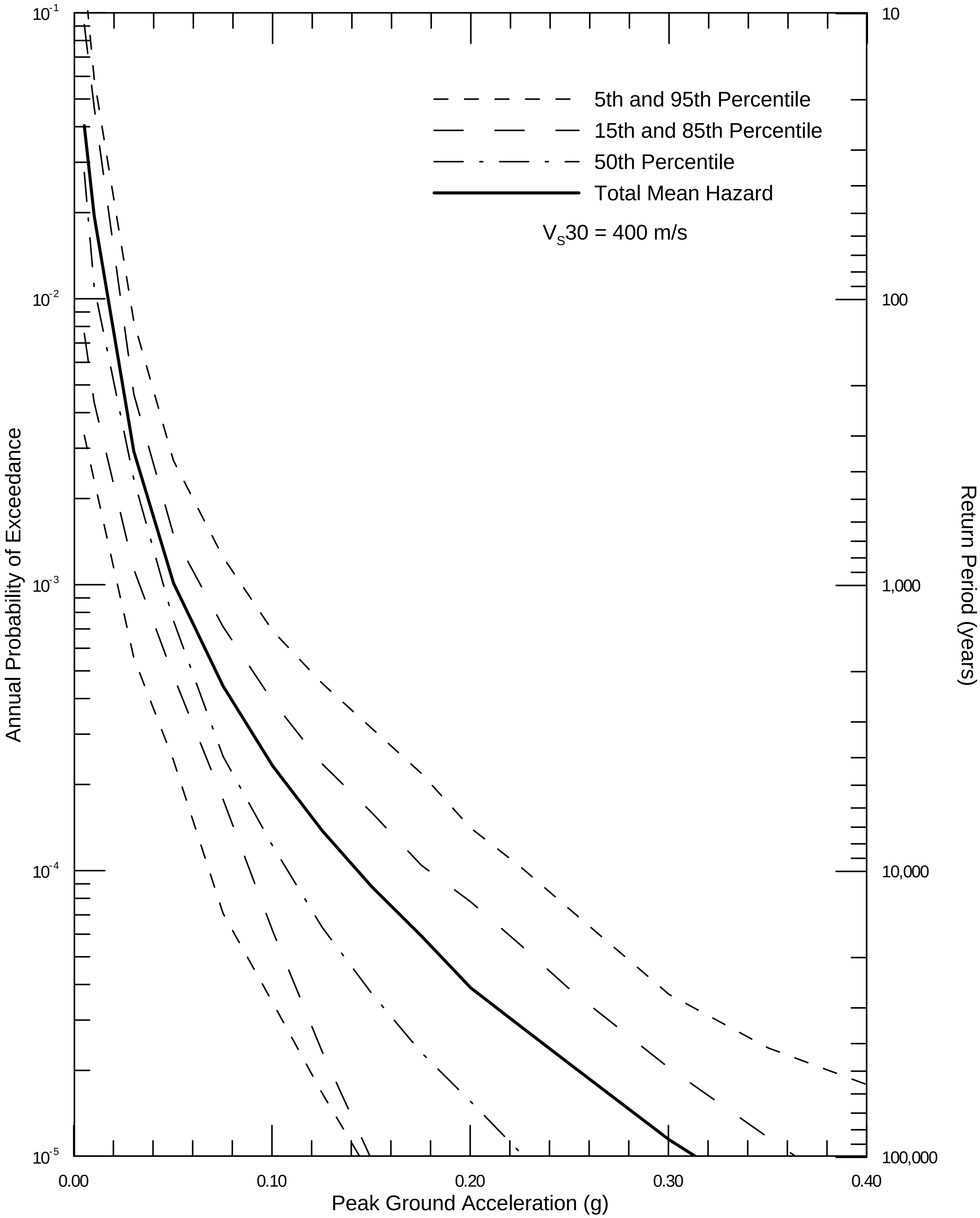

URS	Project No. 26818581 Resolution Copper Mining Arizona	SEISMIC HAZARD CURVES FOR PEAK HORIZONTAL ACCELERATION AT NEAR WEST SITE	Figure 22

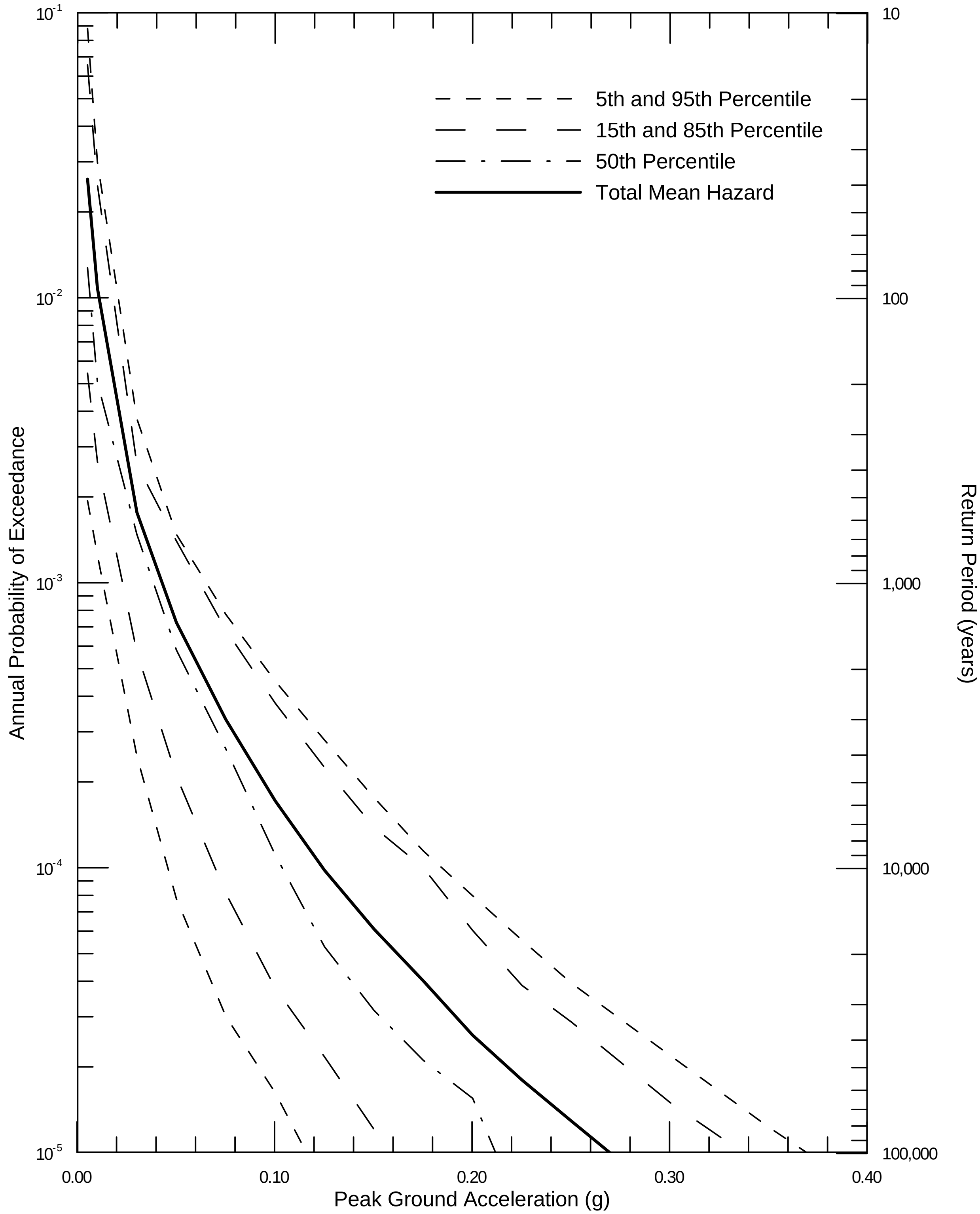

URS	Project No. 26818581	SEISMIC HAZARD CURVES FOR PEAK HORIZONTAL ACCELERATION AT PINTO VALLEY SITE	Figure 23
	Resolution Copper Mining Arizona		

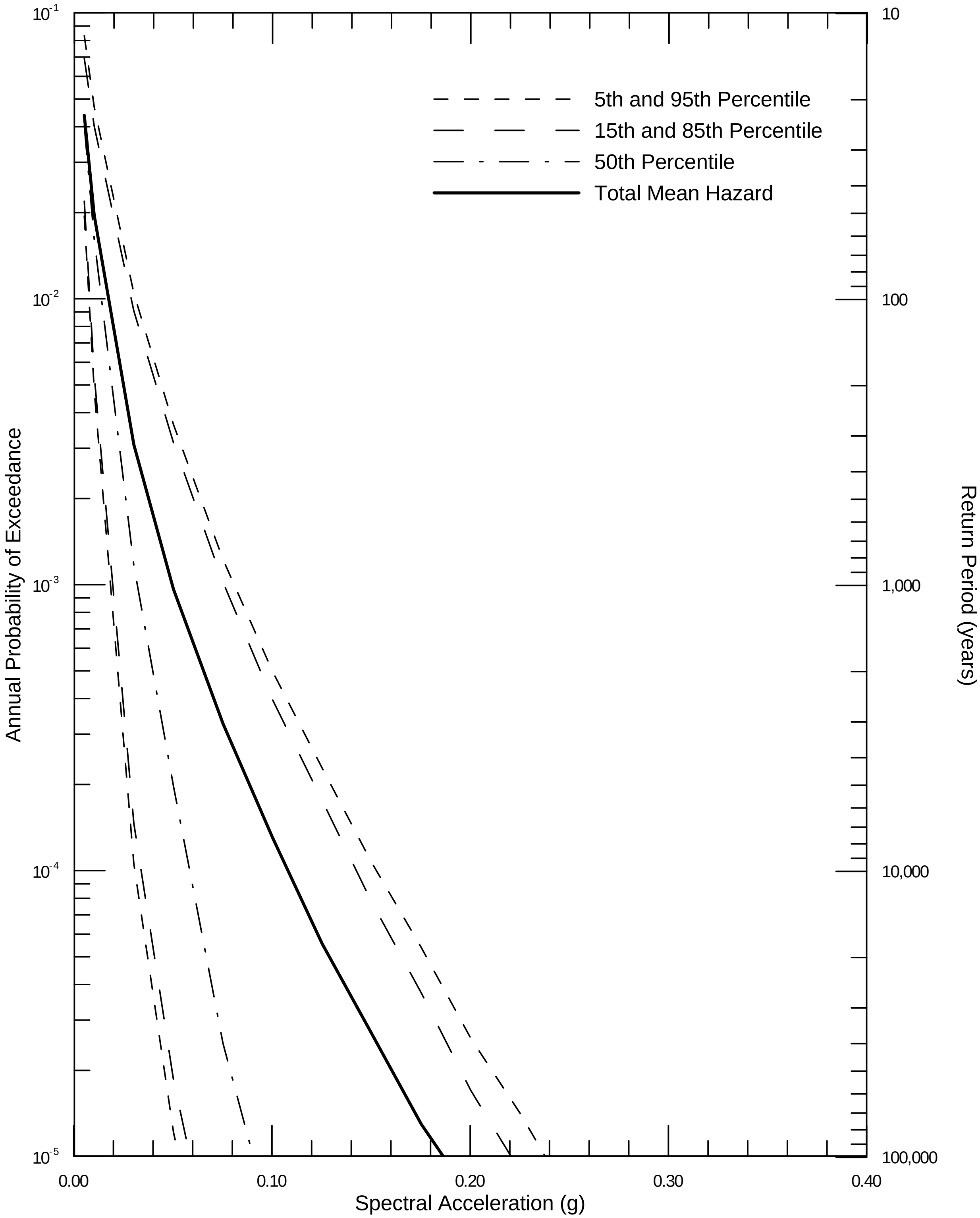

URS	Project No. 26818581 Resolution Copper Mining Arizona	SEISMIC HAZARD CURVES FOR 1.0 SEC HORIZONTAL SPECTRAL ACCELERATION AT FAR WEST 1 SITE	Figure 24

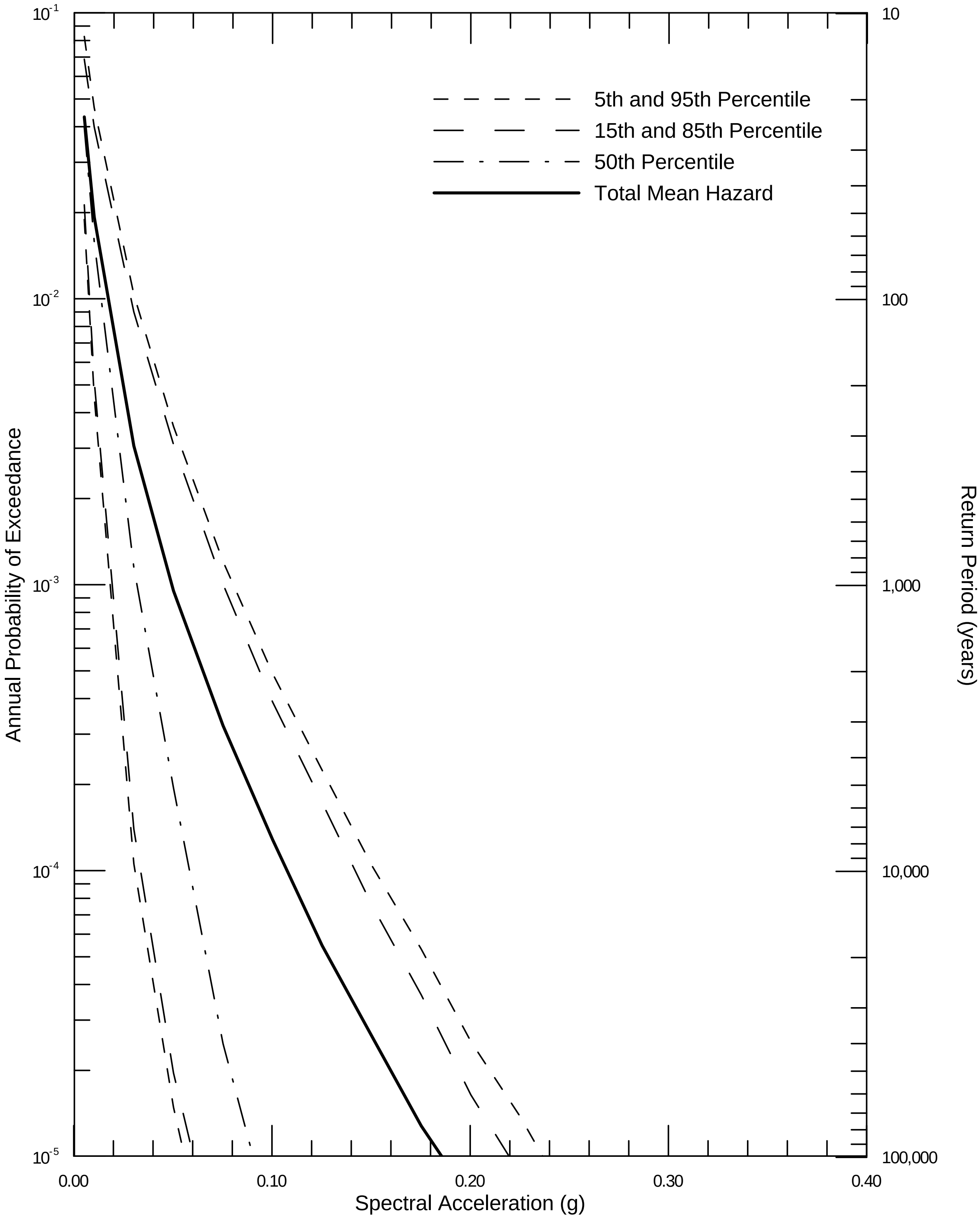

URS

Project No. 26818581

Resolution Copper Mining
Arizona

SEISMIC HAZARD CURVES FOR 1.0 SEC
HORIZONTAL SPECTRAL ACCELERATION
AT FAR WEST 2 SITE

Figure
25

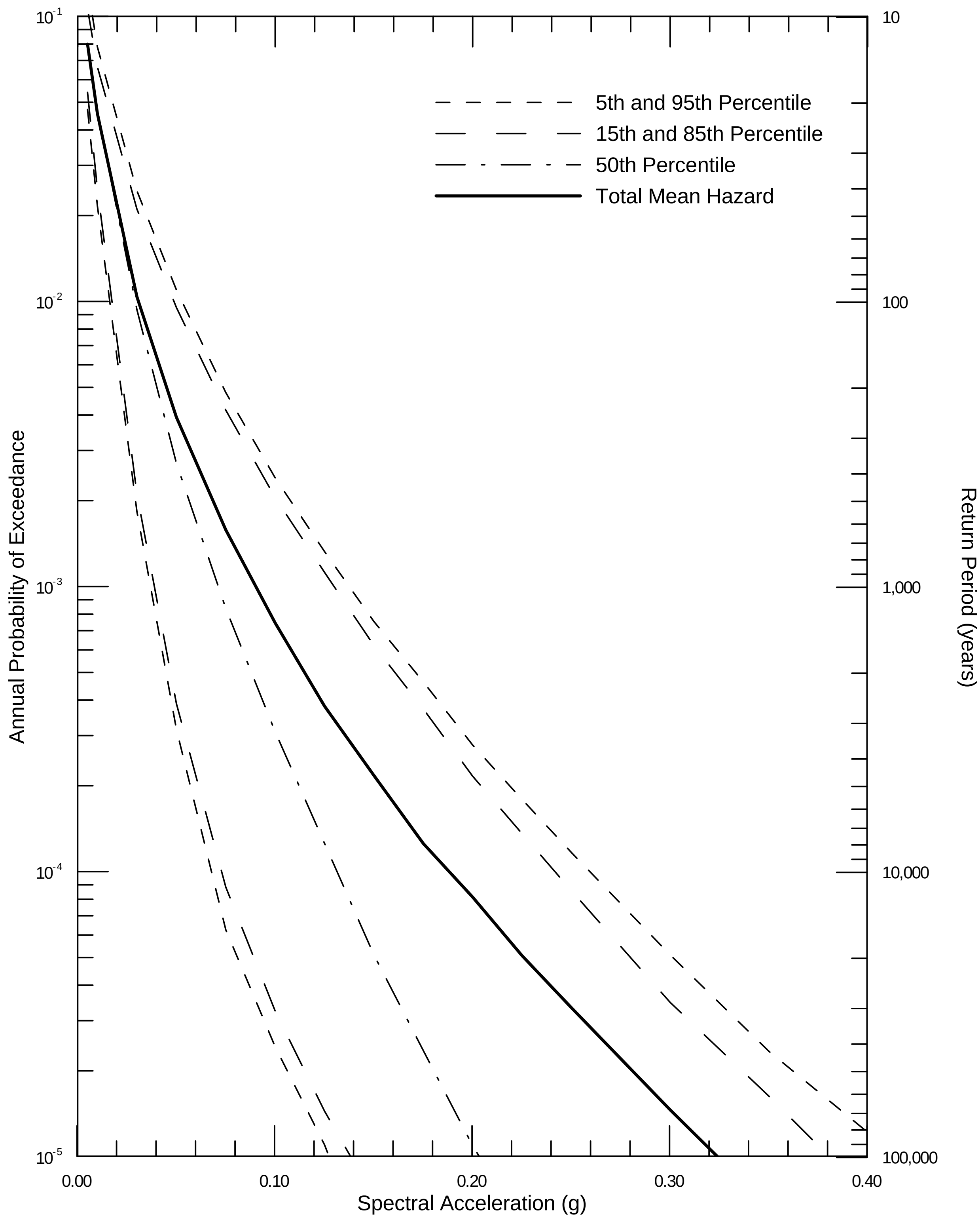

	Project No. 26818581	SEISMIC HAZARD CURVES FOR 1.0 SEC HORIZONTAL SPECTRAL ACCELERATION AT NEAR WEST SITE	Figure 26
URS	Resolution Copper Mining Arizona		

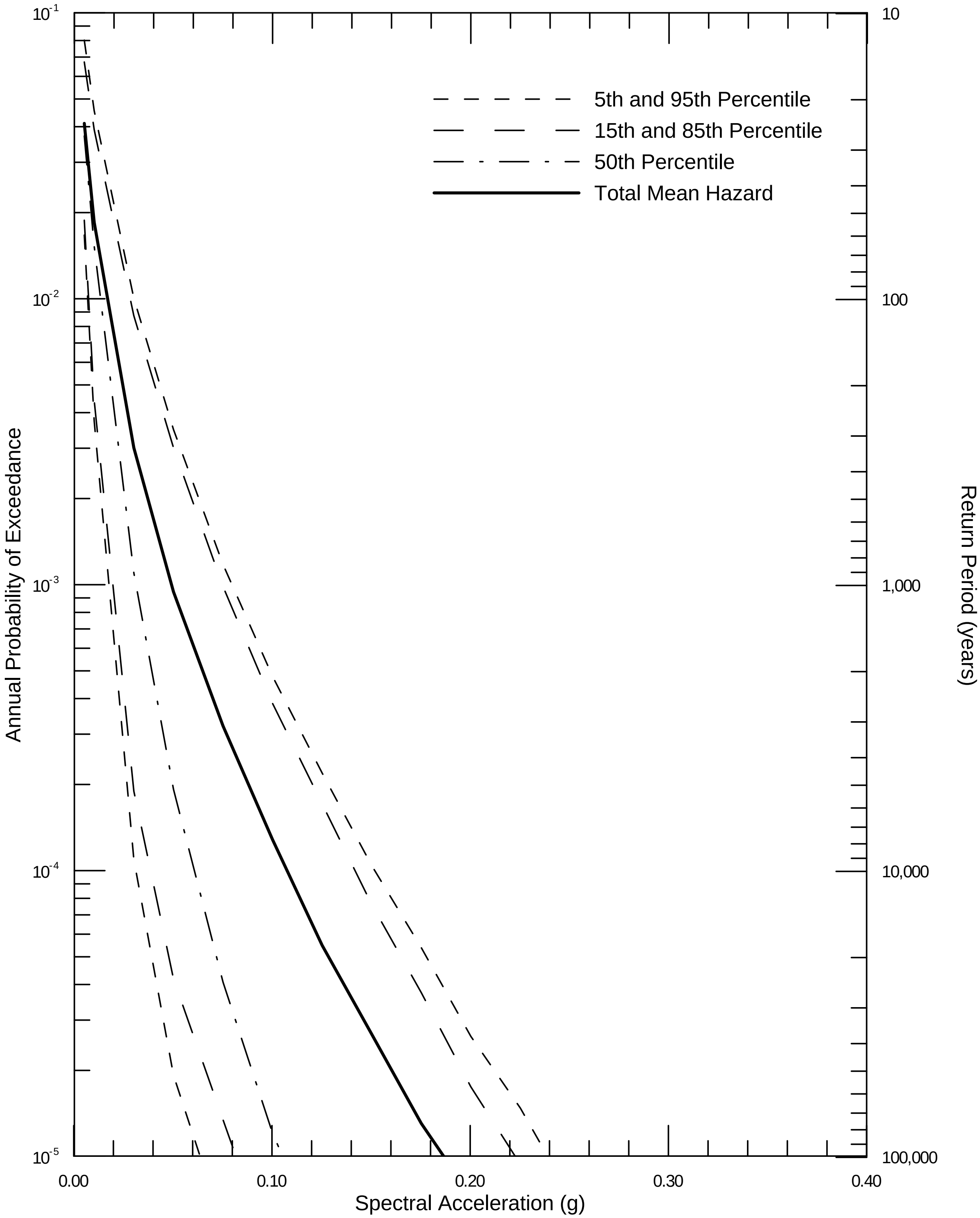

URS	Project No. 26818581	SEISMIC HAZARD CURVES FOR 1.0 SEC HORIZONTAL SPECTRAL ACCELERATION AT PINTO VALLEY SITE	Figure 27
	Resolution Copper Mining Arizona		

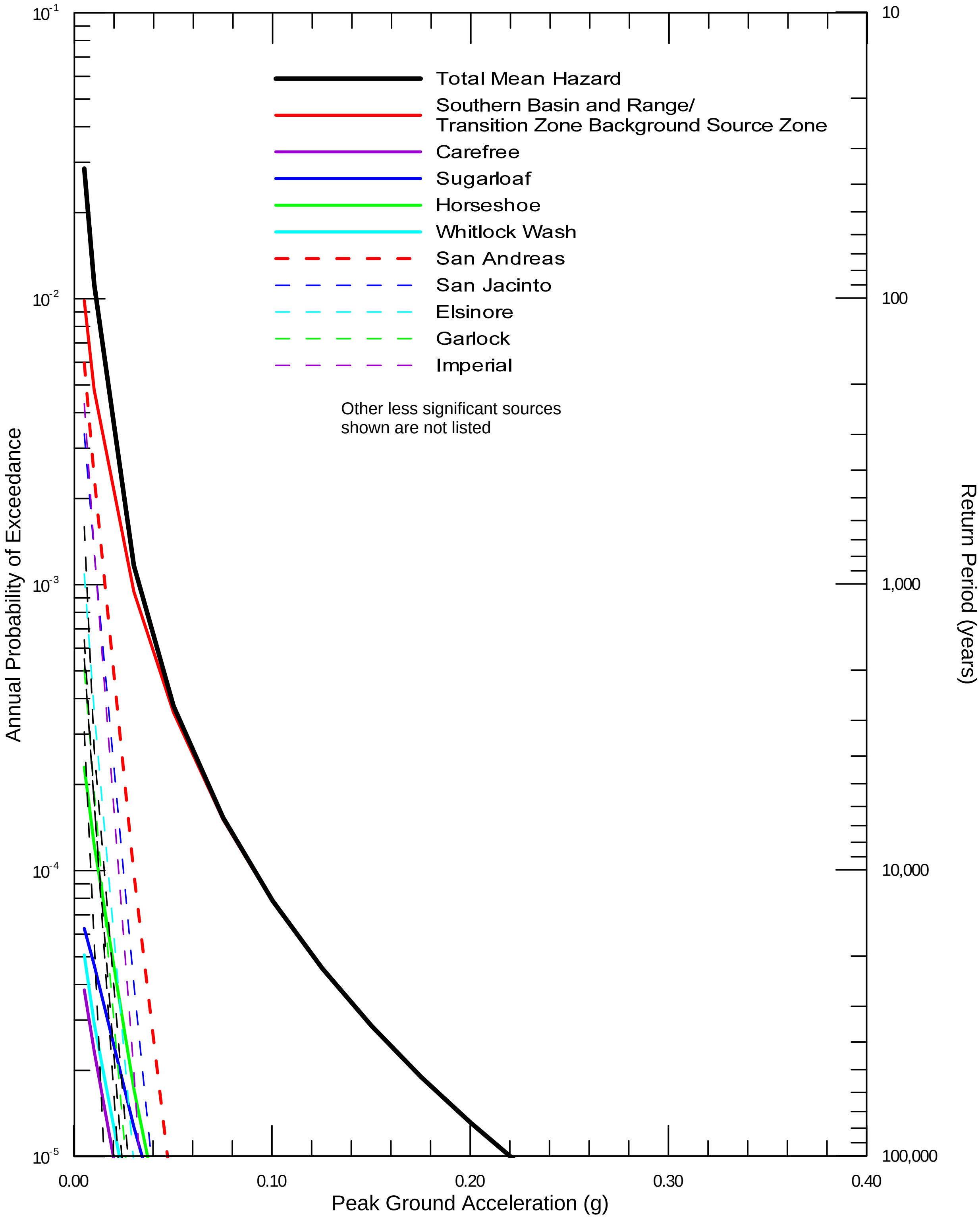

URS	Project No. 26818581 Resolution Copper Mining Arizona	SEISMIC SOURCE CONTRIBUTIONS TO MEAN PEAK HORIZONTAL ACCELERATION HAZARD AT FAR WEST 1 SITE	Figure 28

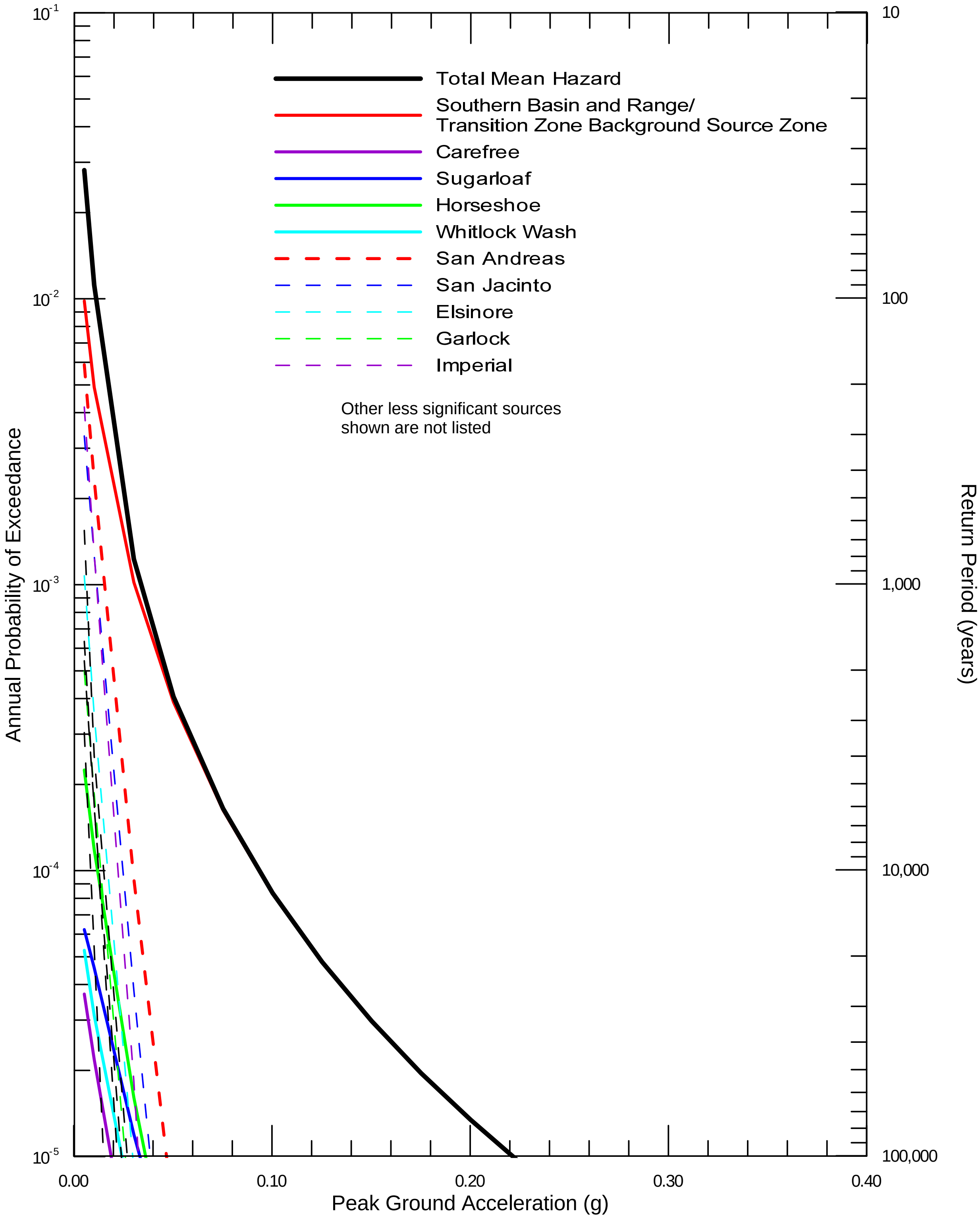

URS	Project No. 26818581 Resolution Copper Mining Arizona	SEISMIC SOURCE CONTRIBUTIONS TO MEAN PEAK HORIZONTAL ACCELERATION HAZARD AT FAR WEST 2 SITE	Figure 29

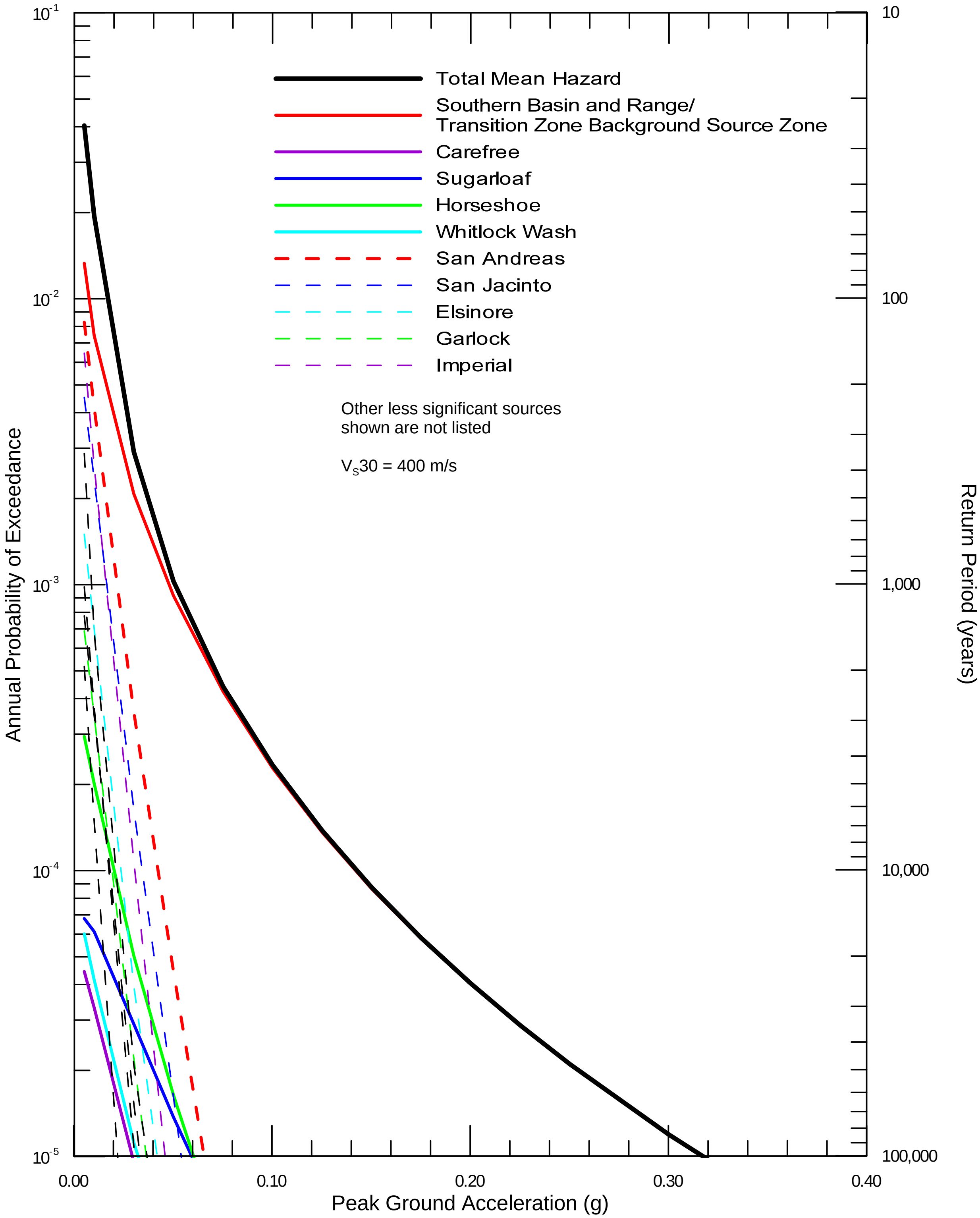

URS	Project No. 26818581 Resolution Copper Mining Arizona	SEISMIC SOURCE CONTRIBUTIONS TO MEAN PEAK HORIZONTAL ACCELERATION HAZARD AT NEAR WEST SITE	Figure 30

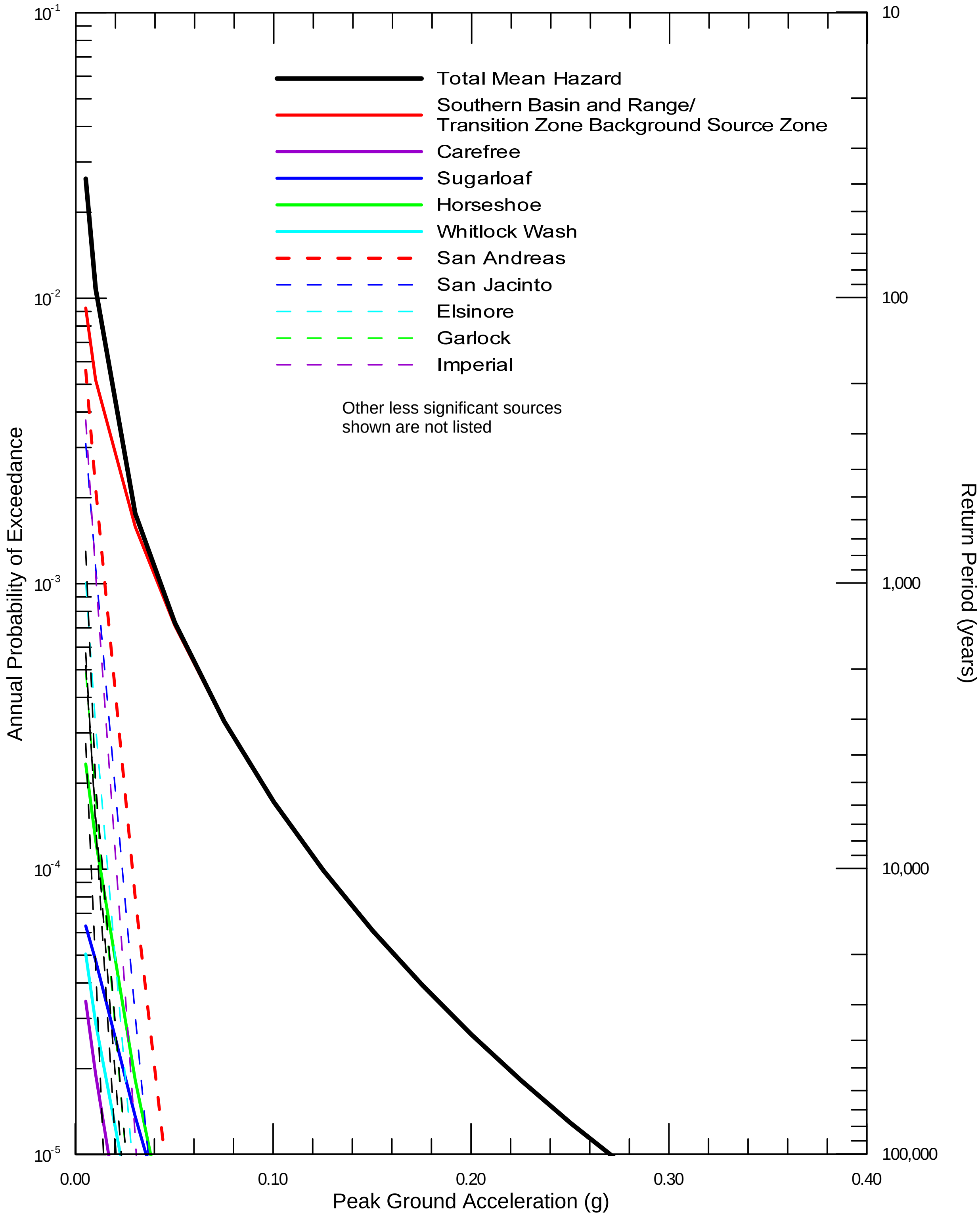

URS	Project No. 26818581 Resolution Copper Mining Arizona	SEISMIC SOURCE CONTRIBUTIONS TO MEAN PEAK HORIZONTAL ACCELERATION HAZARD AT PINTO VALLEY SITE	Figure 31

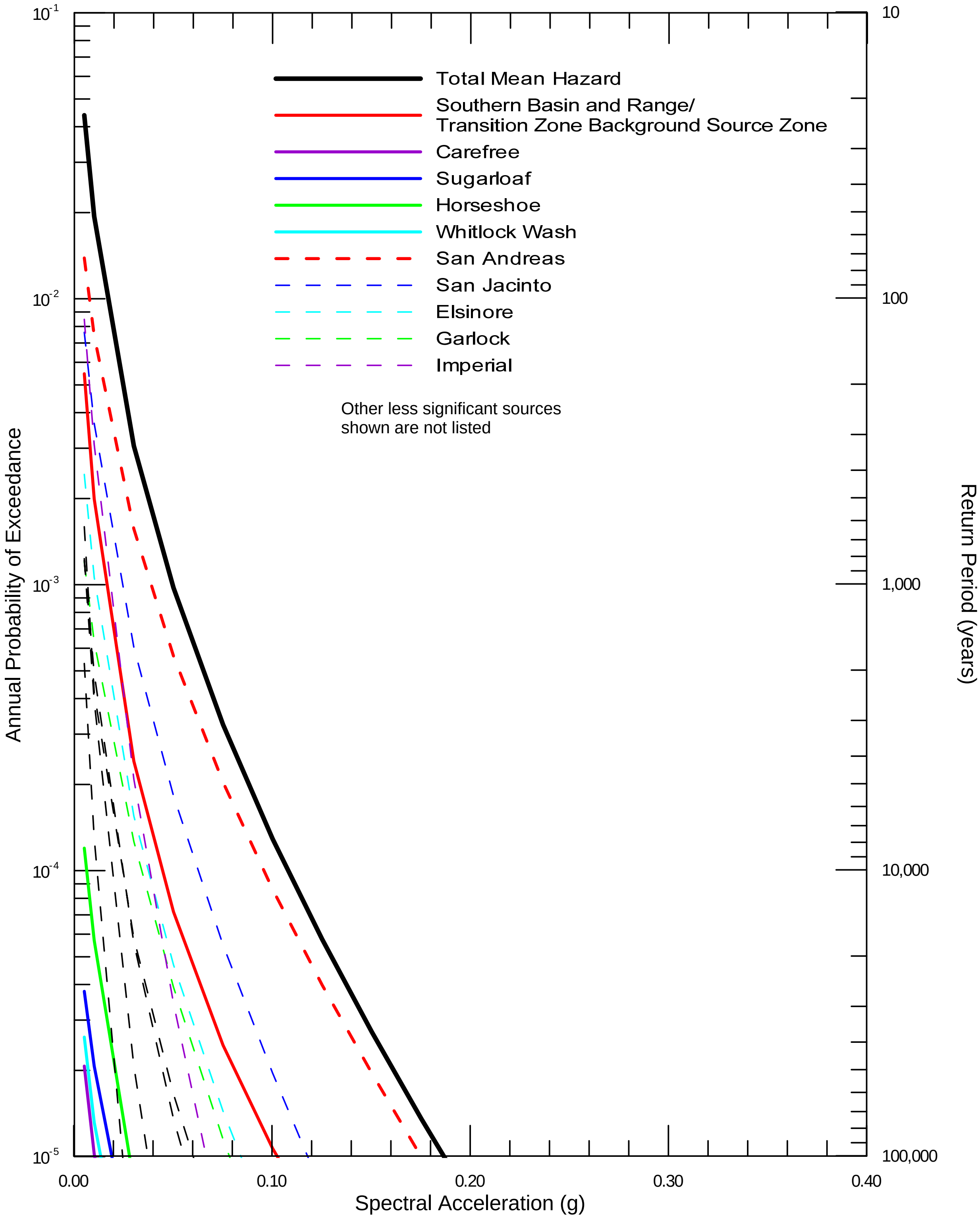

URS	Project No. 26818581 Resolution Copper Mining Arizona	SEISMIC SOURCE CONTRIBUTIONS TO MEAN 1.0 SEC HORIZONTAL SPECTRAL ACCELERATION HAZARD AT FAR WEST 1 SITE	Figure 32

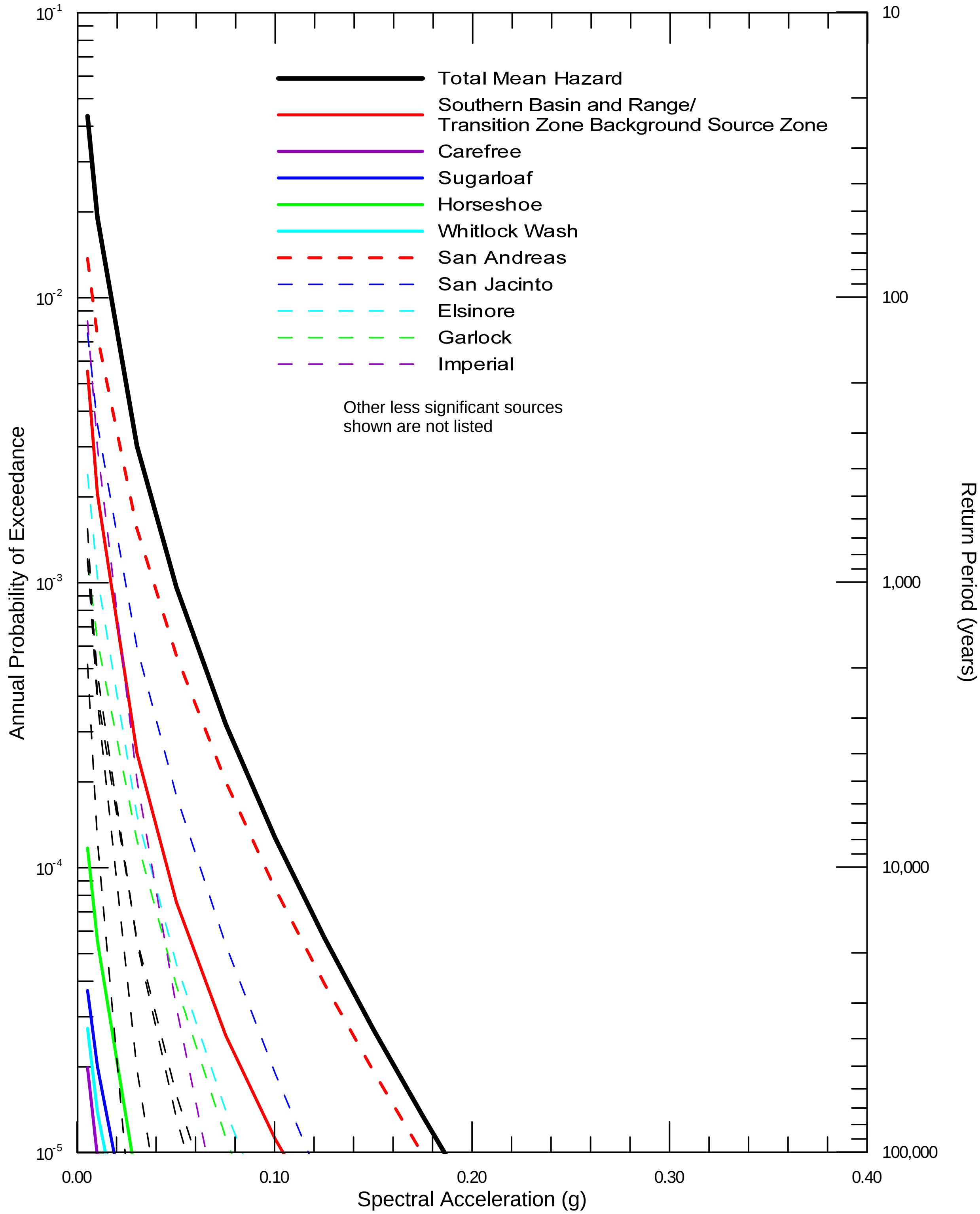

URS	Project No. 26818581 Resolution Copper Mining Arizona	SEISMIC SOURCE CONTRIBUTIONS TO MEAN 1.0 SEC HORIZONTAL SPECTRAL ACCELERATION HAZARD AT FAR WEST 2 SITE	Figure 33

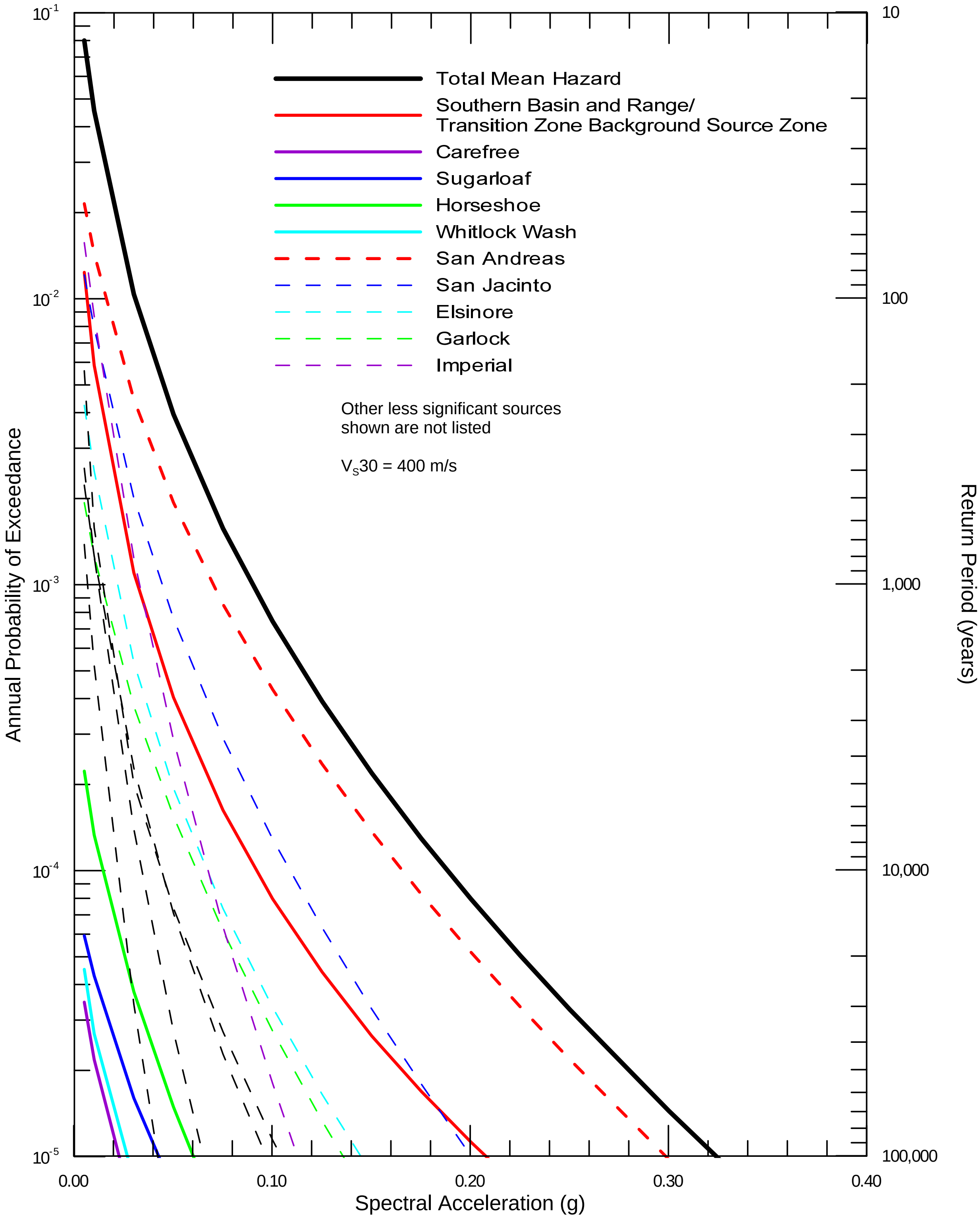

URS	Project No. 26818581 Resolution Copper Mining Arizona	SEISMIC SOURCE CONTRIBUTIONS TO MEAN 1.0 SEC HORIZONTAL SPECTRAL ACCELERATION HAZARD AT NEAR WEST SITE	Figure 34

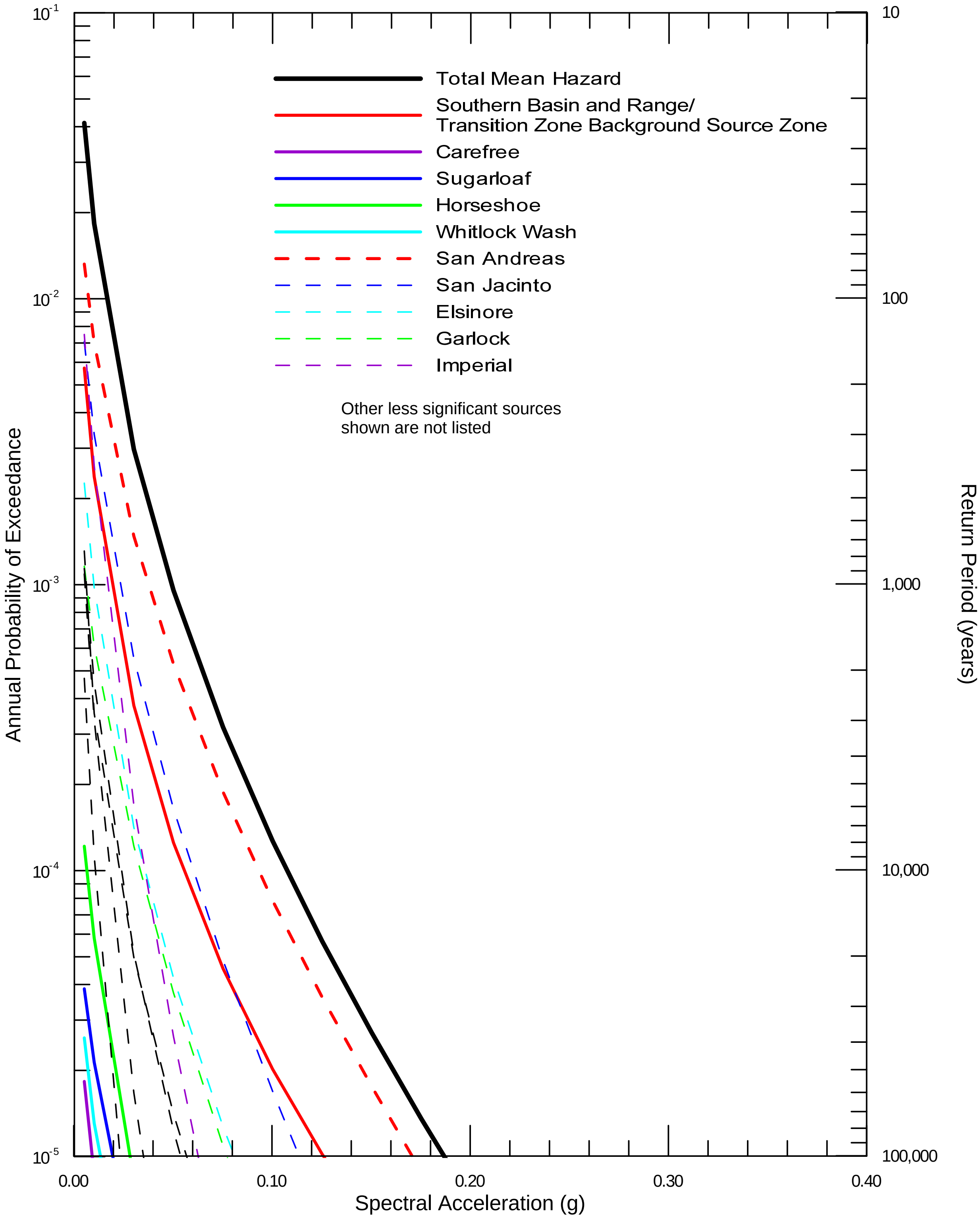

URS	Project No. 26818581 Resolution Copper Mining Arizona	SEISMIC SOURCE CONTRIBUTIONS TO MEAN 1.0 SEC HORIZONTAL SPECTRAL ACCELERATION HAZARD AT PINTO VALLEY SITE	Figure 35

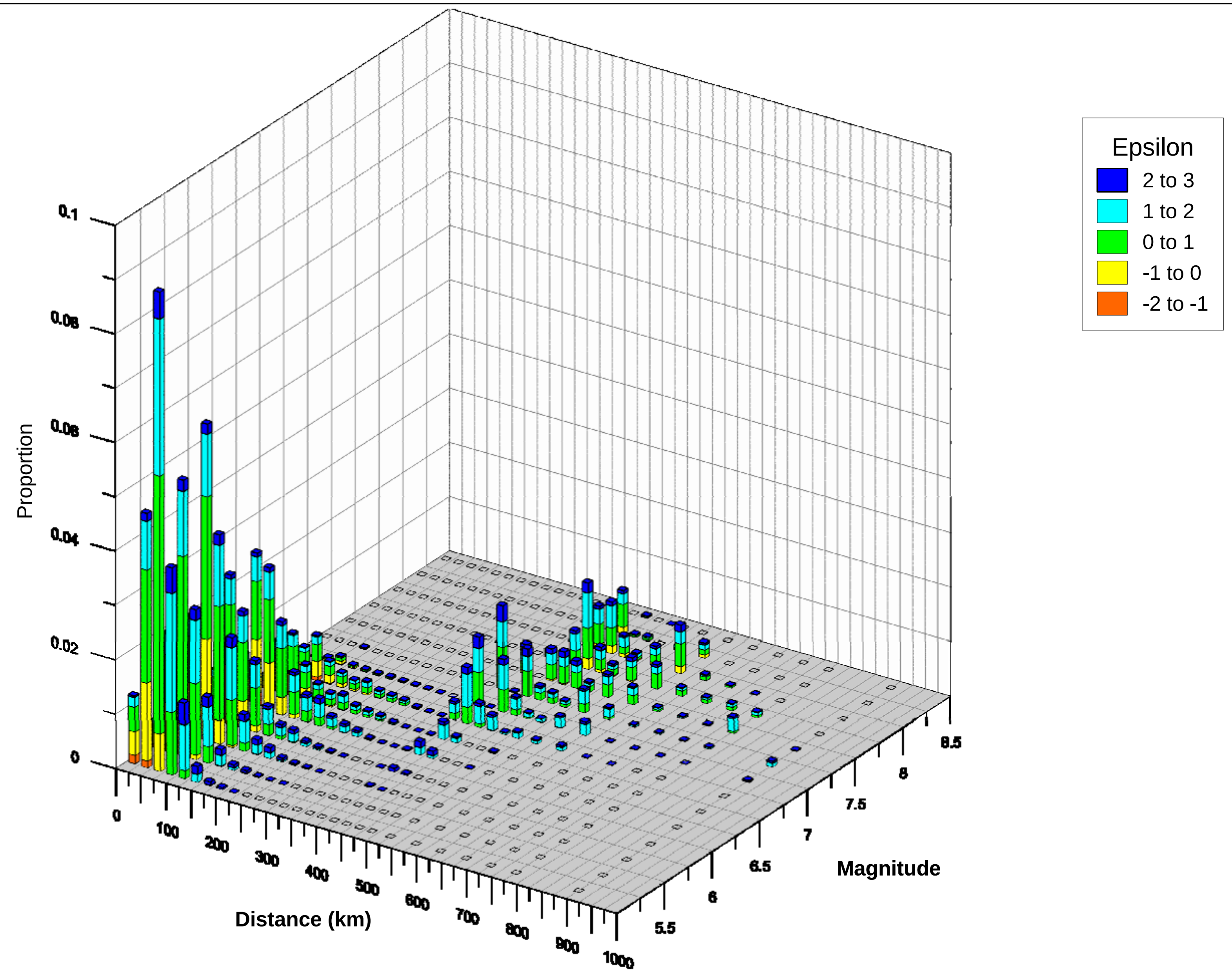

URS	Project No. 26818581 Resolution Copper Mining Arizona	MAGNITUDE AND DISTANCE CONTRIBUTIONS TO THE MEAN PEAK HORIZONTAL ACCELERATION HAZARD AT 100-YEAR RETURN PERIOD AT FAR WEST 1 SITE	Figure 36

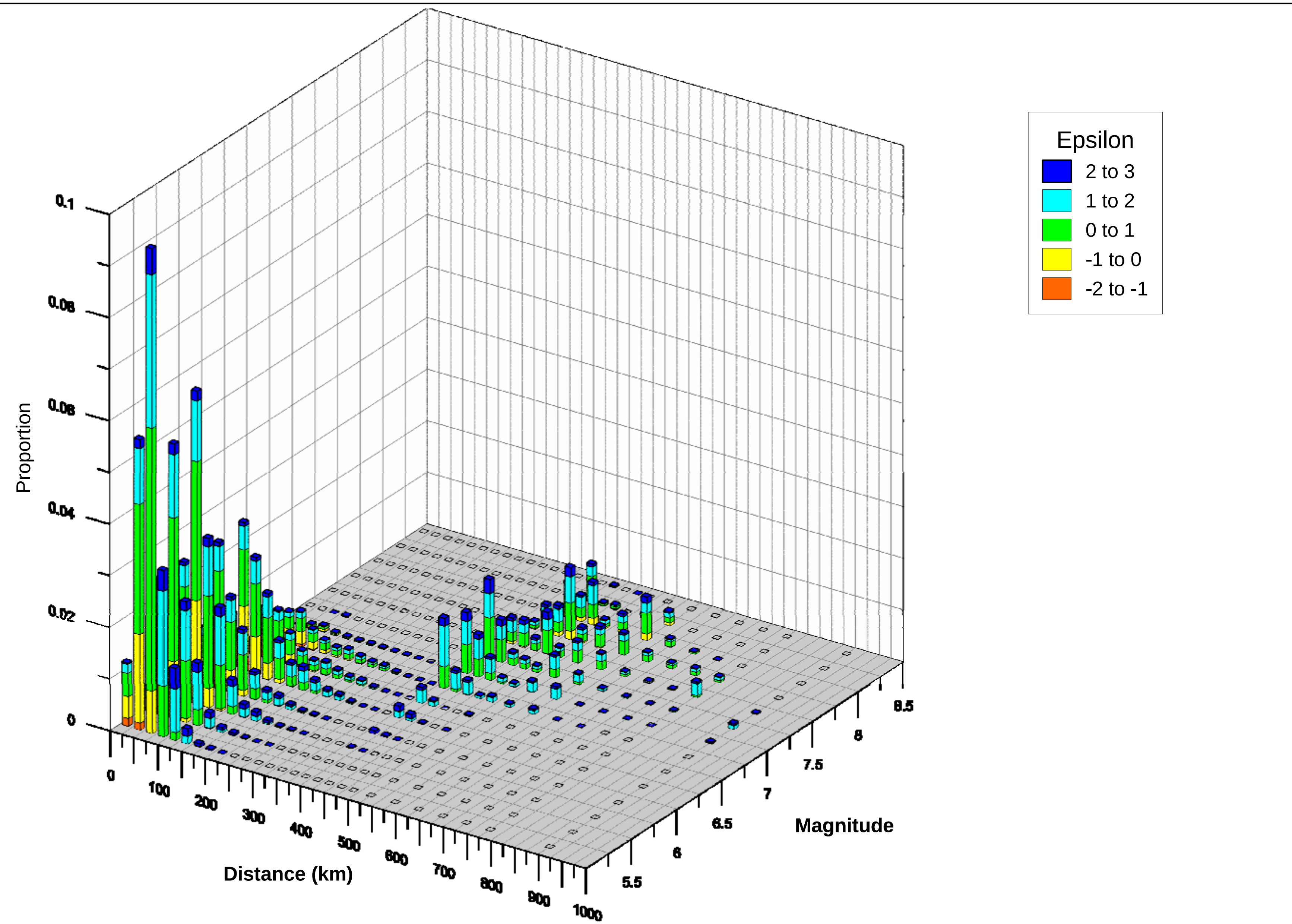

URS	Project No. 26818581 Resolution Copper Mining Arizona	MAGNITUDE AND DISTANCE CONTRIBUTIONS TO THE MEAN PEAK HORIZONTAL ACCELERATION HAZARD AT 100-YEAR RETURN PERIOD AT FAR WEST 2 SITE	Figure 37

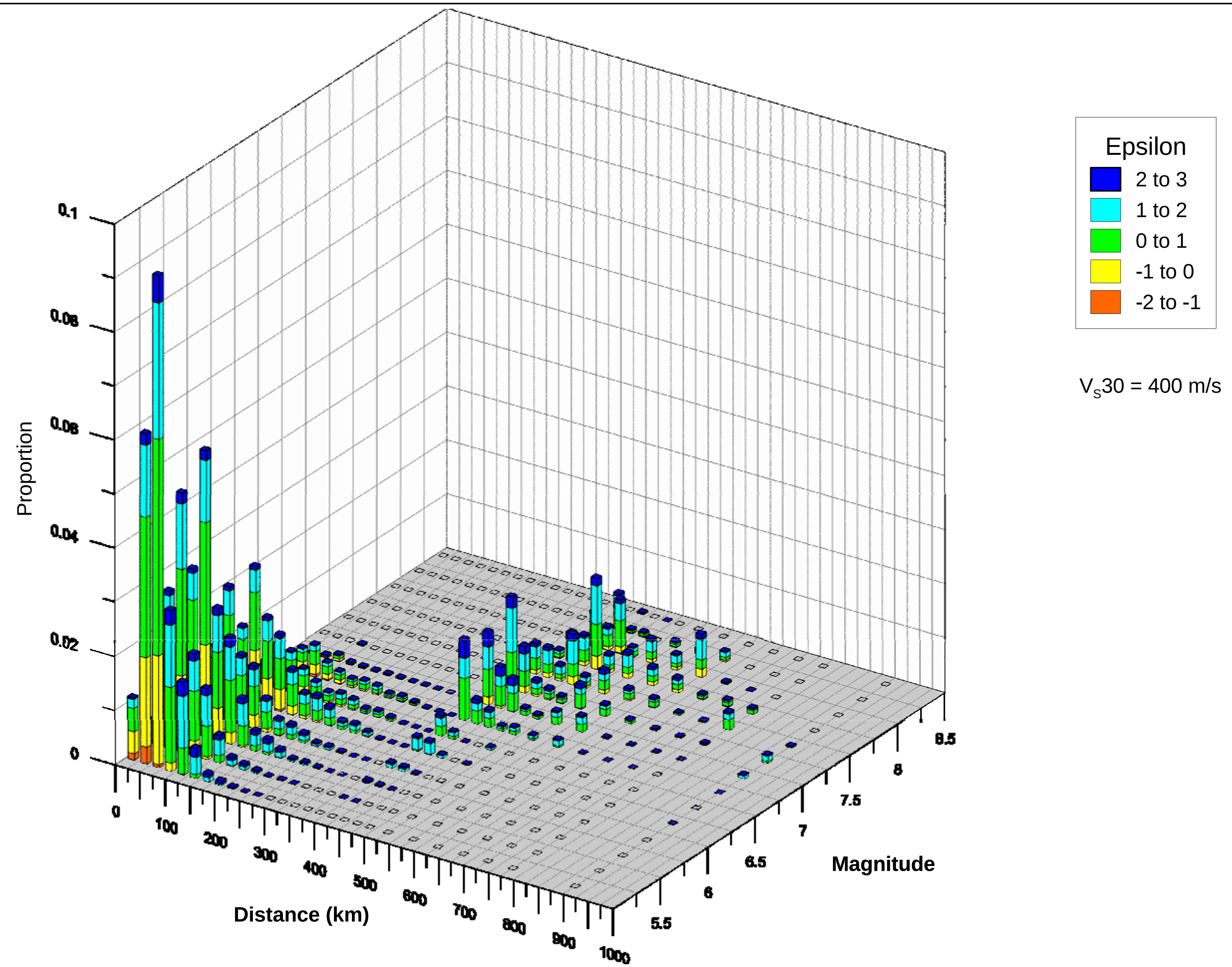

URS	Project No. 26818581 Resolution Copper Mining Arizona	MAGNITUDE AND DISTANCE CONTRIBUTIONS TO THE MEAN PEAK HORIZONTAL ACCELERATION HAZARD AT 100-YEAR RETURN PERIOD AT NEAR WEST SITE	Figure 38

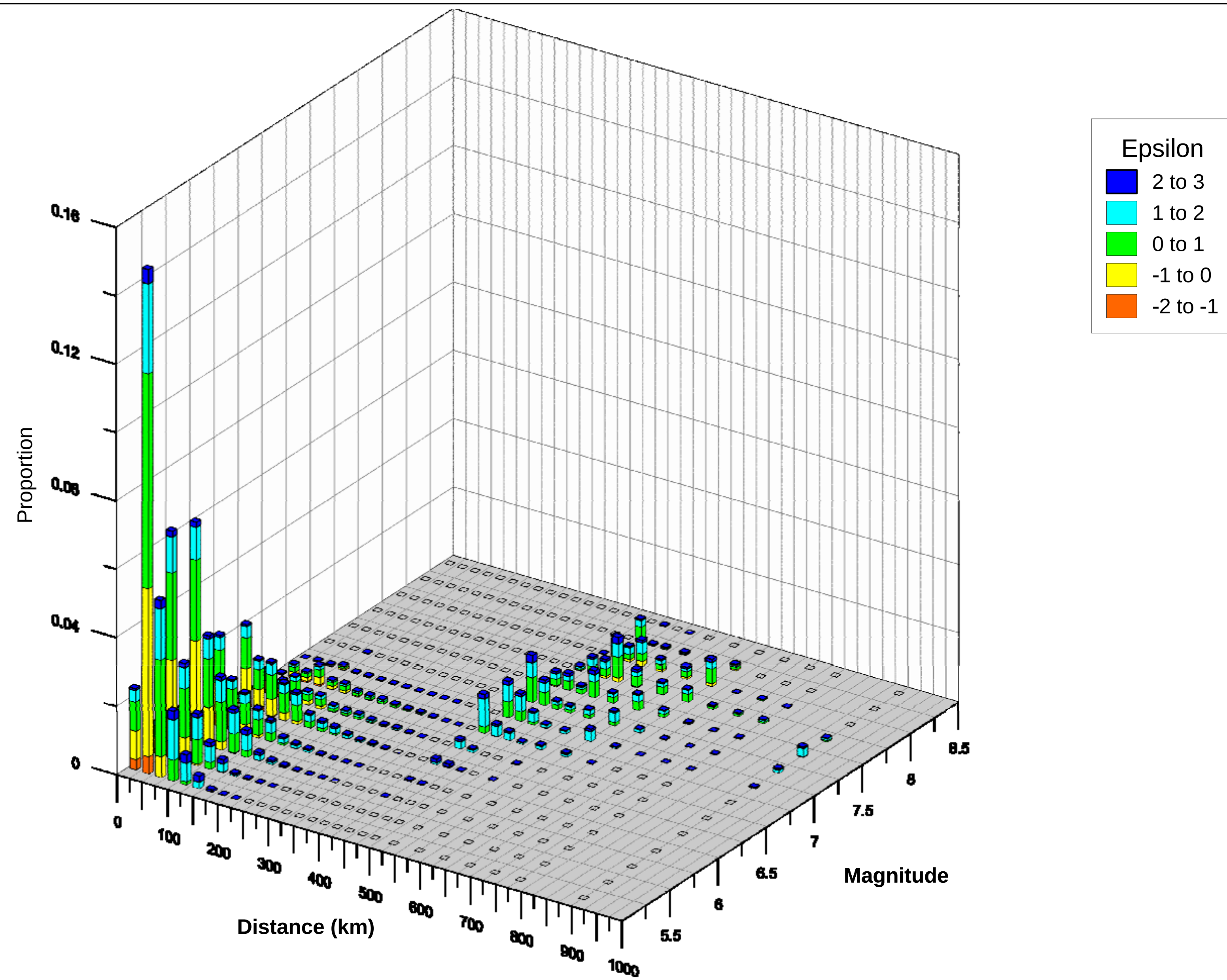

URS	Project No. 26818581 Resolution Copper Mining Arizona	MAGNITUDE AND DISTANCE CONTRIBUTIONS TO THE MEAN PEAK HORIZONTAL ACCELERATION HAZARD AT 100-YEAR RETURN PERIOD AT PINTO VALLEY SITE	Figure 39

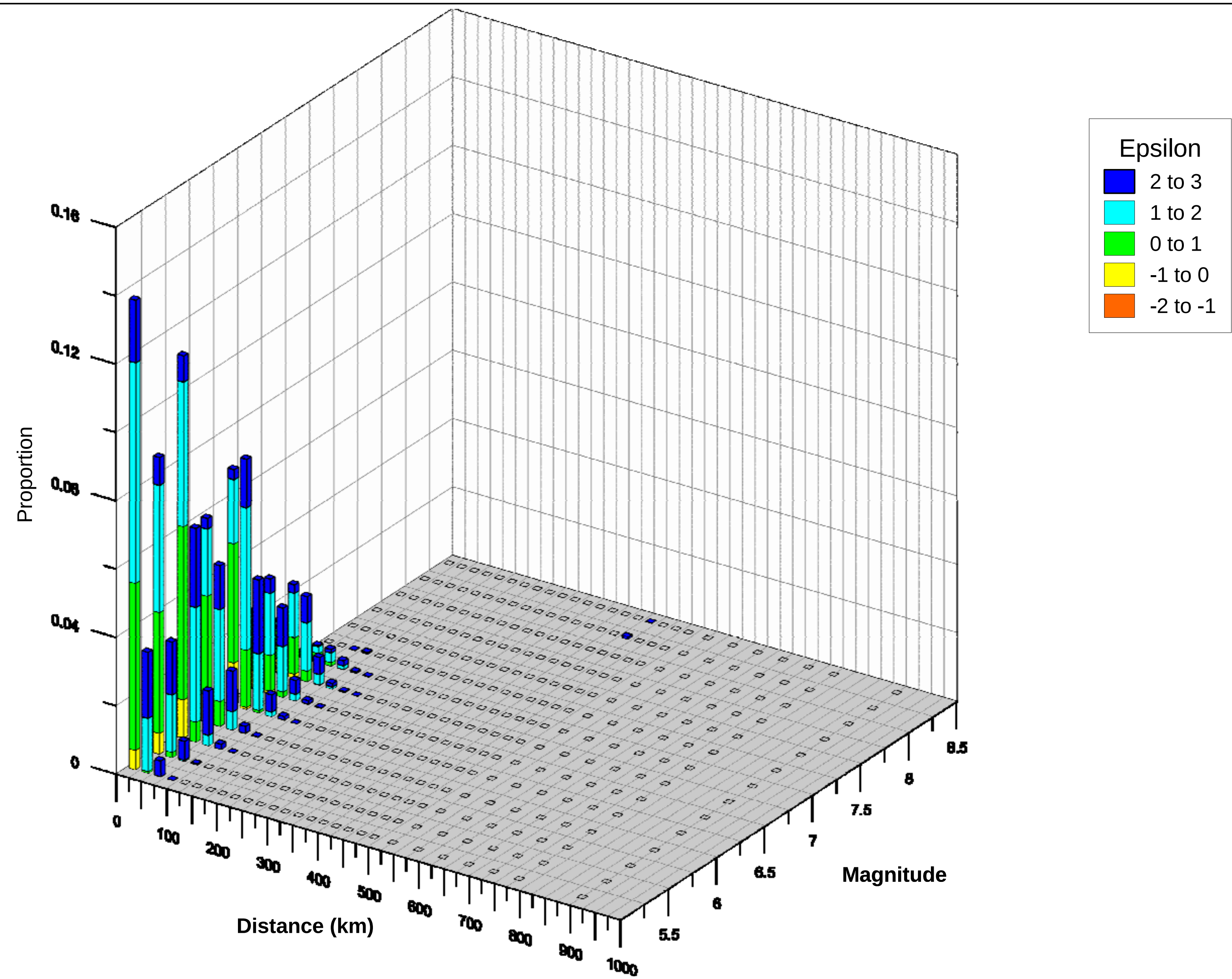

URS

Project No. 26818581

Resolution Copper Mining
Arizona

MAGNITUDE AND DISTANCE CONTRIBUTIONS TO THE MEAN PEAK HORIZONTAL ACCELERATION HAZARD AT 10,000-YEAR RETURN PERIOD AT FAR WEST 1 SITE

Figure 40

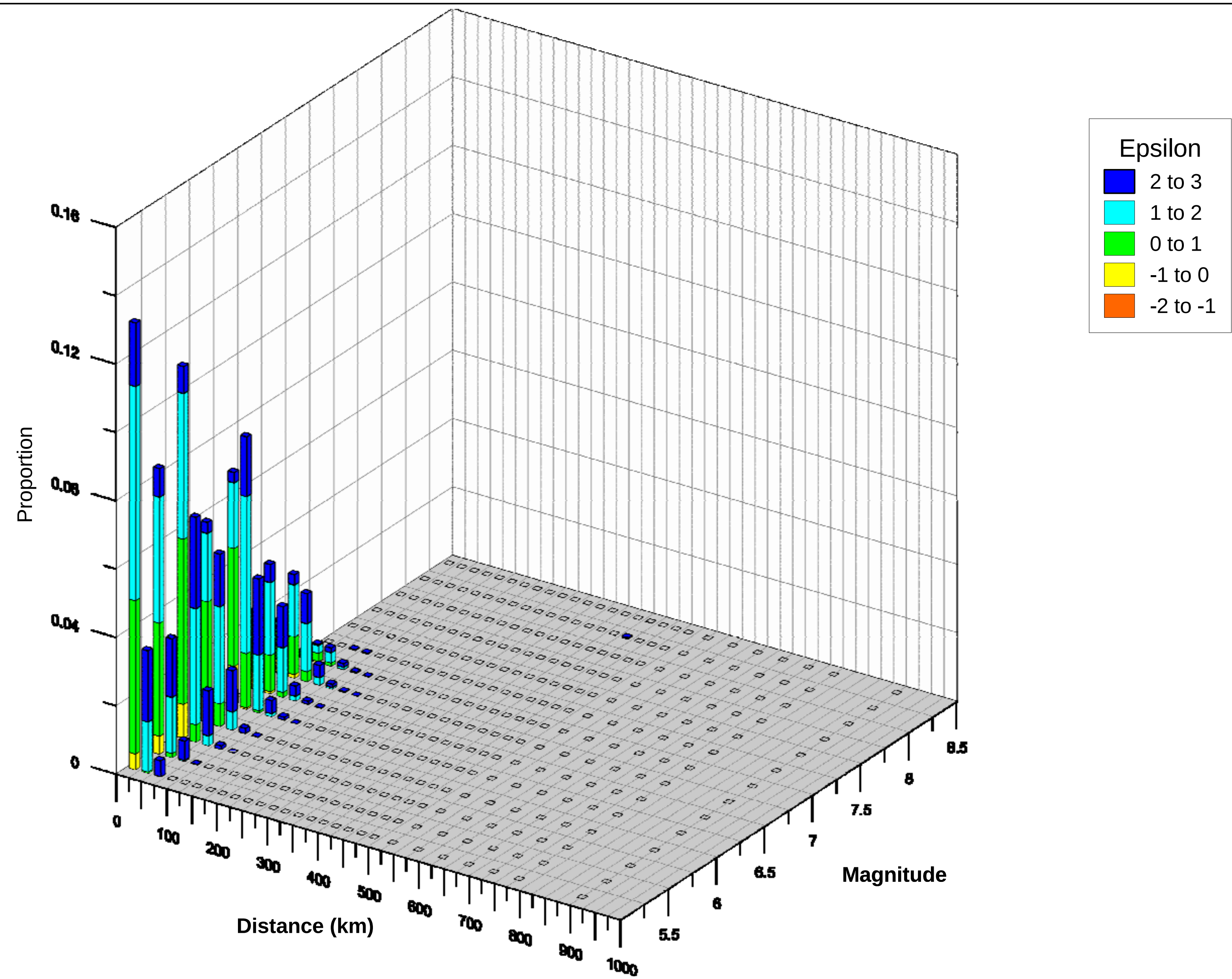

URS

Project No. 26818581

Resolution Copper Mining
Arizona

MAGNITUDE AND DISTANCE CONTRIBUTIONS TO THE MEAN PEAK HORIZONTAL ACCELERATION HAZARD AT 10,000-YEAR RETURN PERIOD AT FAR WEST 2 SITE

Figure 41

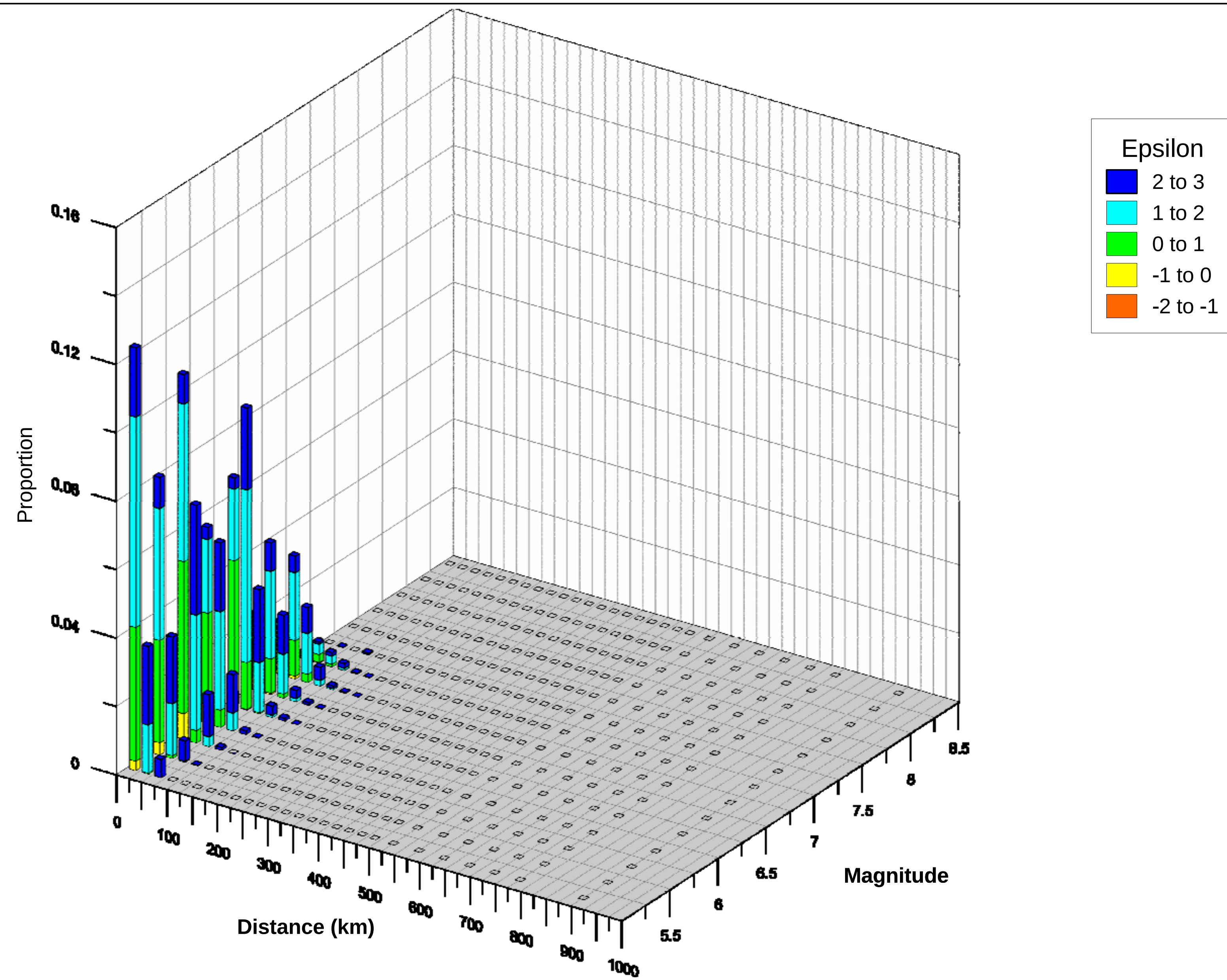

URS

Project No. 26818581

Resolution Copper Mining
Arizona

MAGNITUDE AND DISTANCE CONTRIBUTIONS TO THE MEAN PEAK HORIZONTAL ACCELERATION HAZARD AT 10,000-YEAR RETURN PERIOD AT NEAR WEST SITE

Figure 42

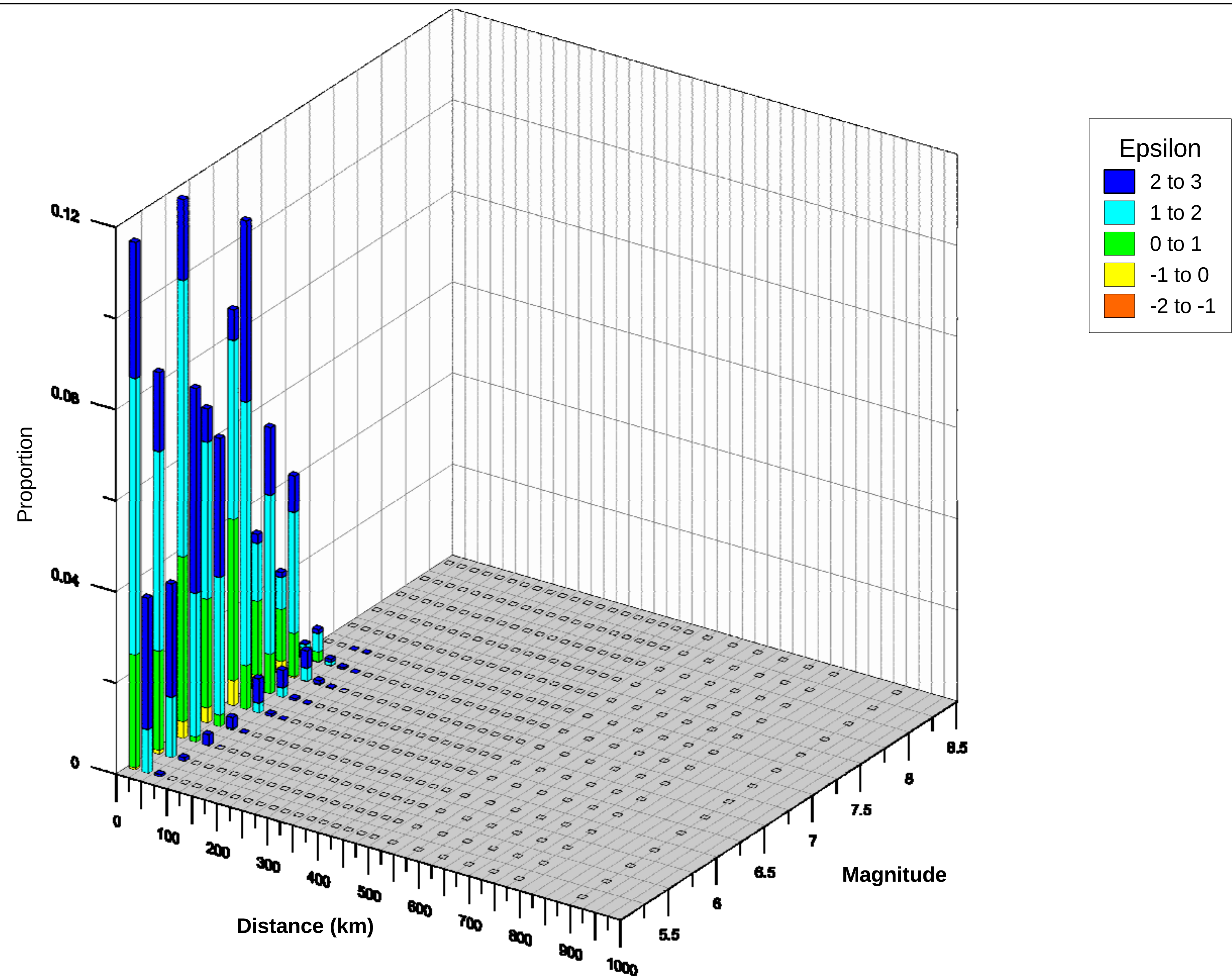

URS	Project No. 26818581 Resolution Copper Mining Arizona	MAGNITUDE AND DISTANCE CONTRIBUTIONS TO THE MEAN PEAK HORIZONTAL ACCELERATION HAZARD AT 10,000-YEAR RETURN PERIOD AT PINTO VALLEY SITE	Figure 43

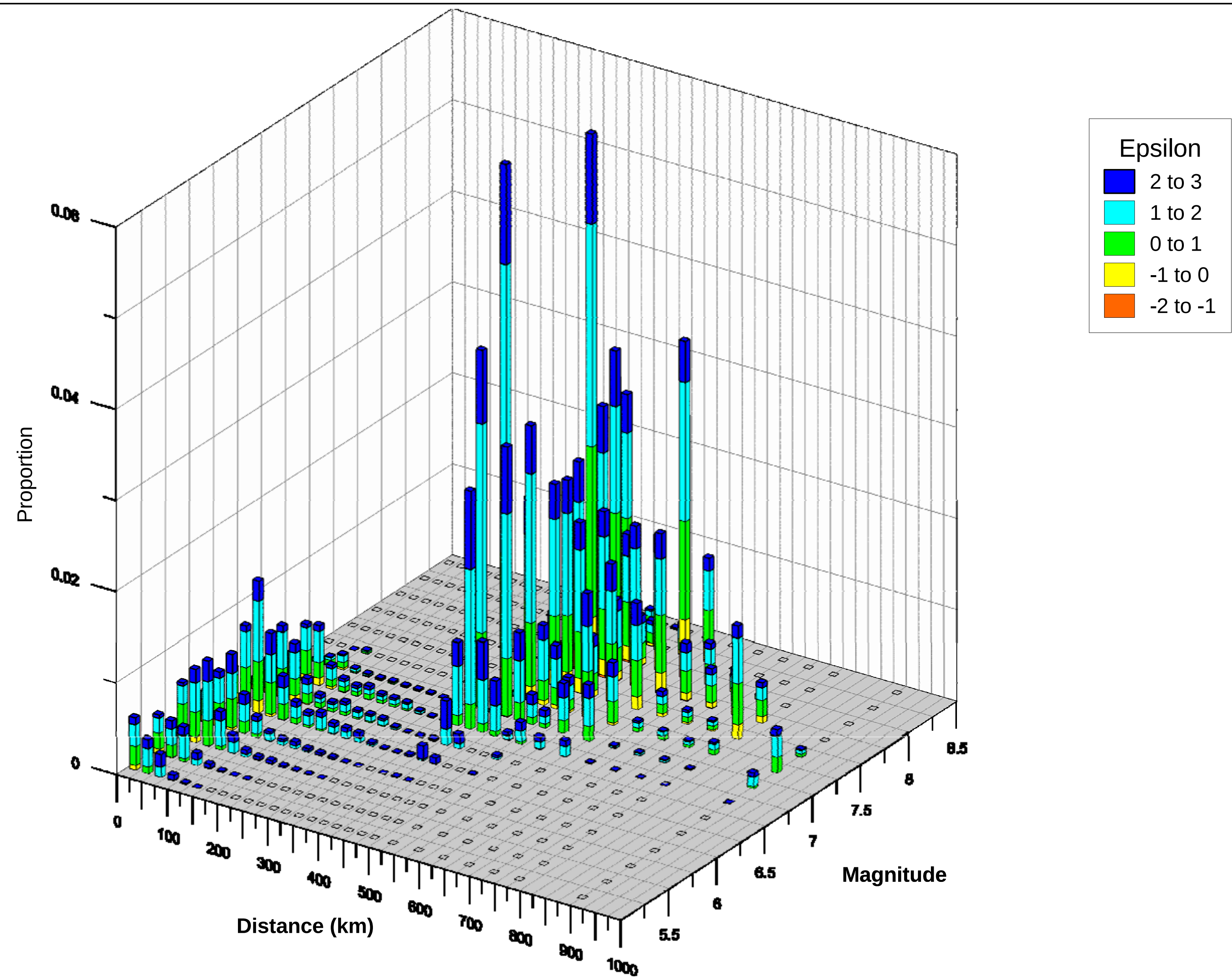

URS	Project No. 26818581 Resolution Copper Mining Arizona	MAGNITUDE AND DISTANCE CONTRIBUTIONS TO THE MEAN 1.0 SEC HORIZONTAL SPECTRAL ACCELERATION HAZARD AT 100-YEAR RETURN PERIOD AT FAR WEST 1 SITE	Figure 44

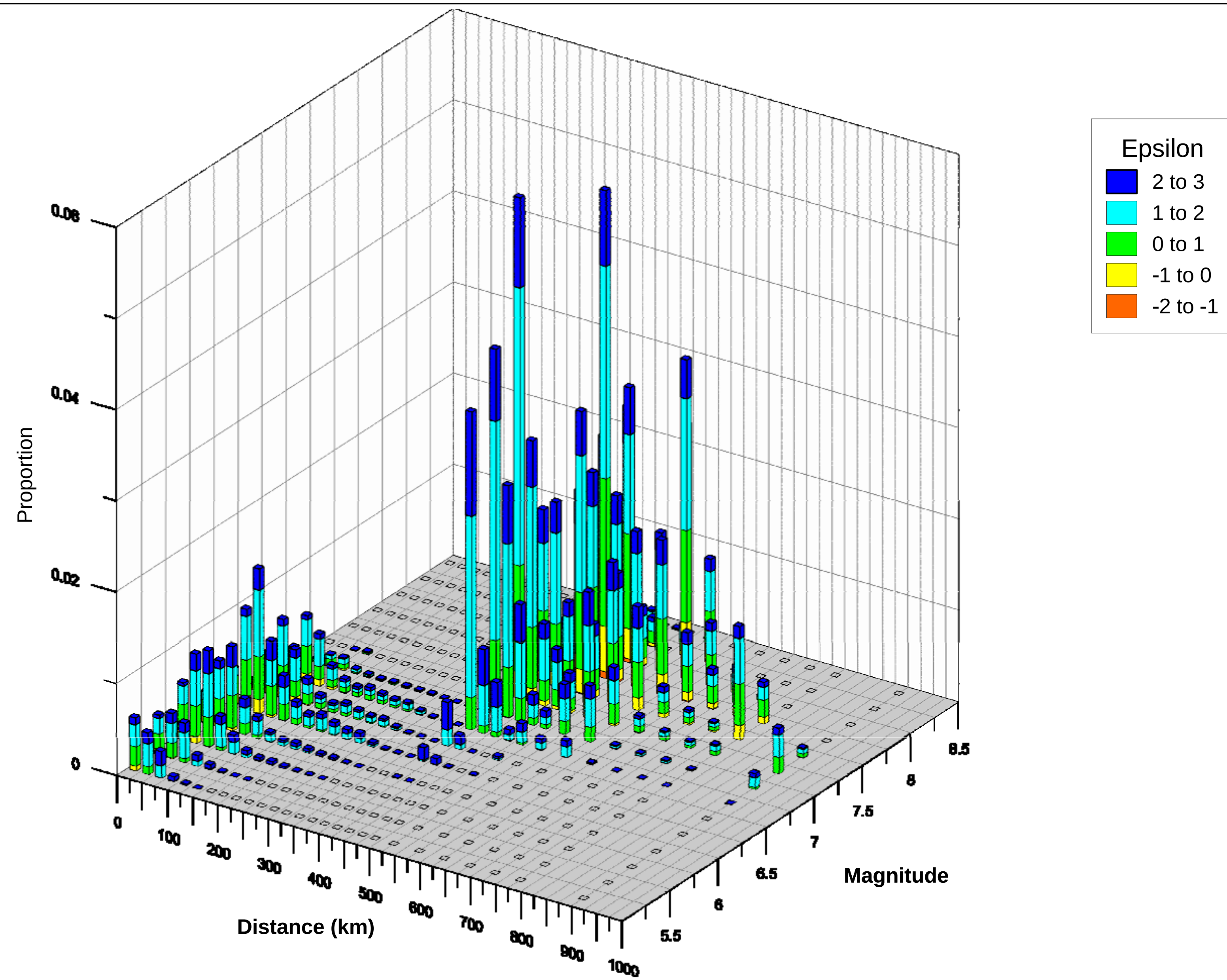

URS	Project No. 26818581 Resolution Copper Mining Arizona	MAGNITUDE AND DISTANCE CONTRIBUTIONS TO THE MEAN 1.0 SEC HORIZONTAL SPECTRAL ACCELERATION HAZARD AT 100-YEAR RETURN PERIOD AT FAR WEST 2 SITE	Figure 45

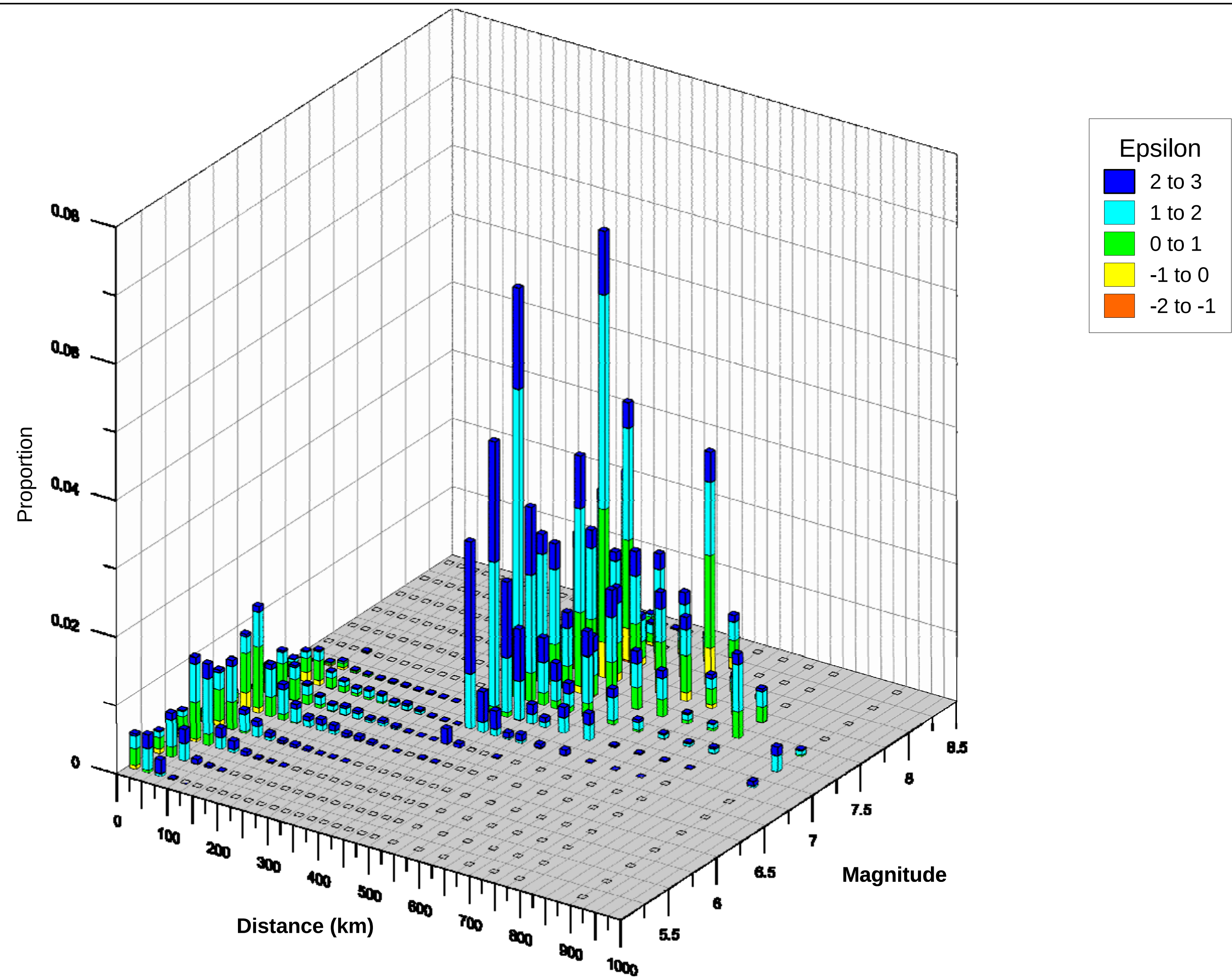

URS	Project No. 26818581 Resolution Copper Mining Arizona	MAGNITUDE AND DISTANCE CONTRIBUTIONS TO THE MEAN 1.0 SEC HORIZONTAL SPECTRAL ACCELERATION HAZARD AT 100-YEAR RETURN PERIOD AT NEAR WEST SITE	Figure 46

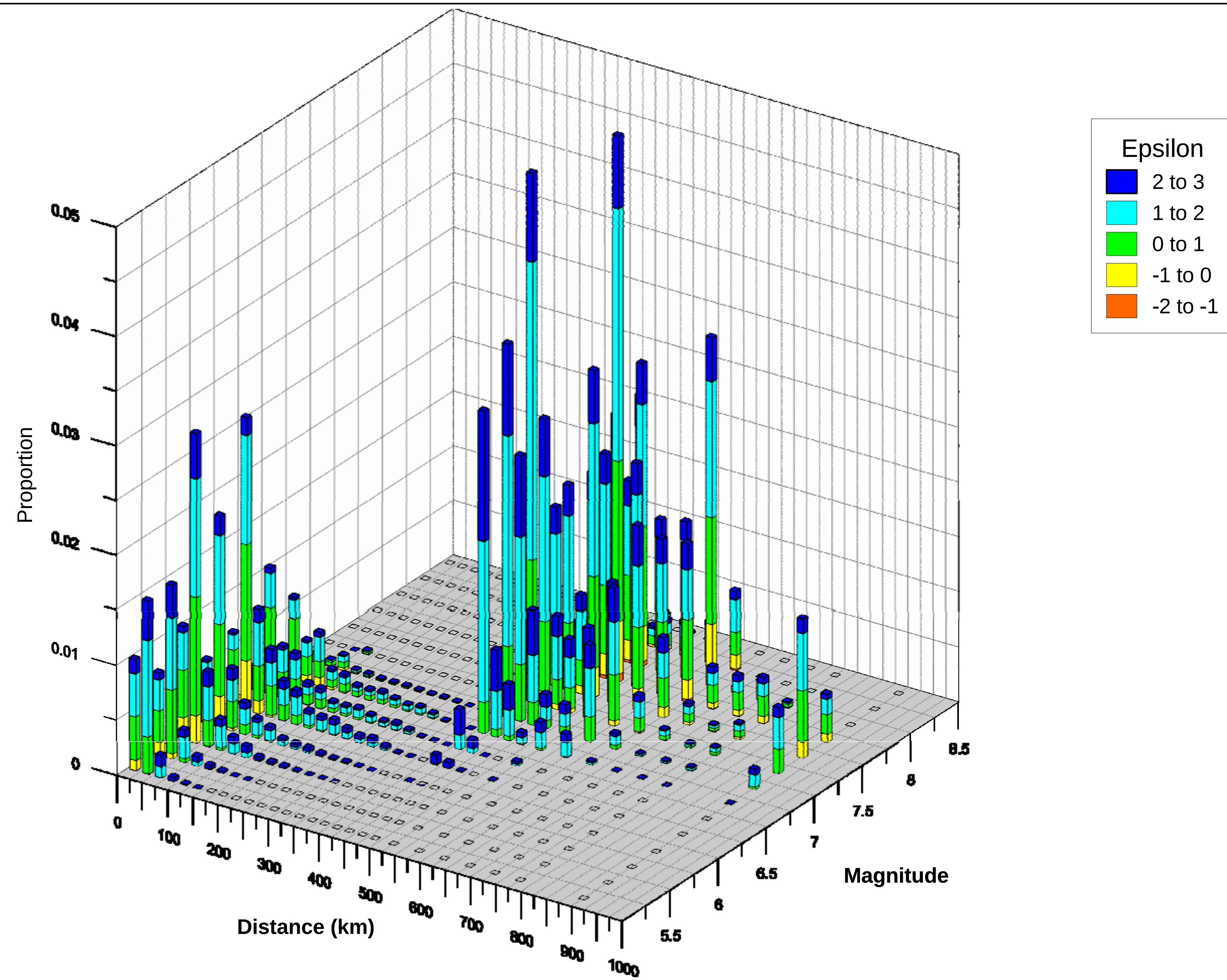

URS	Project No. 26818581 Resolution Copper Mining Arizona	MAGNITUDE AND DISTANCE CONTRIBUTIONS TO THE MEAN 1.0 SEC HORIZONTAL SPECTRAL ACCELERATION HAZARD AT 100-YEAR RETURN PERIOD AT PINTO VALLEY SITE	Figure 47

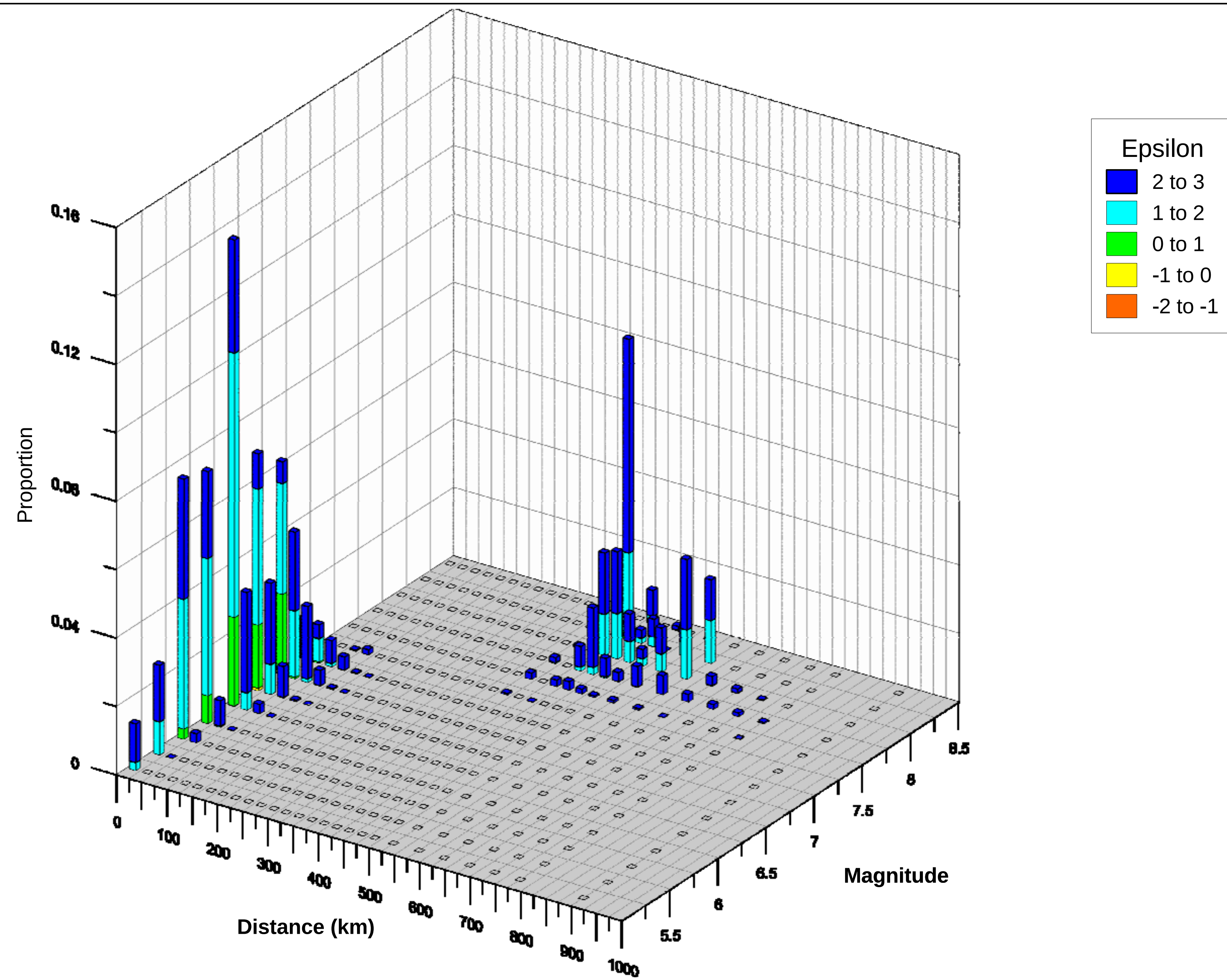

URS	Project No. 26818581 Resolution Copper Mining Arizona	MAGNITUDE AND DISTANCE CONTRIBUTIONS TO THE MEAN 1.0 SEC HORIZONTAL SPECTRAL ACCELERATION HAZARD AT 10,000-YEAR RETURN PERIOD AT FAR WEST 1 SITE	Figure 48

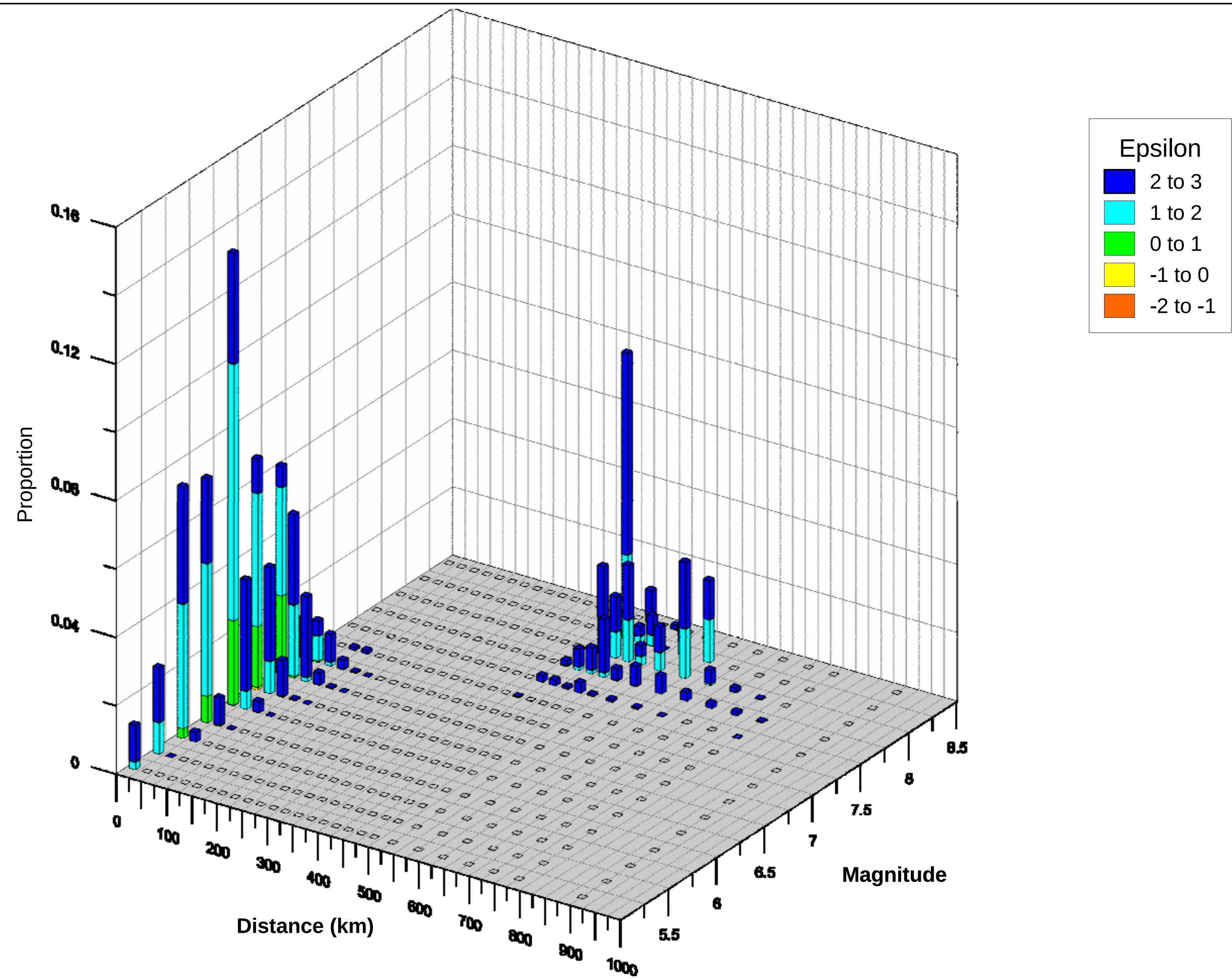

URS

Project No. 26818581

Resolution Copper Mining
Arizona

MAGNITUDE AND DISTANCE CONTRIBUTIONS TO THE MEAN 1.0 SEC HORIZONTAL SPECTRAL ACCELERATION HAZARD AT 10,000-YEAR RETURN PERIOD AT FAR WEST 2 SITE

Figure 49

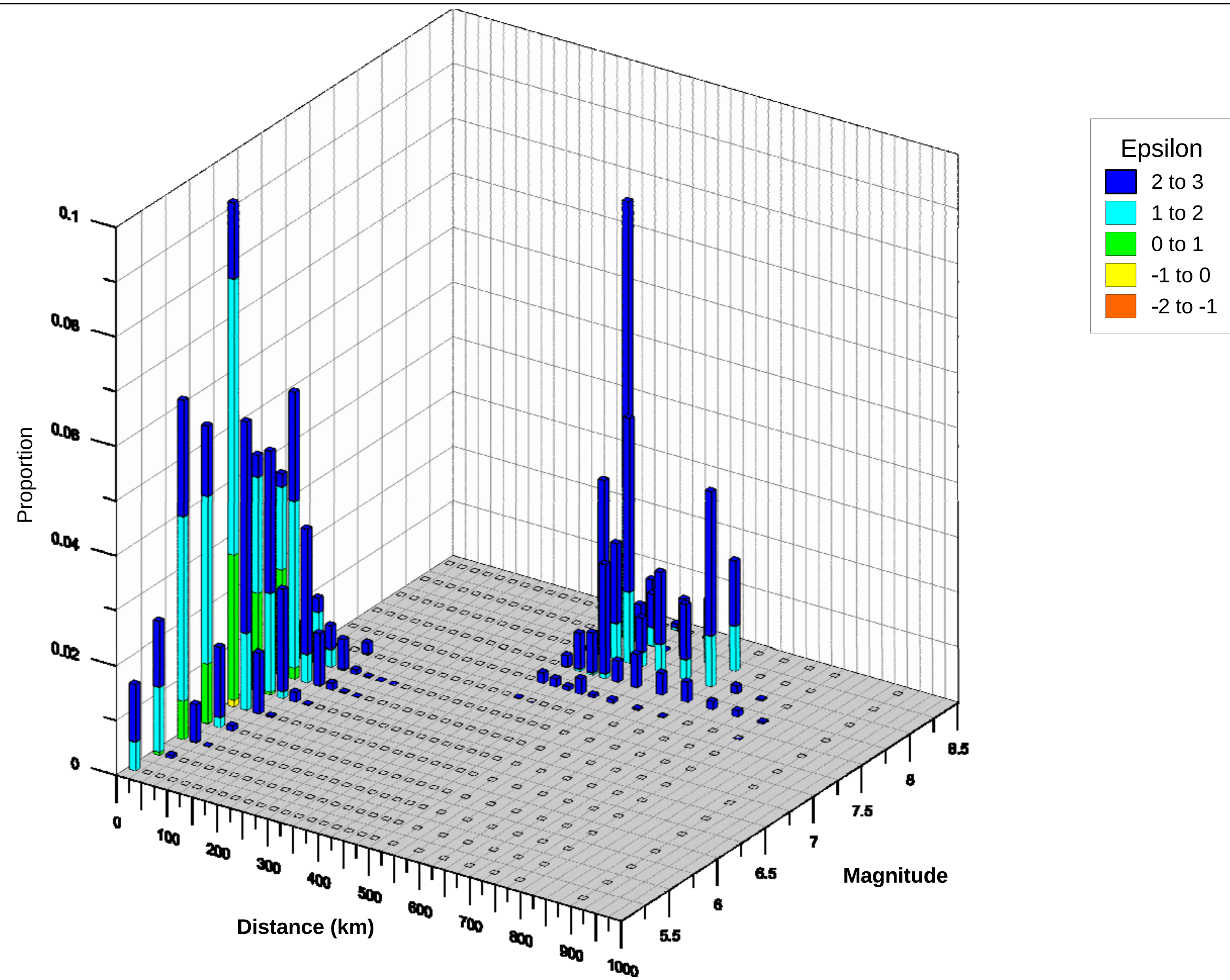

URS	Project No. 26818581 Resolution Copper Mining Arizona	MAGNITUDE AND DISTANCE CONTRIBUTIONS TO THE MEAN 1.0 SEC HORIZONTAL SPECTRAL ACCELERATION HAZARD AT 10,000-YEAR RETURN PERIOD AT NEAR WEST SITE	Figure 50

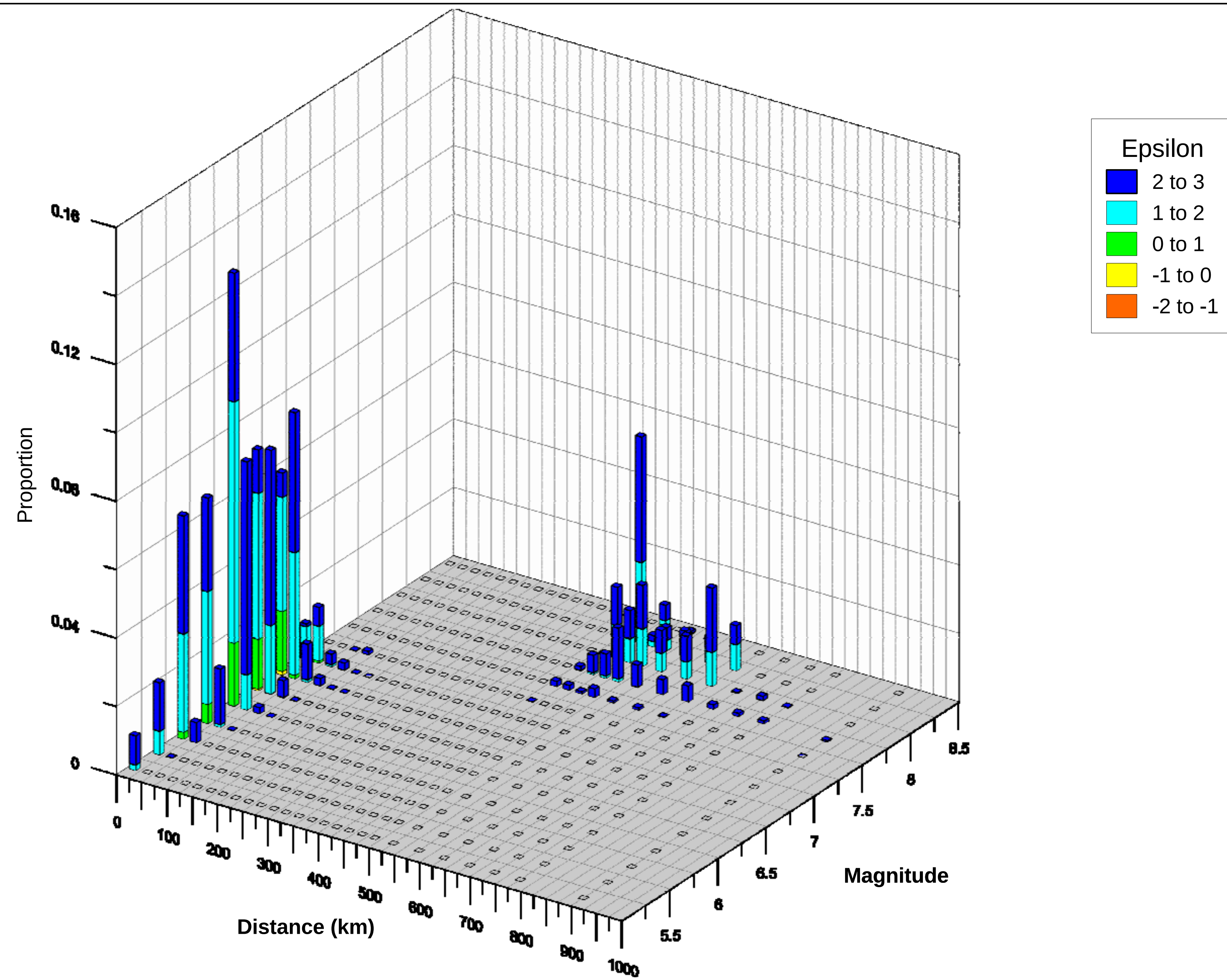

URS	Project No. 26818581	MAGNITUDE AND DISTANCE CONTRIBUTIONS TO THE MEAN 1.0 SEC HORIZONTAL SPECTRAL ACCELERATION HAZARD AT 10,000-YEAR RETURN PERIOD AT PINTO VALLEY SITE	Figure 51
	Resolution Copper Mining Arizona		

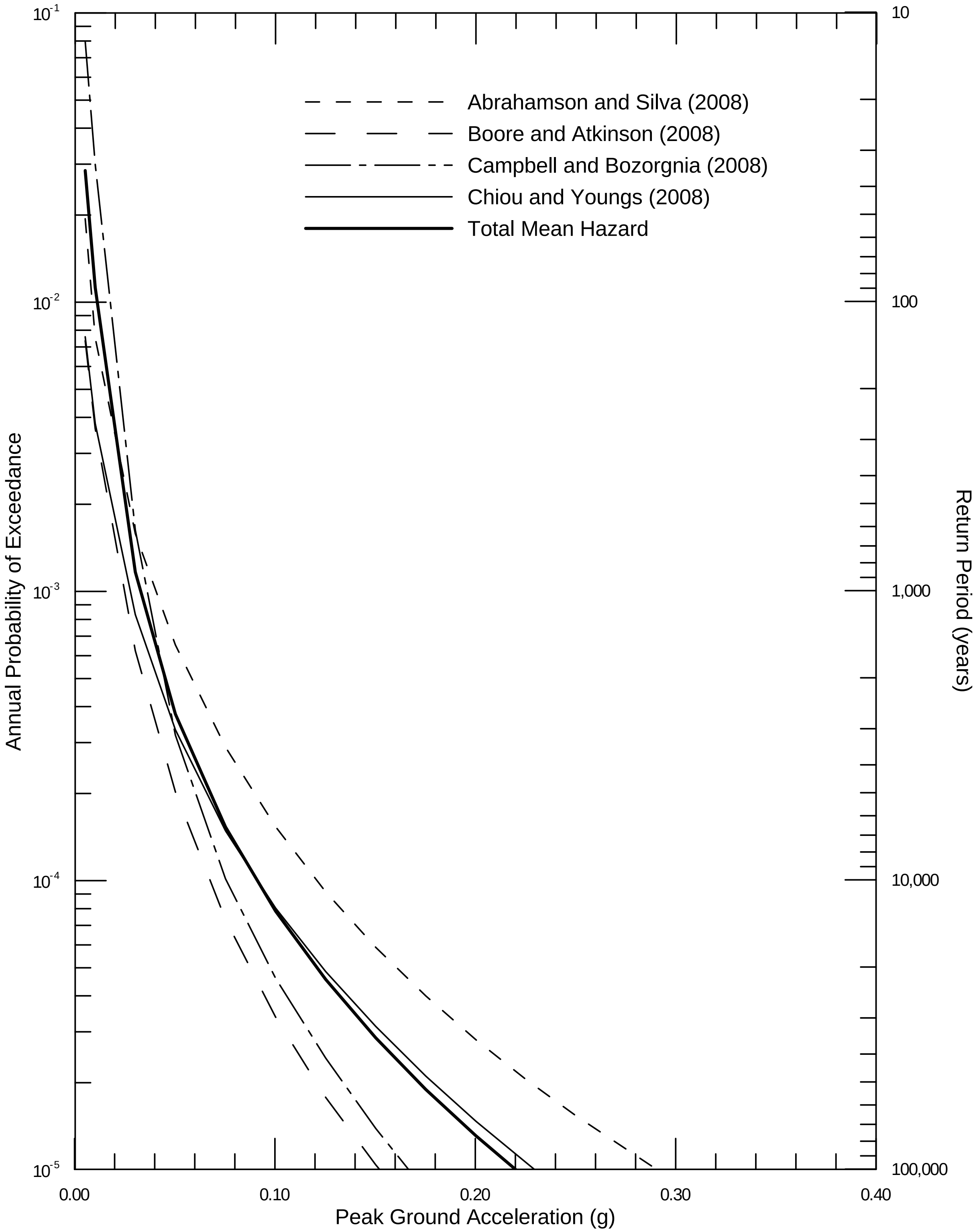

URS	Project No. 26818581	SENSITIVITY OF THE PEAK HORIZONTAL ACCELERATION HAZARD TO THE SELECTION OF GROUND MOTION PREDICTION MODELS AT FAR WEST 1 SITE	Figure 52
	Resolution Copper Mining Arizona		

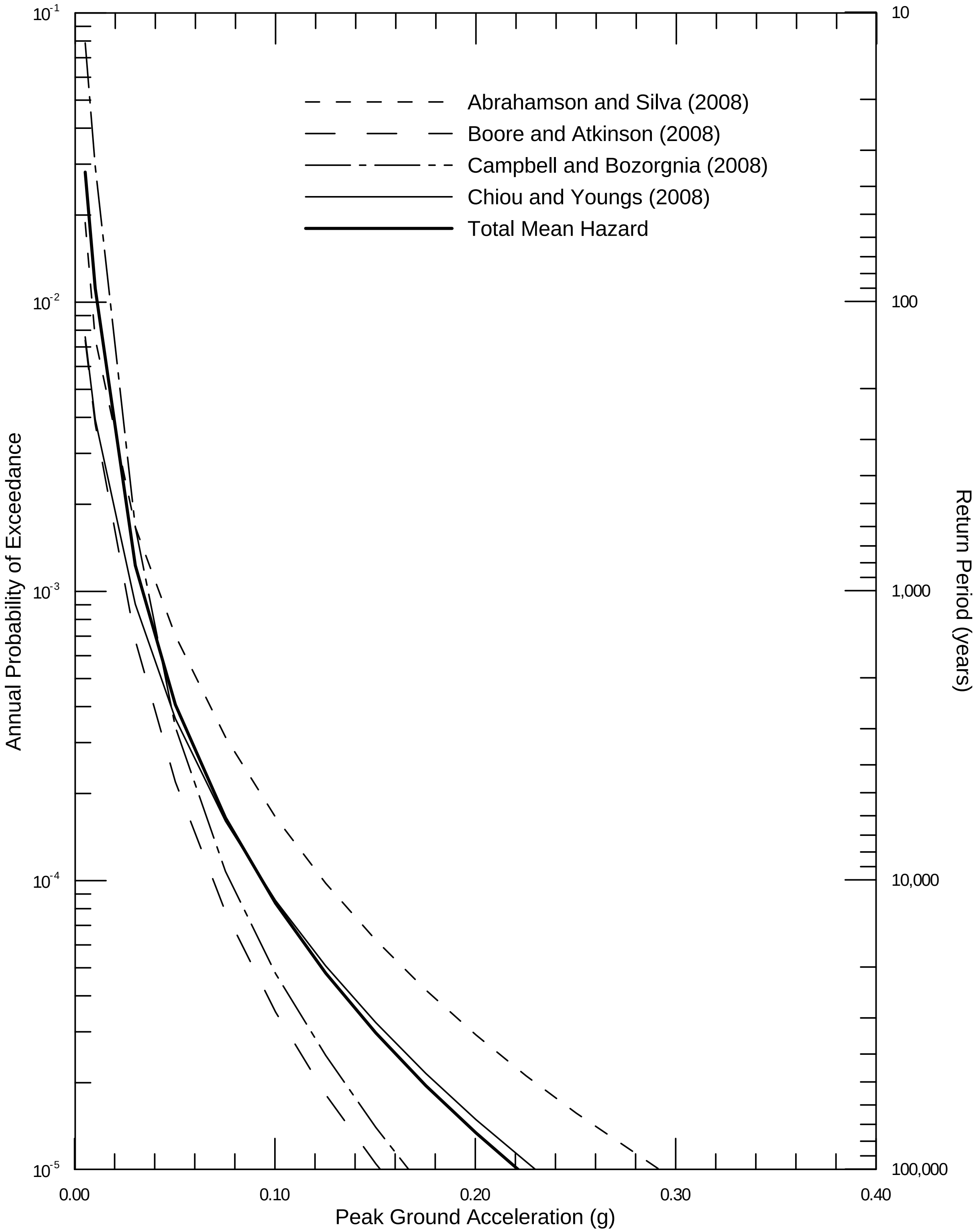

URS	Project No. 26818581 Resolution Copper Mining Arizona	SENSITIVITY OF THE PEAK HORIZONTAL ACCELERATION HAZARD TO THE SELECTION OF GROUND MOTION PREDICTION MODELS AT FAR WEST 2 SITE	Figure 53

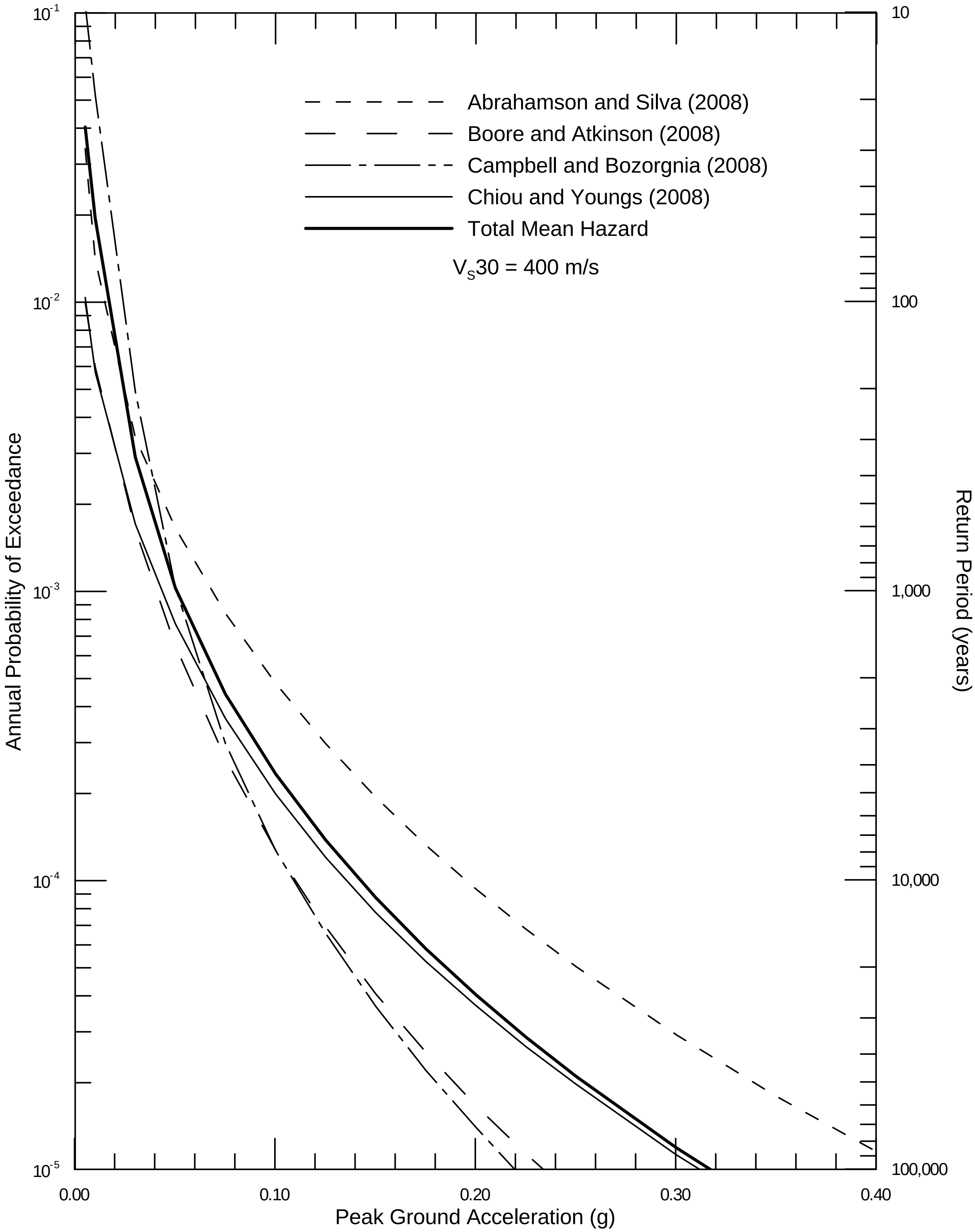

URS	Project No. 26818581	SENSITIVITY OF THE PEAK HORIZONTAL ACCELERATION HAZARD TO THE SELECTION OF GROUND MOTION PREDICTION MODELS AT NEAR WEST SITE	Figure 54
	Resolution Copper Mining Arizona		

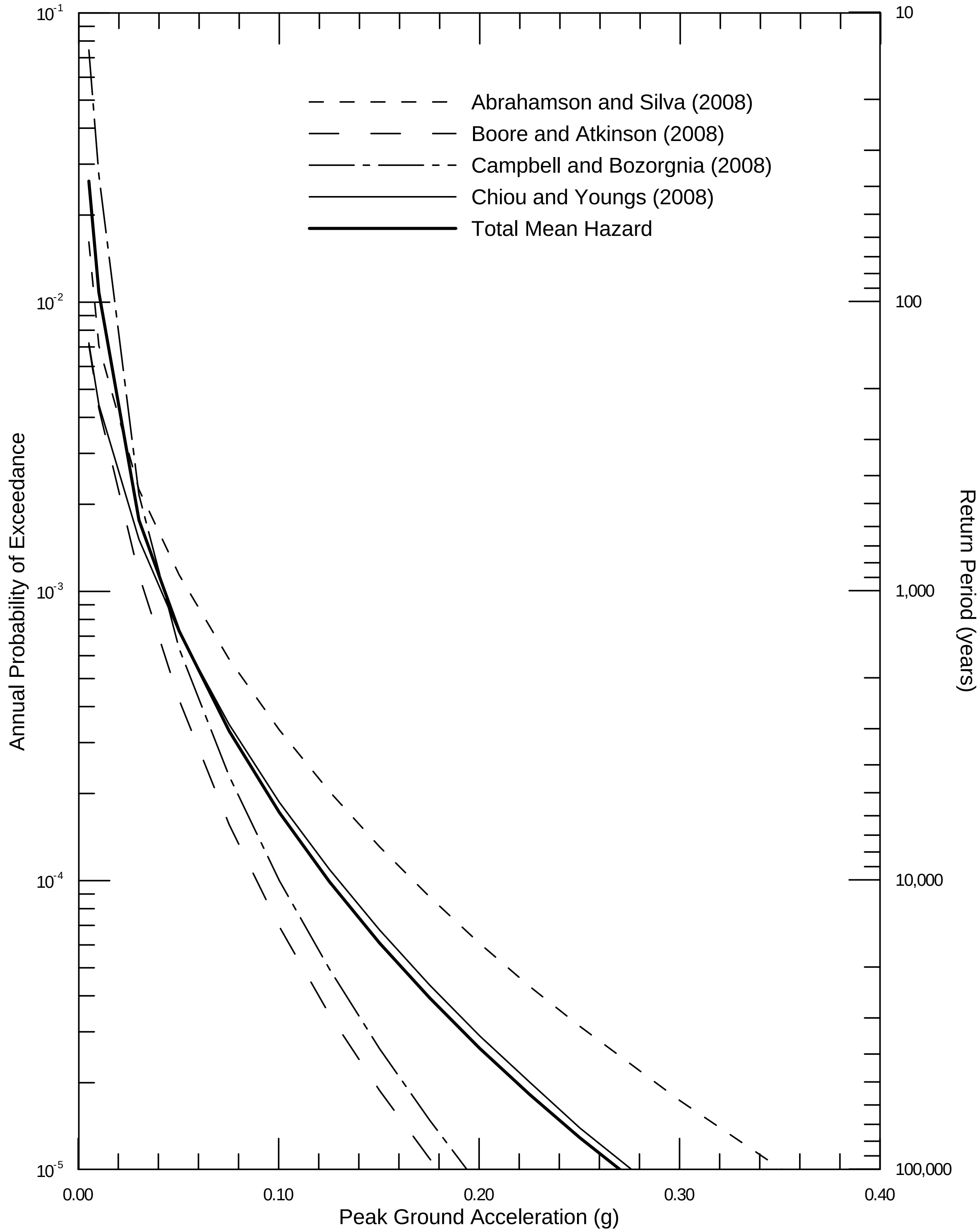

URS	Project No. 26818581 Resolution Copper Mining Arizona	SENSITIVITY OF THE PEAK HORIZONTAL ACCELERATION HAZARD TO THE SELECTION OF GROUND MOTION PREDICTION MODELS AT PINTO VALLEY SITE	Figure 55

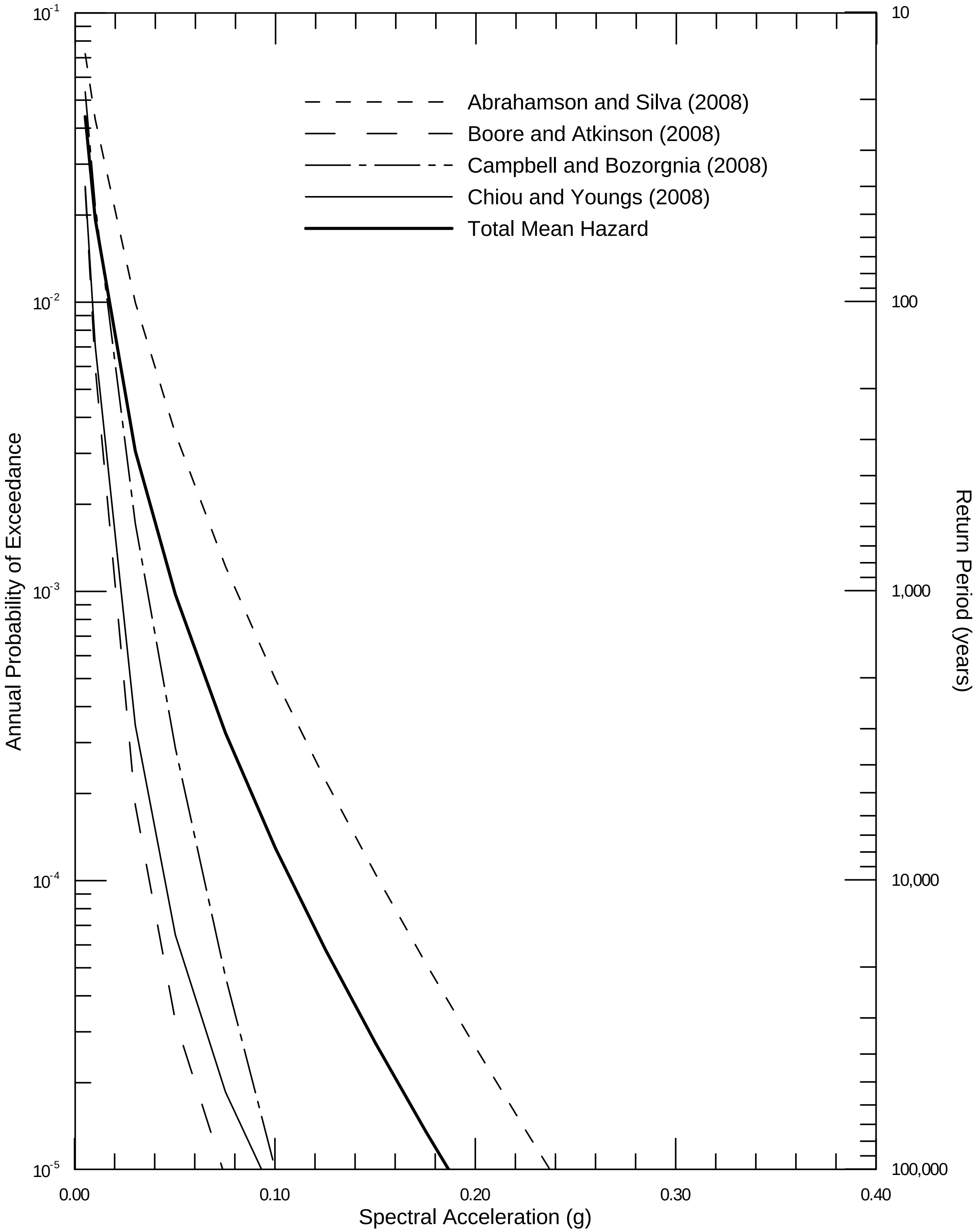

URS	Project No. 26818581 Resolution Copper Mining Arizona	SENSITIVITY OF THE 1.0 SEC HORIZONTAL SPECTRAL ACCELERATION HAZARD TO THE SELECTION OF GROUND MOTION PREDICTION MODELS AT FAR WEST 1 SITE	Figure 56

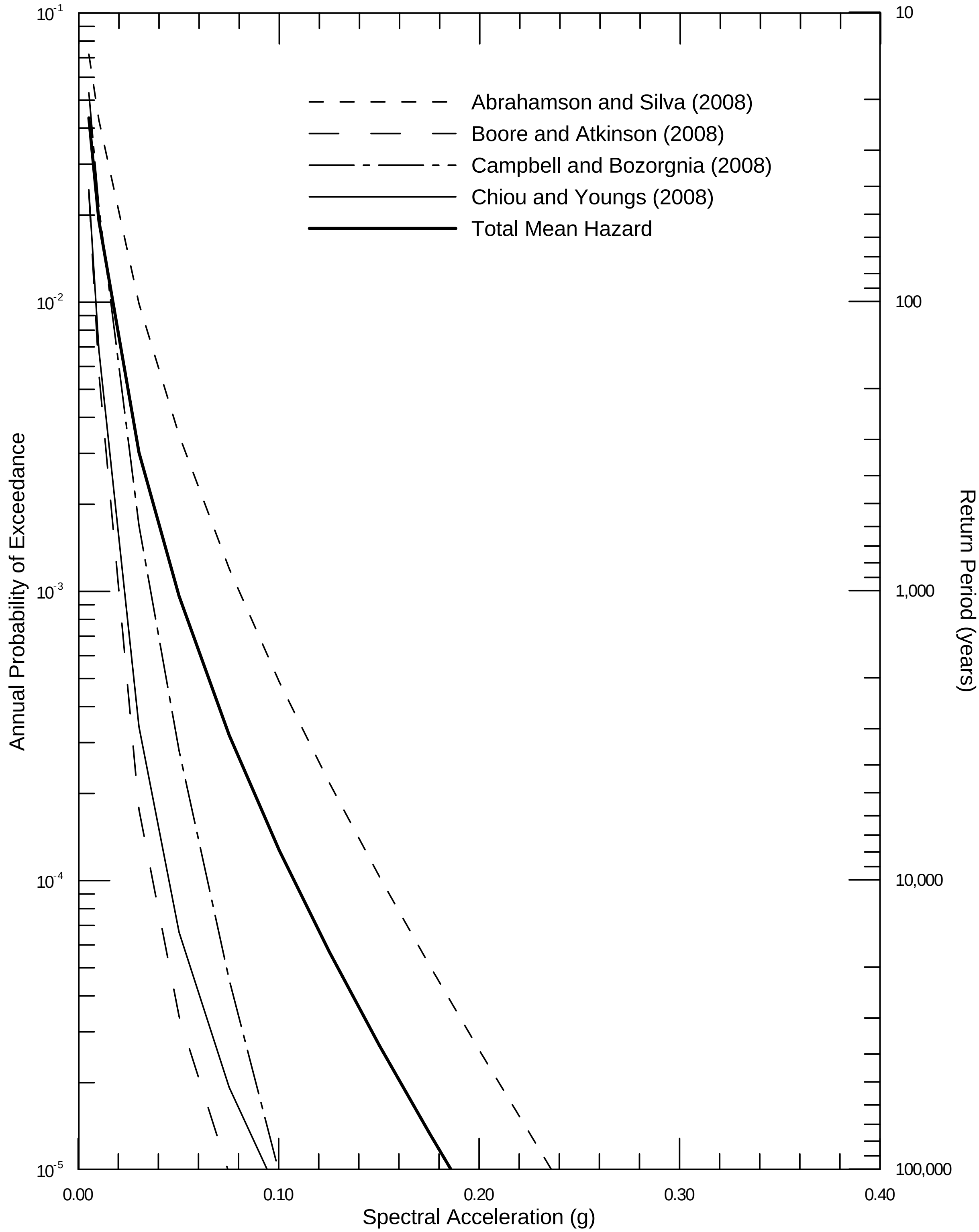

URS	Project No. 26818581	SENSITIVITY OF THE 1.0 SEC HORIZONTAL SPECTRAL ACCELERATION HAZARD TO THE SELECTION OF GROUND MOTION PREDICTION MODELS AT FAR WEST 2 SITE	Figure 57
	Resolution Copper Mining Arizona		

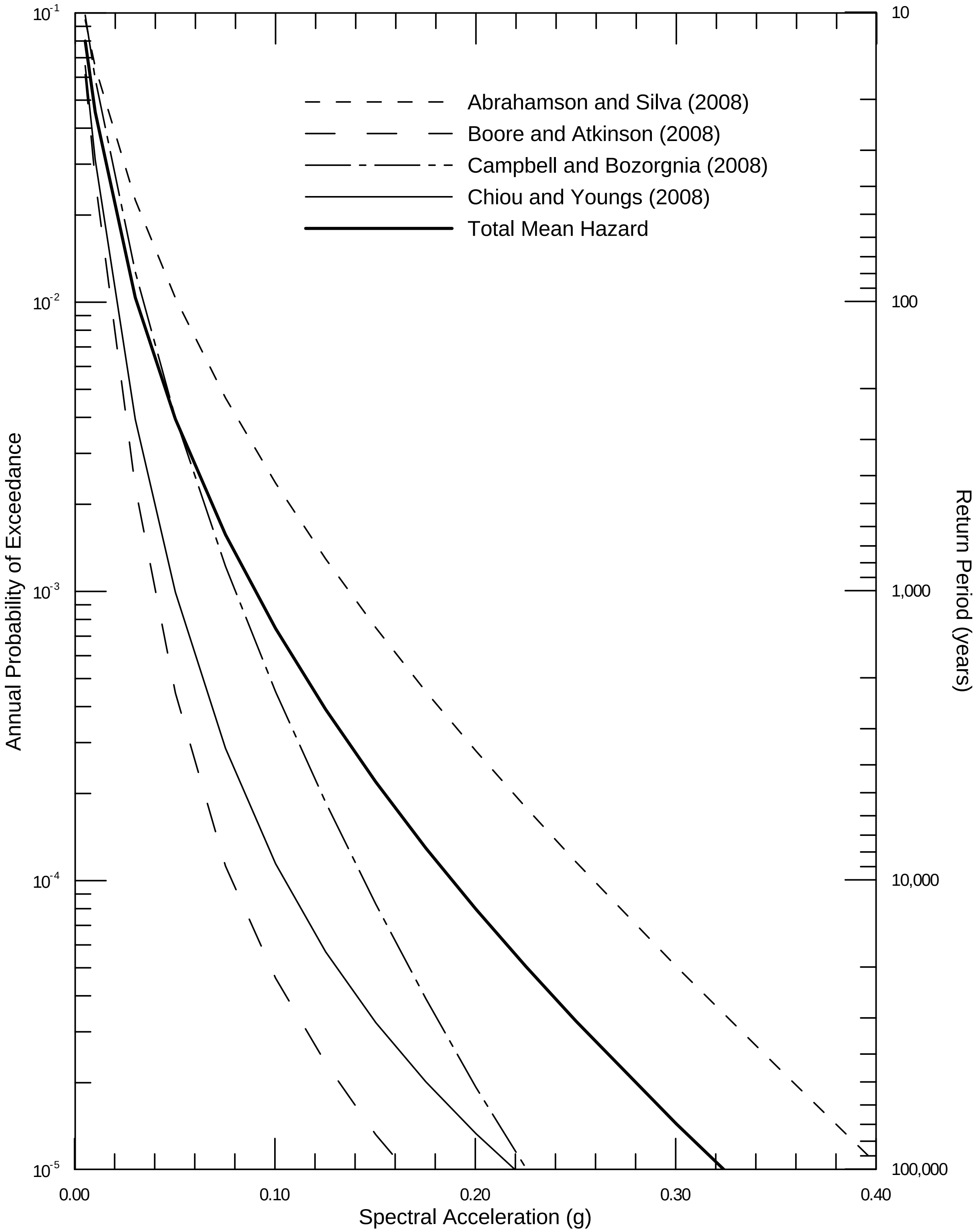

URS	Project No. 26818581	SENSITIVITY OF THE 1.0 SEC HORIZONTAL SPECTRAL ACCELERATION HAZARD TO THE SELECTION OF GROUND MOTION PREDICTION MODELS AT NEAR WEST SITE	Figure 58
	Resolution Copper Mining Arizona		

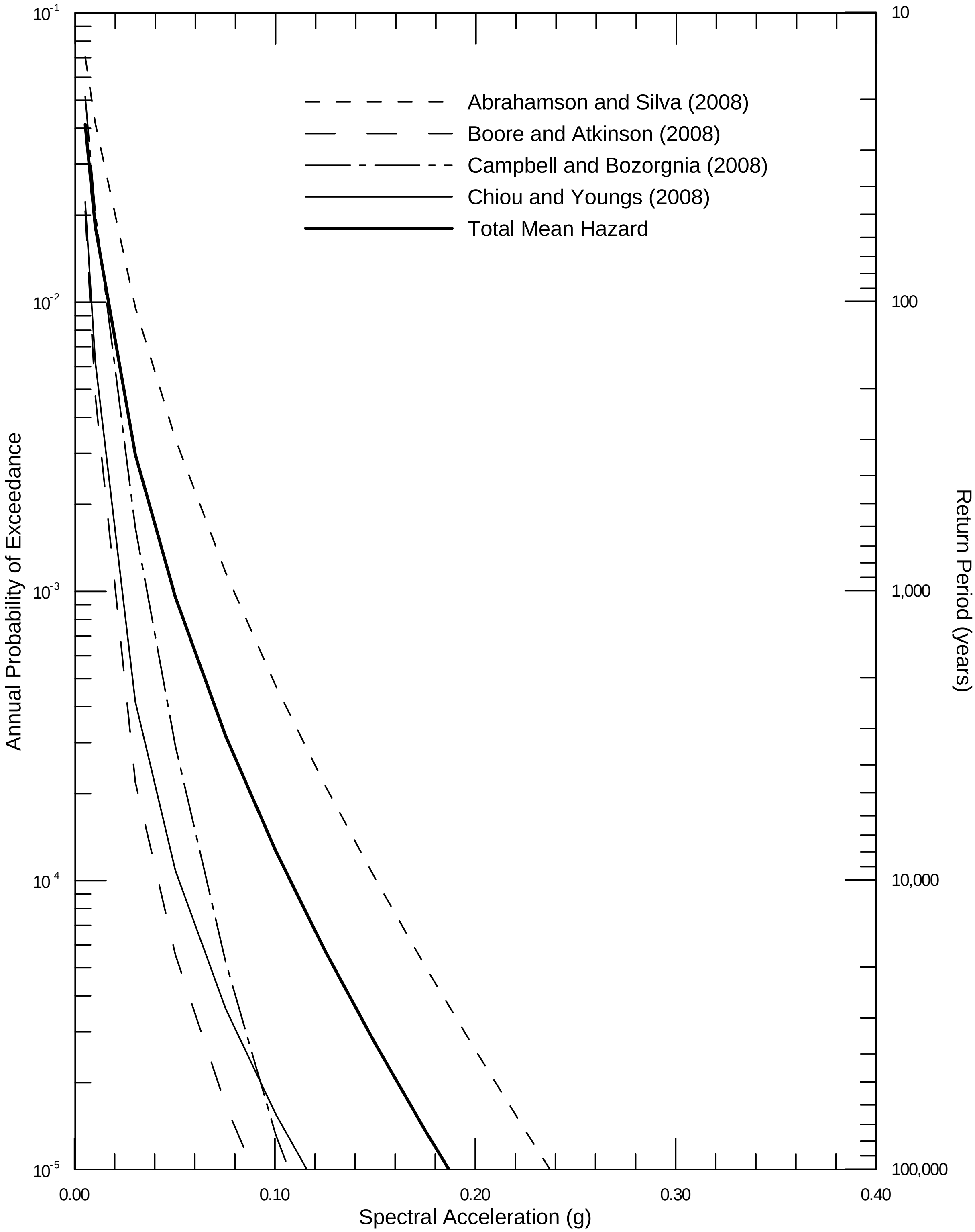

URS	Project No. 26818581	SENSITIVITY OF THE 1.0 SEC HORIZONTAL SPECTRAL ACCELERATION HAZARD TO THE SELECTION OF GROUND MOTION PREDICTION MODELS AT PINTO VALLEY SITE	Figure 59
	Resolution Copper Mining Arizona		

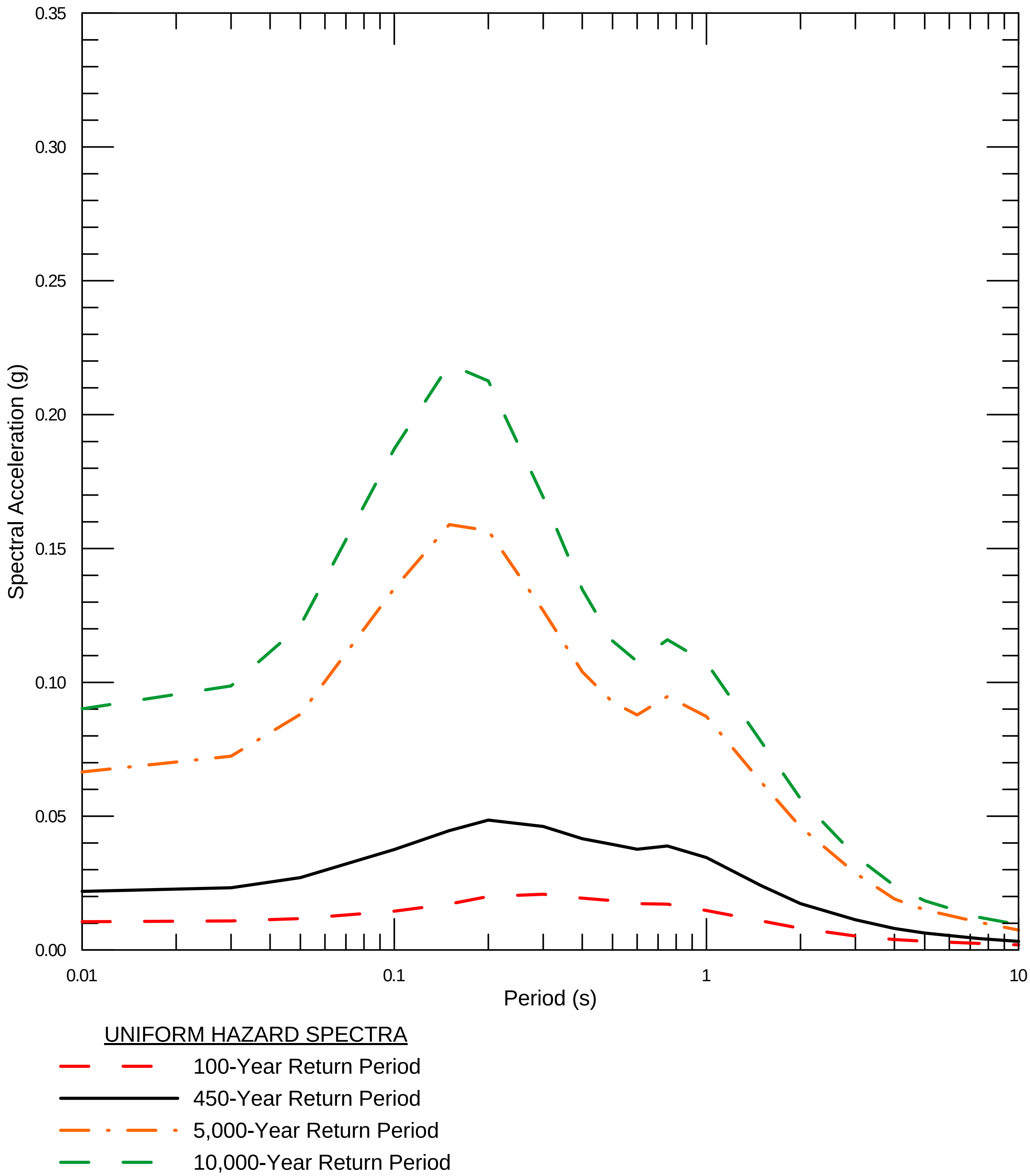

URS	Project No. 26818581	5%-DAMPED UNIFORM HAZARD SPECTRA AT FAR WEST 1 SITE ON ROCK	Figure 60
	Resolution Copper Mining Arizona		

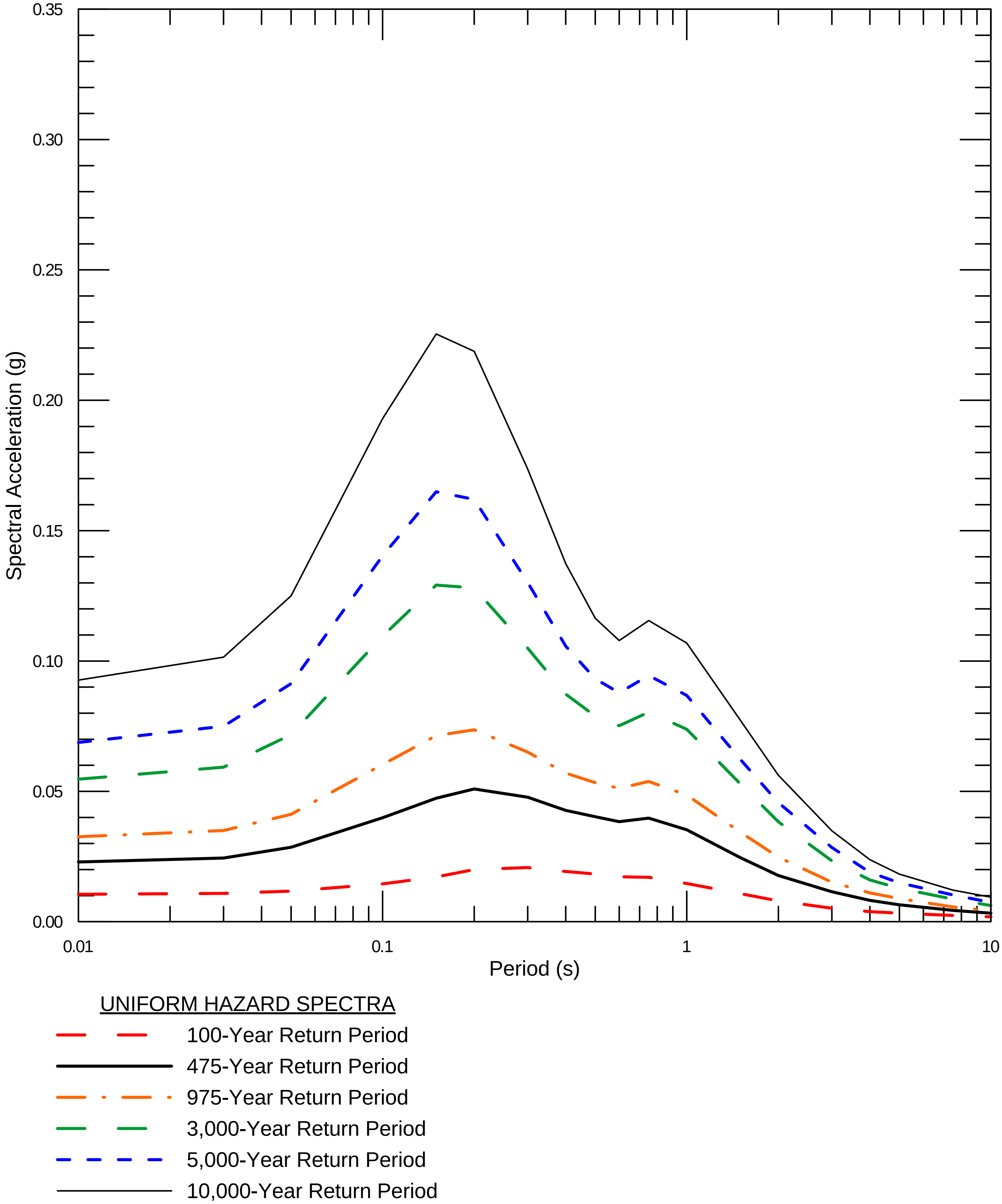

URS	Project No. 26818581 Resolution Copper Mining Arizona	5%-DAMPED UNIFORM HAZARD SPECTRA AT FAR WEST 2 SITE	Figure 61

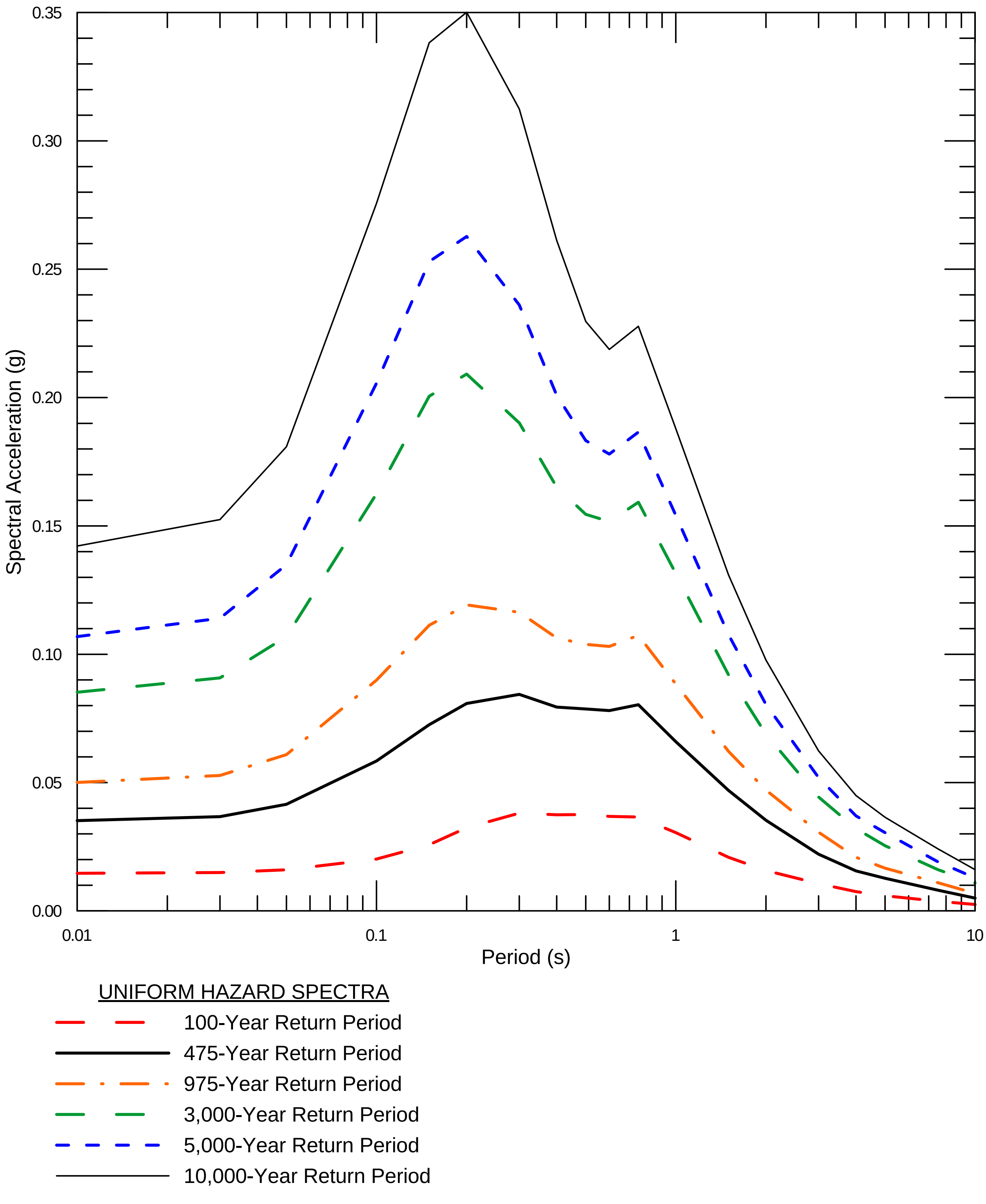

URS	Project No. 26818581 Resolution Copper Mining Arizona	5%-DAMPED UNIFORM HAZARD SPECTRA AT NEAR WEST SITE	Figure 62

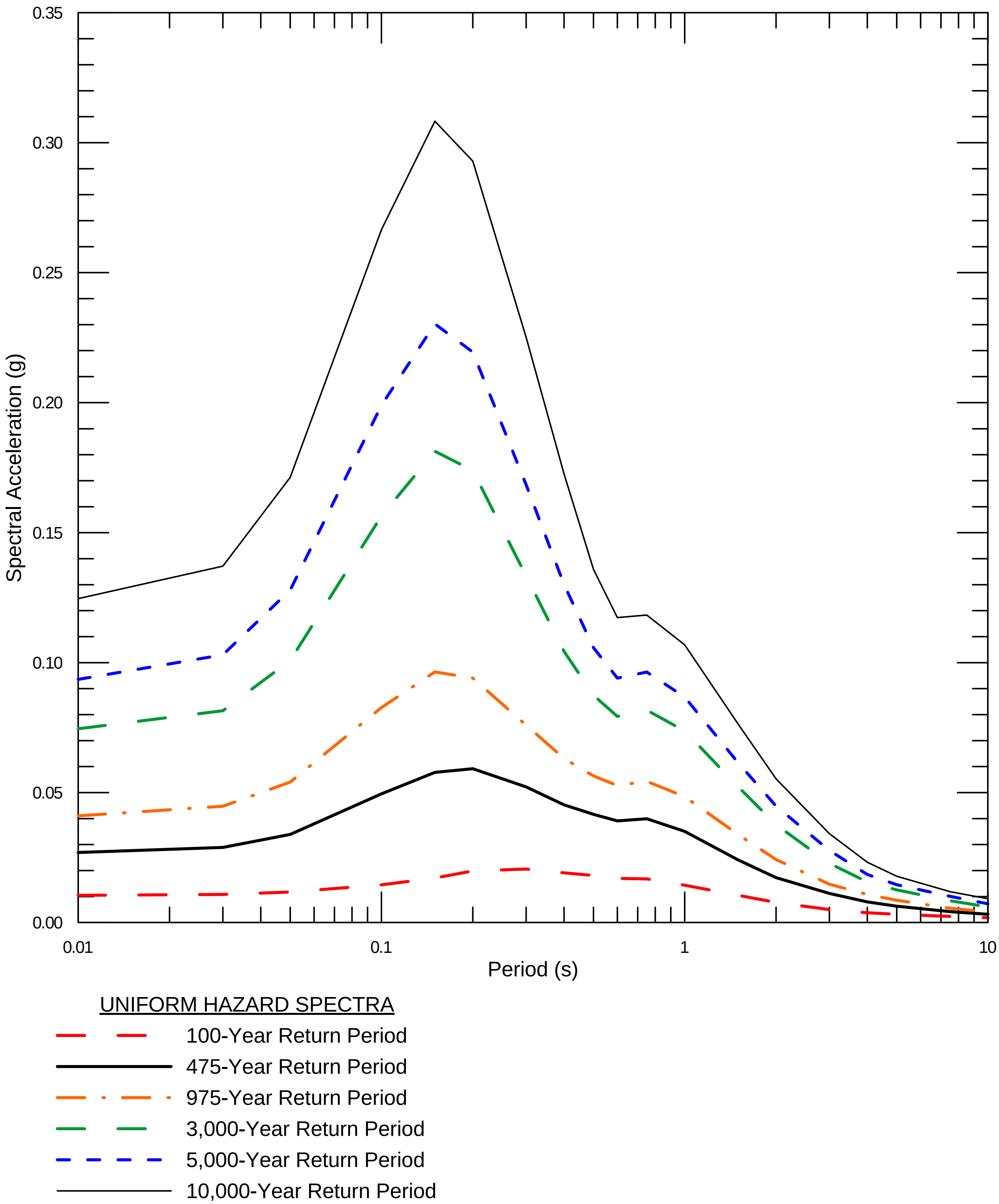

URS	Project No. 26818581	5%-DAMPED UNIFORM HAZARD SPECTRA AT PINTO VALLEY SITE	Figure 63
	Resolution Copper Mining Arizona		

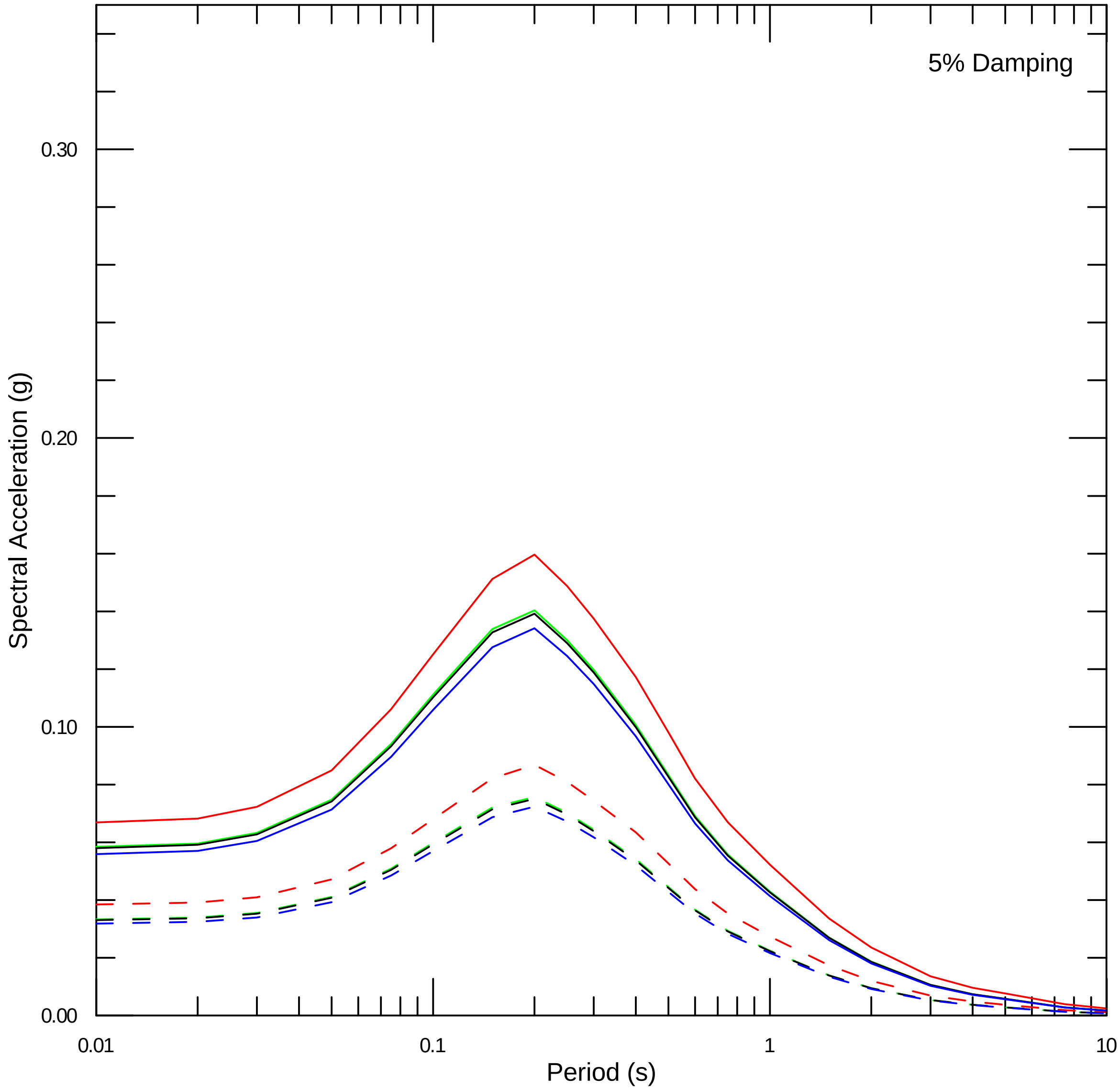

Pinto Valley - Median	Sugarloaf fault
Pinto Valley - 84th Percentile	**M**6.6
Near West - Median	Dip = 50°
Near West - 84th Percentile	Normal Fault
Far West 1 - Median	Far West 1: R_{RUP} = 54.6 km
Far West 1 - 84th Percentile	Far West 2: R_{RUP} = 56.5 km
Far West 2 - Median	Near West: R_{RUP} = 48.6 km
Far West 2 - 84th Percentile	Pinto Valley: R_{RUP} = 54.8 km

URS	Project No. 26818581 Resolution Copper Mining Arizona	MEDIAN AND 84th-PERCENTILE SUGARLOAF FAULT **M**6.6 MCE HORIZONTAL ACCELERATION RESPONSE SPECTRA	Figure 64

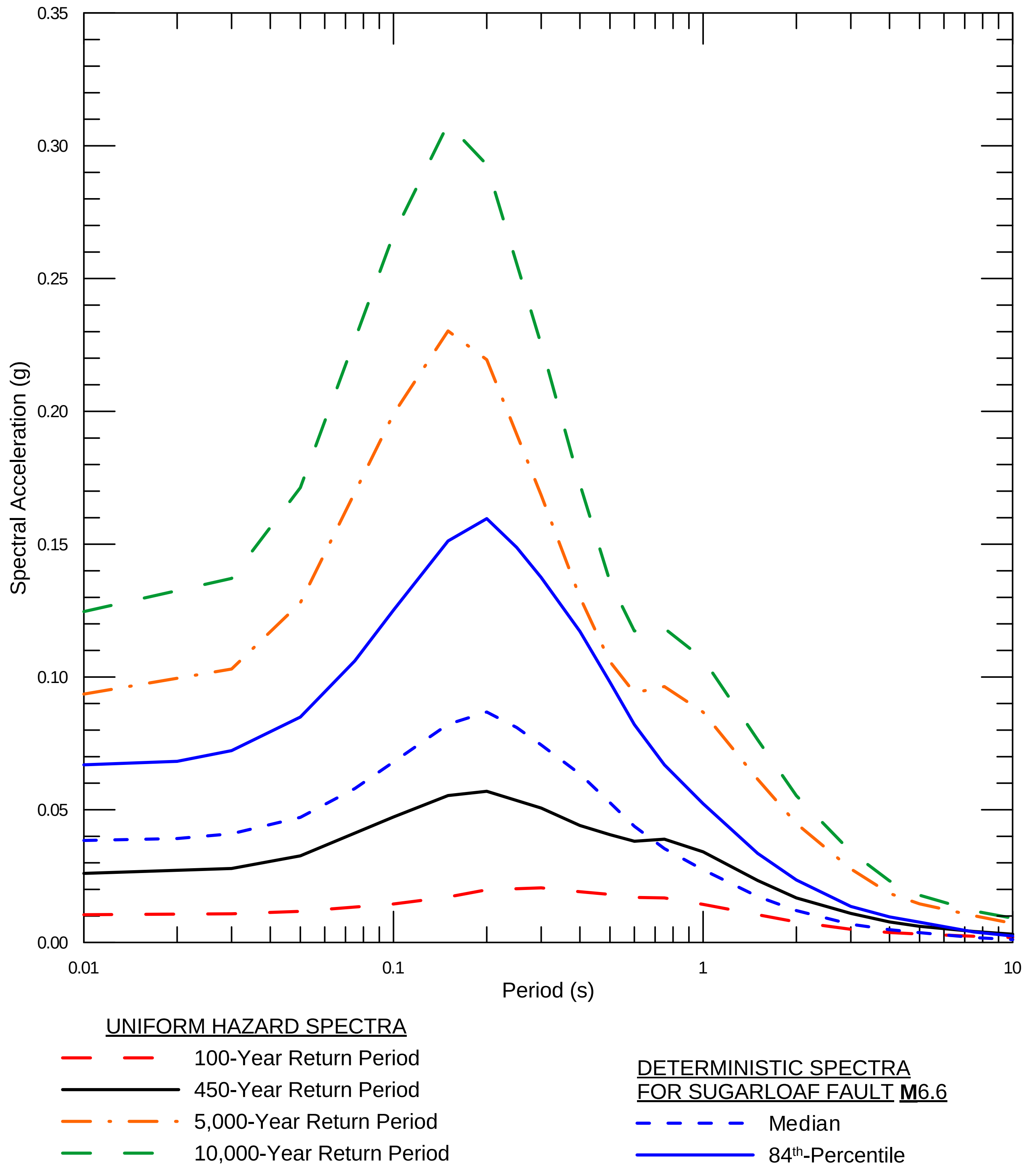

URS	Project No. 26818581	5%-DAMPED UNIFORM HAZARD SPECTRA AND DETERMINISTIC SPECTRA AT PINTO VALLEY SITE	Figure 65
	Resolution Copper Mining Arizona		

Unit	Depth (m)	V_S (m/sec)
Alluvium (Qal)	24	200 ± 50
Quaternary & Tertiary Basaltic fill Deposits	170	400 ± 100
Basalt - Tertiary and Younger Volcanics		~1800 ± 150
? — ? — ?	? — ?	? — ? — ?
Units like Apache Leaf tuff other volcanic units, and possibly Paleozoic sedmentary units	600 - 900	?
Pinal Schist		> 2000

URS

Project No. 26818581

Resolution Copper Mining, Arizona

STRATIGRAPHY AND V_S AT FAR WEST 1

Figure 66

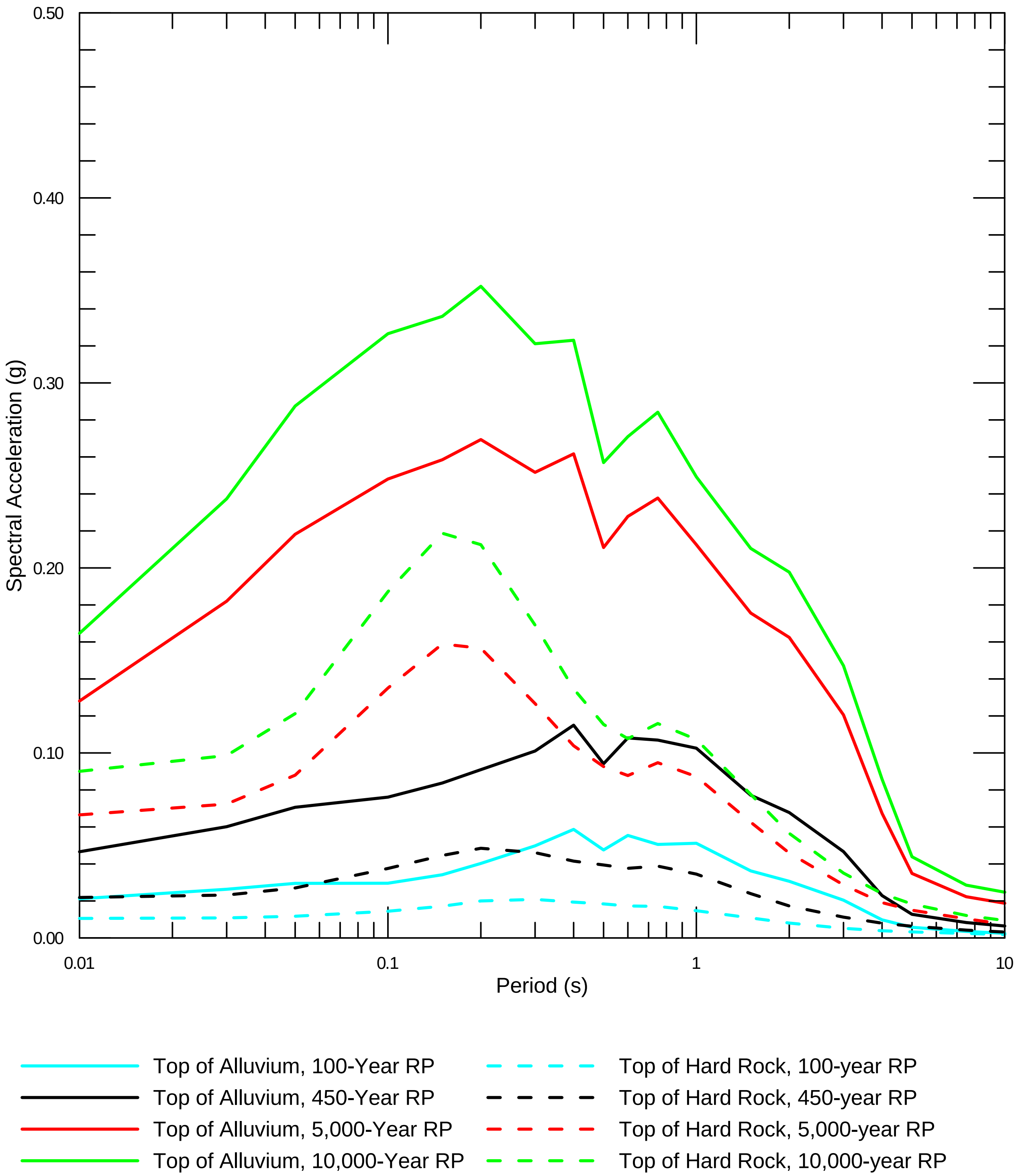

URS	Project No. 26818581	UHS AT FAR WEST 1 AT THE TOP OF HARD ROCK AND ALLUVIUM	Figure 67
	Resolution Copper Mining Arizona		

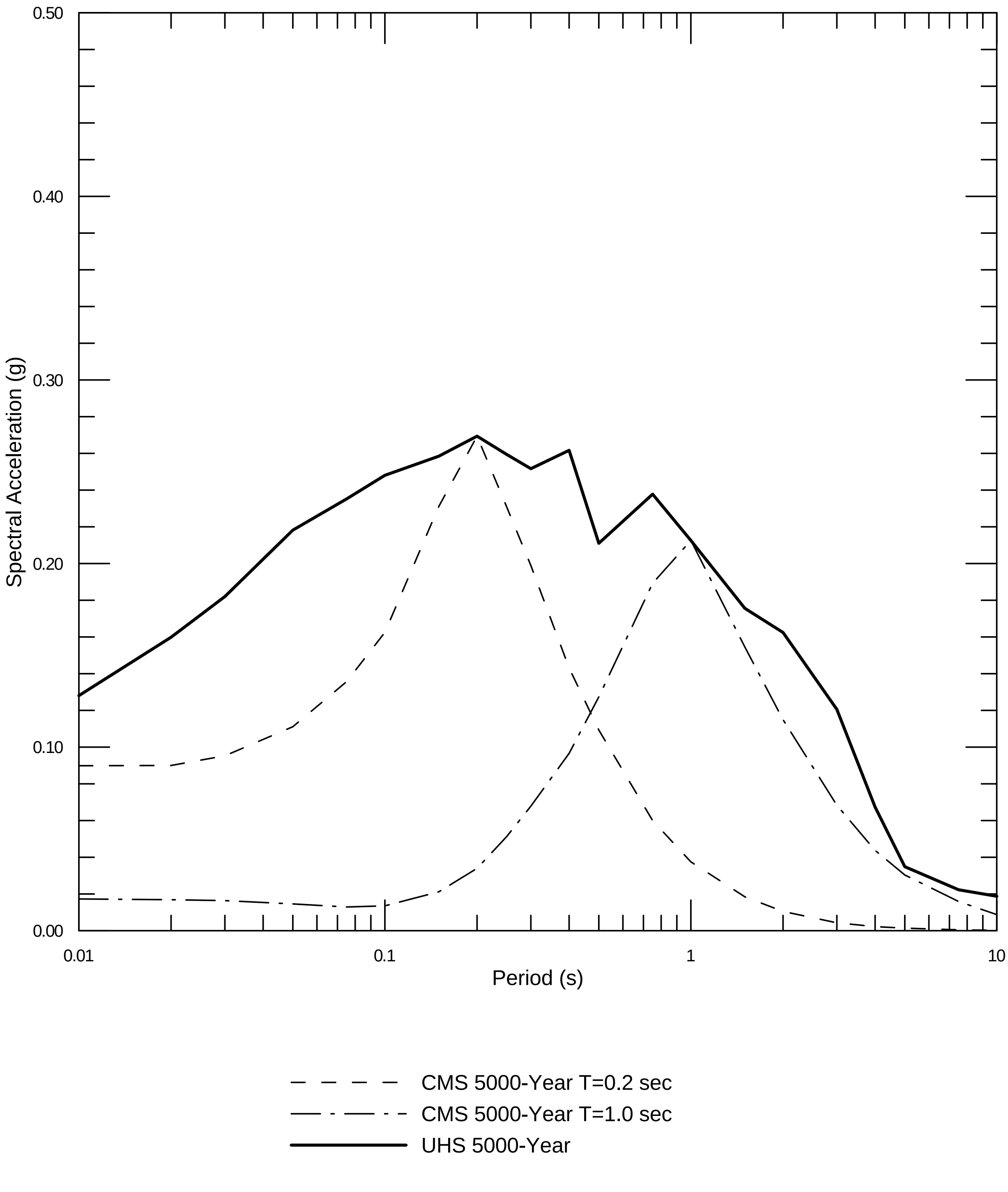

URS	Project No. 26818581	5%-DAMPED 5000-YEAR RETURN PERIOD UHS FOR TOP OF ALLUVIUM AND CMS AT FAR WEST 1 SITE	Figure 68
	Resolution Copper Mining Arizona		

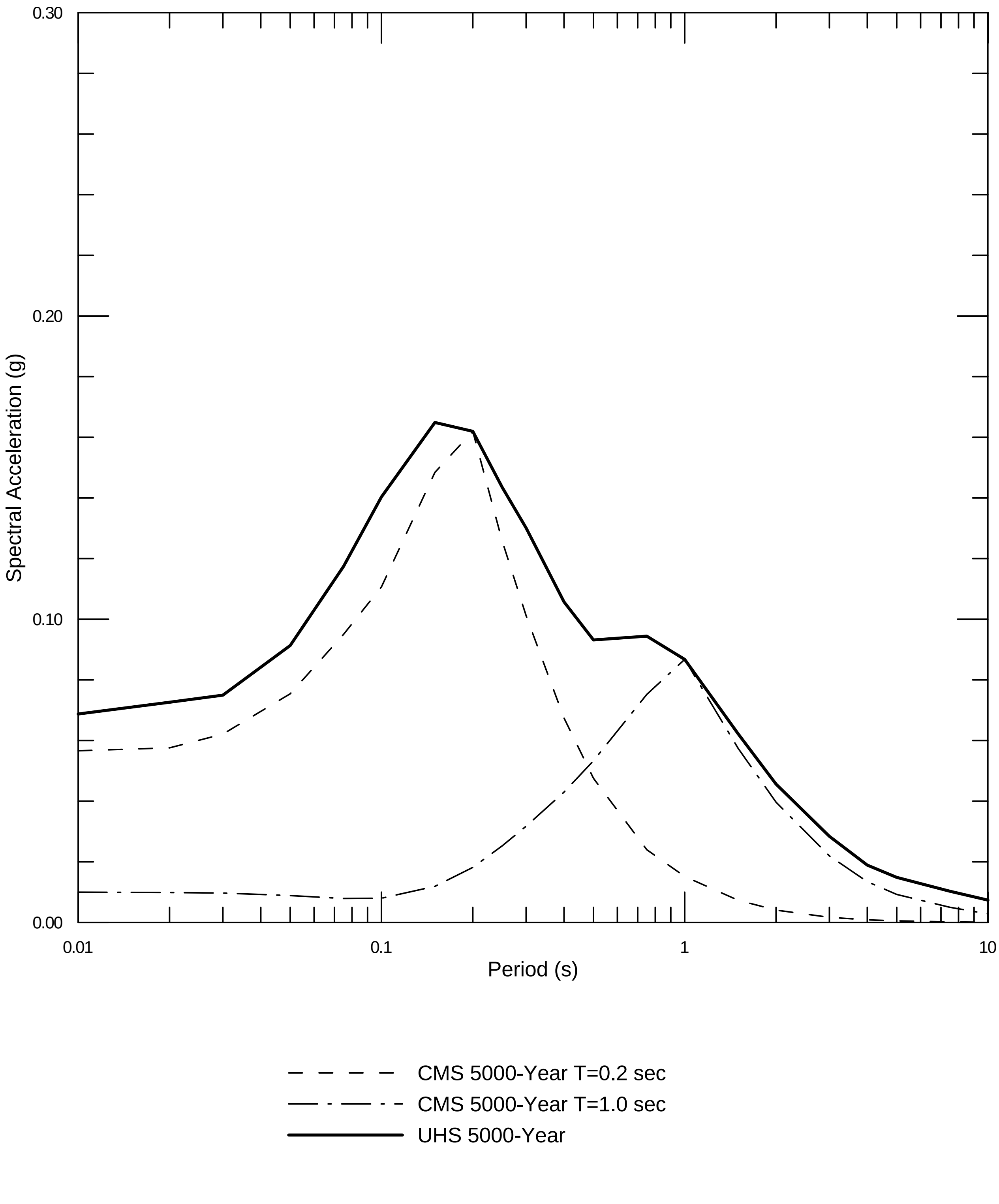

URS	Project No. 26818581 Resolution Copper Mining Arizona	5%-DAMPED 5000-YEAR RETURN PERIOD UHS AND CMS AT FAR WEST 2 SITE	Figure 69

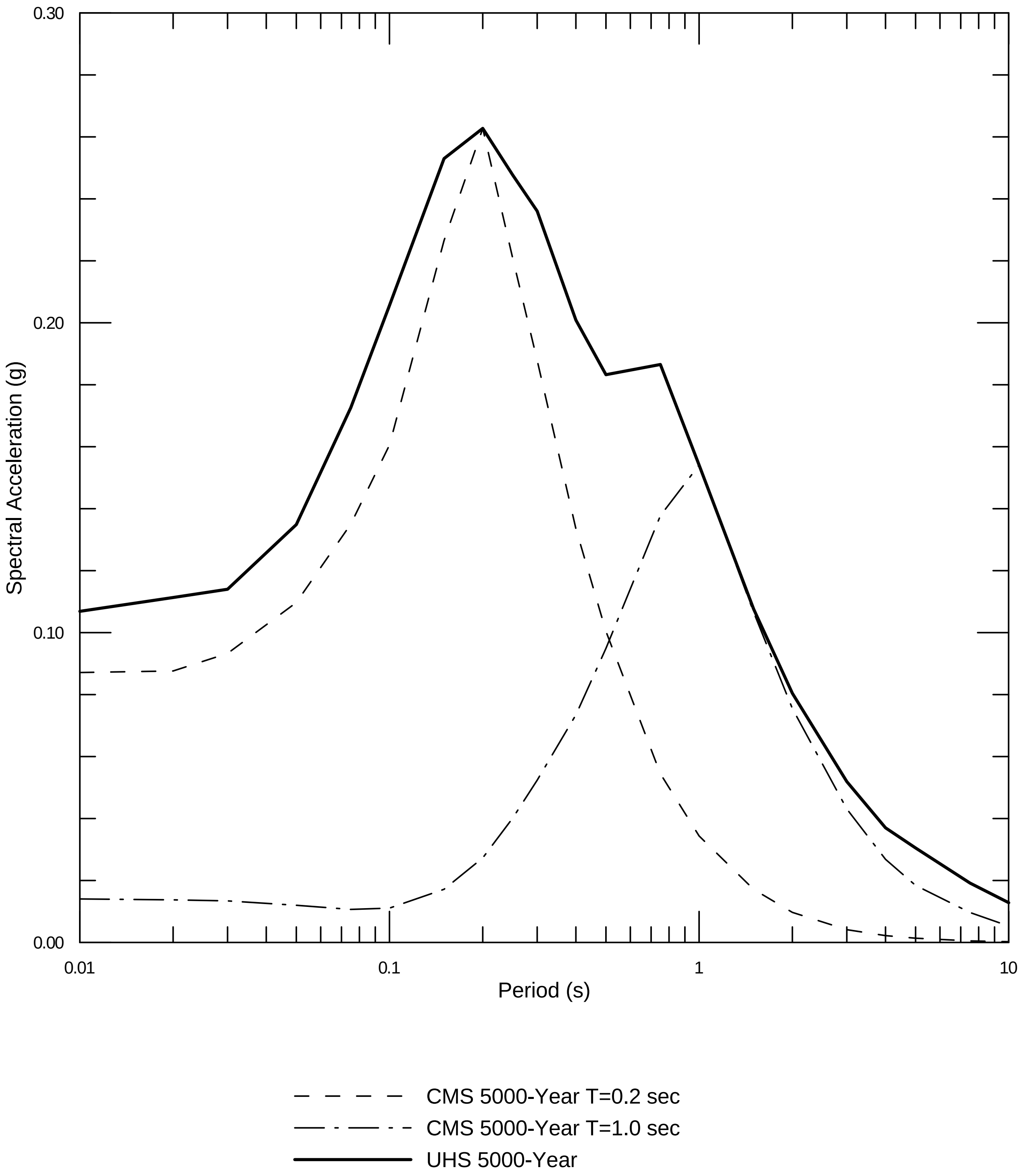

URS	Project No. 26818581 Resolution Copper Mining Arizona	5%-DAMPED 5000-YEAR RETURN PERIOD UHS AND CMS AT NEAR WEST SITE	Figure 70

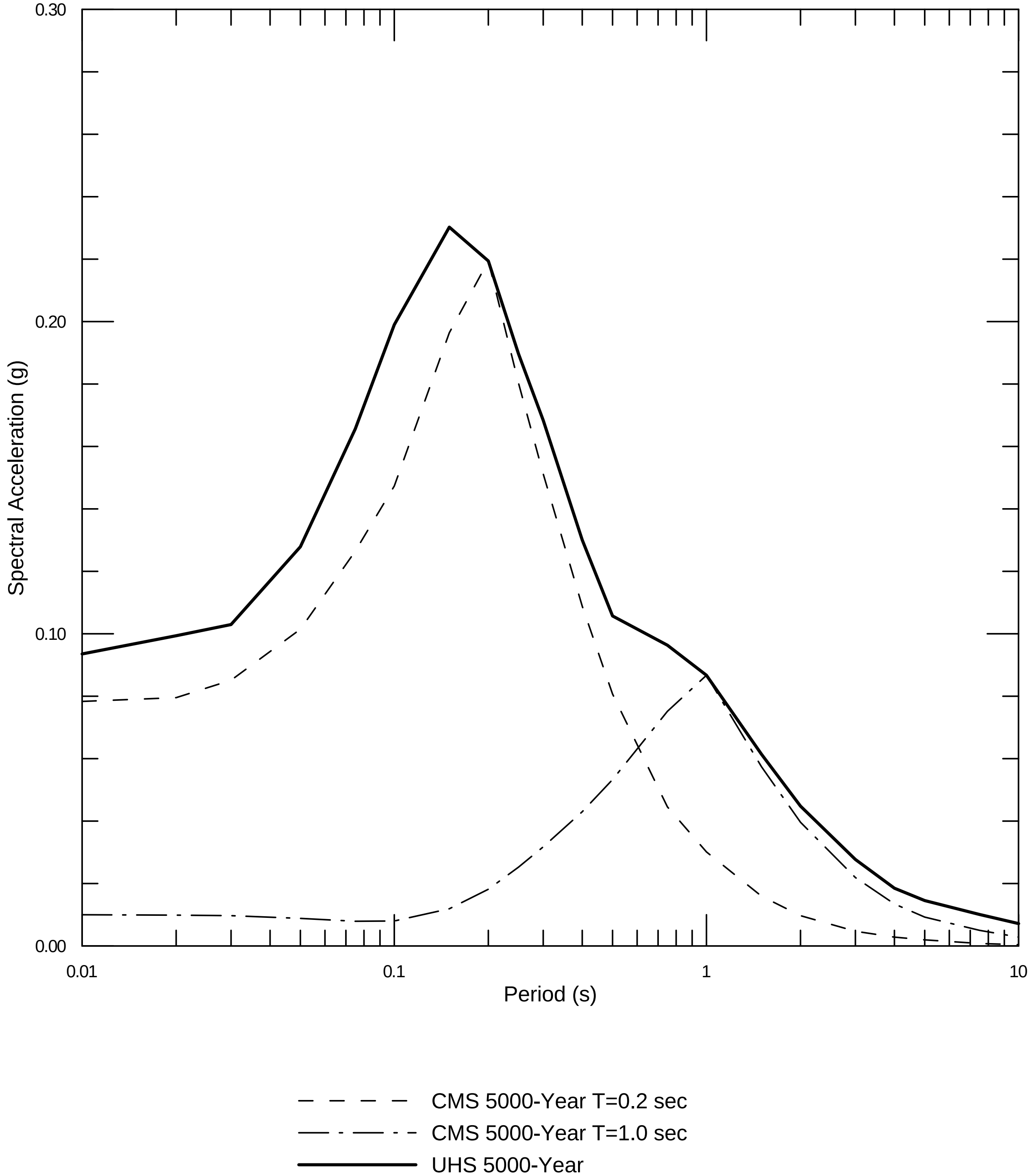

URS	Project No. 26818581 Resolution Copper Mining Arizona	5%-DAMPED 5000-YEAR RETURN PERIOD UHS AND CMS AT PINTO VALLEY SITE	Figure 71

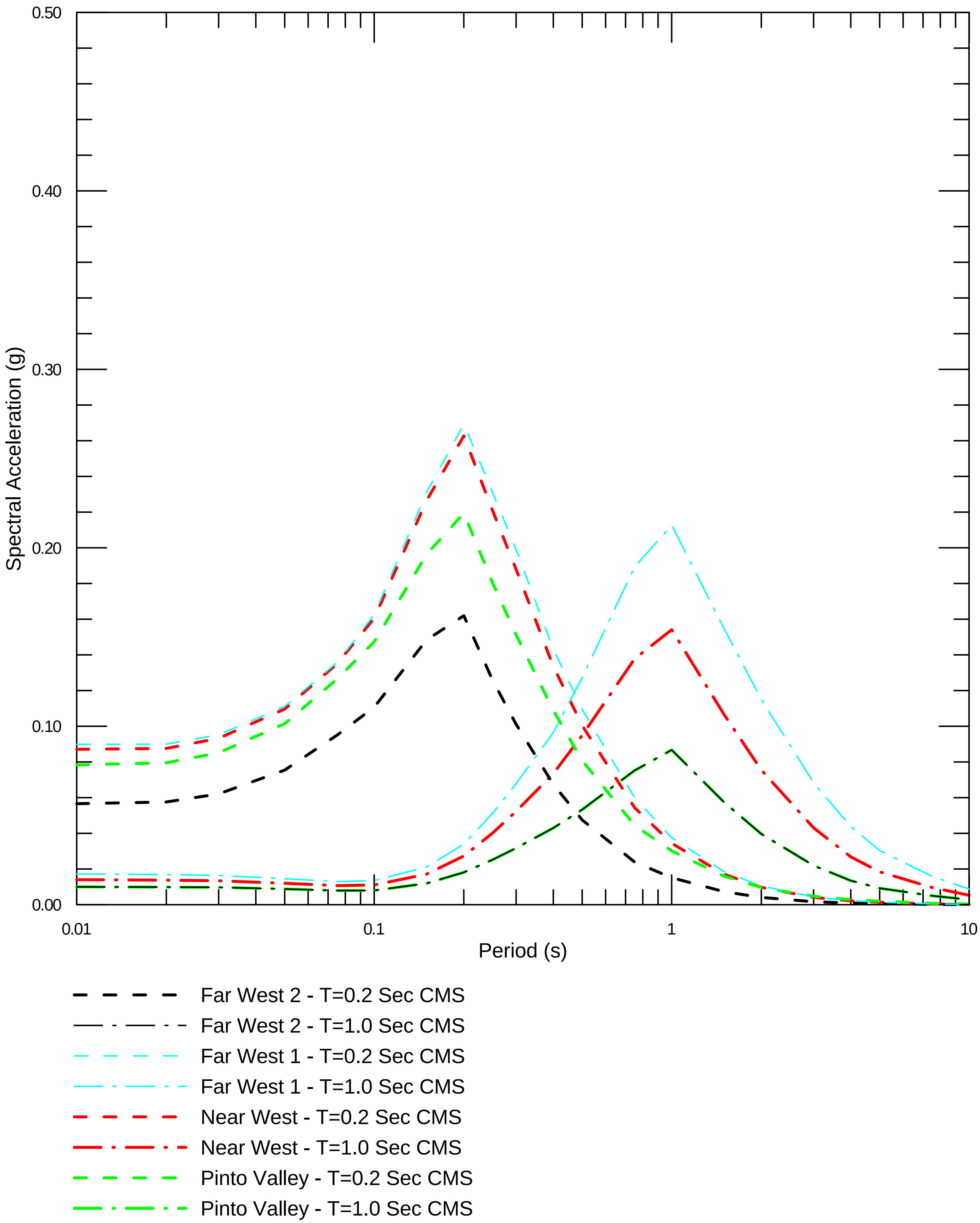

URS	Project No. 26818581 Resolution Copper Mining Arizona	5,000-YEAR RETURN PERIOD CMS FOR 0.2 AND 1.0 SEC SPECTRAL ACCELERATION	Figure 72

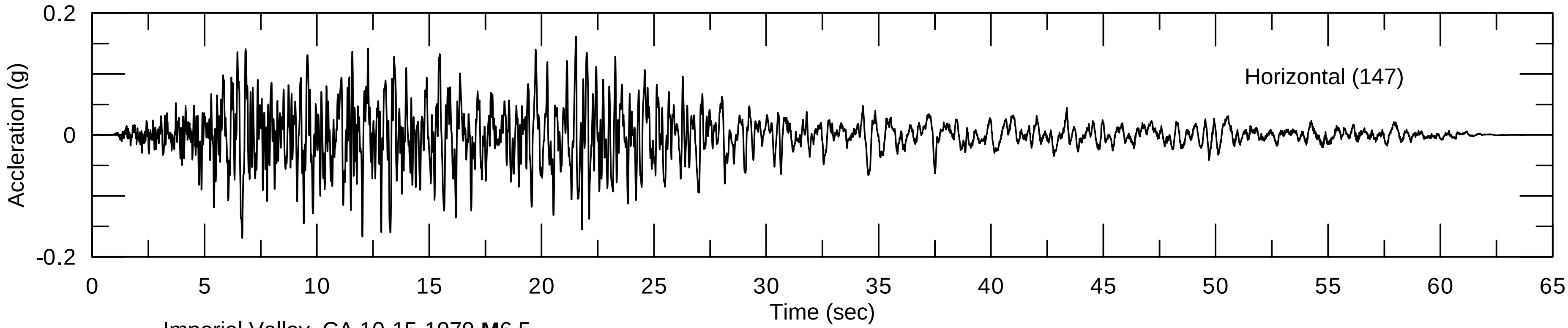

Imperial Valley, CA 10-15-1979 **M**6.5
Cerro Prieto
Dist=15.19 km
V_S30 = 659.6 m/s

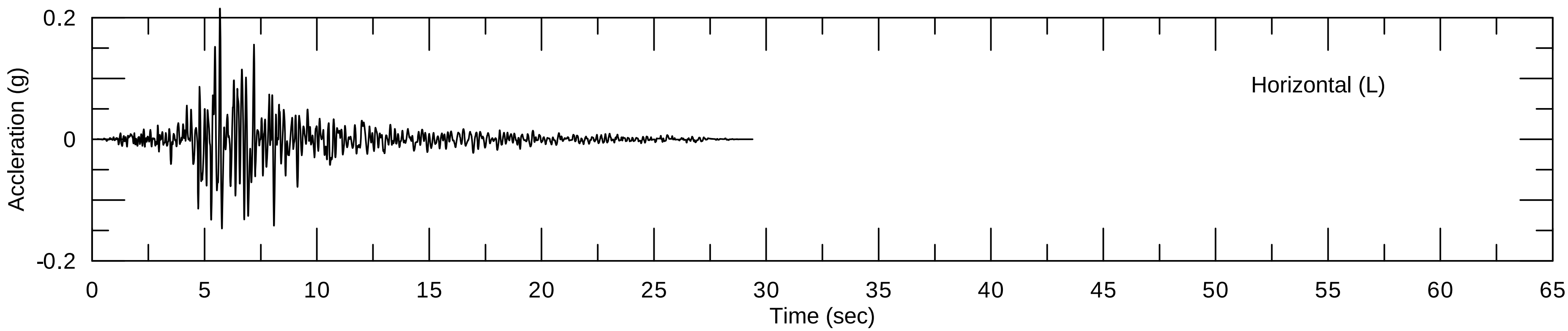

Kozani, Greece 1995 **M**6.4
Kozani
Dist=19.5 km
V_S30 = 659.6 m/s

URS	Project No. 26818294 Resolution Copper Arizona	SEED TIME HISTORIES FOR 0.2 SEC CMS SPECTRUM 1979 IMPERIAL VALLEY AND 1995 KOZANI	Figure 73

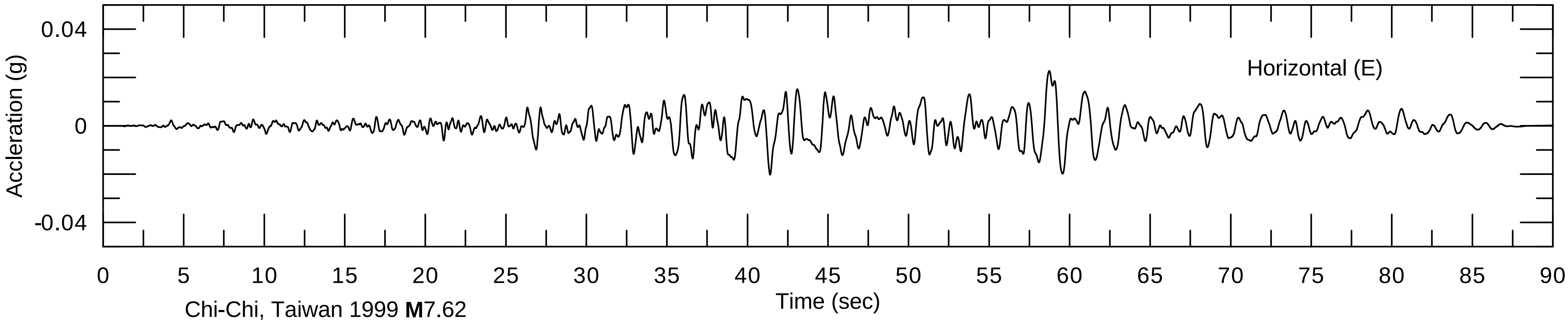

Chi-Chi, Taiwan 1999 **M**7.62
KAU046
Dist= 162 km
V_S30 =204.2 m/s

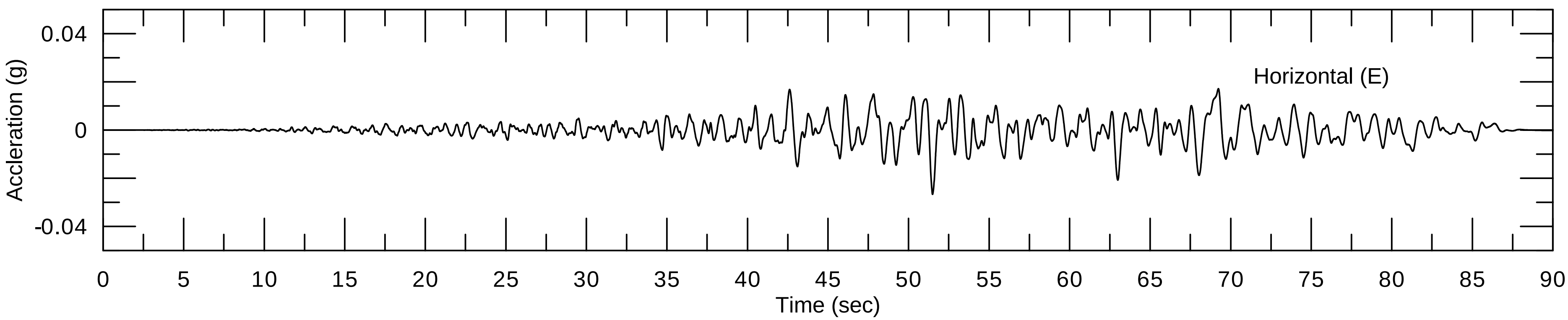

Chi-Chi, Taiwan 1999 **M**7.62
KAU081
Dist= 161 km
V_S30 =272.4 m/s

URS	Project No. 26818294 Resolution Copper Arizona	SEED TIME HISTORIES FOR 1.0 SEC CMS SPECTRUM 1999 CHI-CHI	Figure 74

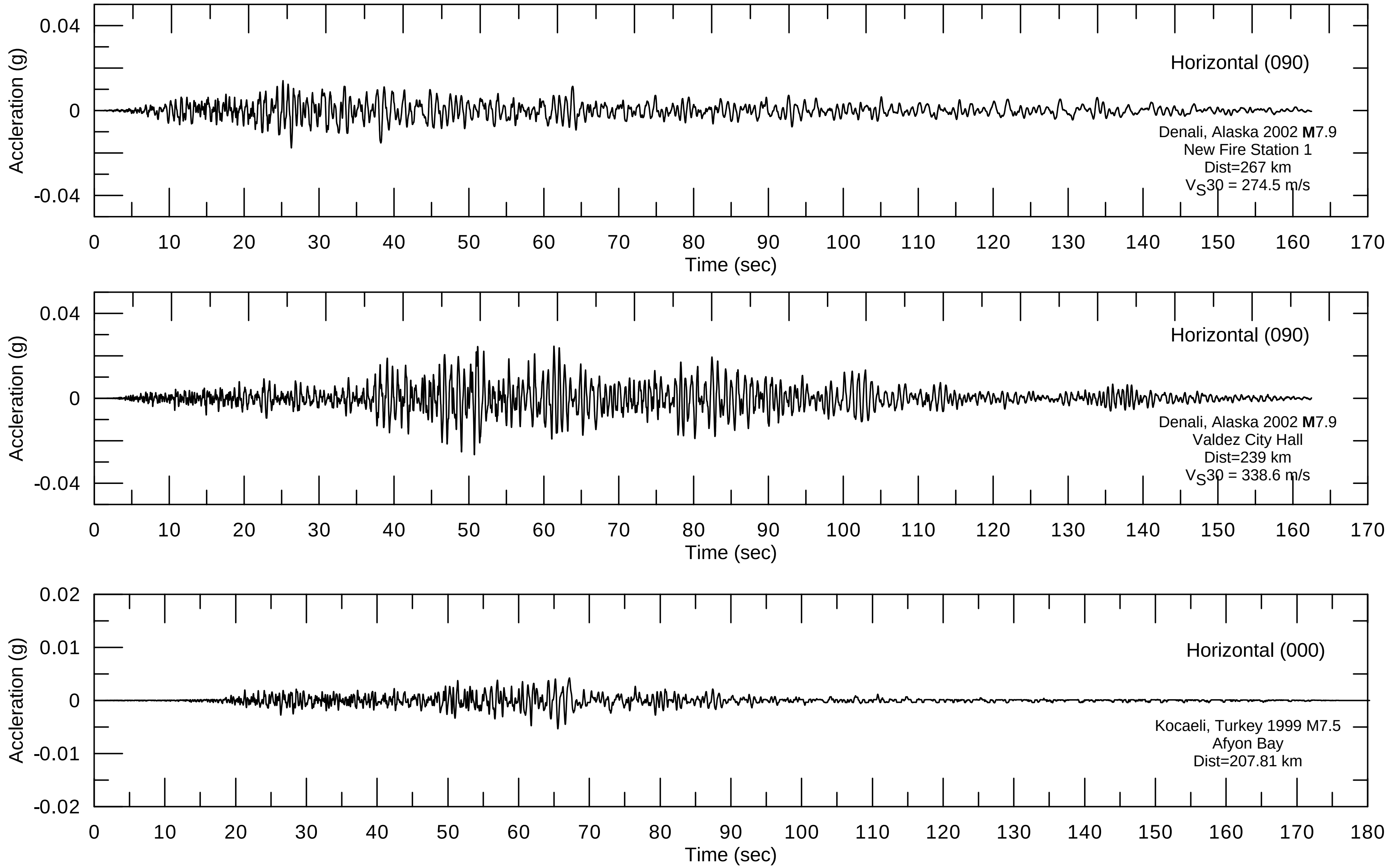

URS	Project No. 26818581 Resolution Copper Arizona	SEED TIME HISTORIES FOR 1.0 SEC CMS SPECTRUM 1999 KOCAELI AND 2002 DENALI	Figure 75

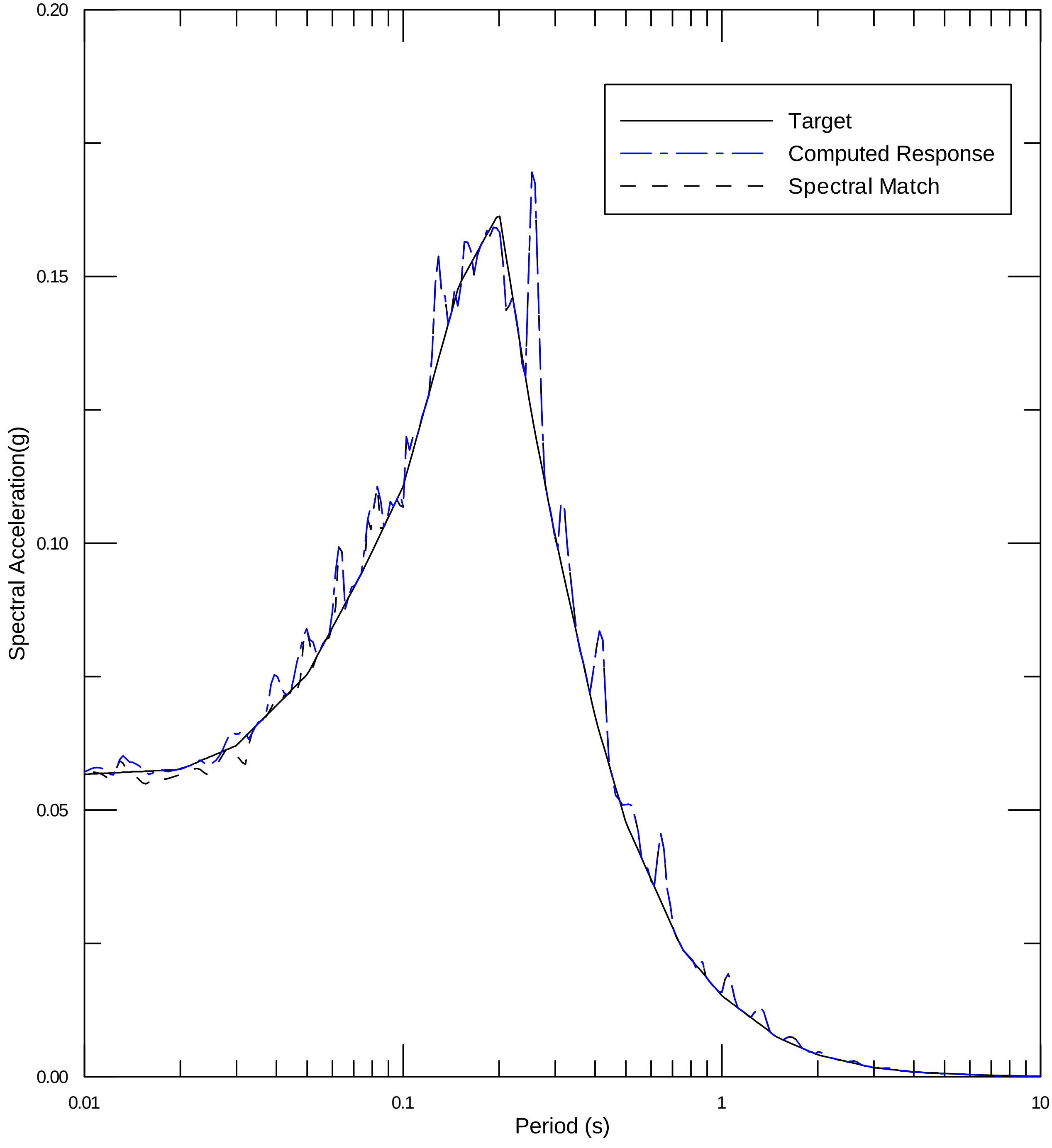

URS

Project No. 26818581

Resolution Copper
Arizona

SPECTRAL MATCH TO HORIZONTAL
5,000-YEAR RETURN PERIOD 0.2 SEC CMS SPECTRUM
1979 IMPERIAL VALEY - CERRO PRIETO (147)
FOR FAR WEST 2 (ROCK) SITE

Figure
76

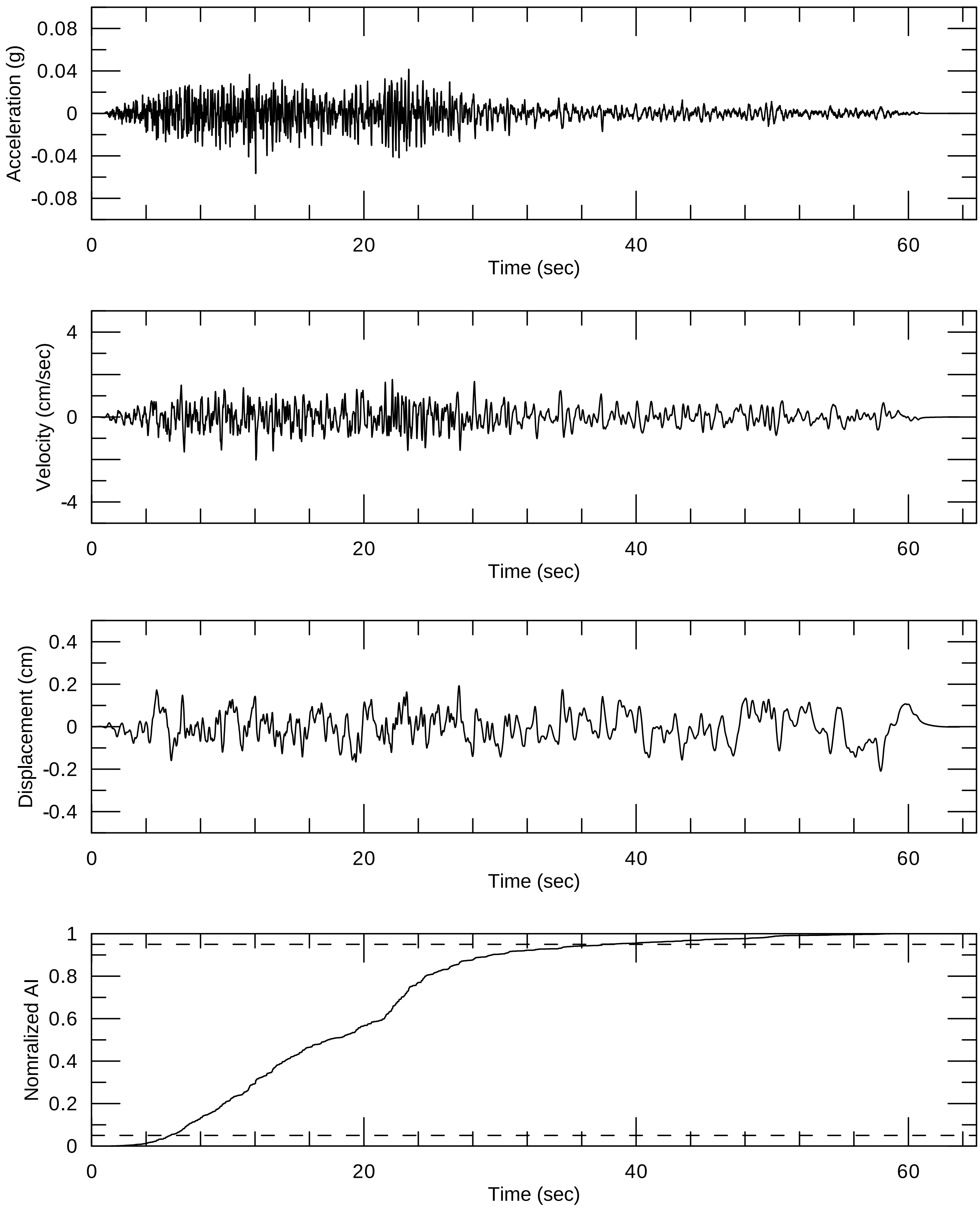

Project No. 26818581	TIME HISTORIES SPECTRALLY MATCHED TO HORIZONTAL 5,000-YEAR RETURN PERIOD 0.2 SEC CMS SPECTRUM 1979 IMPERIAL VALLEY-CERRO PRIETO (147) FOR FAR WEST 2 (ROCK) SITE	Figure 77
Resolution Copper Arizona		

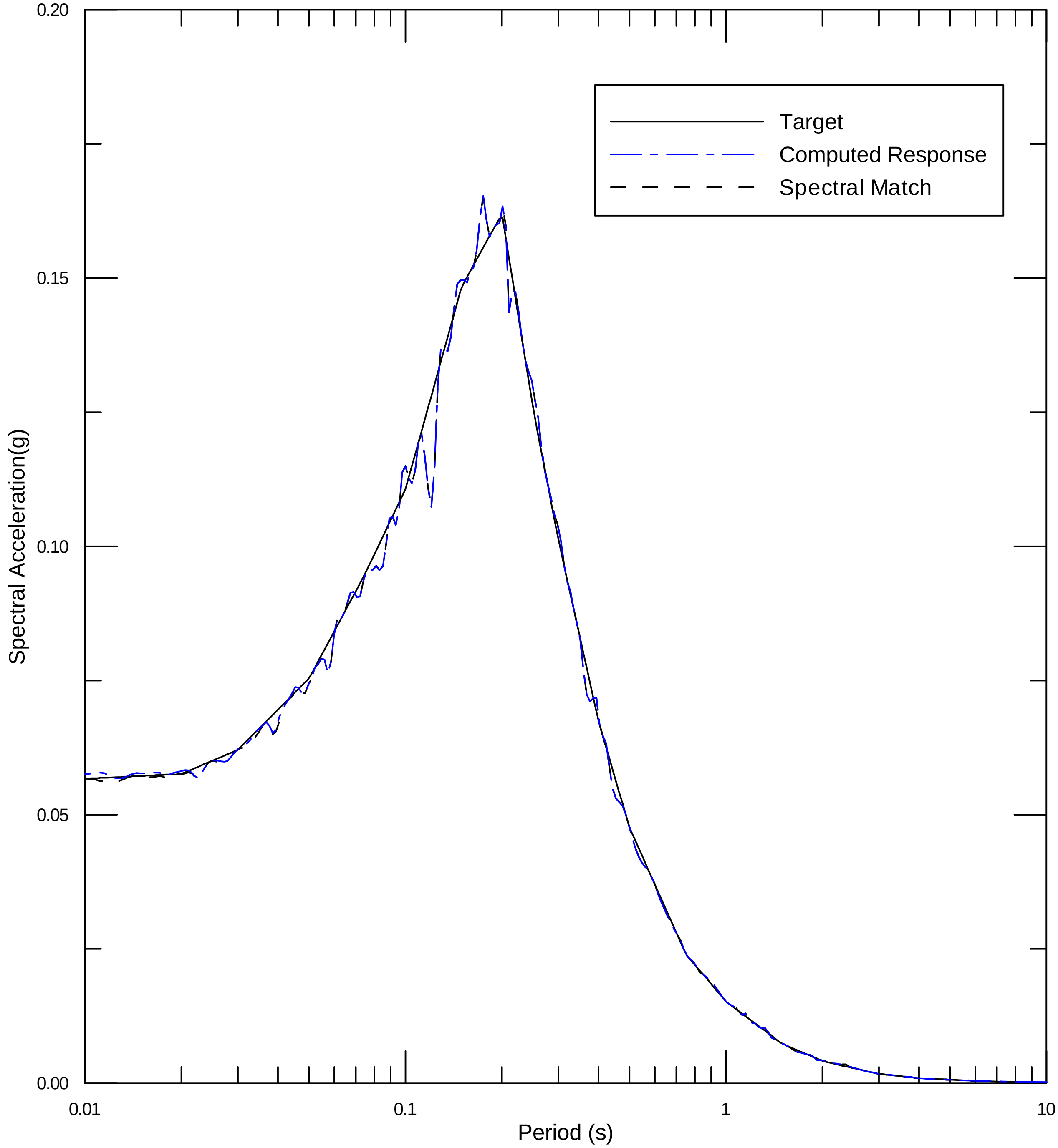

URS	Project No. 26818581 Resolution Copper Arizona	SPECTRAL MATCH TO HORIZONTAL 5,000-YEAR RETURN PERIOD0.2 SEC CMS SPECTRUM 1995 KOZANI - KOZANI (L) FOR FAR WEST 2 (ROCK) SITE	Figure 78

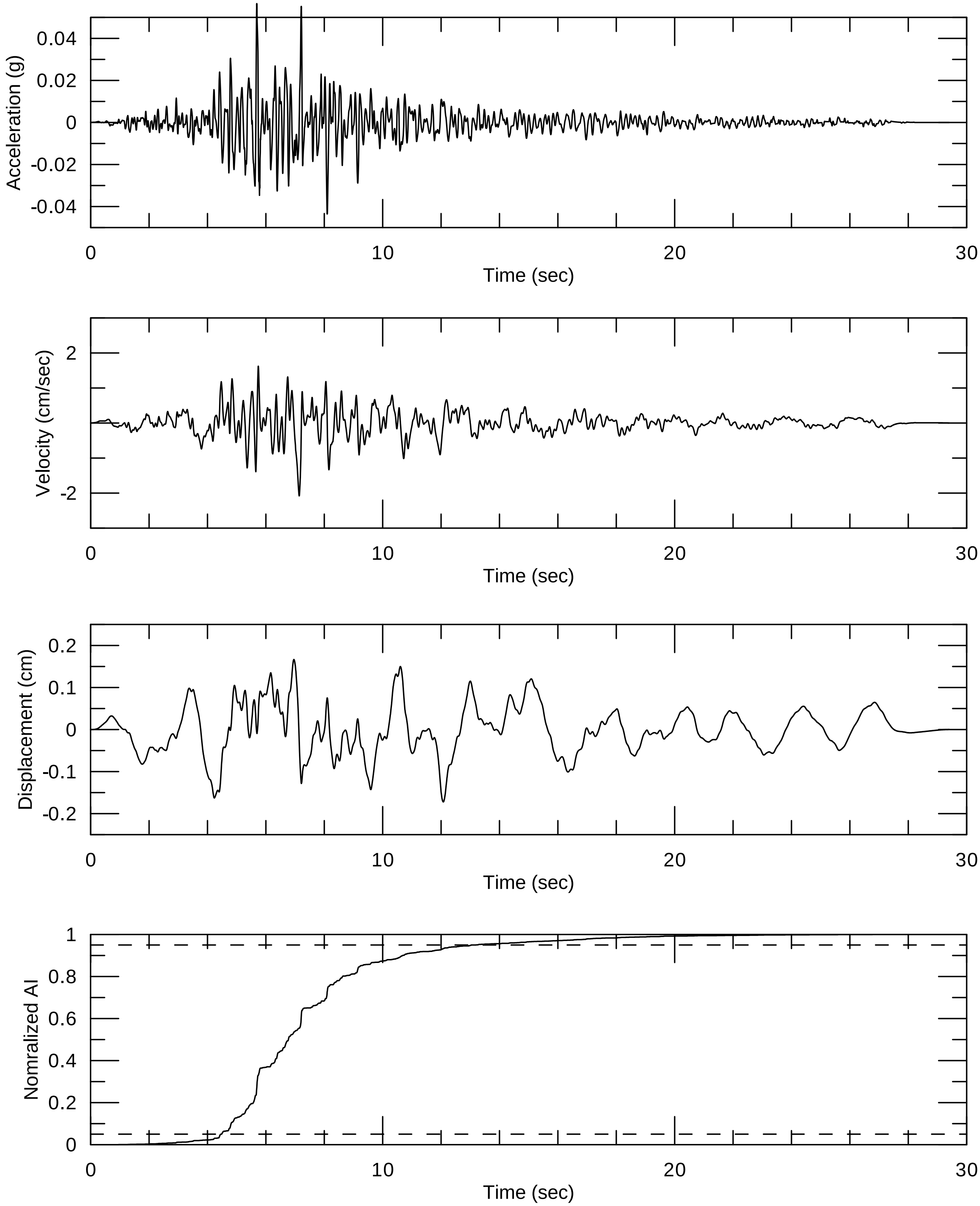

URS	Project No. 26818581 Resolution Copper Arizona	TIME HISTORIES SPECTRALLY MATCHED TO HORIZONTAL 5,000-YEAR RETURN PERIOD 0.2 SEC CMS SPECTRUM 1995 KOZANI- KOZANI (L) FOR FAR WEST 2 (ROCK) SITE	Figure 79

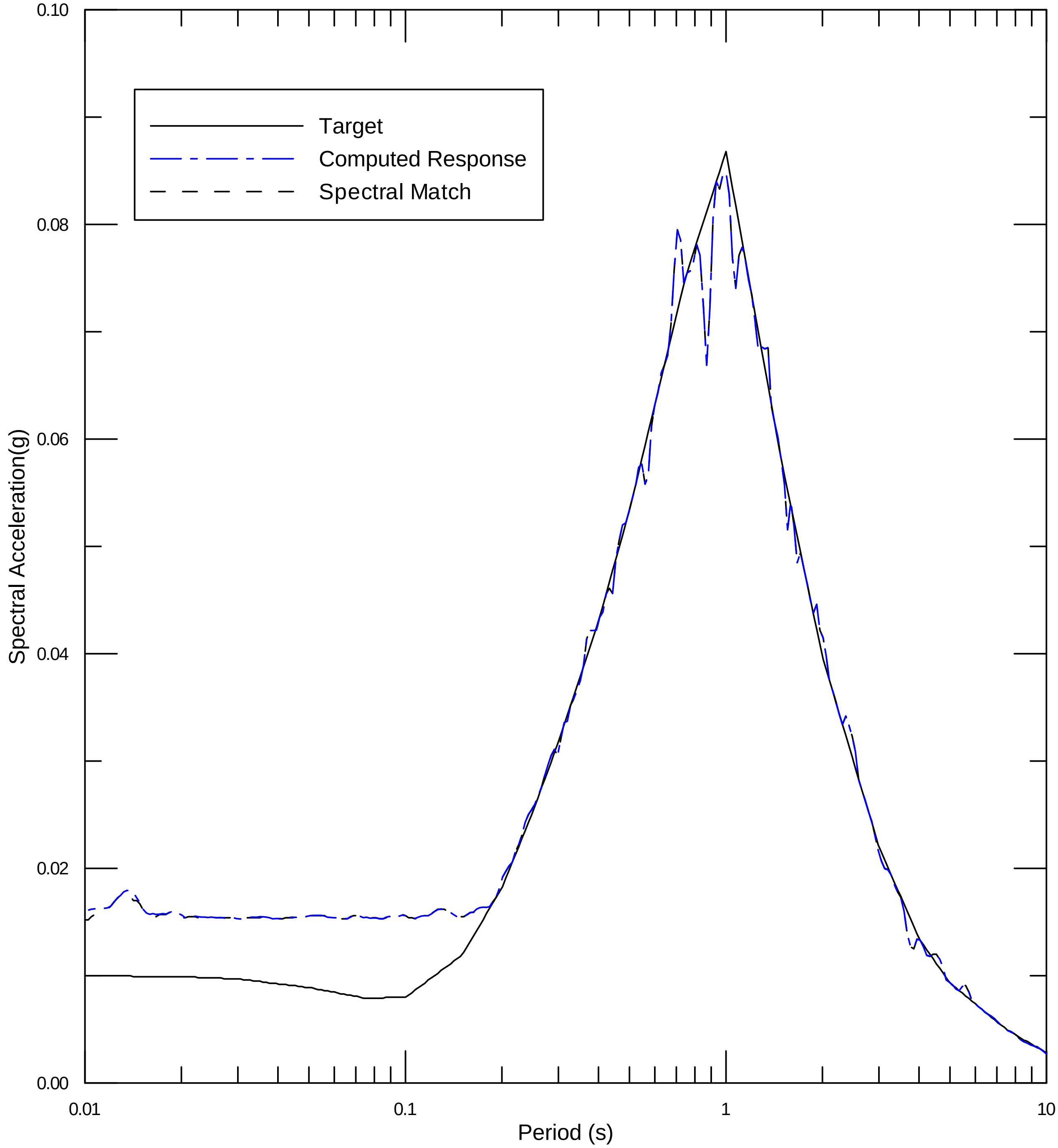

URS	Project No. 26818581 Resolution Copper Arizona	SPECTRAL MATCH TO HORIZONTAL 5,000-YEAR RETURN PERIOD 1.0 SEC CMS SPECTRUM 1999 CHI-CHI - KAU046 (E) FOR FAR WEST 2 (ROCK) SITE	Figure 80

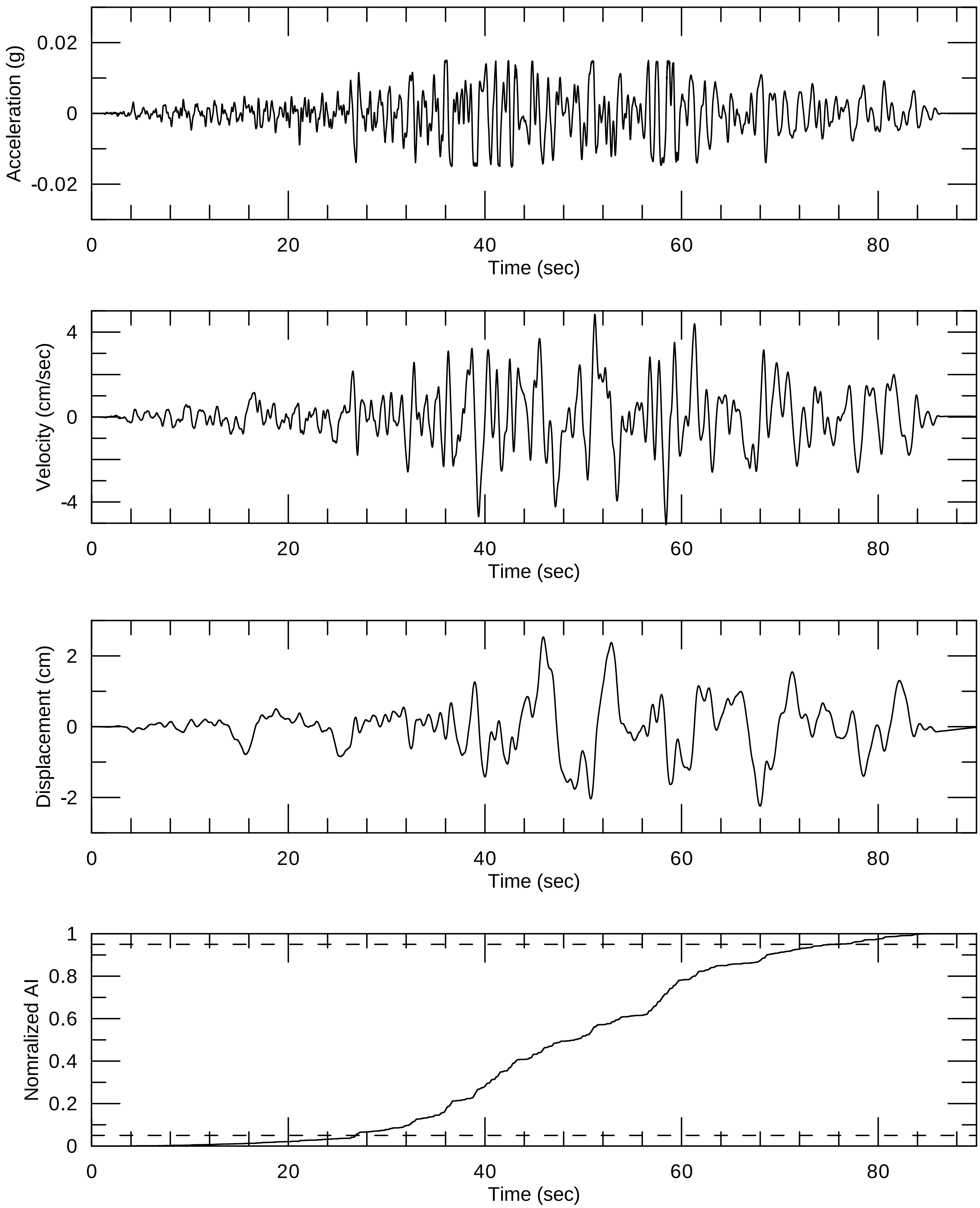

URS

Project No. 26818581

Resolution Copper
Arizona

TIME HISTORIES SPECTRALLY MATCHED TO HORIZONTAL 5,000-YEAR RETURN PERIOD 1.0 SEC CMS SPECTRUM 1999 CHI-CHI - NAU046 (E) FOR FAR WEST 2 (ROCK) SITE

Figure 81

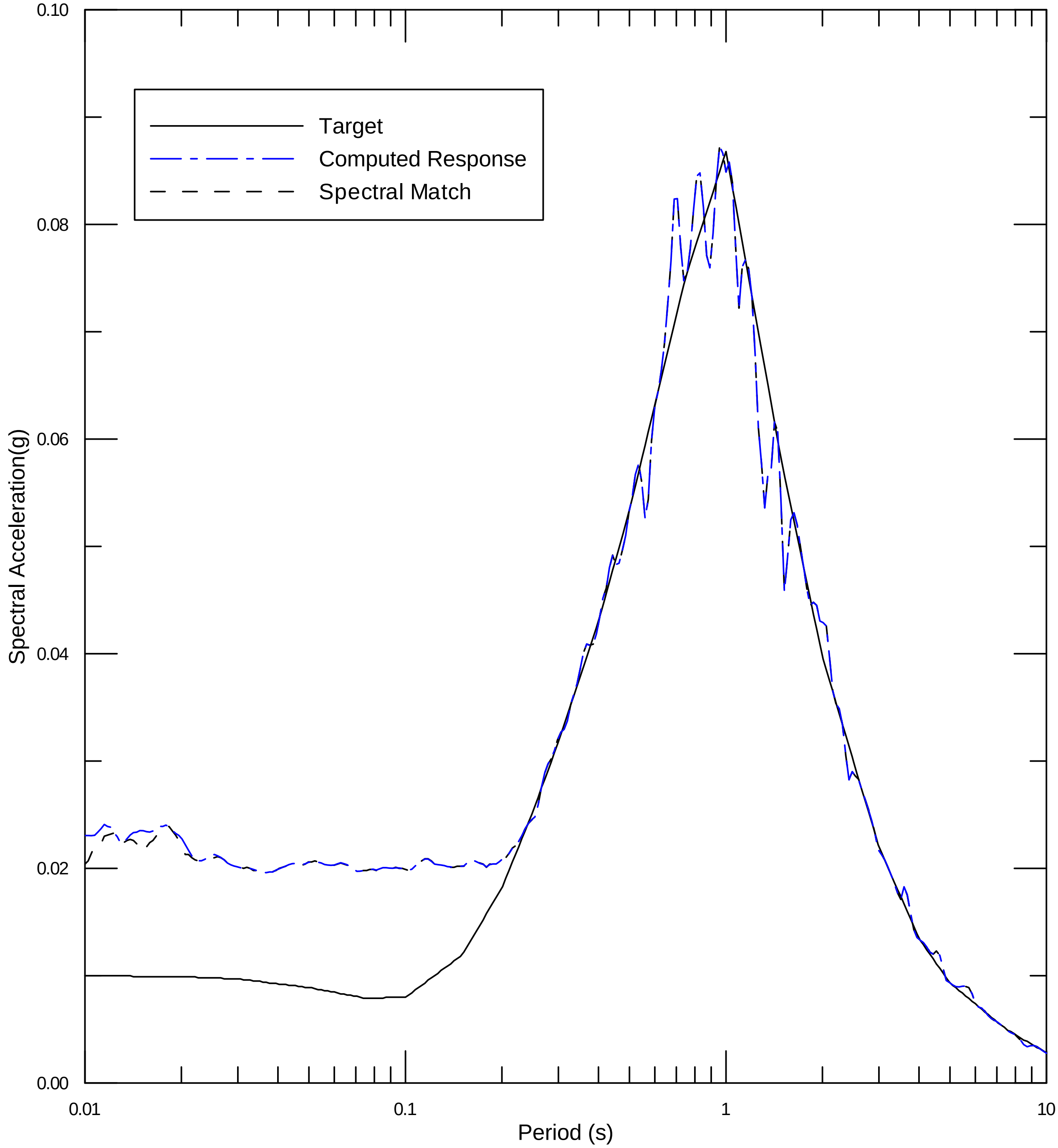

URS	Project No. 26818581 Resolution Copper Arizona	SPECTRAL MATCH TO HORIZONTAL 5,000-YEAR RETURN PERIOD 1.0 SEC CMS SPECTRUM 1999 CHI-CHI - KAU081 (E) FOR FAR WEST 2 (ROCK) SITE	Figure 82

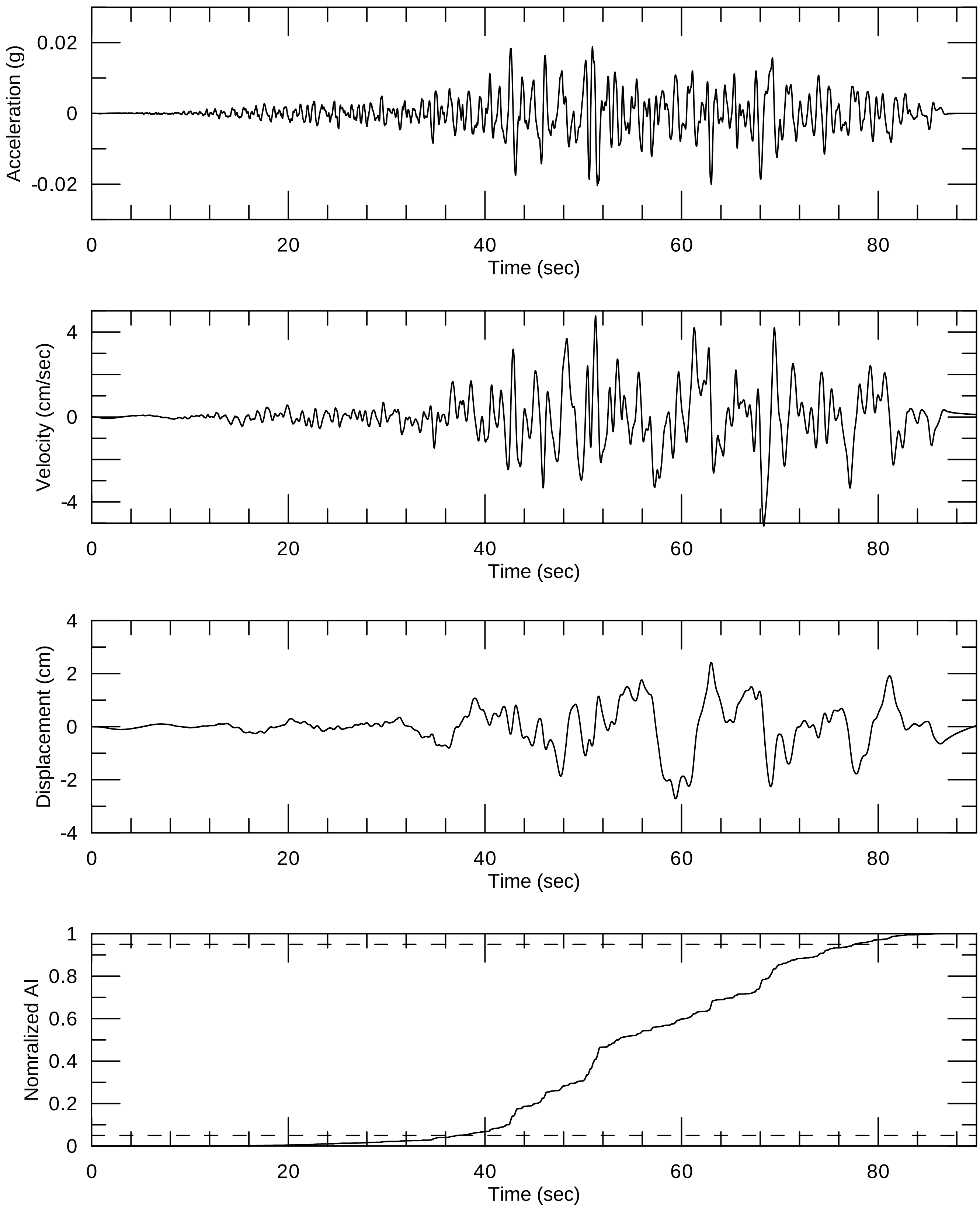

URS	Project No. 26818581 Resolution Copper Arizona	TIME HISTORIES SPECTRALLY MATCHED TO HORIZONTAL 5,000-YEAR RETURN PERIOD 1.0 SEC CMS SPECTRUM 1999 CHI-CHI - KAU081 (E) FOR FOR FAR WEST 2 (ROCK) SITE	Figure 83

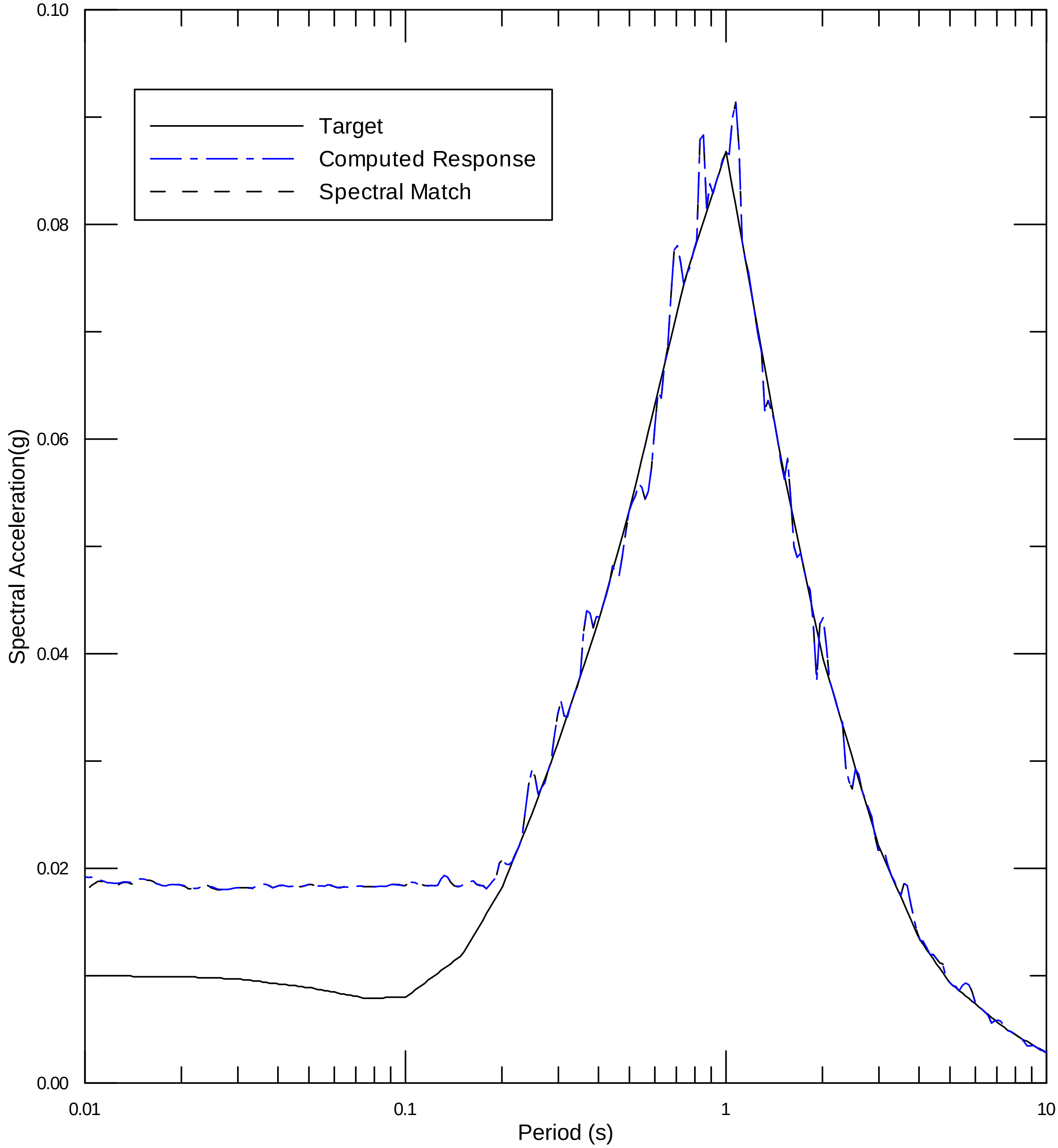

URS	Project No. 26818581 Resolution Copper Arizona	SPECTRAL MATCH TO HORIZONTAL 5,000-YEAR RETURN PERIOD 1.0 SEC CMS SPECTRUM 2002 DENALI - FIRE STATION 1 (090) FOR FAR WEST 2 (ROCK) SITE	Figure 84

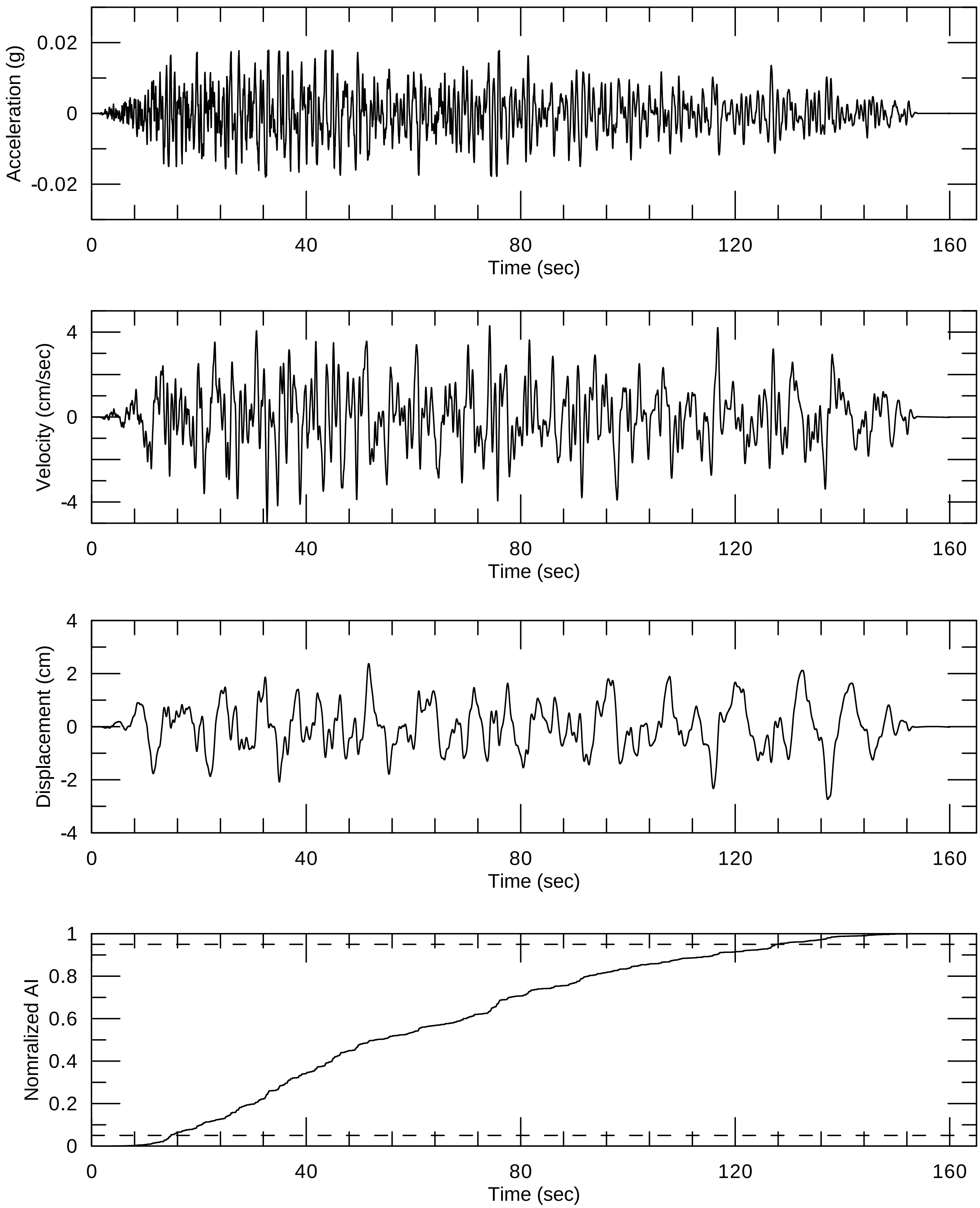

URS	Project No. 26818581 Resolution Copper Arizona	TIME HISTORIES SPECTRALLY MATCHED TO HORIZONTAL 5,000-YEAR RETURN PERIOD 1.0 SEC CMS SPECTRUM 2002 DENALI - FIRE STATION 1 (090) FOR FAR WEST 2 (ROCK) SITE	Figure 85

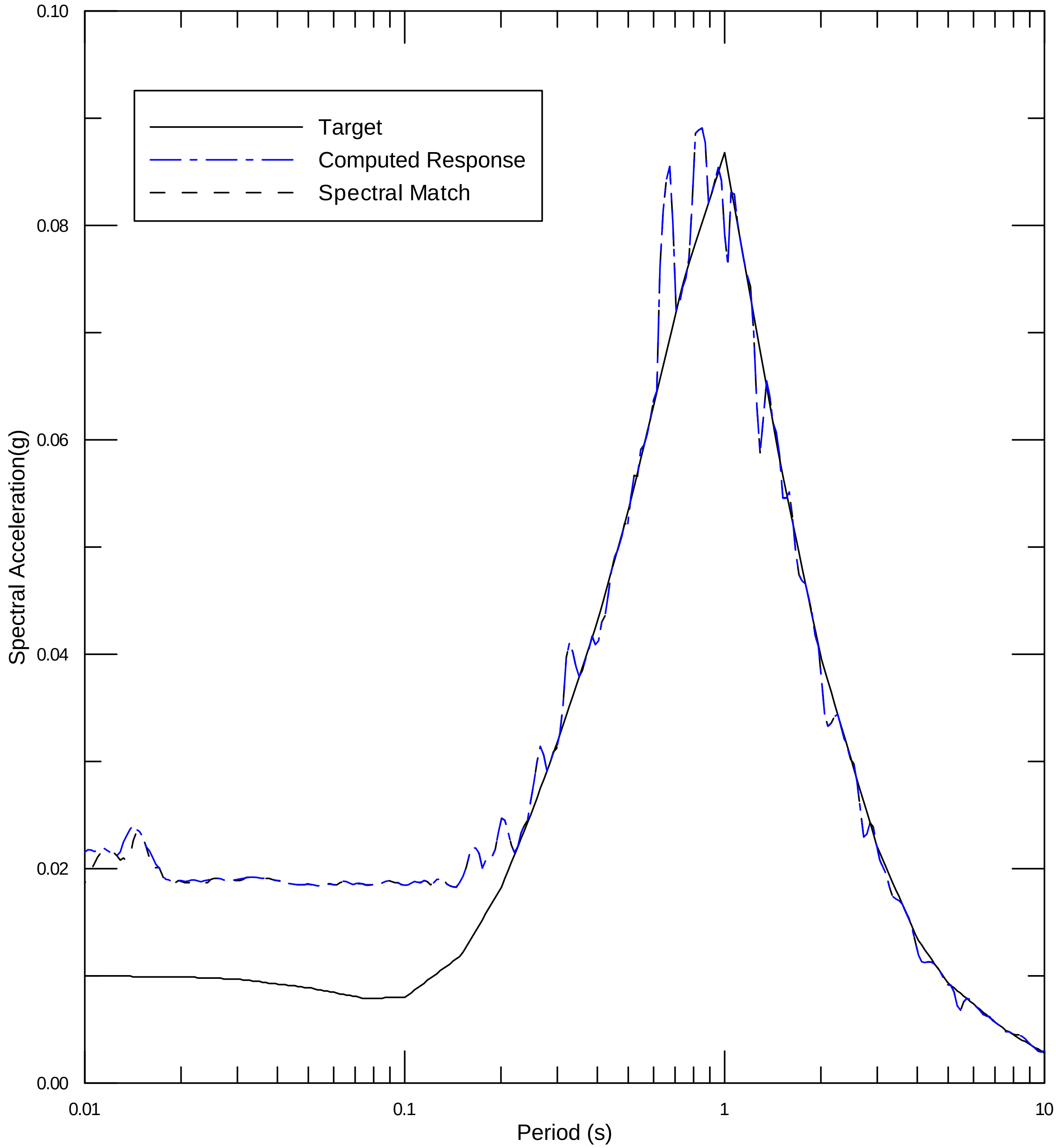

URS	Project No. 26818581 Resolution Copper Arizona	SPECTRAL MATCH TO HORIZONTAL 5,000-YEAR RETURN PERIOD 1.0 SEC CMS SPECTRUM 2002 DENALI - VALDEZ CITY HALL (090) FOR FAR WEST 2 (ROCK) SITE	Figure 86

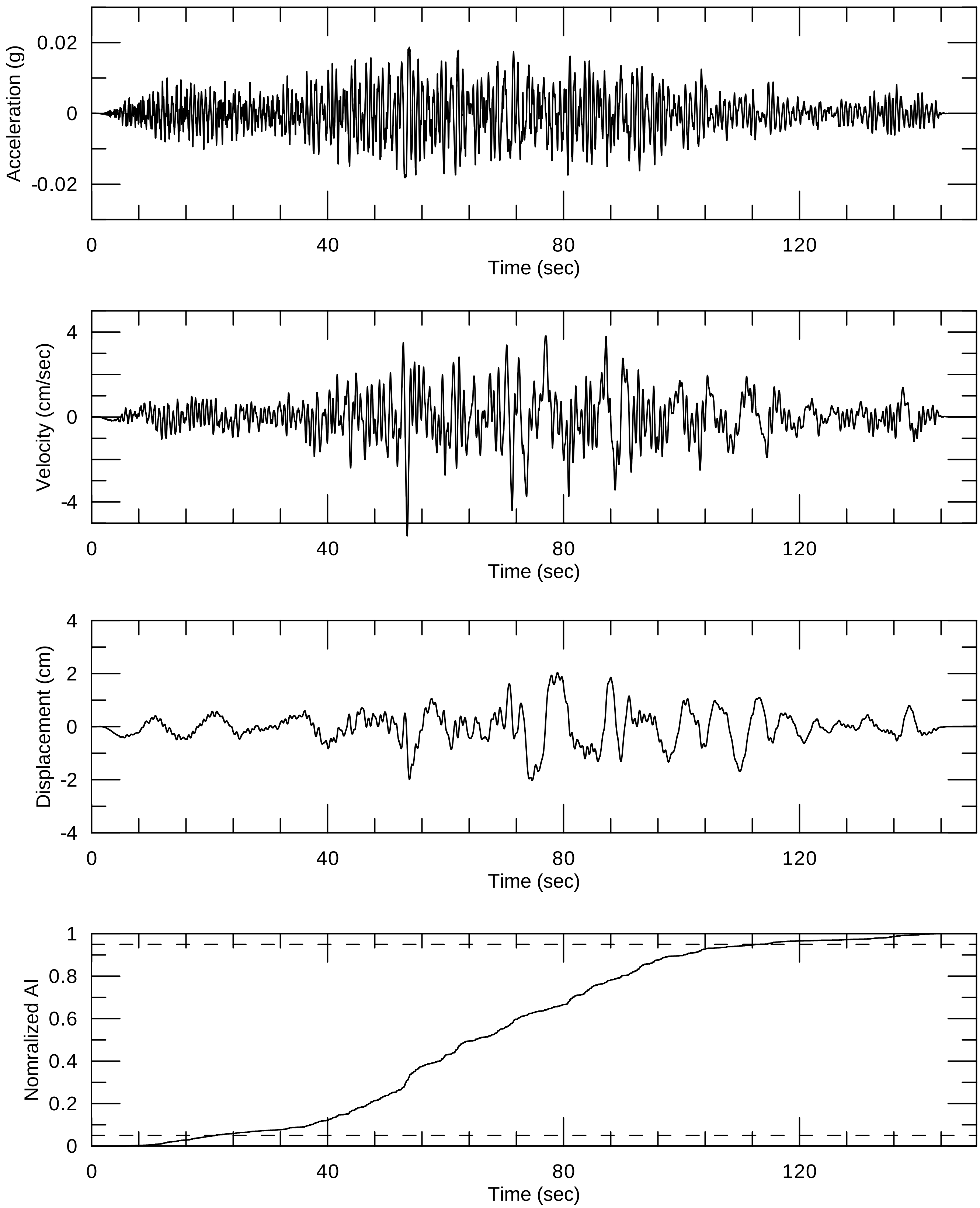

URS	Project No. 26818581 Resolution Copper Arizona	TIME HISTORIES SPECTRALLY MATCHED TO HORIZONTAL 5,000-YEAR RETURN PERIOD 1.0 SEC CMS SPECTRUM 2002 DENALI - VALDEZ CITY HALL (090) FOR FAR WEST 2 (ROCK) SITE	Figure 87

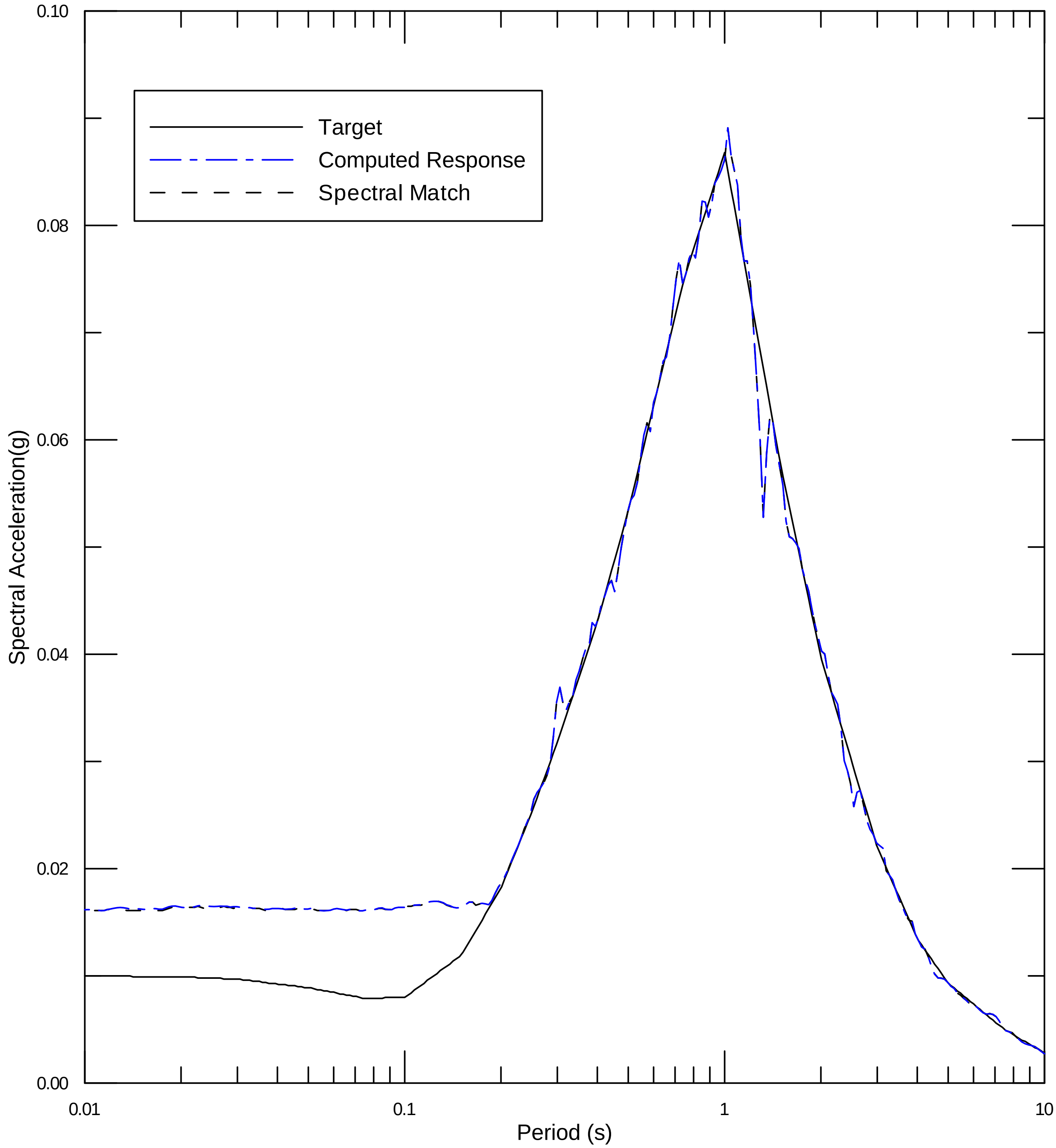

URS	Project No. 26818581 Resolution Copper Arizona	SPECTRAL MATCH TO HORIZONTAL 5,000-YEAR RETURN PERIOD 1.0 SEC CMS SPECTRUM 1999 KOCAELI - AFYON (000) FOR FAR WEST 2 (ROCK) SITE	Figure 88

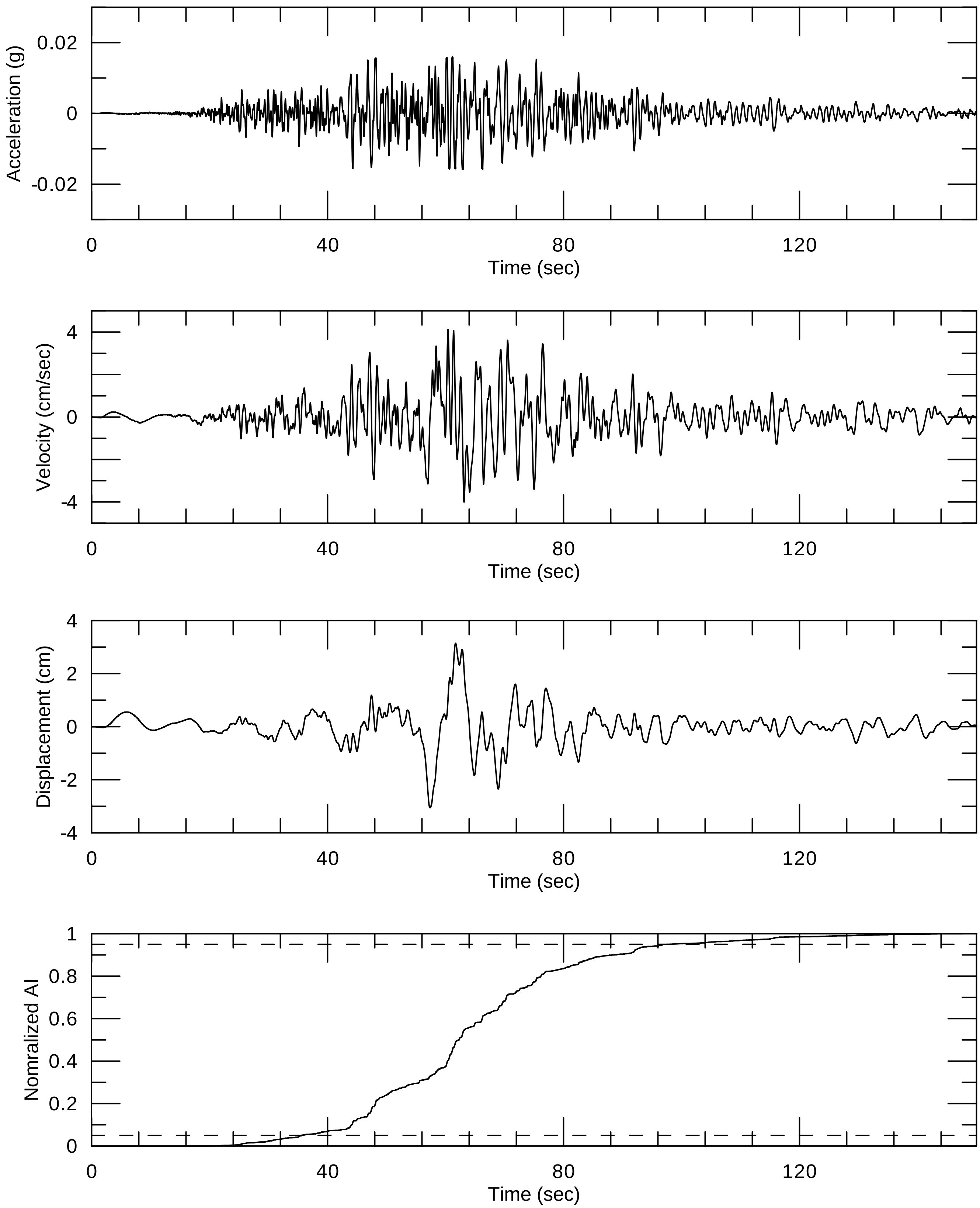

URS

Project No. 26818581

Resolution Copper
Arizona

TIME HISTORIES SPECTRALLY MATCHED TO HORIZONTAL 5,000-YEAR RETURN PERIOD 1.0 SEC CMS SPECTRUM 1999 KOCAELI - AFYON (000) FOR FAR WEST 2 (ROCK) SITE

Figure 89

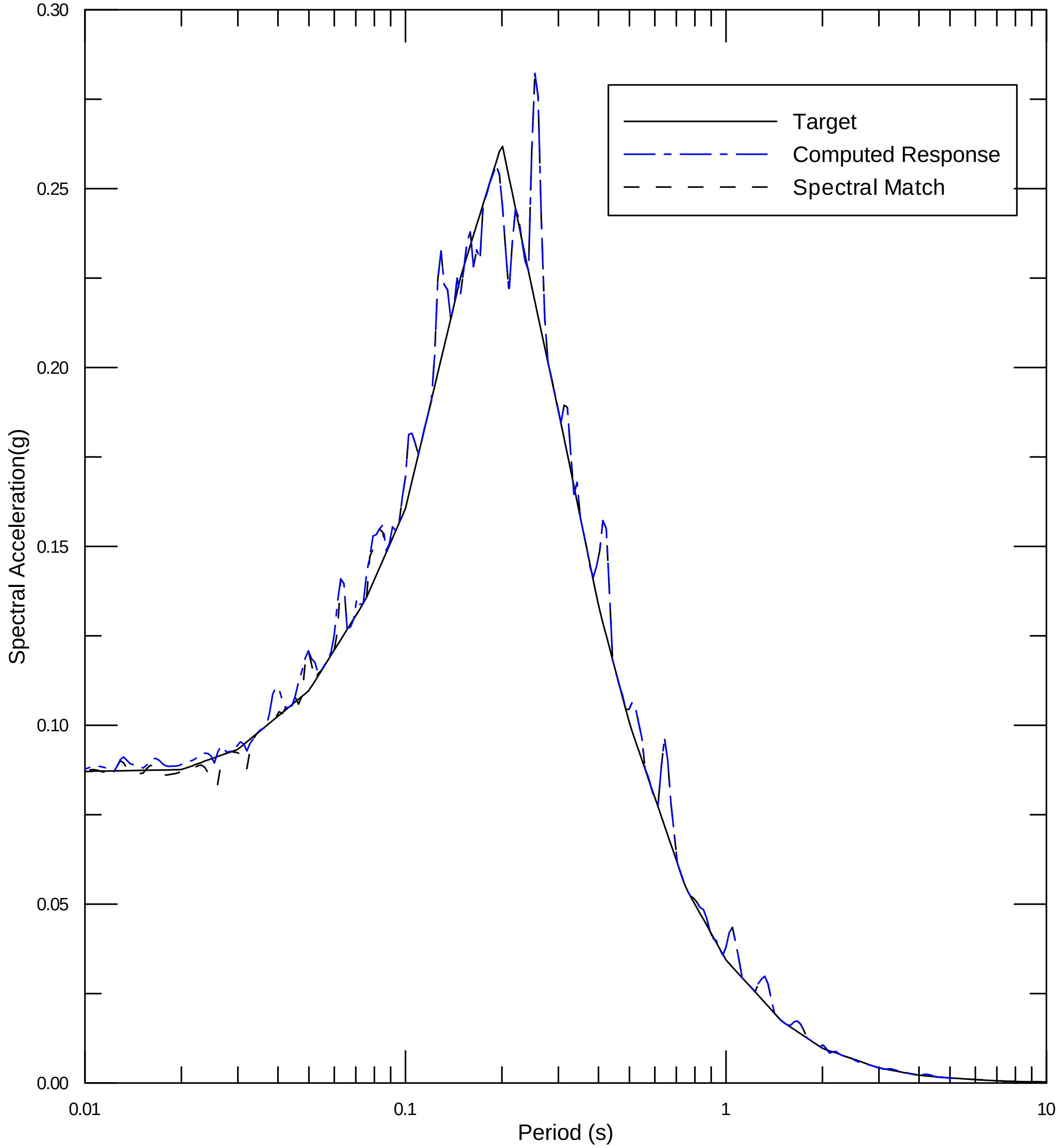

URS	Project No. 26818581 Resolution Copper Arizona	SPECTRAL MATCH TO HORIZONTAL 5,000-YEAR RETURN PERIOD 0.2 SEC CMS SPECTRUM 1979 IMPERIAL VALEY - CERRO PRIETO (147) FOR NEAR WEST SITE	Figure 90

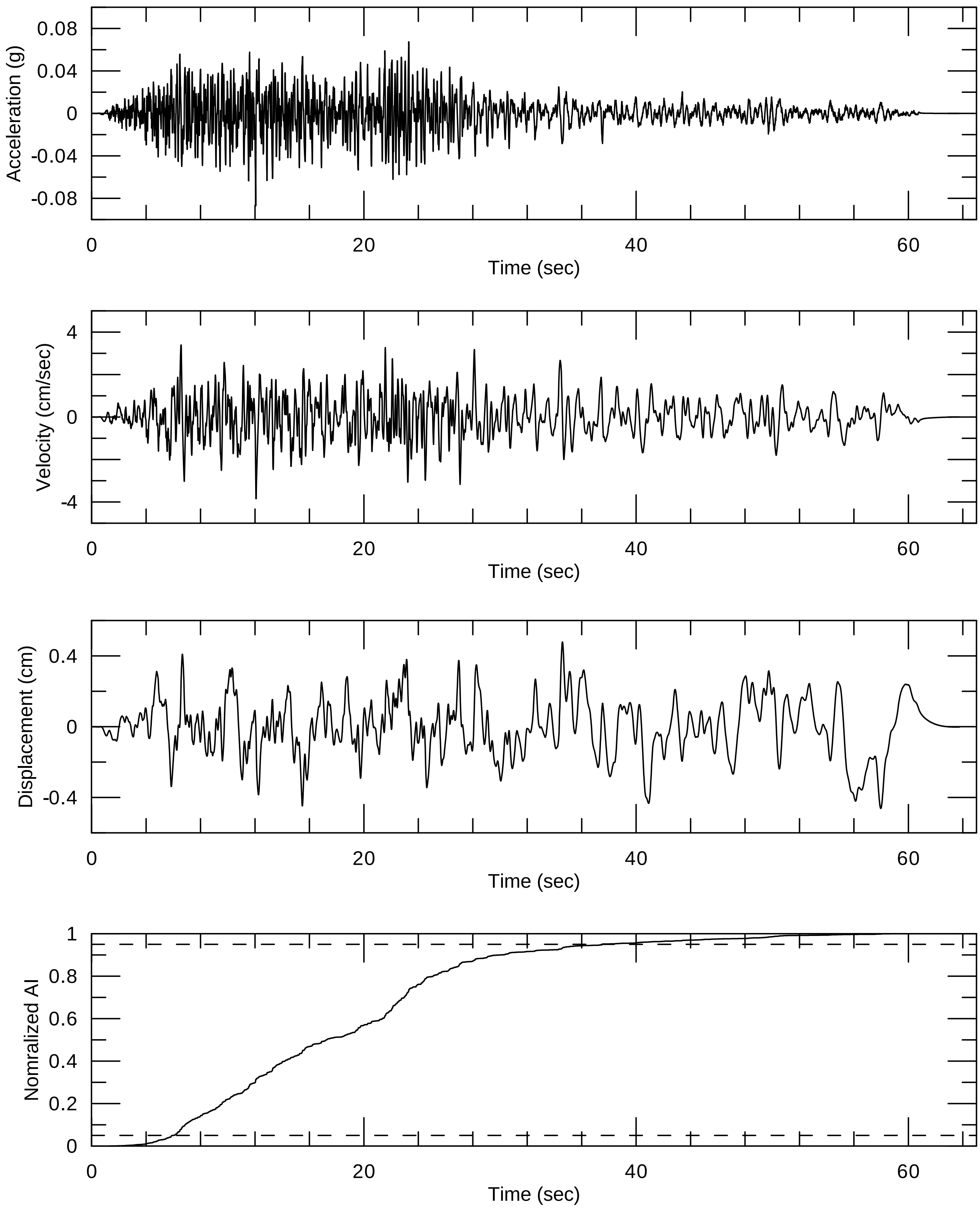

URS	Project No. 26818581 Resolution Copper Arizona	TIME HISTORIES SPECTRALLY MATCHED TO HORIZONTAL 5,000-YEAR RETURN PERIOD 0.2 SEC CMS SPECTRUM 1979 IMPERIAL VALLEY-CERRO PRIETO (147) FOR NEAR WEST SITE	Figure 91

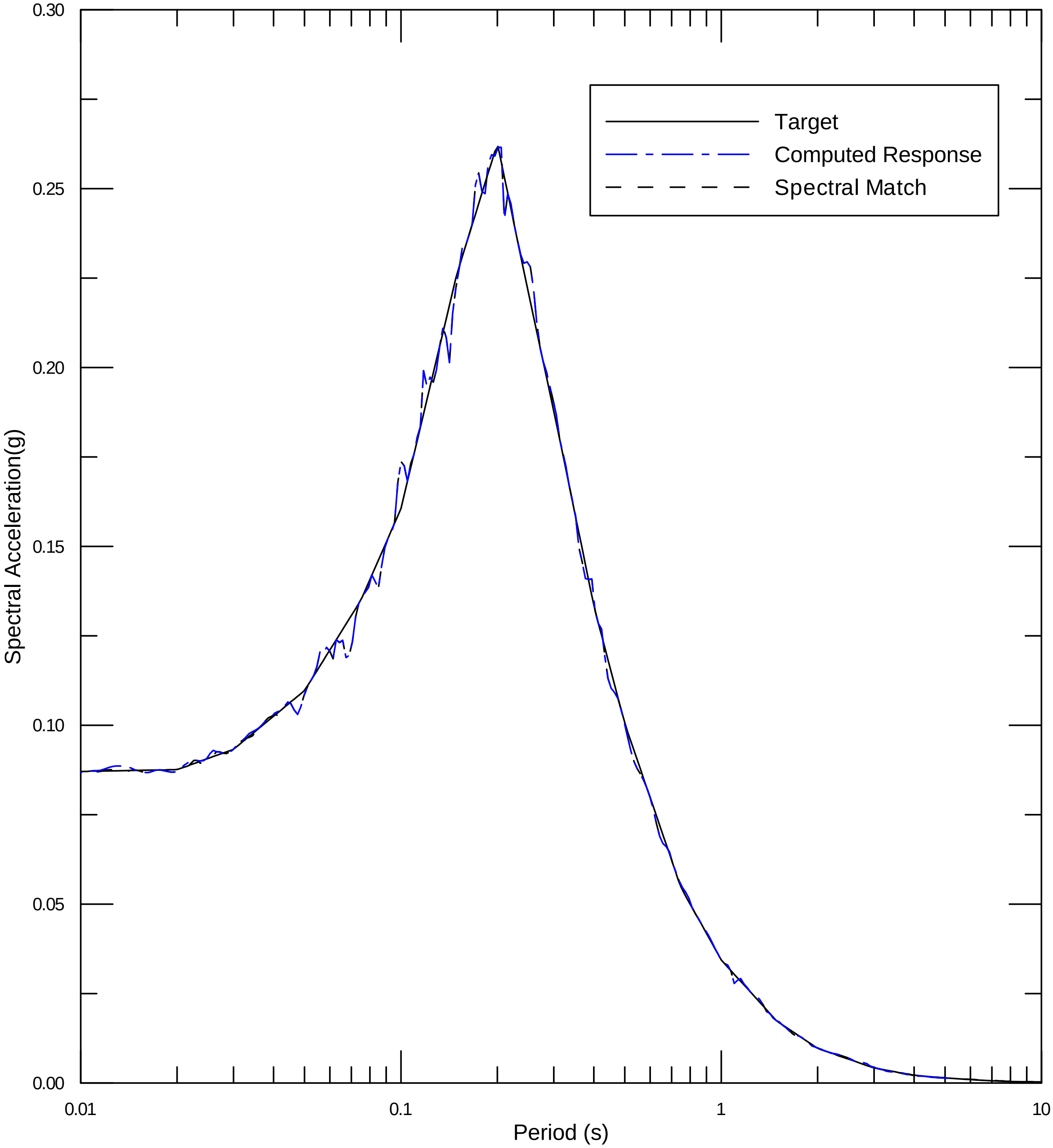

URS	Project No. 26818581	SPECTRAL MATCH TO HORIZONTAL 5,000-YEAR RETURN PERIOD0.2 SEC CMS SPECTRUM 1995 KOZANI - KOZANI (L) FOR NEAR WEST SITE	Figure 92
	Resolution Copper Arizona		

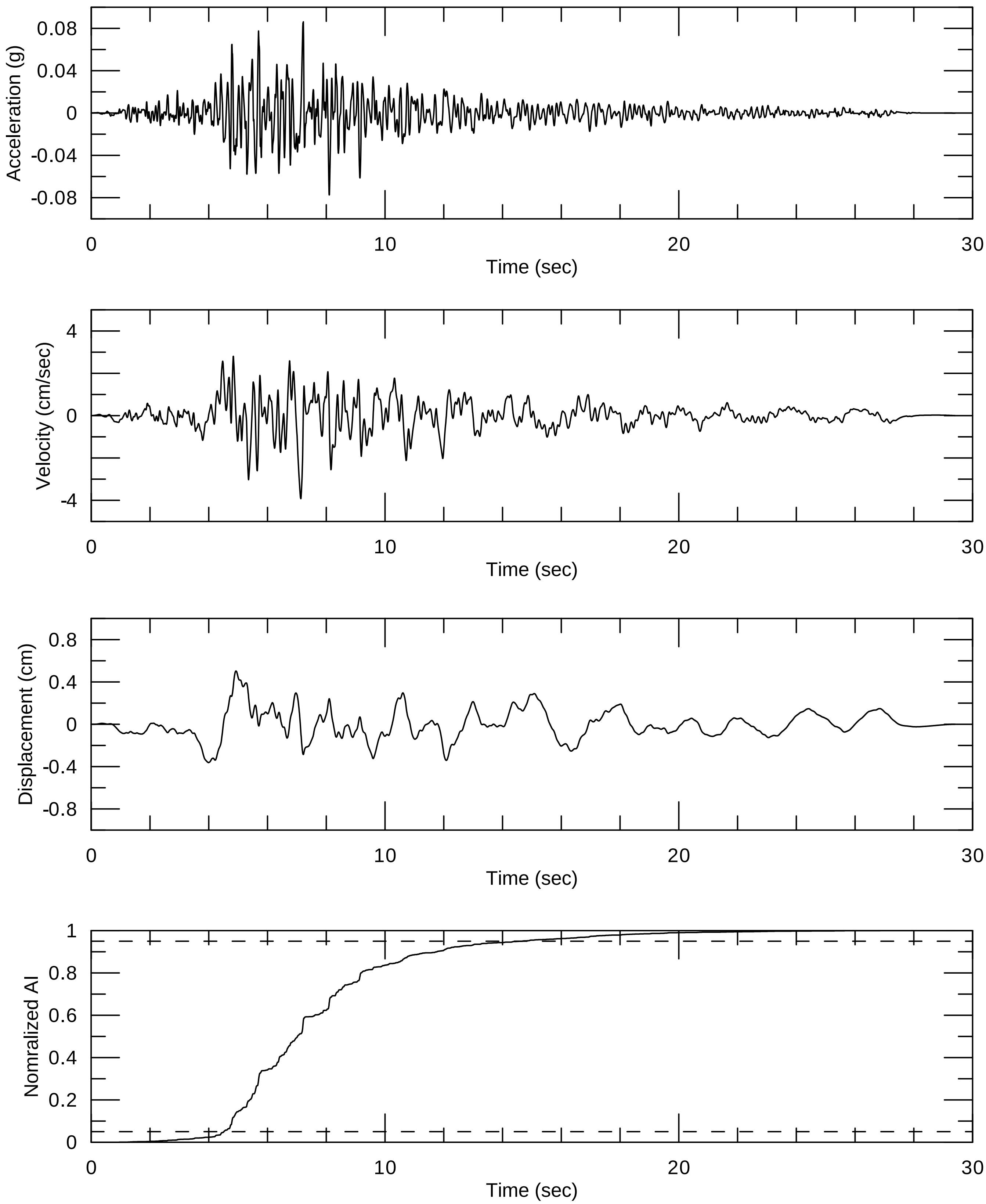

URS	Project No. 26818581 Resolution Copper Arizona	TIME HISTORIES SPECTRALLY MATCHED TO HORIZONTAL 5,000-YEAR RETURN PERIOD 0.2 SEC CMS SPECTRUM 1995 KOZANI- KOZANI (L) FOR NEAR WEST SITE	Figure 93

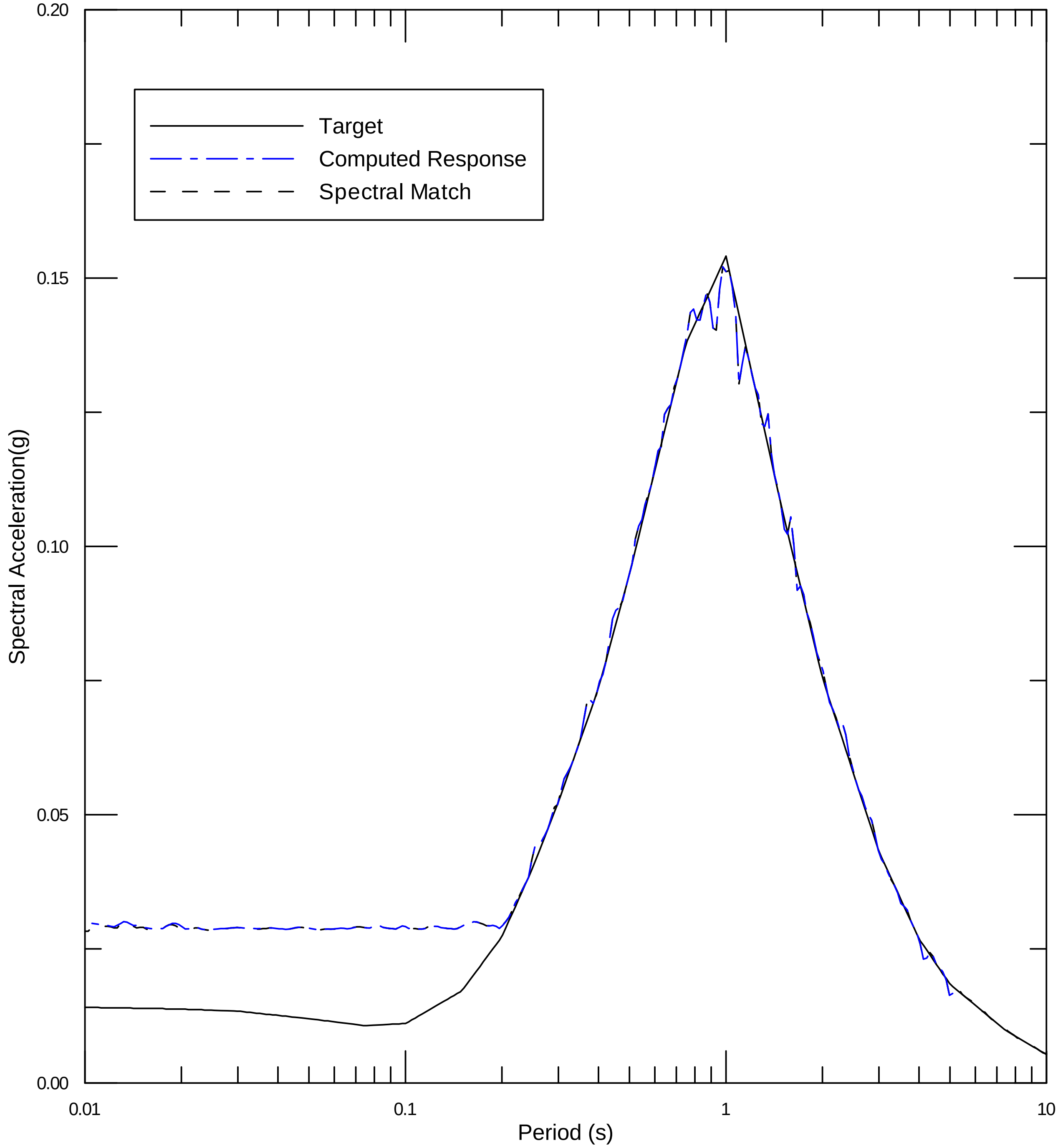

URS

Project No. 26818581

Resolution Copper
Arizona

SPECTRAL MATCH TO HORIZONTAL
5,000-YEAR RETURN PERIOD 1.0 SEC CMS SPECTRUM
1999 CHI-CHI - KAU046 (E)
FOR NEAR WEST SITE

Figure
94

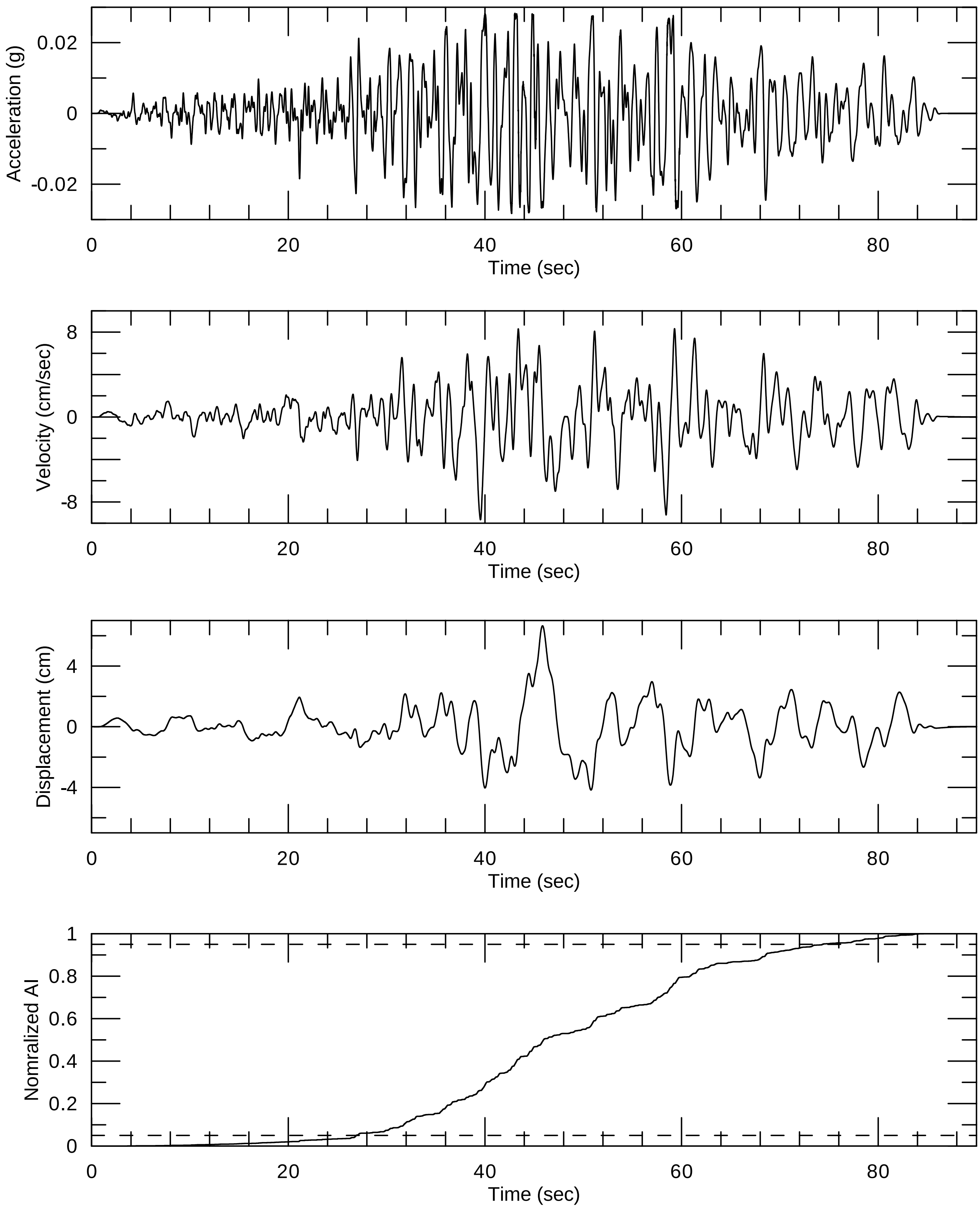

URS	Project No. 26818581 Resolution Copper Arizona	TIME HISTORIES SPECTRALLY MATCHED TO HORIZONTAL 5,000-YEAR RETURN PERIOD 1.0 SEC CMS SPECTRUM 1999 CHI-CHI - KAU046 (E) FOR NEAR WEST SITE	Figure 95

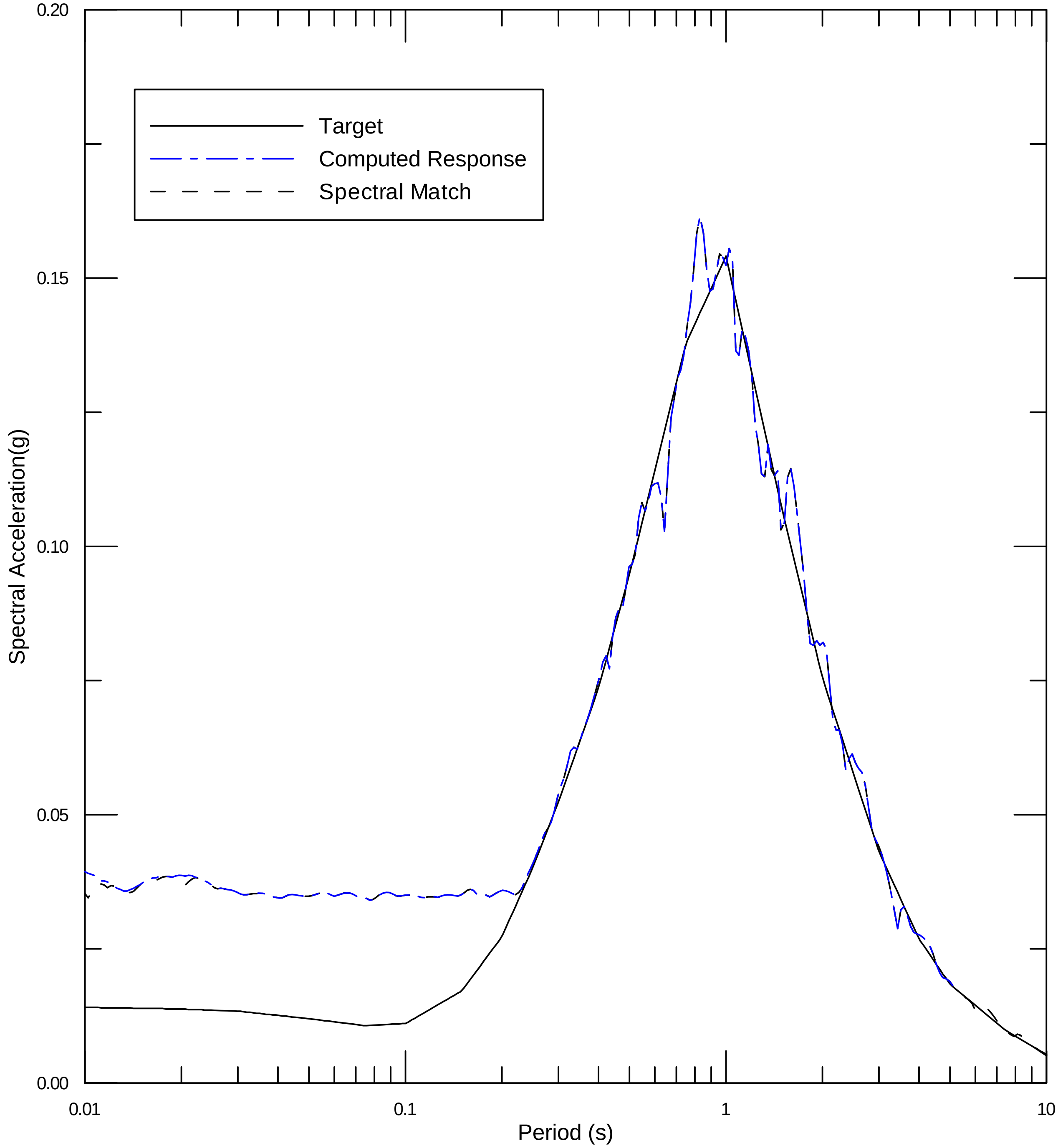

URS	Project No. 26818581 Resolution Copper Arizona	SPECTRAL MATCH TO HORIZONTAL 5,000-YEAR RETURN PERIOD 1.0 SEC CMS SPECTRUM 1999 CHI-CHI - KAU081 (E) FOR NEAR WEST SITE	Figure 96

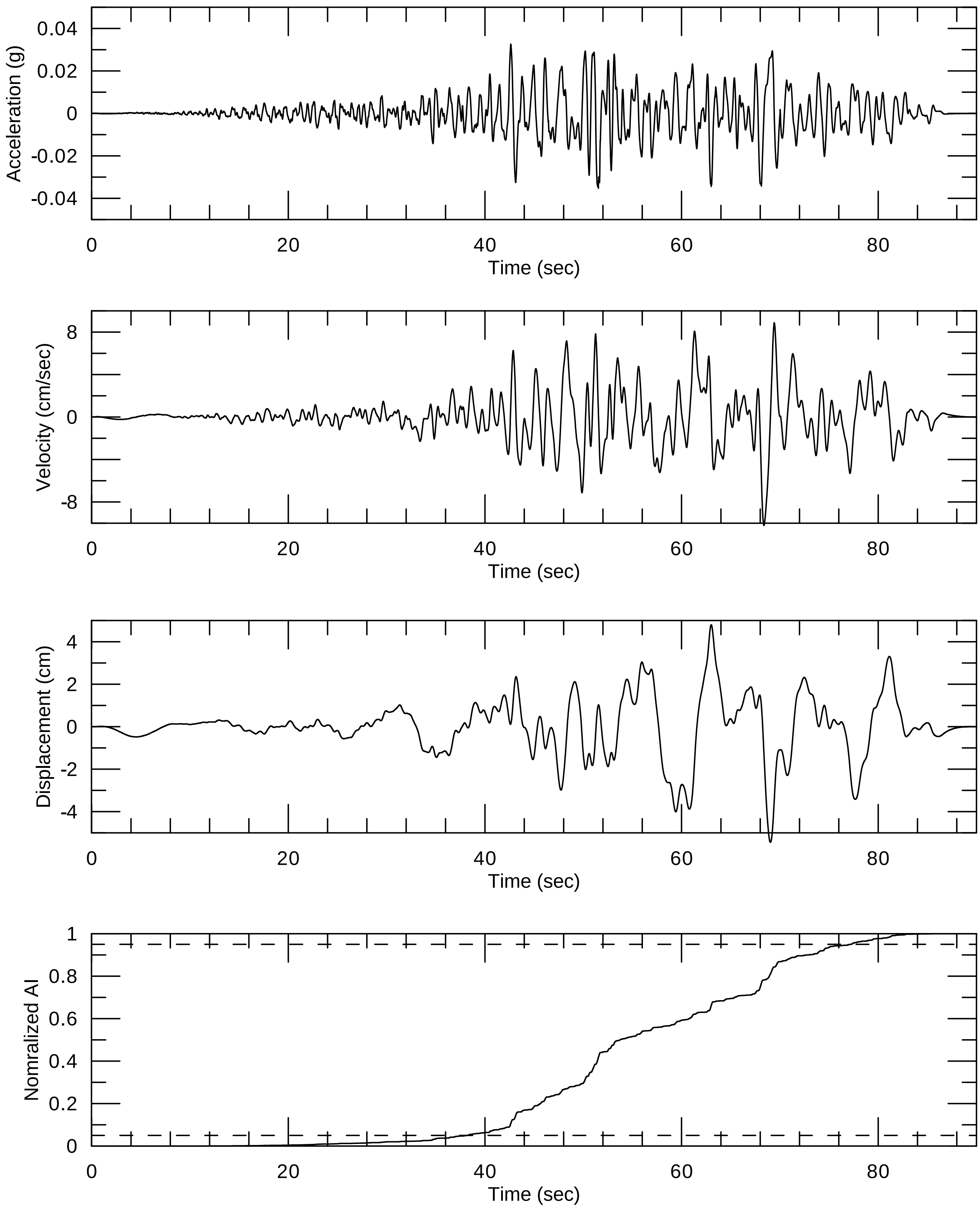

URS

Project No. 26818581

Resolution Copper
Arizona

TIME HISTORIES SPECTRALLY MATCHED TO
HORIZONTAL 5,000-YEAR RETURN PERIOD 1.0 SEC
CMS SPECTRUM 1999 CHI-CHI - KAU081 (E)
FOR NEAR WEST SITE

Figure
97

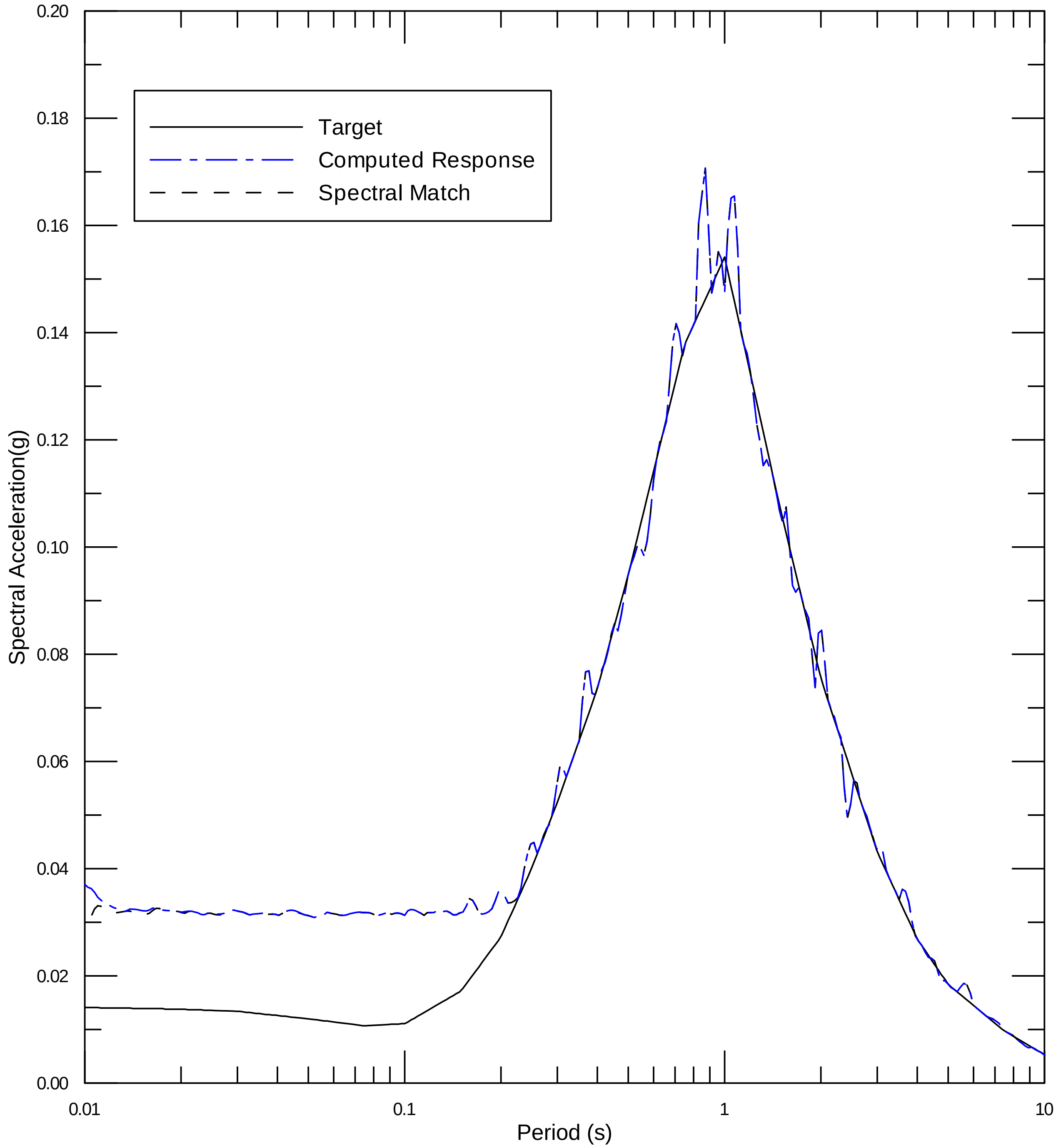

URS	Project No. 26818581 Resolution Copper Arizona	SPECTRAL MATCH TO HORIZONTAL 5,000-YEAR RETURN PERIOD 1.0 SEC CMS SPECTRUM 2002 DENALI - FIRE STATION 1 (090) FOR NEAR WEST SITE	Figure 98

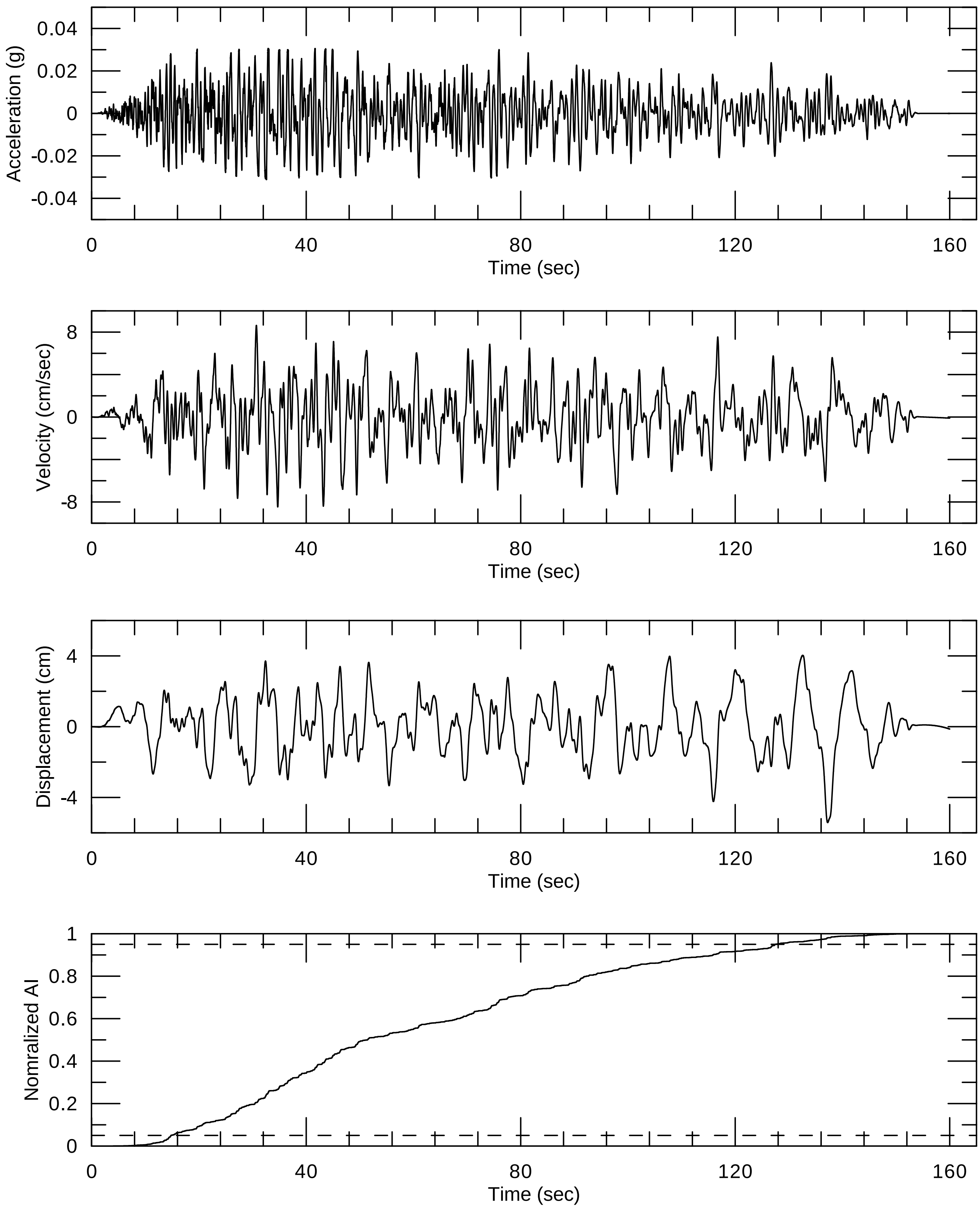

URS	Project No. 26818581 Resolution Copper Arizona	TIME HISTORIES SPECTRALLY MATCHED TO HORIZONTAL 5,000-YEAR RETURN PERIOD 1.0 SEC CMS SPECTRUM 2002 DENALI - FIRE STATION 1 (090) FOR NEAR WEST SITE	Figure 99

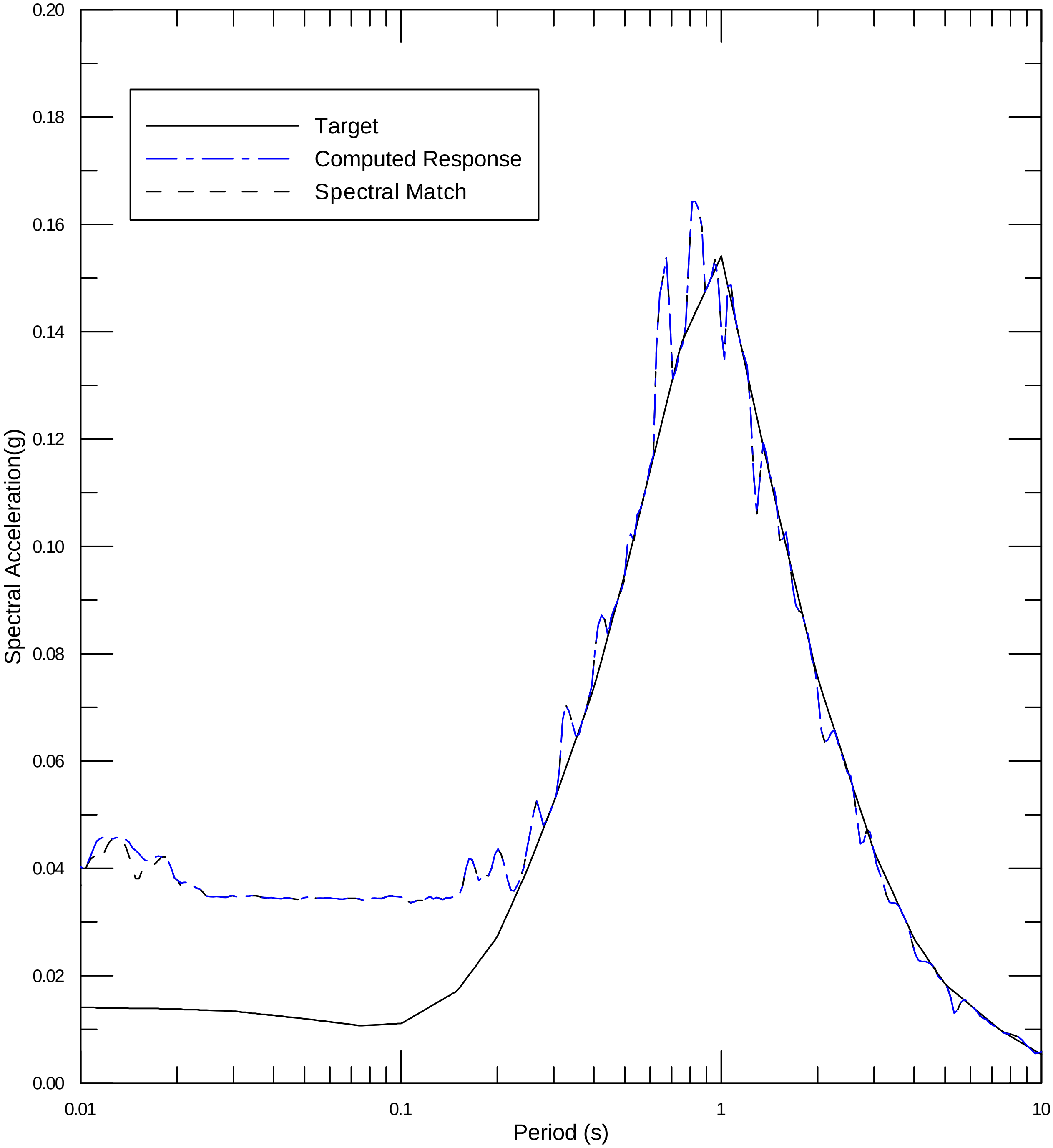

URS	Project No. 26818581	SPECTRAL MATCH TO HORIZONTAL 5,000-YEAR RETURN PERIOD 1.0 SEC CMS SPECTRUM 2002 DENALI - VALDEZ CITY HALL (090) FOR NEAR WEST SITE	Figure 100
	Resolution Copper Arizona		

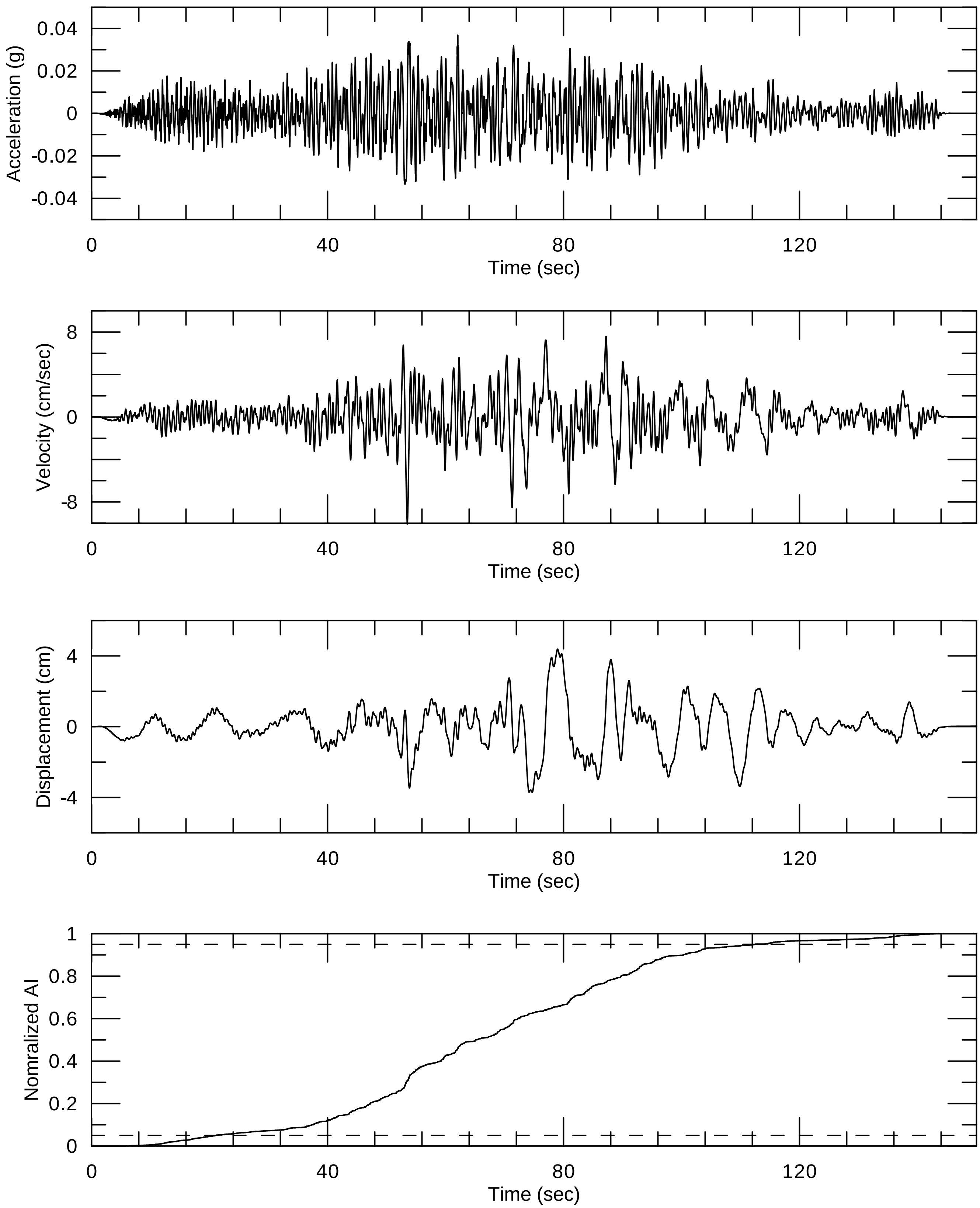

URS	Project No. 26818581 Resolution Copper Arizona	TIME HISTORIES SPECTRALLY MATCHED TO HORIZONTAL 5,000-YEAR RETURN PERIOD 1.0 SEC CMS SPECTRUM 2002 DENALI - VALDEZ CITY HALL (090) FOR NEAR WEST SITE	Figure 101

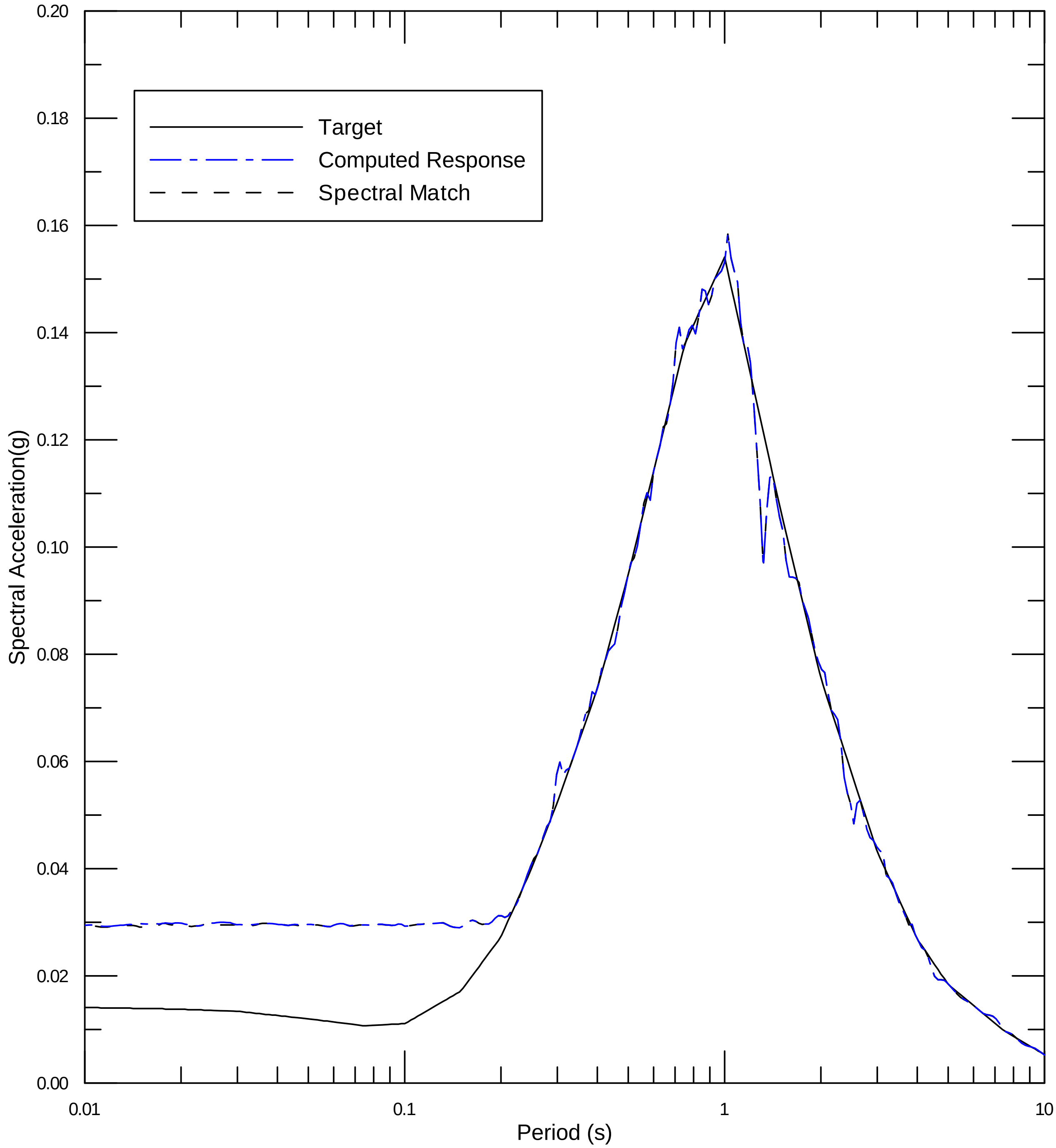

URS

Project No. 26818581

Resolution Copper
Arizona

SPECTRAL MATCH TO HORIZONTAL
5,000-YEAR RETURN PERIOD 1.0 SEC CMS SPECTRUM
1999 KOCAELI - AFYON (000)
FOR NEAR WEST SITE

Figure
102

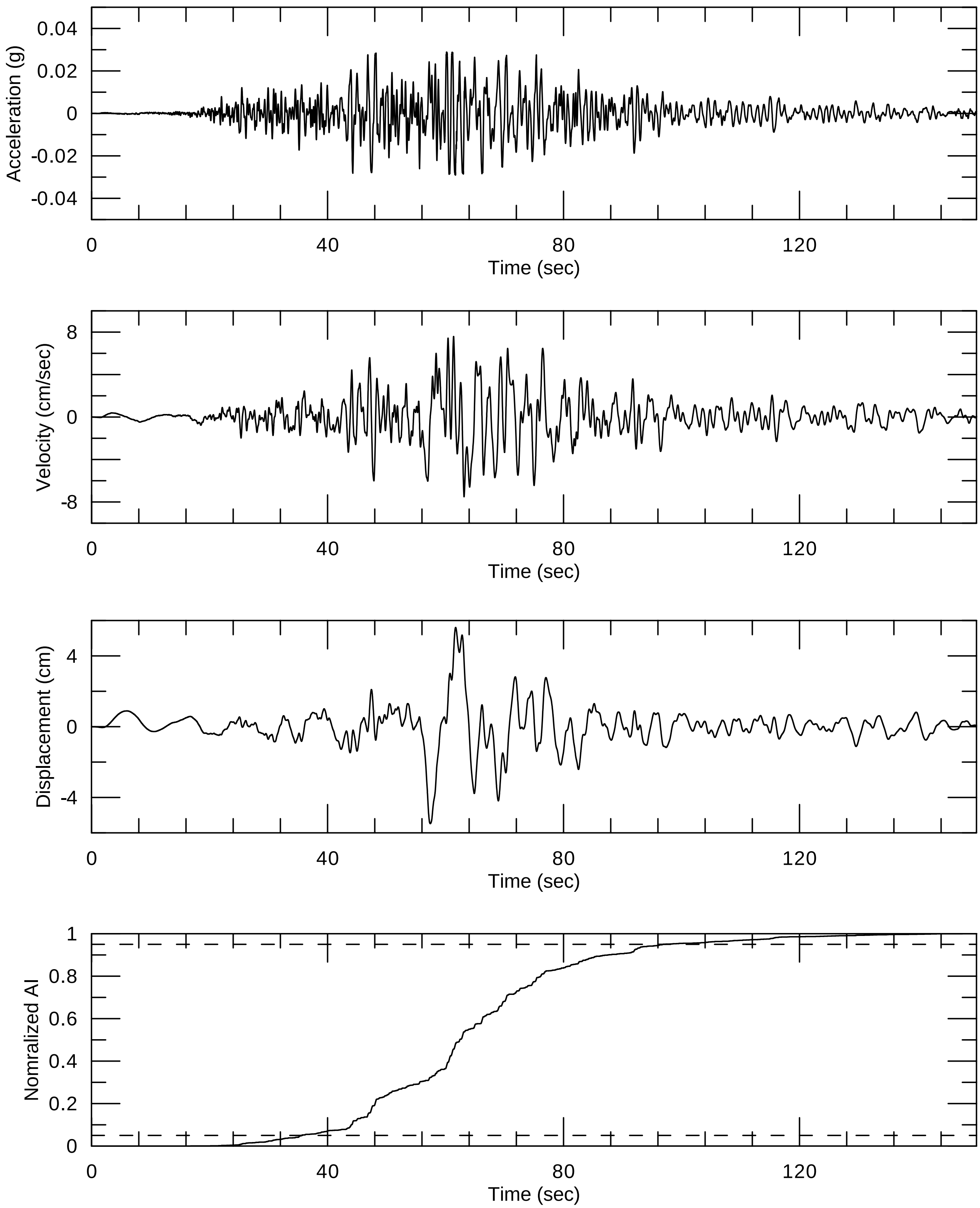

URS	Project No. 26818581 Resolution Copper Arizona	TIME HISTORIES SPECTRALLY MATCHED TO HORIZONTAL 5,000-YEAR RETURN PERIOD 1.0 SEC CMS SPECTRUM 1999 KOCAELI - AFYON (000) FOR NEAR WEST SITE	Figure 103

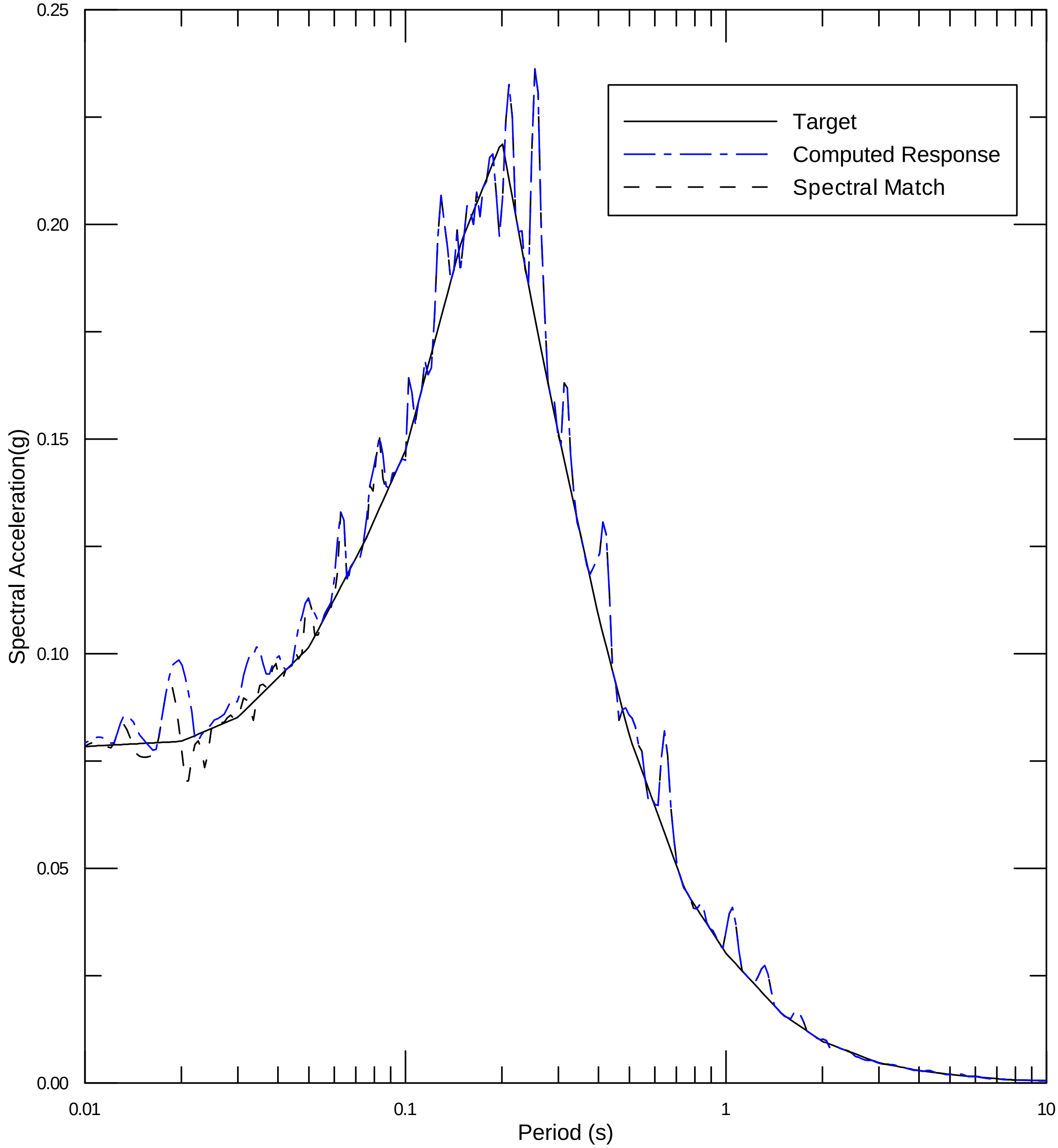

URS	Project No. 26818581 Resolution Copper Arizona	SPECTRAL MATCH TO HORIZONTAL 5,000-YEAR RETURN PERIOD 0.2 SEC CMS SPECTRUM 1979 IMPERIAL VALEY - CERRO PRIETO (147) FOR PINTO VALLEY SITE	Figure 104

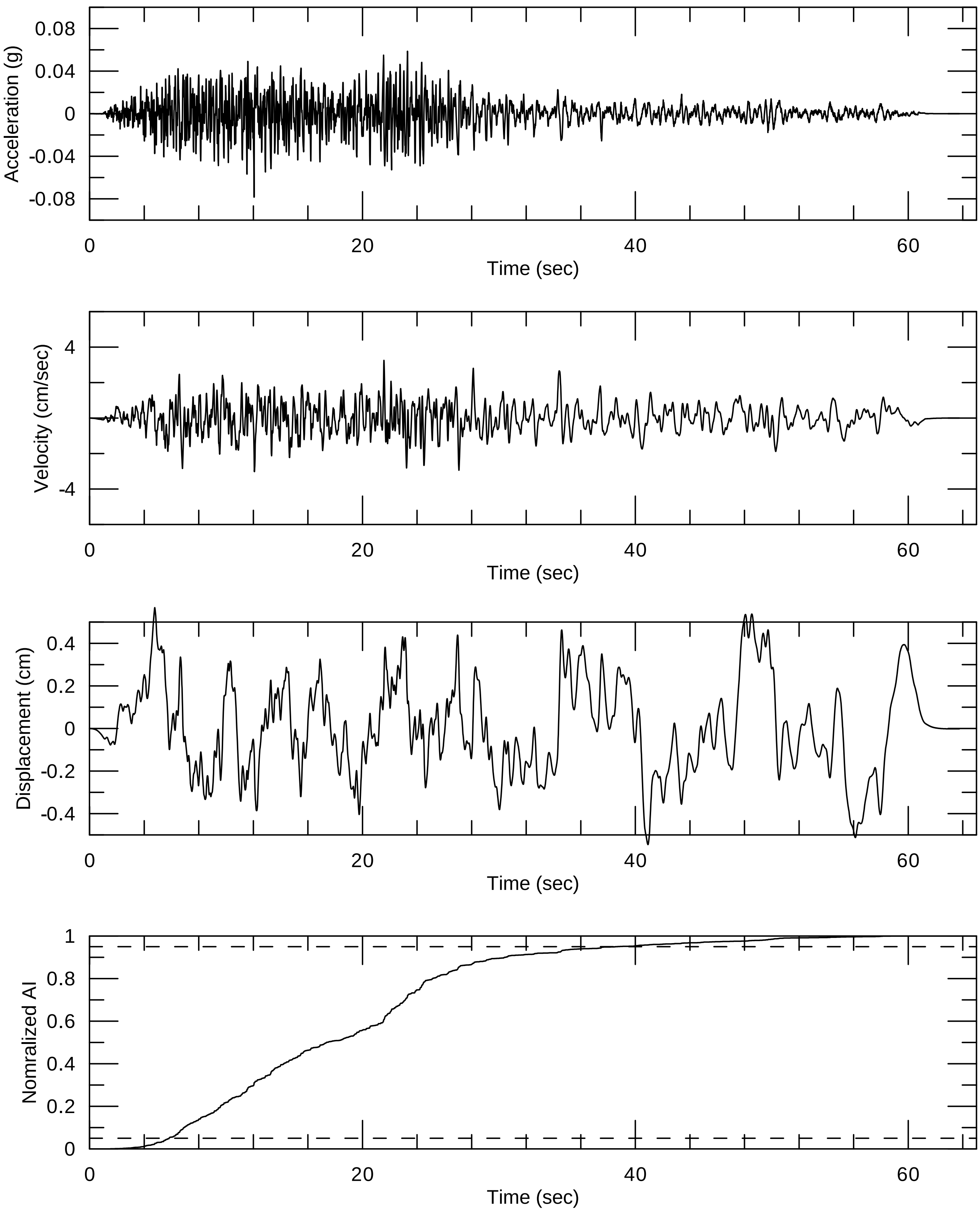

URS	Project No. 26818581 Resolution Copper Arizona	TIME HISTORIES SPECTRALLY MATCHED TO HORIZONTAL 5,000-YEAR RETURN PERIOD 0.2 SEC CMS SPECTRUM 1979 IMPERIAL VALLEY-CERRO PRIETO (147) FOR PINTO VALLEY SITE	Figure 105

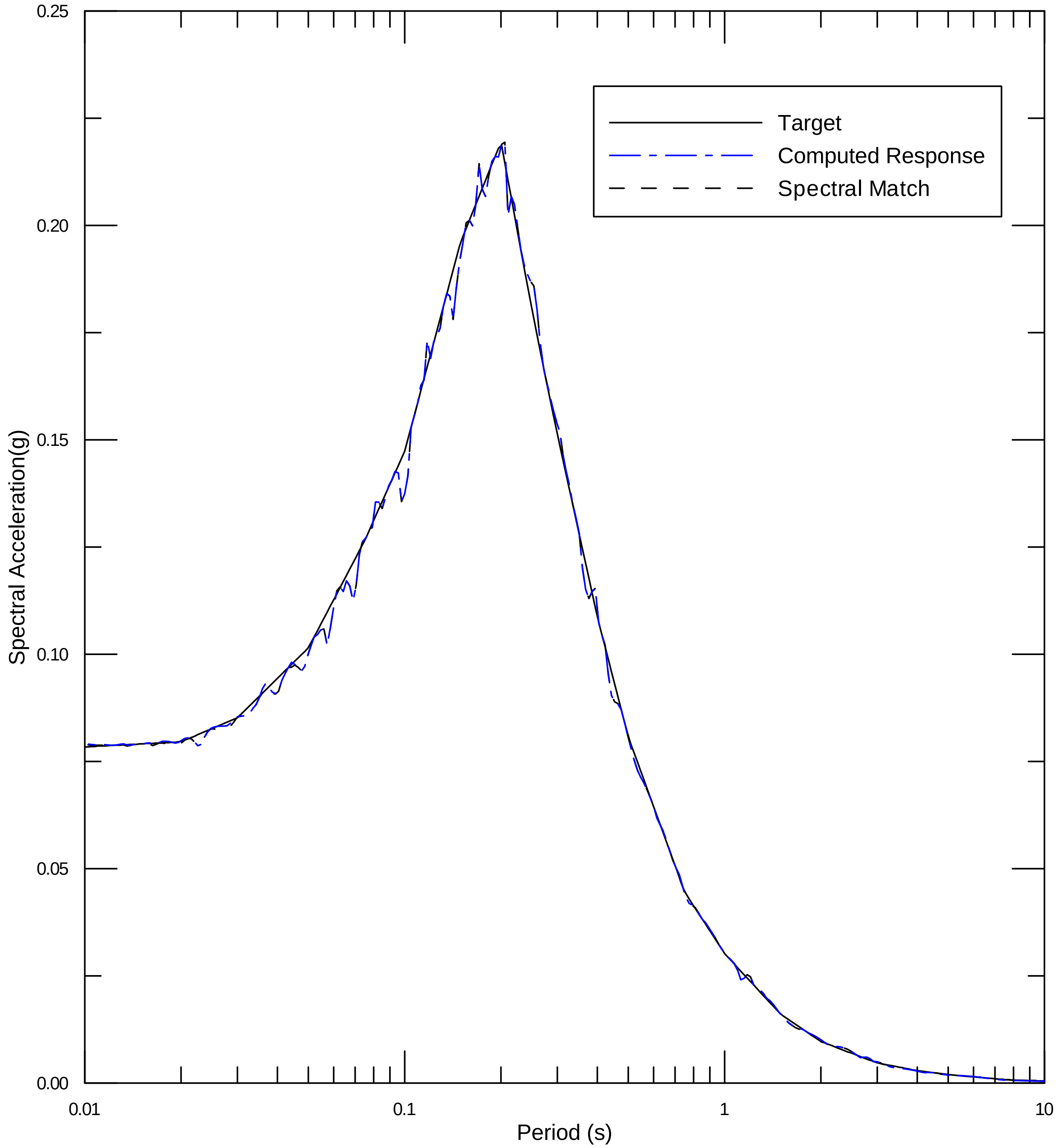

URS

Project No. 26818581

Resolution Copper
Arizona

SPECTRAL MATCH TO HORIZONTAL
5,000-YEAR RETURN PERIOD0.2 SEC CMS SPECTRUM
1995 KOZANI - KOZANI (L)
FOR PINTO VALLEY SITE

Figure
106

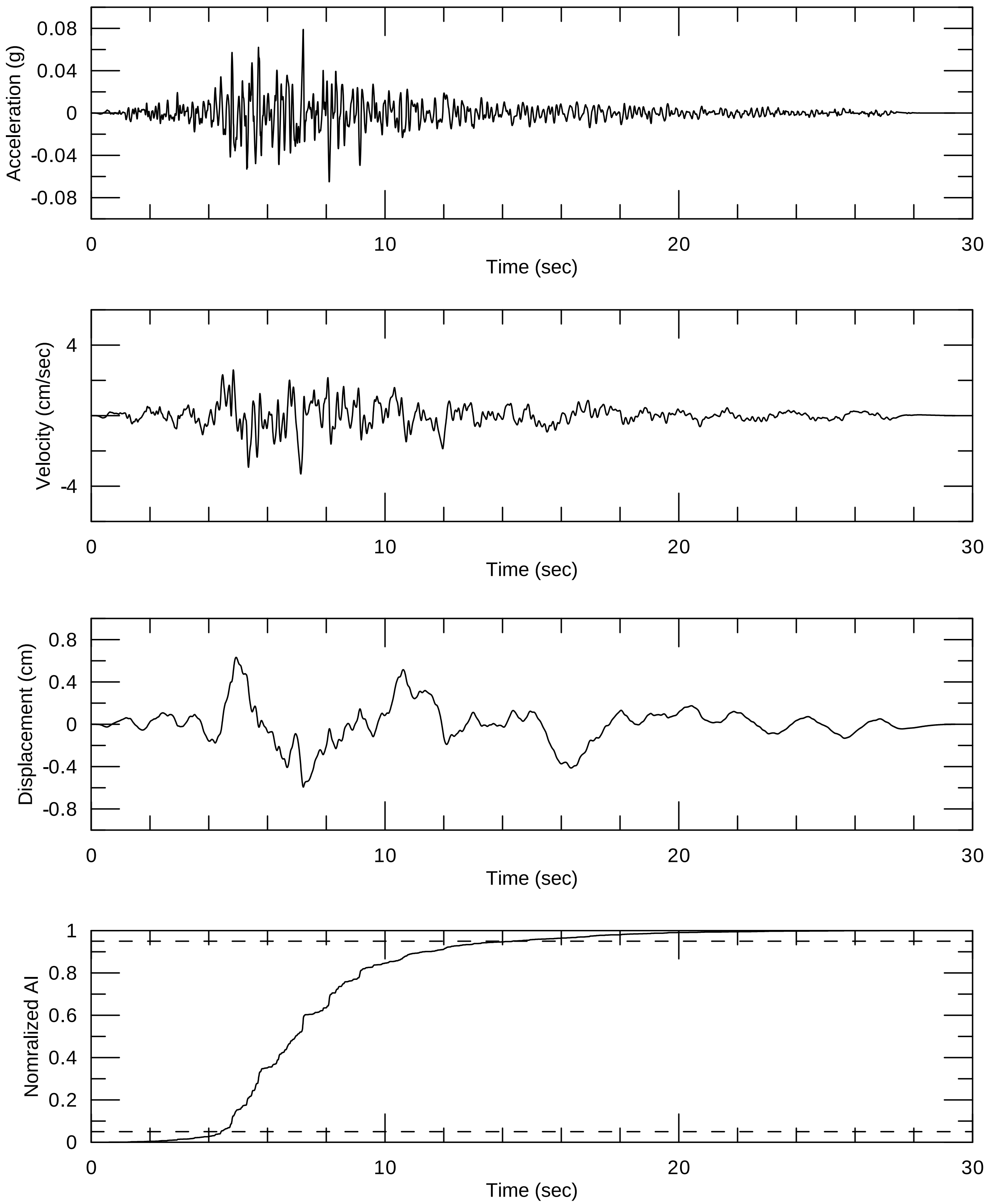

URS	Project No. 26818581 Resolution Copper Arizona	TIME HISTORIES SPECTRALLY MATCHED TO HORIZONTAL 5,000-YEAR RETURN PERIOD 0.2 SEC CMS SPECTRUM 1995 KOZANI- KOZANI (L) FOR PINTO VALLEY SITE	Figure 107

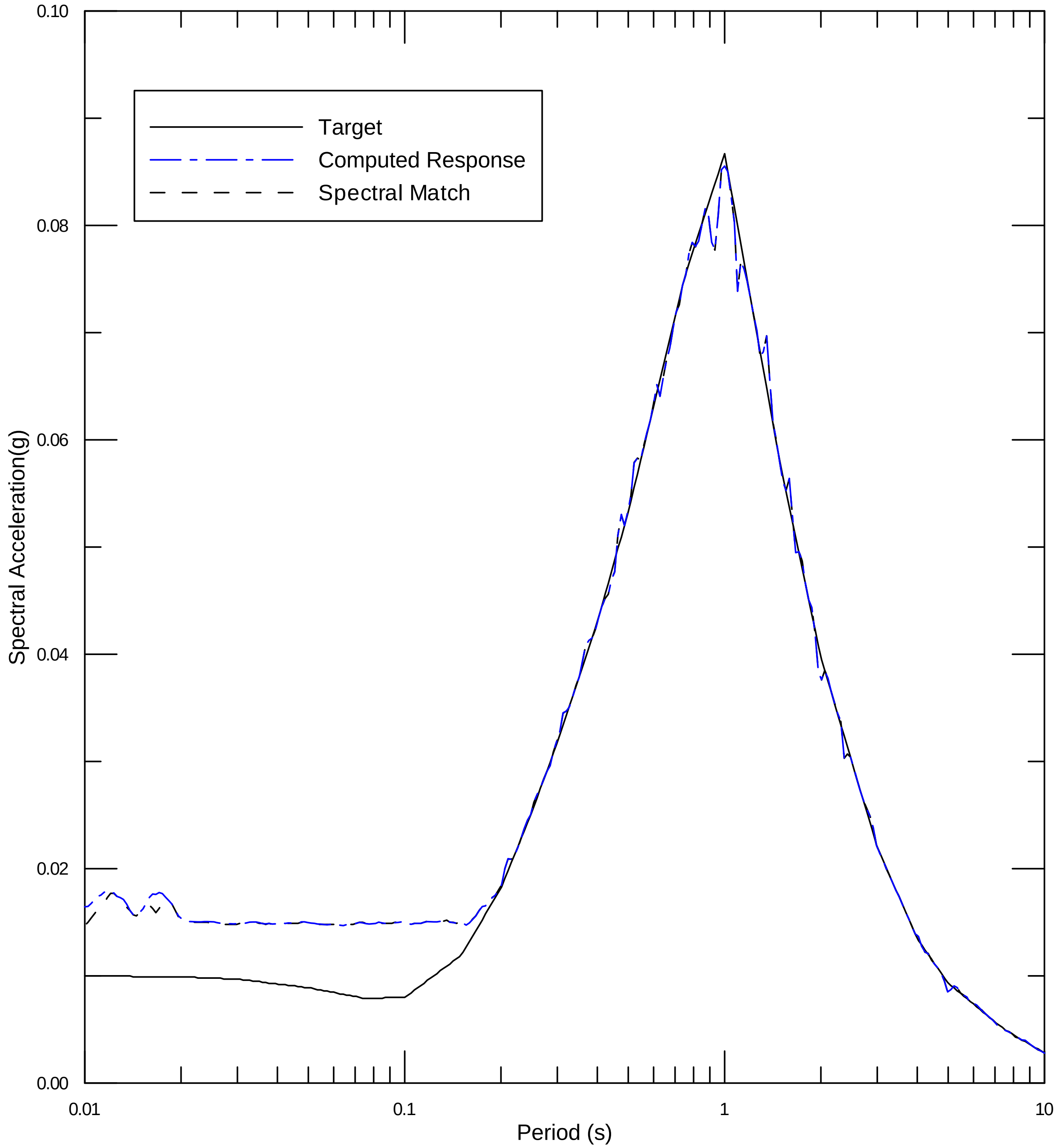

URS

Project No. 26818581

Resolution Copper
Arizona

SPECTRAL MATCH TO HORIZONTAL
5,000-YEAR RETURN PERIOD 1.0 SEC CMS SPECTRUM
1999 CHI-CHI - KAU046 (E)
FOR PINTO VALLEY SITE

Figure
108

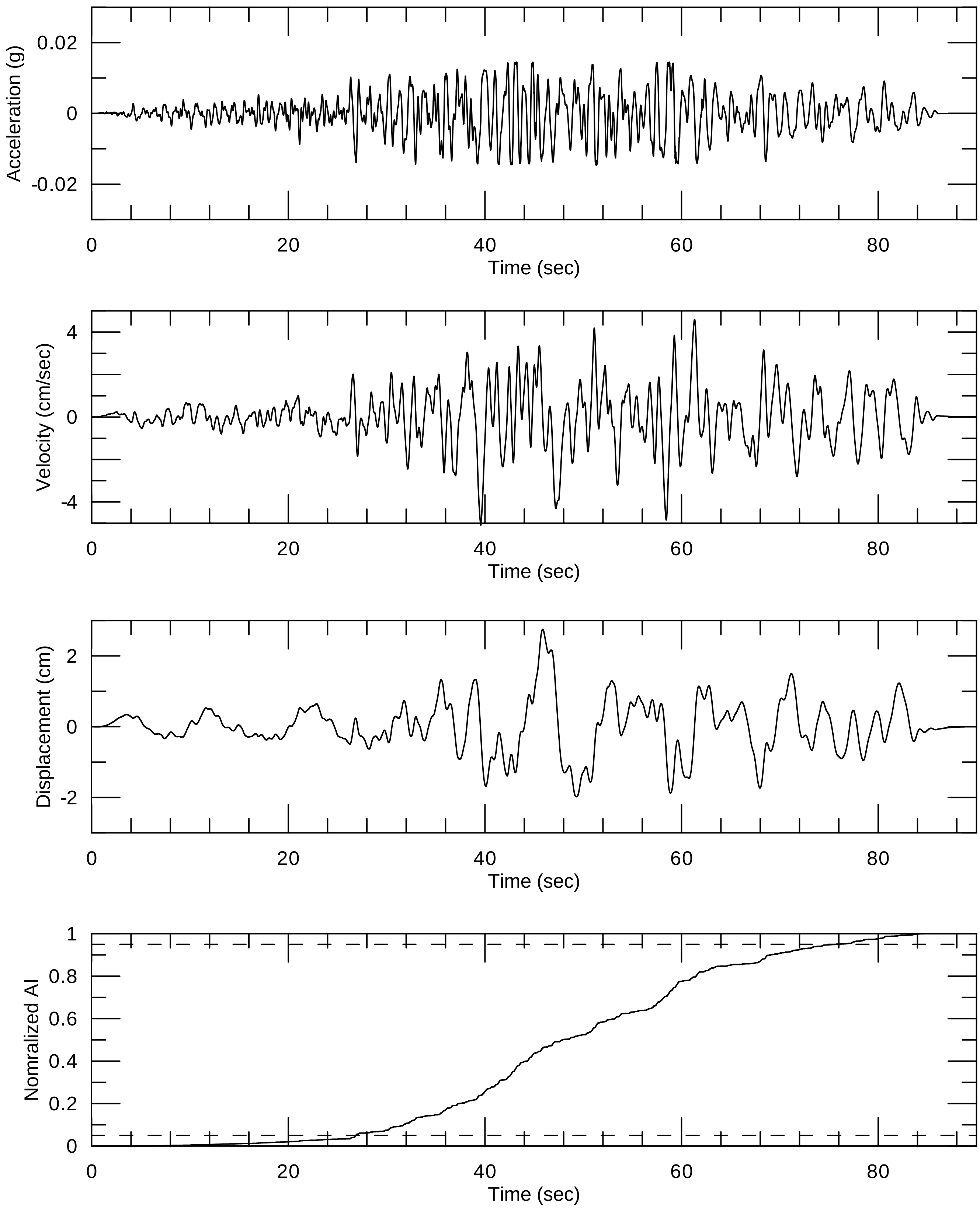

URS	Project No. 26818581	TIME HISTORIES SPECTRALLY MATCHED TO HORIZONTAL 5,000-YEAR RETURN PERIOD 1.0 SEC CMS SPECTRUM 1999 CHI-CHI - KAU046 (E) FOR PINTO VALLEY SITE	Figure 109
	Resolution Copper Arizona		

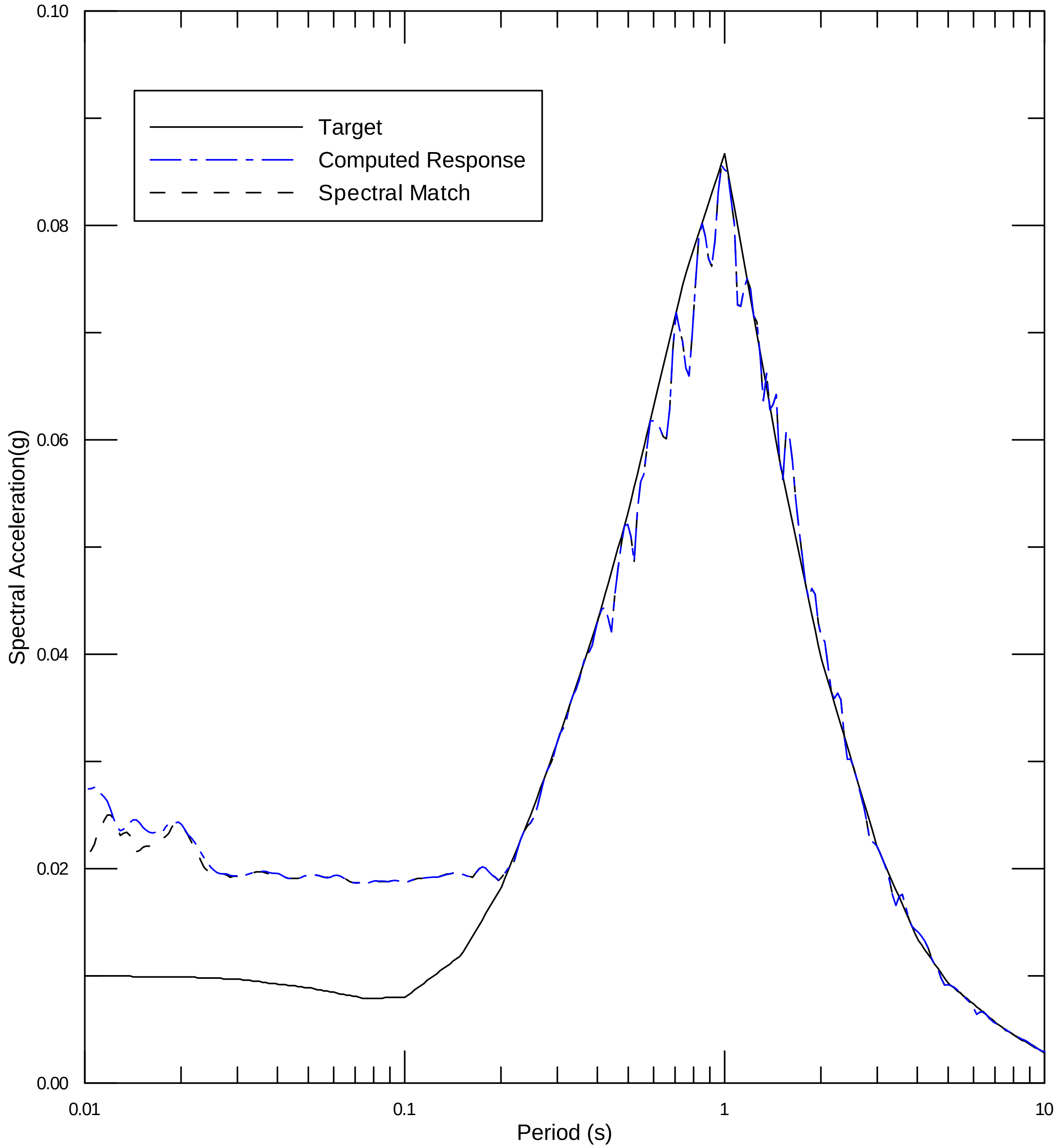

URS

Project No. 26818581

Resolution Copper
Arizona

SPECTRAL MATCH TO HORIZONTAL
5,000-YEAR RETURN PERIOD 1.0 SEC CMS SPECTRUM
1999 CHI-CHI - KAU081 (E)
FOR PINTO VALLEY SITE

Figure
110

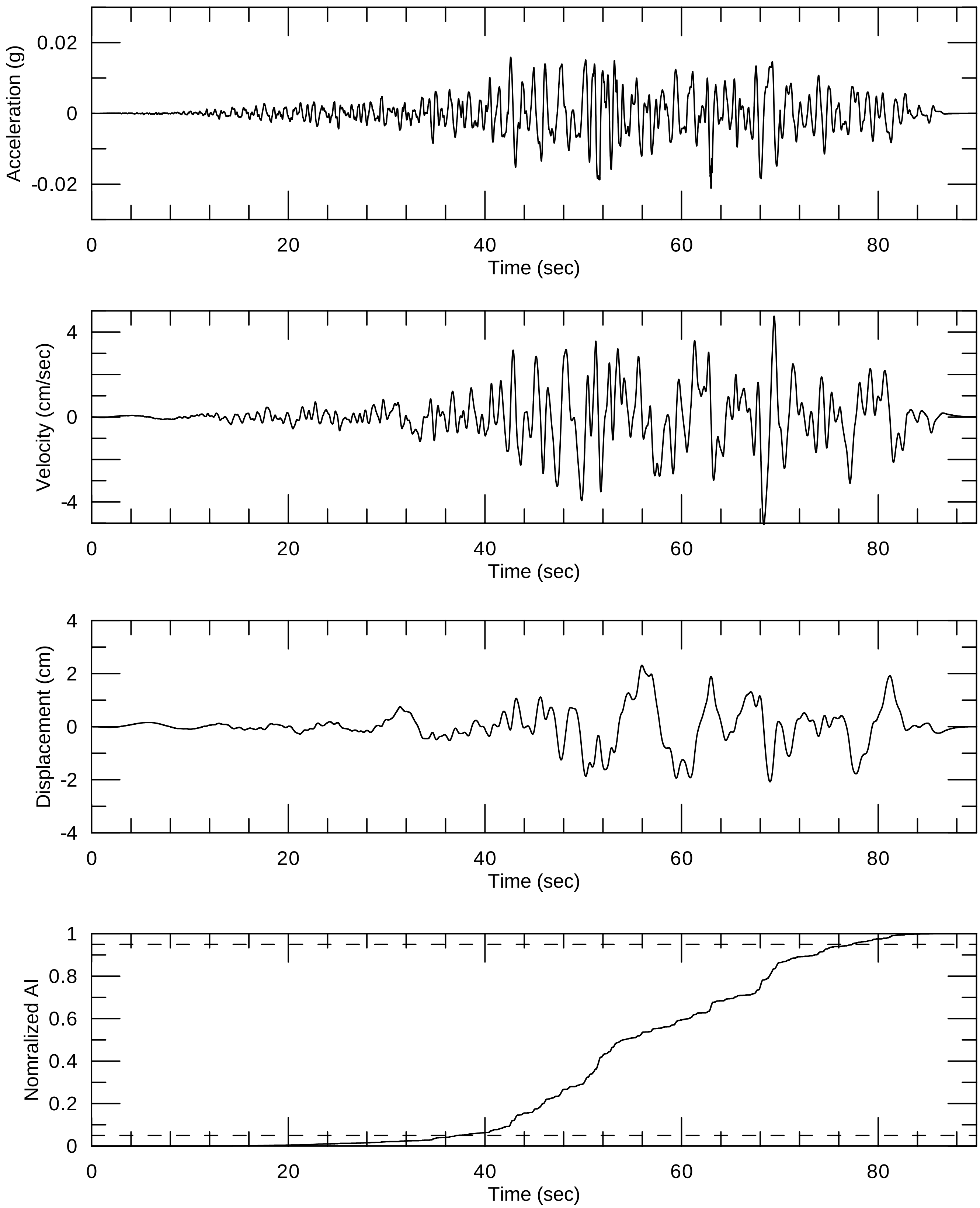

URS

Project No. 26818581

Resolution Copper
Arizona

TIME HISTORIES SPECTRALLY MATCHED TO
HORIZONTAL 5,000-YEAR RETURN PERIOD 1.0 SEC
CMS SPECTRUM 1999 CHI-CHI - KAU081 (E)
FOR PINTO VALLEY SITE

Figure
111

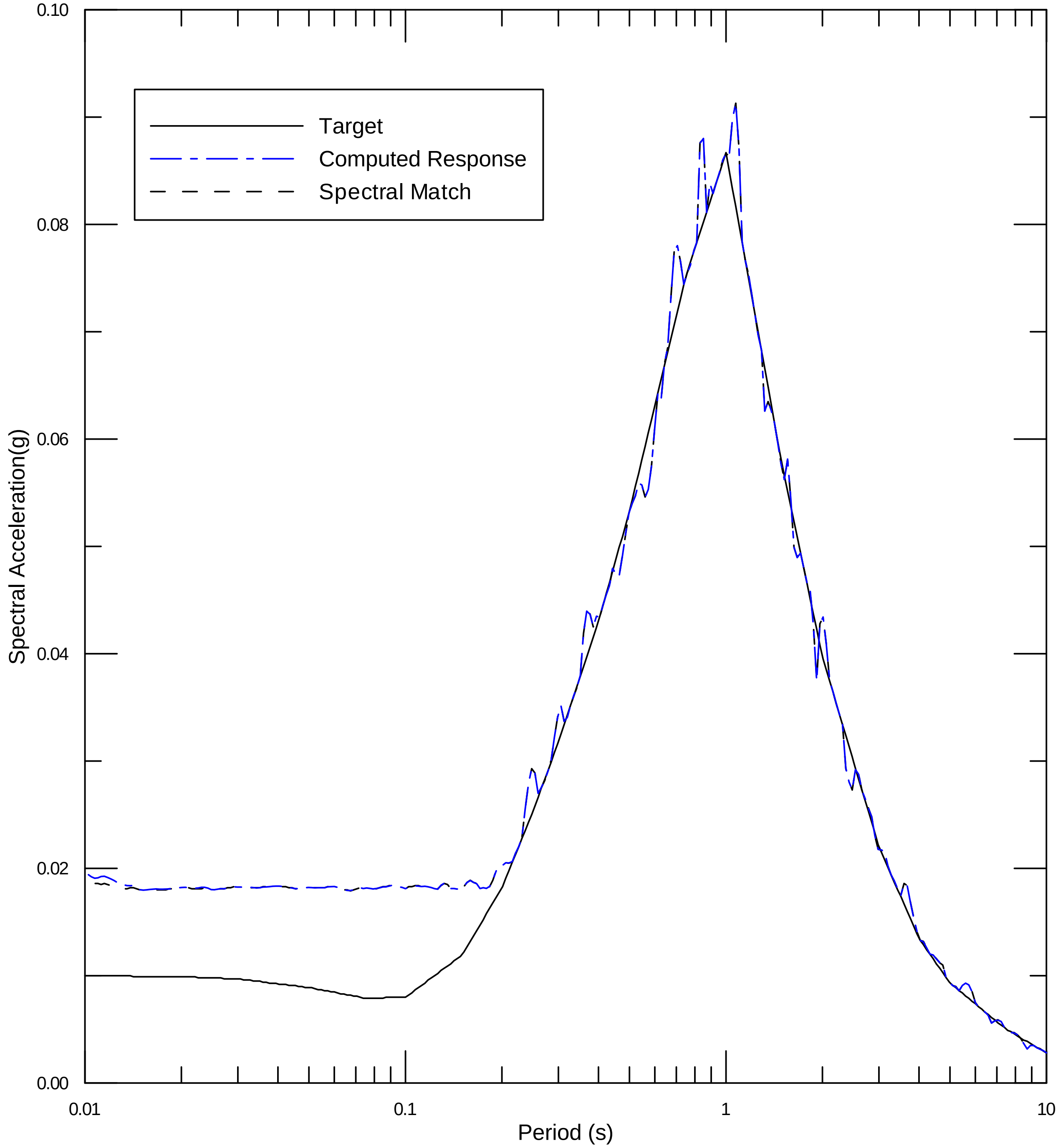

URS	Project No. 26818581	SPECTRAL MATCH TO HORIZONTAL 5,000-YEAR RETURN PERIOD 1.0 SEC CMS SPECTRUM DENALI 2002 - FIRE STATION 1 (090) FOR PINTO VALLEY SITE	Figure 112
	Resolution Copper Arizona		

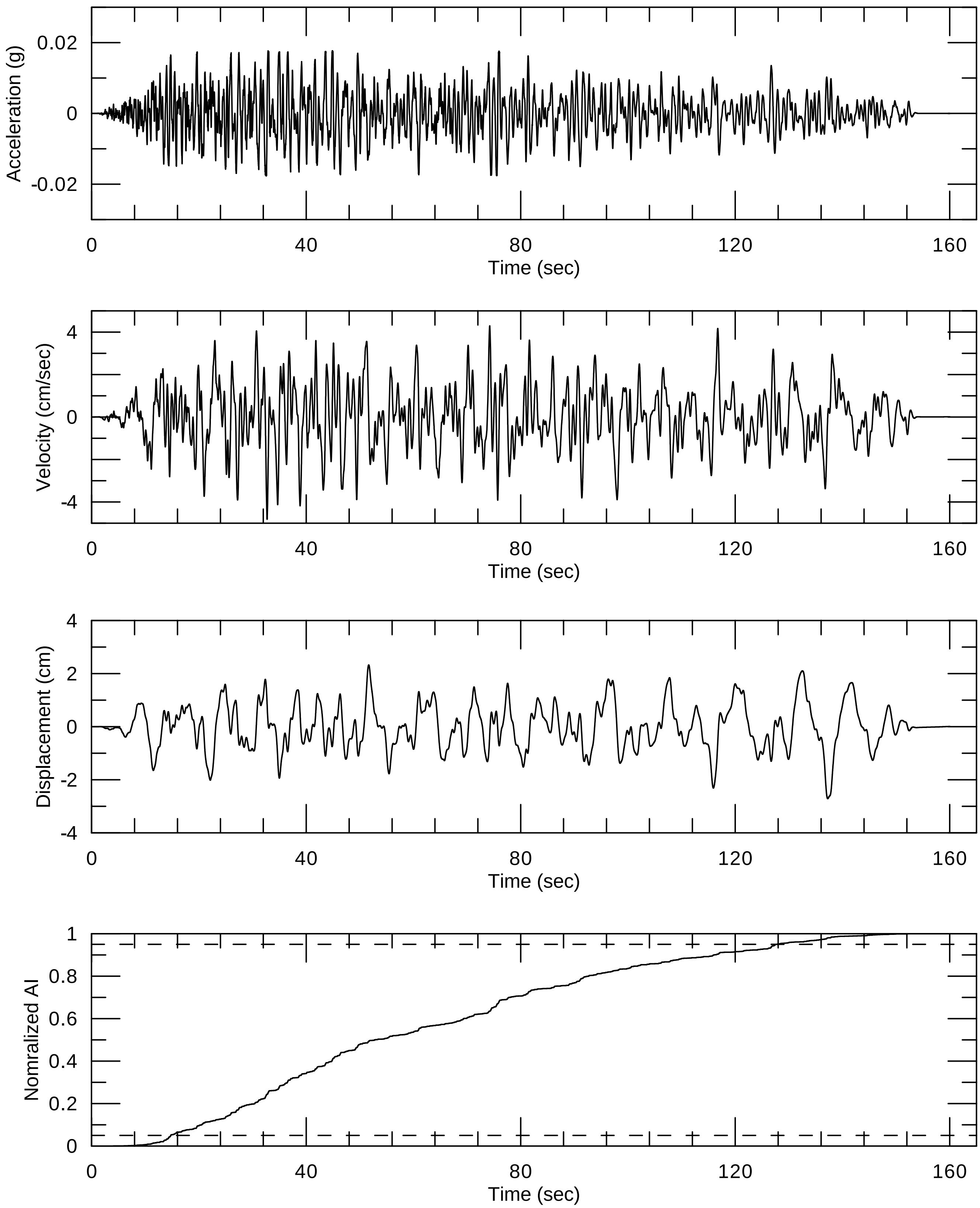

URS	Project No. 26818581 Resolution Copper Arizona	TIME HISTORIES SPECTRALLY MATCHED TO HORIZONTAL 5,000-YEAR RETURN PERIOD 1.0 SEC CMS SPECTRUM 2002 DENALI - FIRE STATION 1 (090) FOR PINTO VALLEY SITE	Figure 113

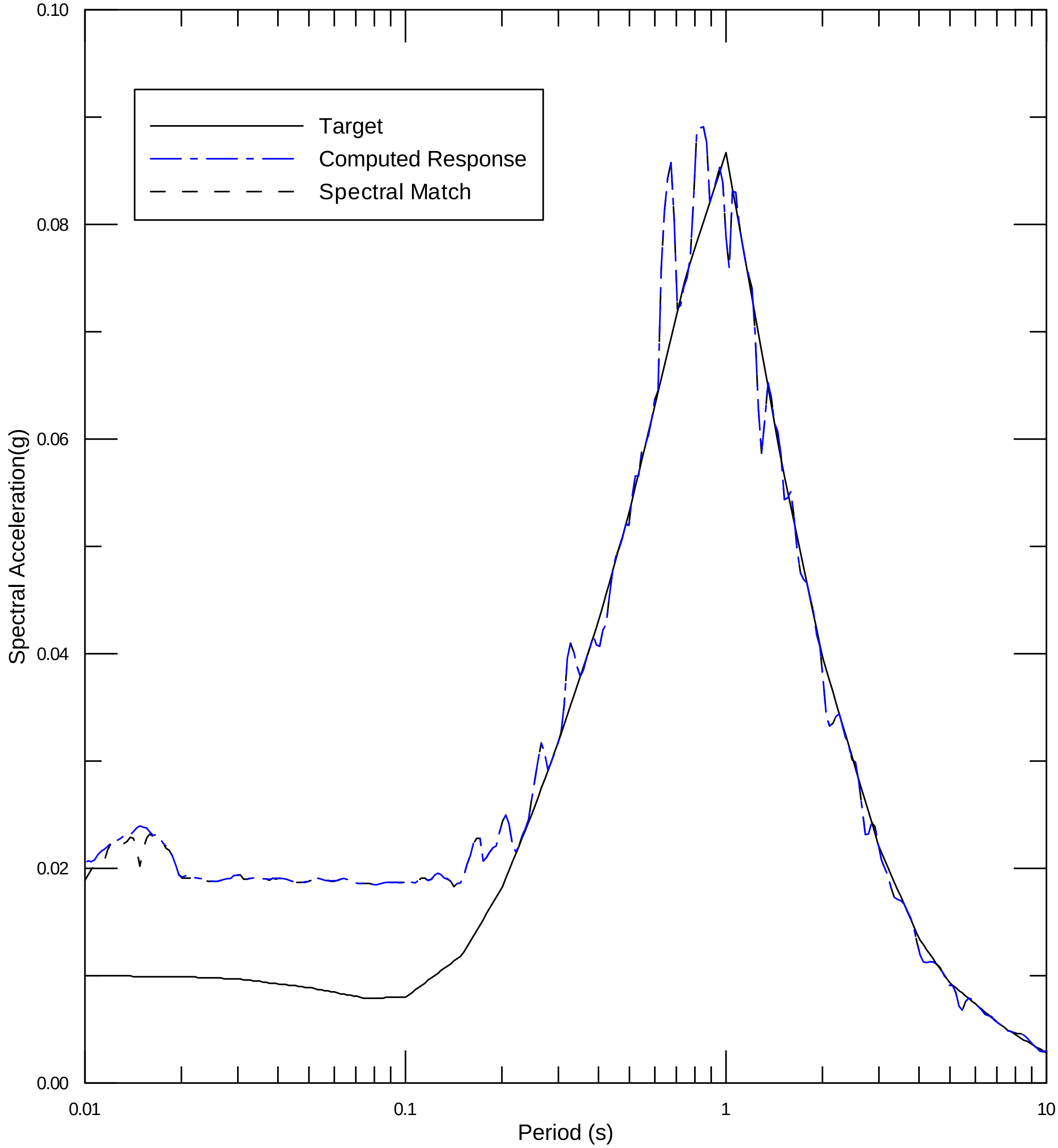

URS	Project No. 26818581 Resolution Copper Arizona	SPECTRAL MATCH TO HORIZONTAL 5,000-YEAR RETURN PERIOD 1.0 SEC CMS SPECTRUM 2002 DENALI - VALDEZ CITY HALL (090) FOR PINTO VALLEY SITE	Figure 114

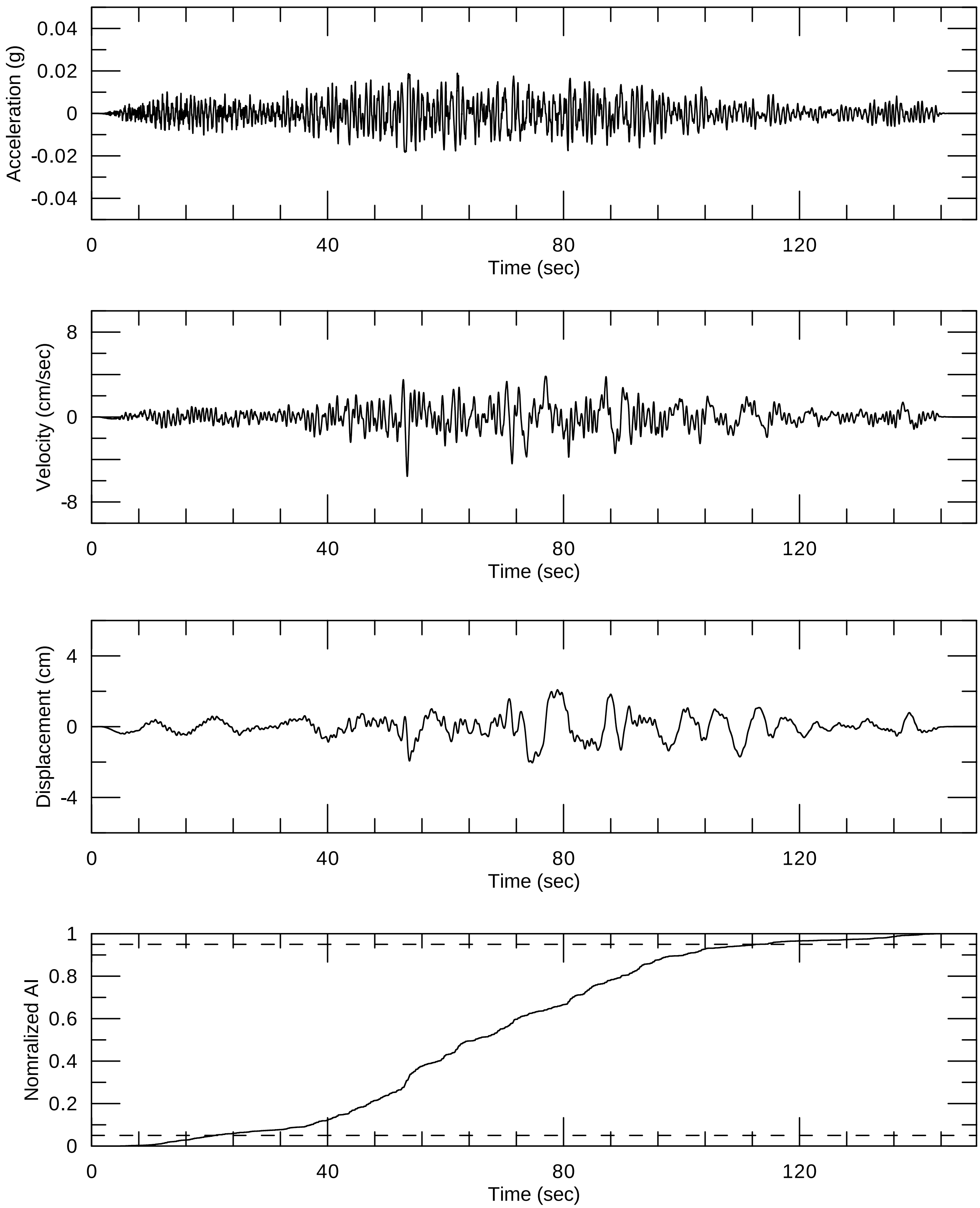

URS

Project No. 26818581

Resolution Copper
Arizona

TIME HISTORIES SPECTRALLY MATCHED TO HORIZONTAL 5,000-YEAR RETURN PERIOD 1.0 SEC CMS SPECTRUM 2002 DENALI - VALDEZ CITY HALL (090) FOR PINTO VALLEY SITE

Figure 115

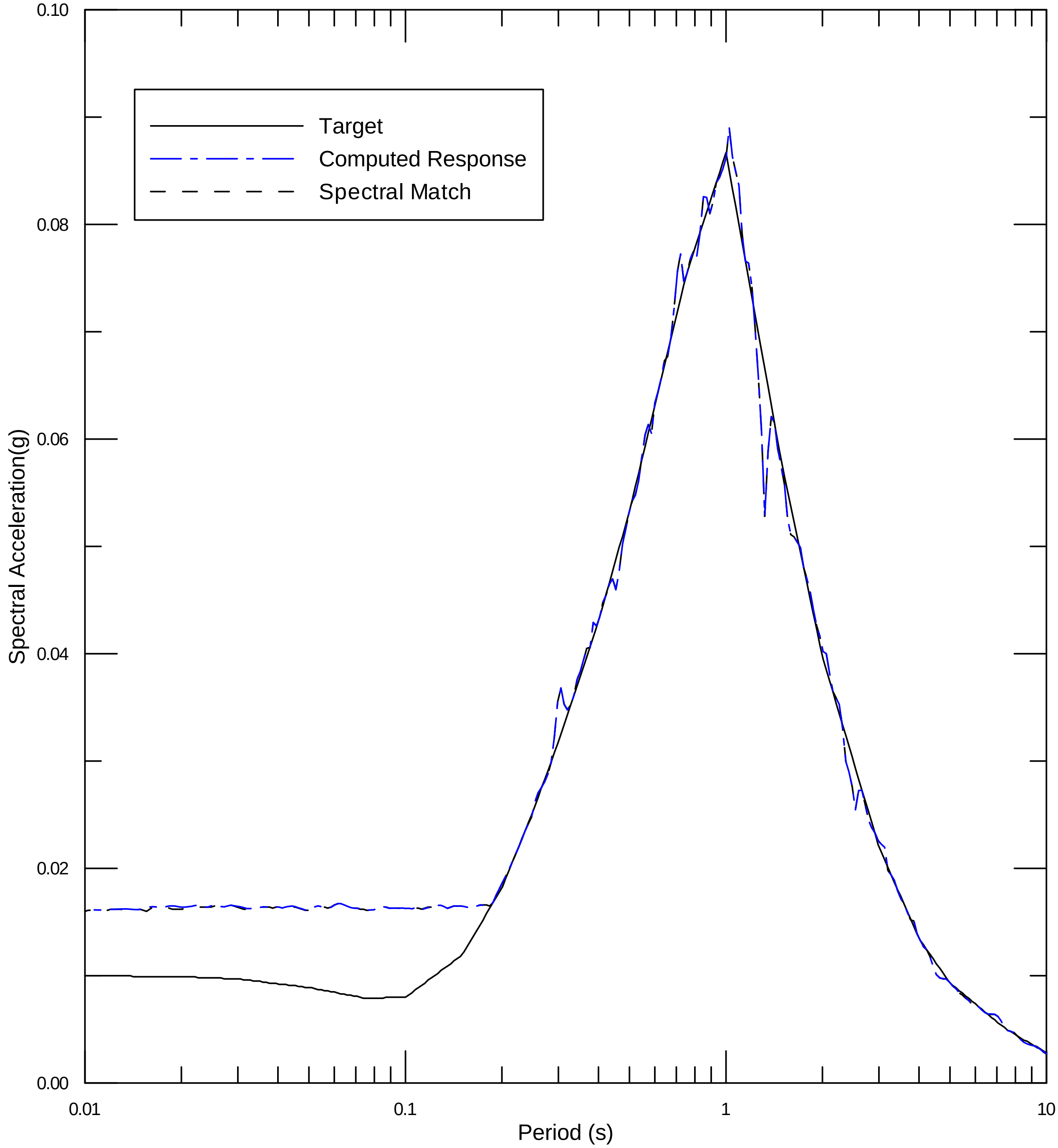

URS	Project No. 26818581 Resolution Copper Arizona	SPECTRAL MATCH TO HORIZONTAL 5,000-YEAR RETURN PERIOD 1.0 SEC CMS SPECTRUM 1999 KOCAELI - AFYON (000) FOR PINTO VALLEY SITE	Figure 116

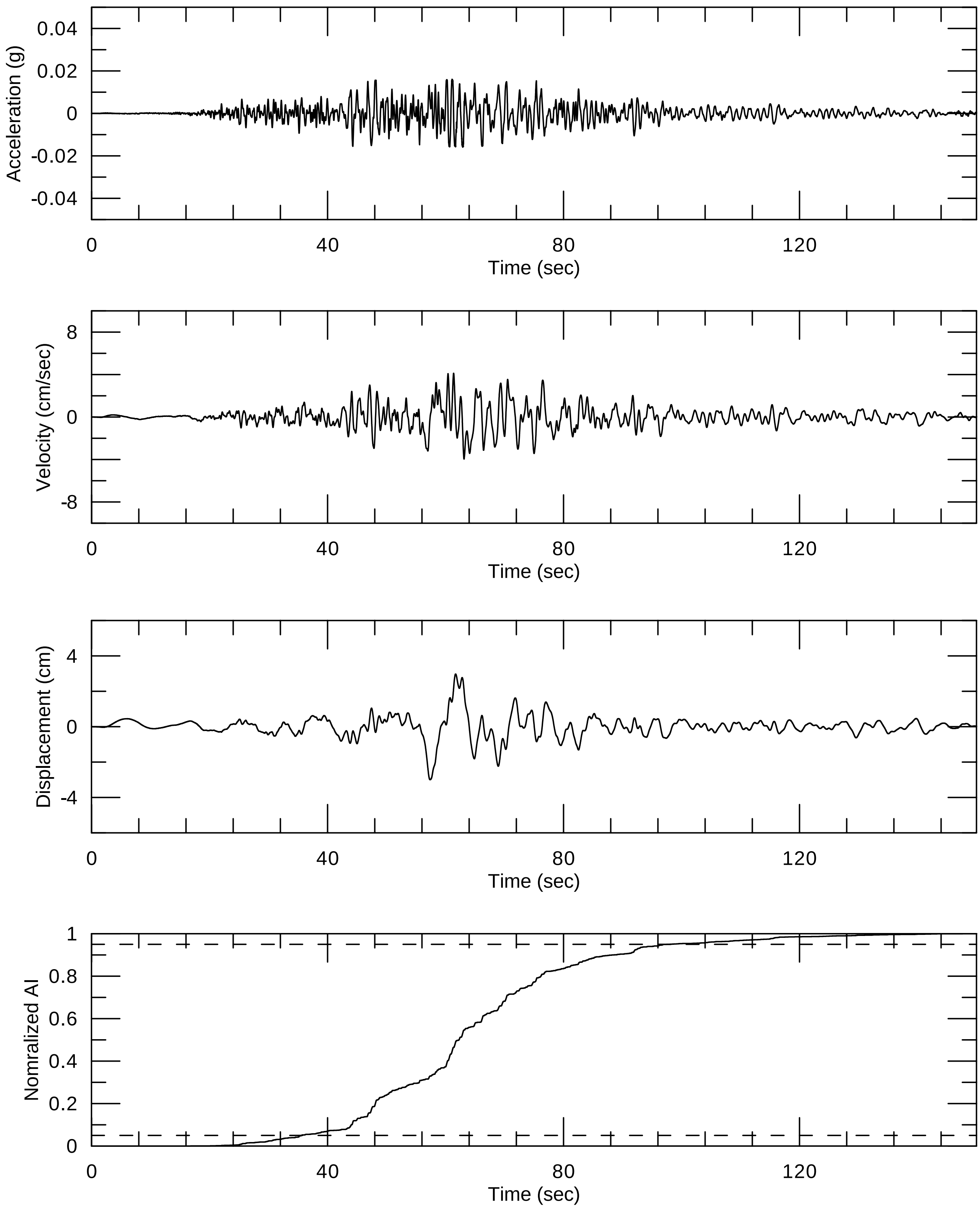

URS	Project No. 26818581	TIME HISTORIES SPECTRALLY MATCHED TO HORIZONTAL 5,000-YEAR RETURN PERIOD 1.0 SEC CMS SPECTRUM 1999 KOCAELI - AFYON (000) FOR PINTO VALLEY SITE	Figure 117
	Resolution Copper Arizona		

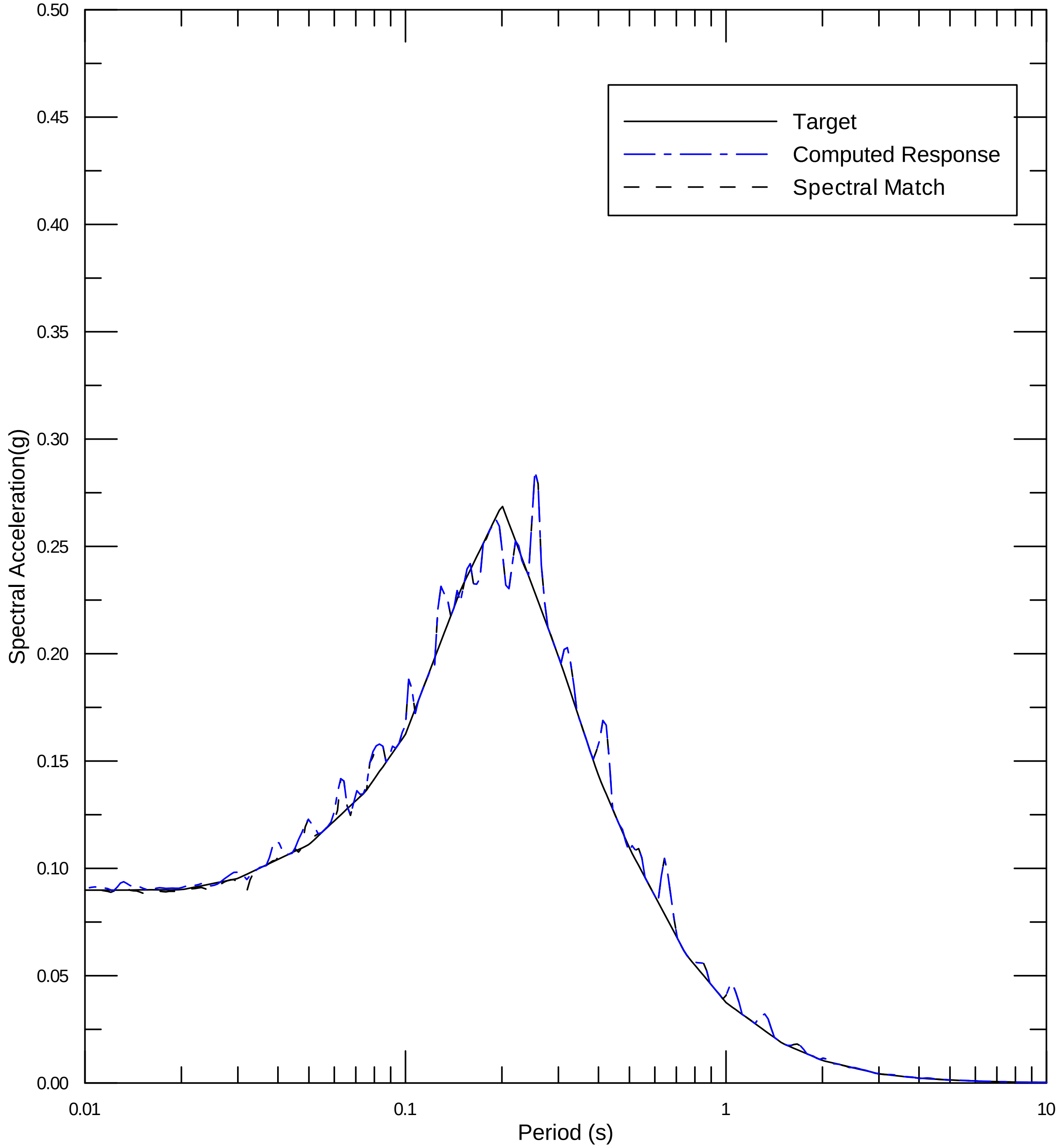

URS	Project No. 26818581 Resolution Copper Arizona	SPECTRAL MATCH TO HORIZONTAL 5,000-YEAR RETURN PERIOD 0.2 SEC CMS SPECTRUM 1979 IMPERIAL VALEY - CERRO PRIETO (147) FOR FAR WEST 1 SITE	Figure 118

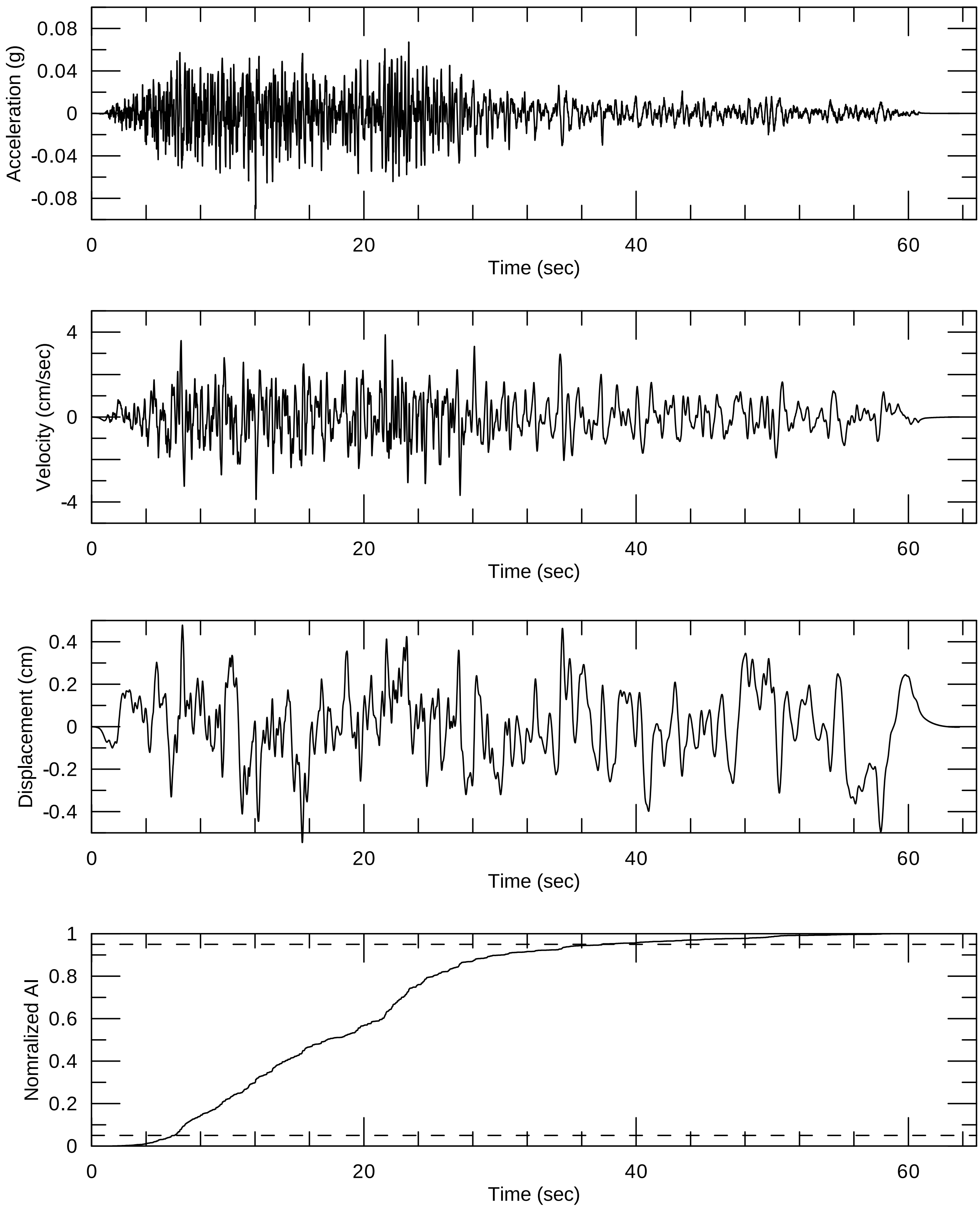

URS	Project No. 26818581 Resolution Copper Arizona	TIME HISTORIES SPECTRALLY MATCHED TO HORIZONTAL 5,000-YEAR RETURN PERIOD 0.2 SEC CMS SPECTRUM 1979 IMPERIAL VALLEY-CERRO PRIETO (147) FOR FAR WEST 1 SITE	Figure 119

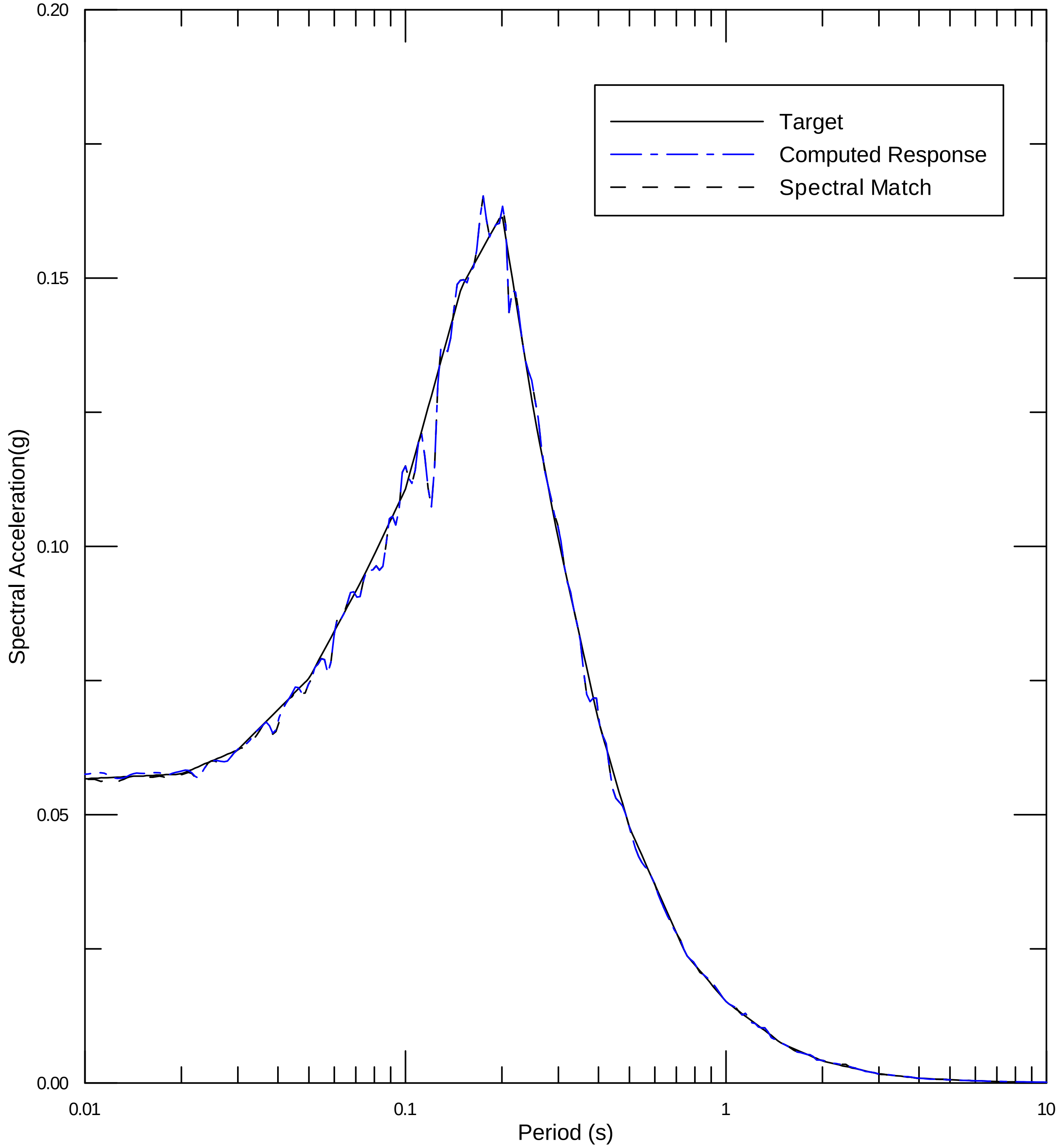

URS	Project No. 26818581	SPECTRAL MATCH TO HORIZONTAL 5,000-YEAR RETURN PERIOD0.2 SEC CMS SPECTRUM 1995 KOZANI - KOZANI (L) FOR FAR WEST 1 SITE	Figure 120
	Resolution Copper Arizona		

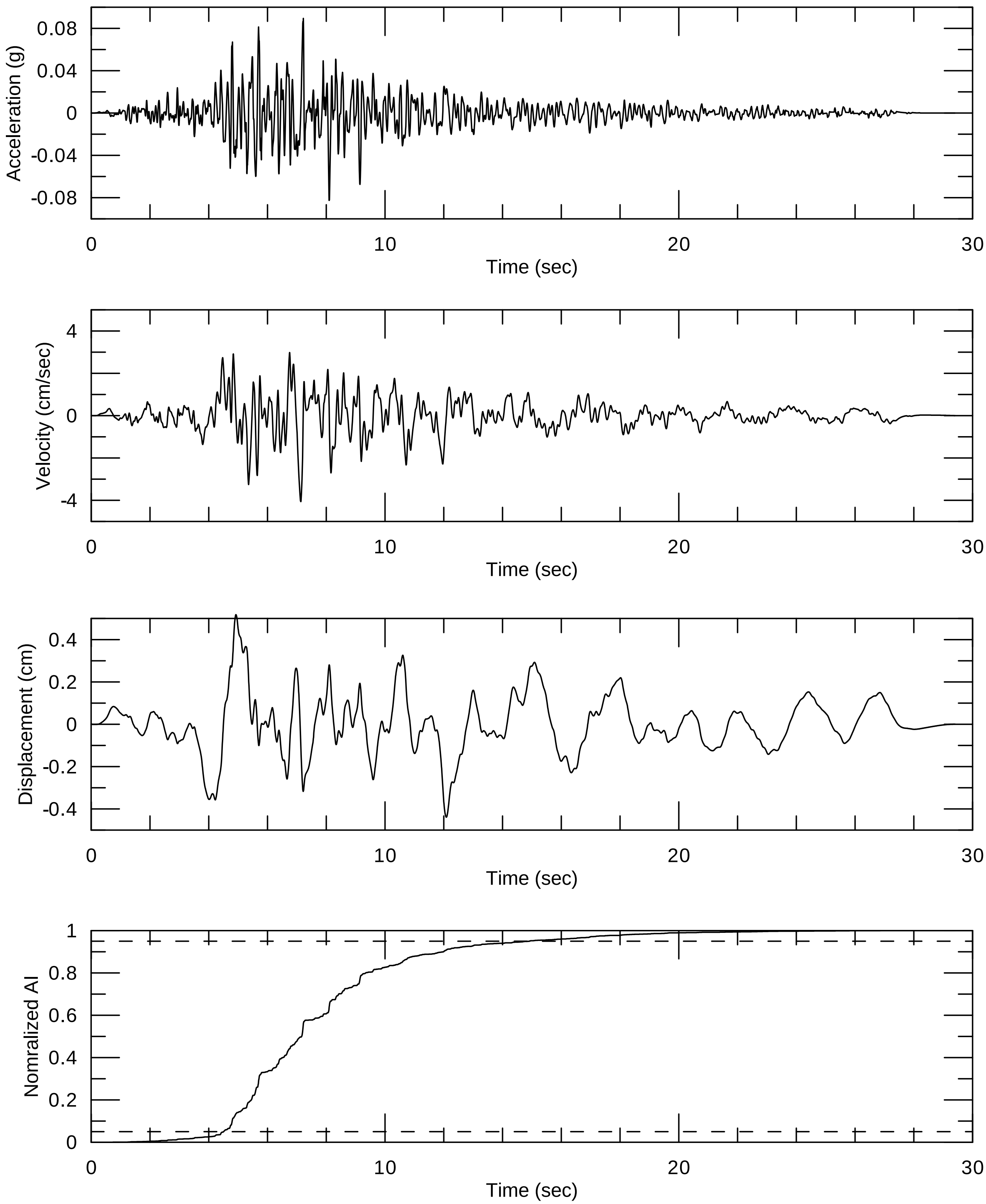

URS	Project No. 26818581 Resolution Copper Arizona	TIME HISTORIES SPECTRALLY MATCHED TO HORIZONTAL 5,000-YEAR RETURN PERIOD 0.2 SEC CMS SPECTRUM 1995 KOZANI- KOZANI (L) FOR FAR WEST 1 SITE	Figure 121

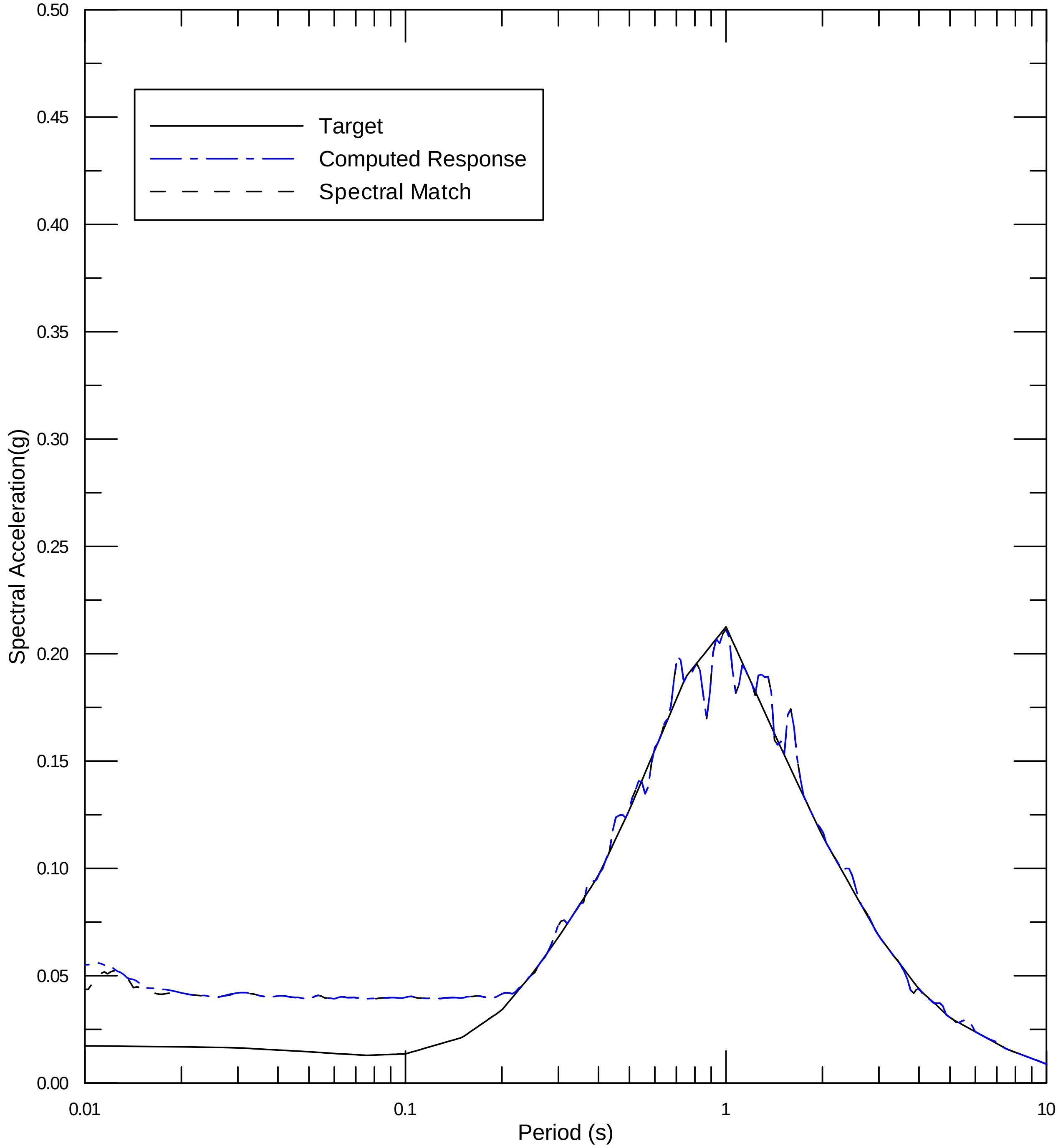

URS	Project No. 26818581 Resolution Copper Arizona	SPECTRAL MATCH TO HORIZONTAL 5,000-YEAR RETURN PERIOD 1.0 SEC CMS SPECTRUM 1999 CHI-CHI - KAU046 (E) FOR FAR WEST 1 SITE	Figure 122

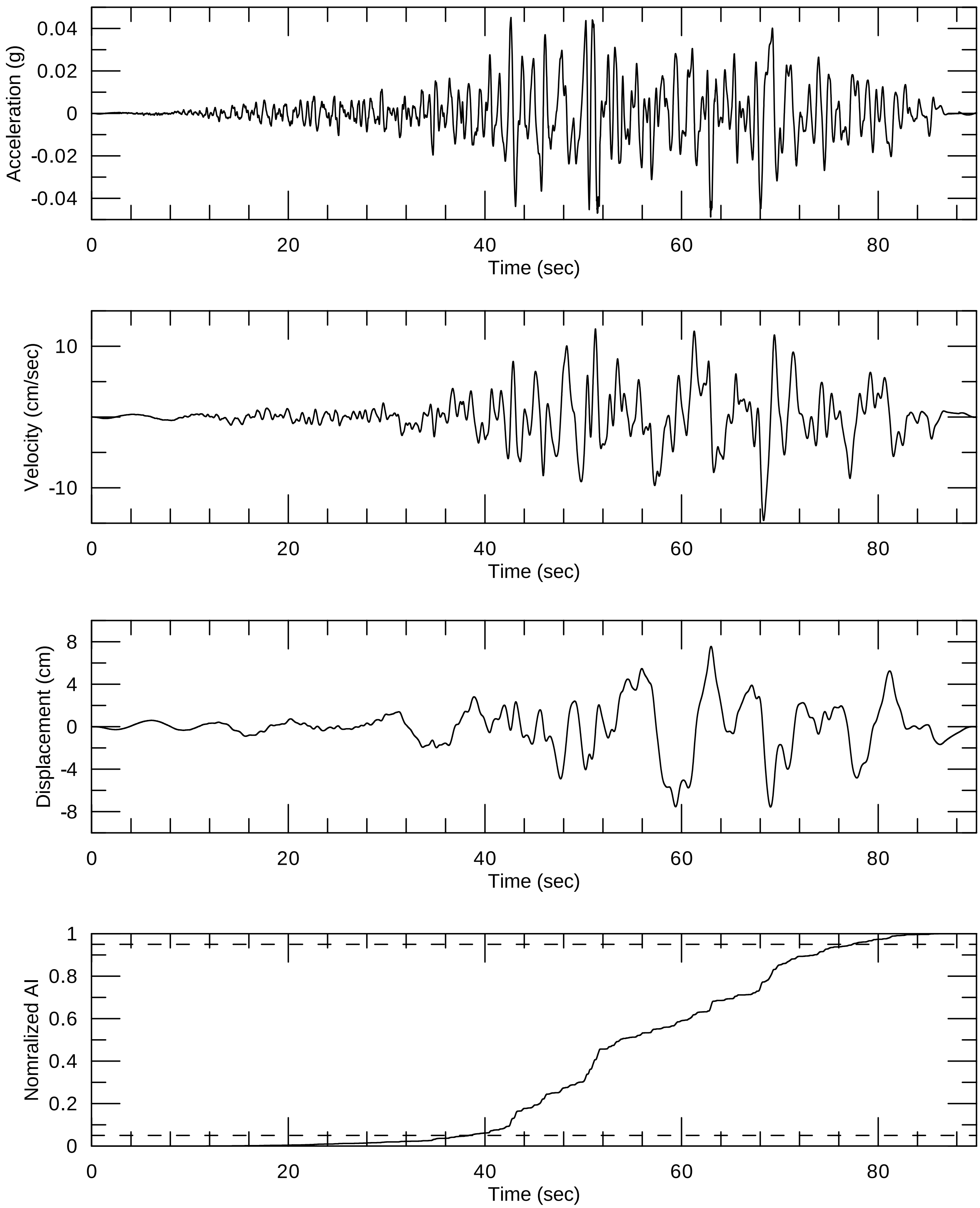

URS	Project No. 26818581 Resolution Copper Arizona	TIME HISTORIES SPECTRALLY MATCHED TO HORIZONTAL 5,000-YEAR RETURN PERIOD 1.0 SEC CMS SPECTRUM 1999 CHI-CHI - KAU081 (E) FOR FOR FAR WEST 1 SITE	Figure 125

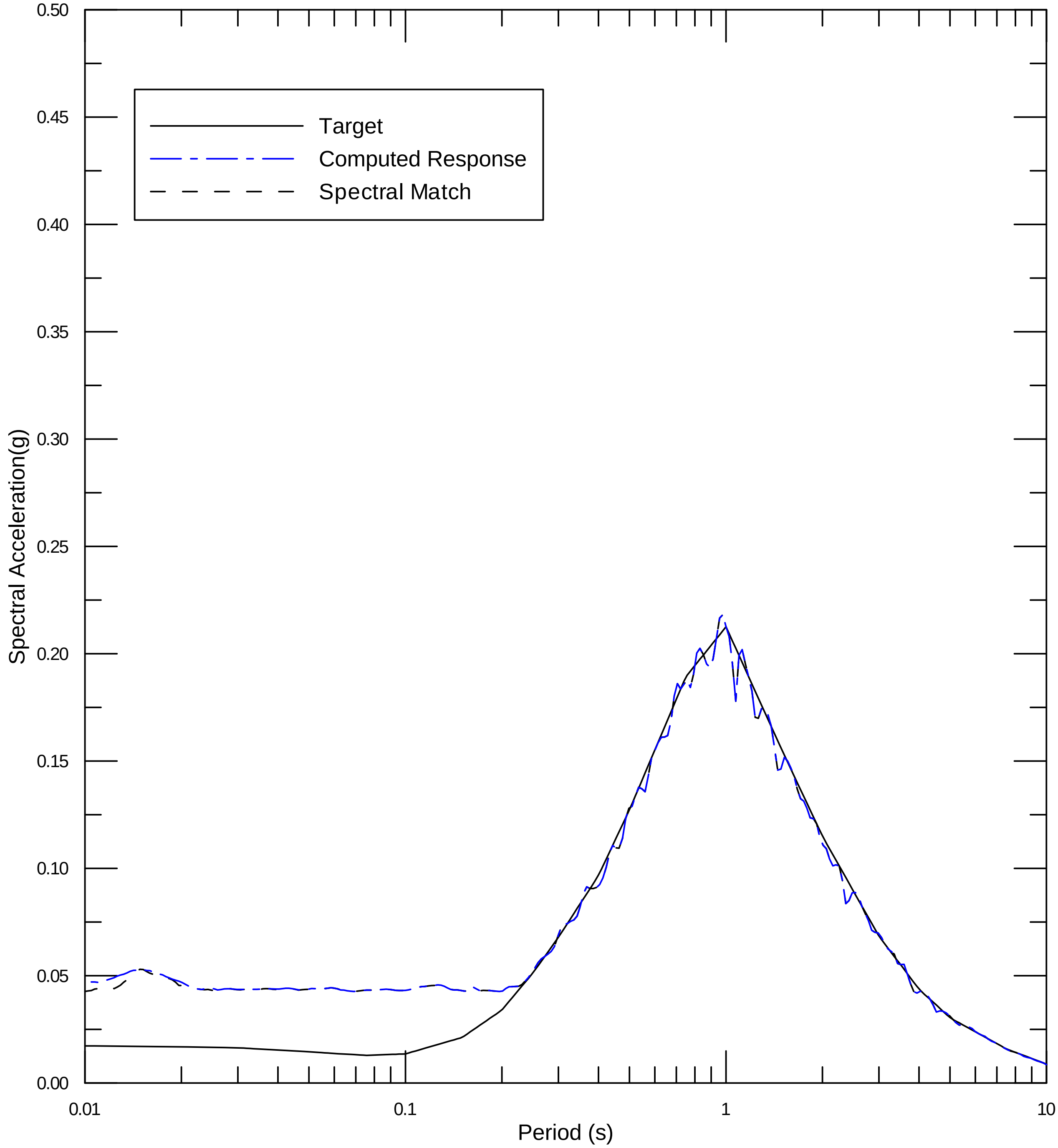

URS	Project No. 26818581 Resolution Copper Arizona	SPECTRAL MATCH TO HORIZONTAL 5,000-YEAR RETURN PERIOD 1.0 SEC CMS SPECTRUM 1999 CHI-CHI - KAU081 (E) FOR FAR WEST 1 SITE	Figure 124

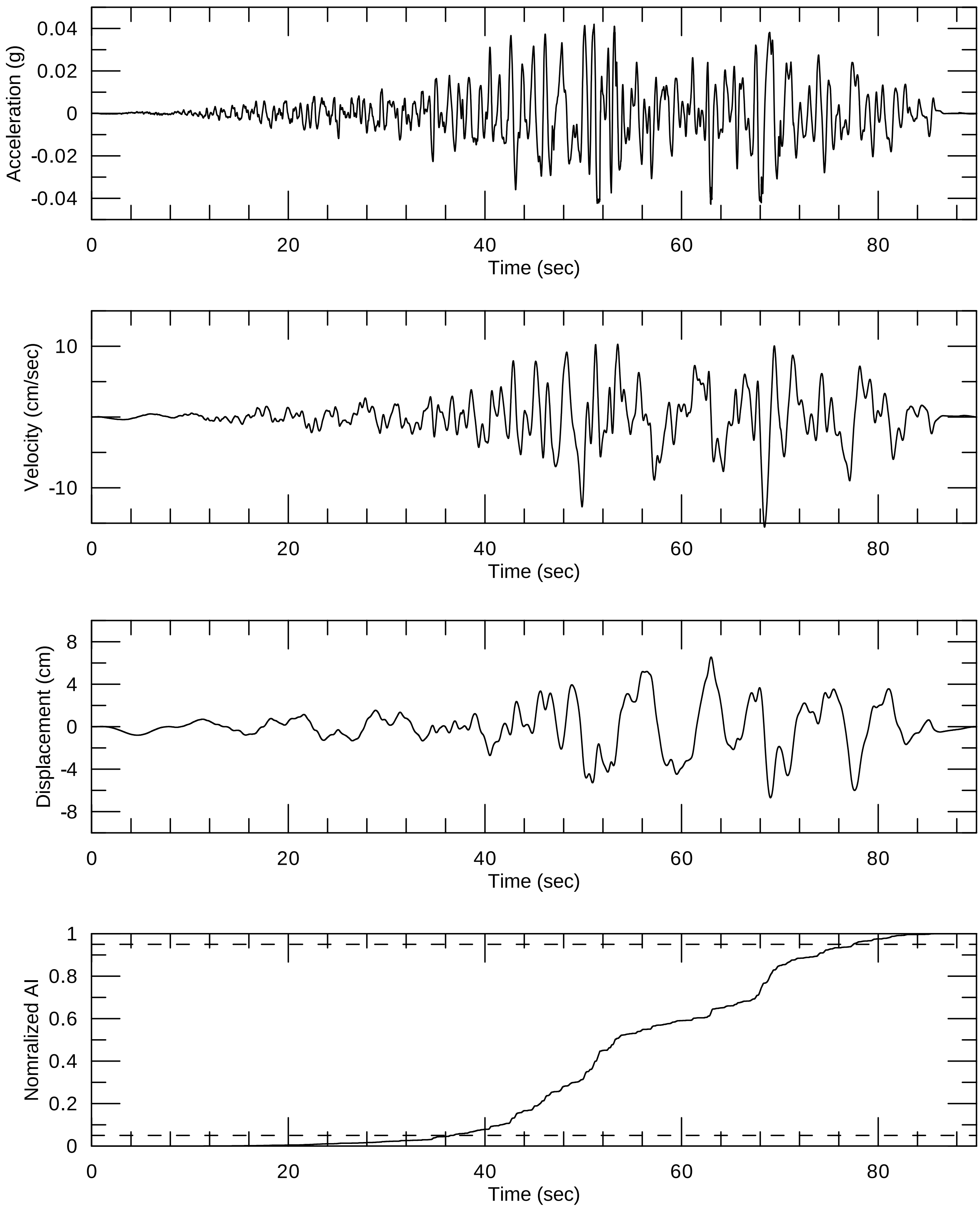

URS	Project No. 26818581 Resolution Copper Arizona	TIME HISTORIES SPECTRALLY MATCHED TO HORIZONTAL 5,000-YEAR RETURN PERIOD 1.0 SEC CMS SPECTRUM 1999 CHI-CHI - KAU081 (E) FOR FOR FAR WEST 1 SITE	Figure 125

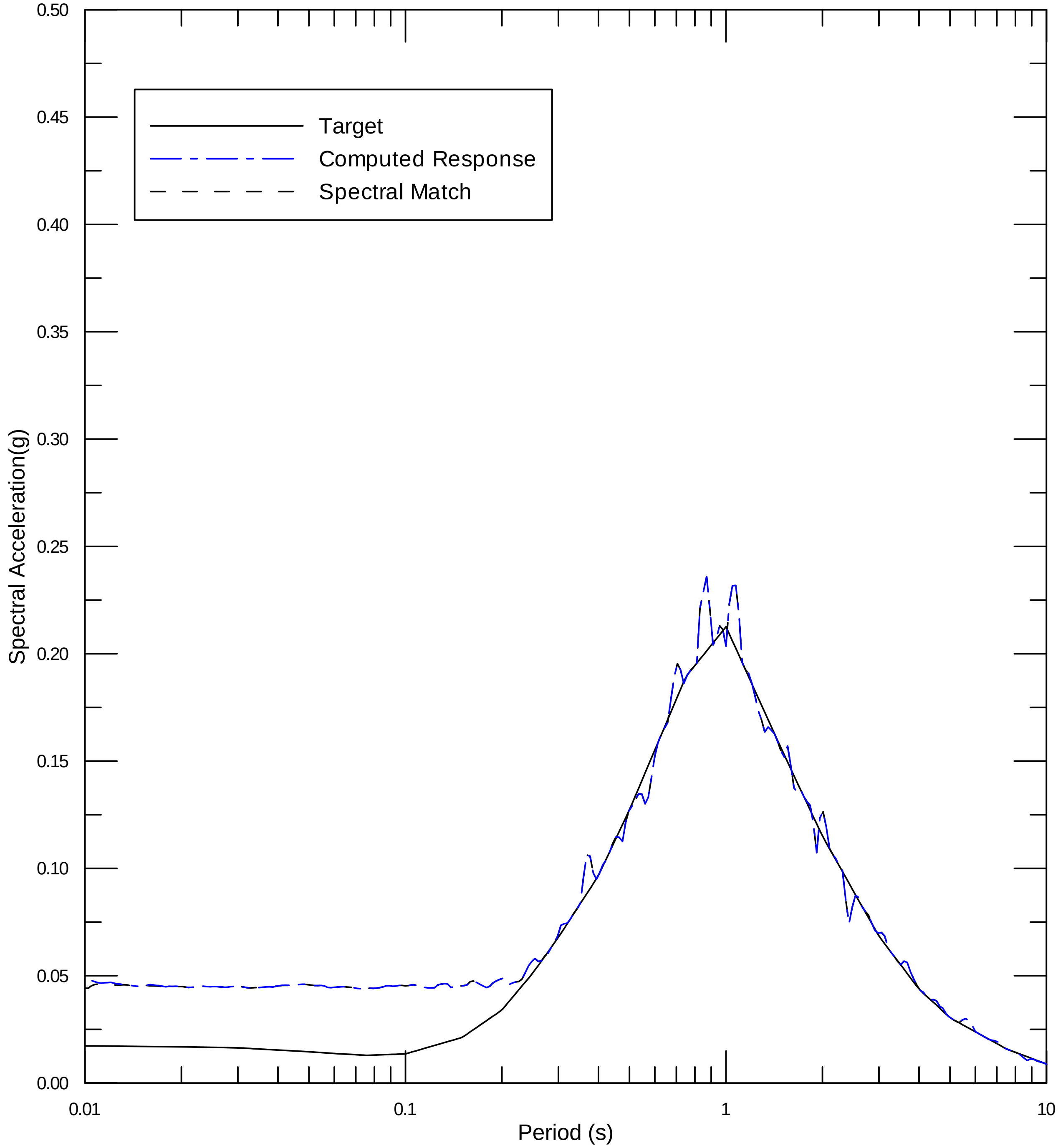

URS

Project No. 26818581

Resolution Copper
Arizona

SPECTRAL MATCH TO HORIZONTAL
5,000-YEAR RETURN PERIOD 1.0 SEC CMS SPECTRUM
2002 DENALI - FIRE STATION 1 (090)
FOR FAR WEST 1 SITE

Figure
126

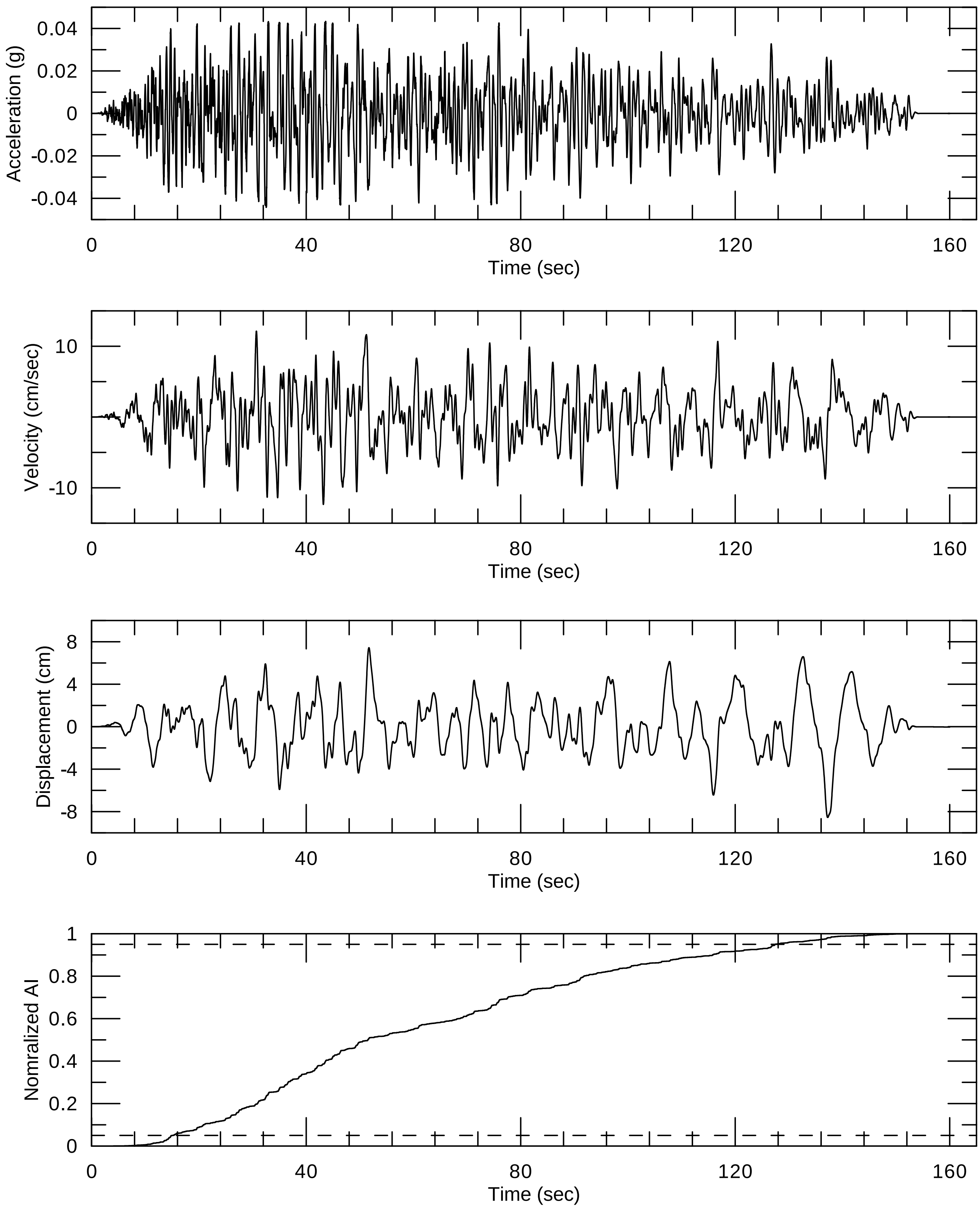

URS	Project No. 26818581 Resolution Copper Arizona	TIME HISTORIES SPECTRALLY MATCHED TO HORIZONTAL 5,000-YEAR RETURN PERIOD 1.0 SEC CMS SPECTRUM 2002 DENALI - FIRE STATION 1 (090) FOR FAR WEST 1 SITE	Figure 127

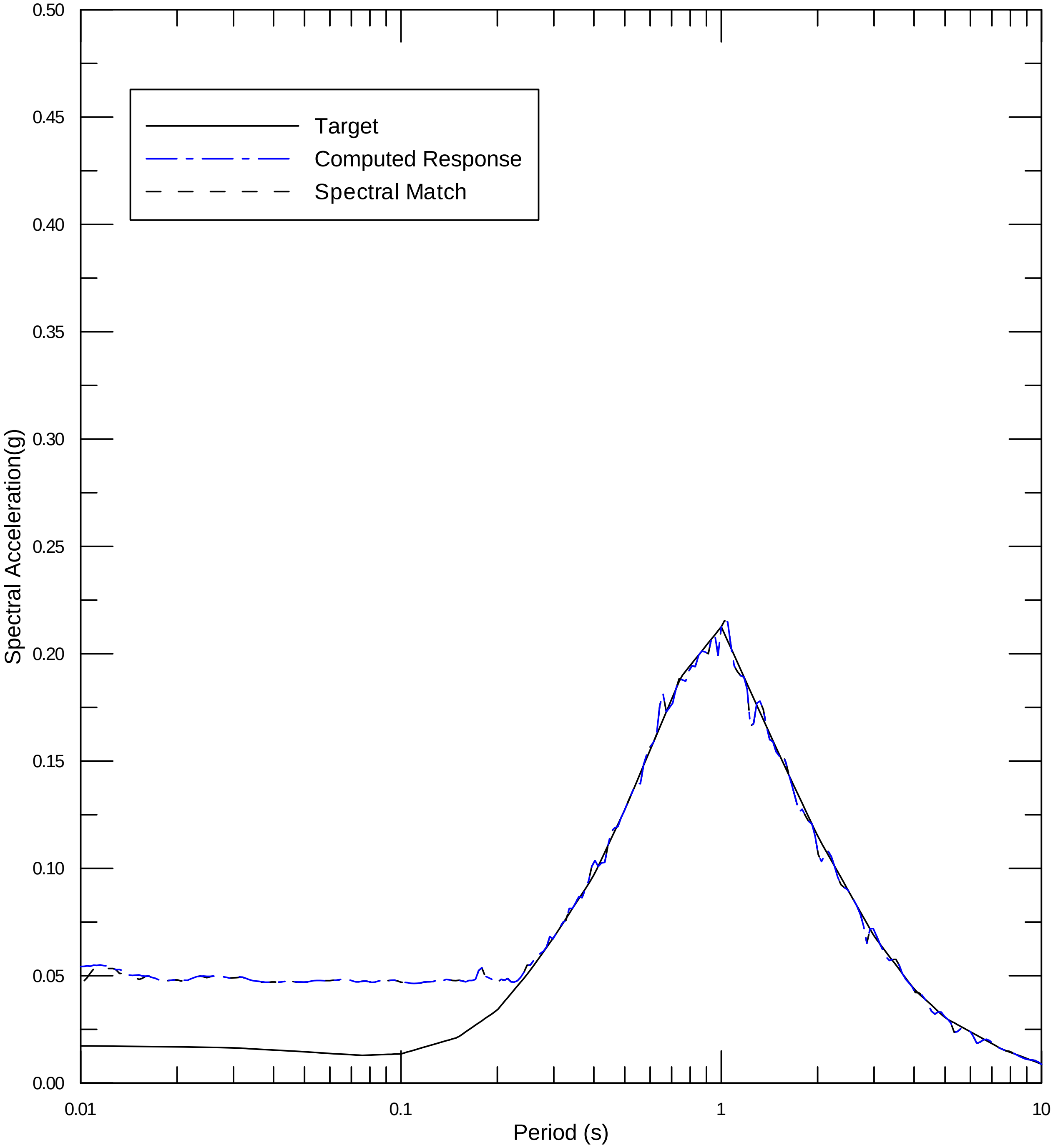

URS	Project No. 26818581 Resolution Copper Arizona	SPECTRAL MATCH TO HORIZONTAL 5,000-YEAR RETURN PERIOD 1.0 SEC CMS SPECTRUM 2002 DENALI - VALDEZ CITY HALL (090) FOR FAR WEST 1 SITE	Figure 128

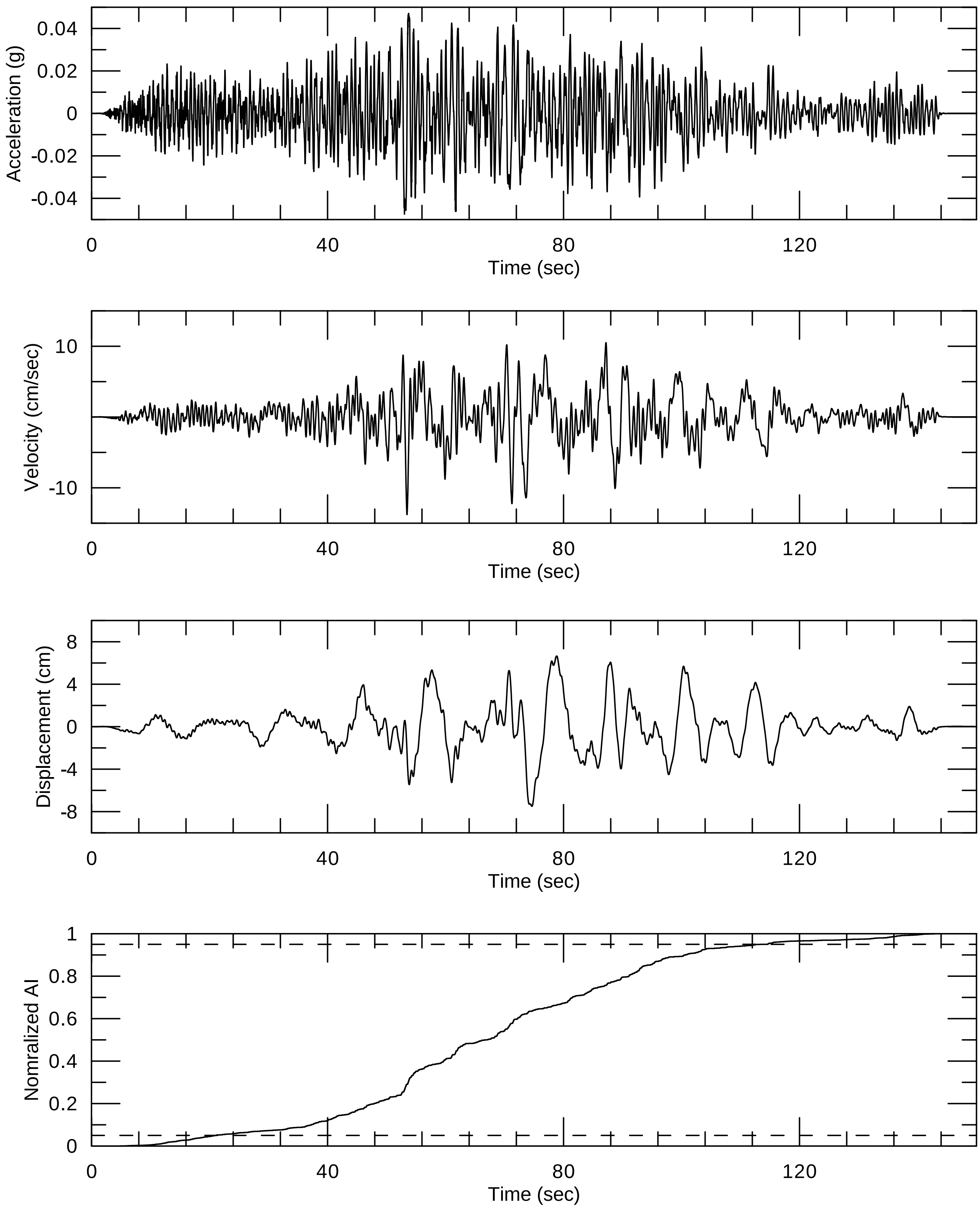

URS	Project No. 26818581 Resolution Copper Arizona	TIME HISTORIES SPECTRALLY MATCHED TO HORIZONTAL 5,000-YEAR RETURN PERIOD 1.0 SEC CMS SPECTRUM 2002 DENALI - VALDEZ CITY HALL (090) FOR FAR WEST 1 SITE	Figure 129

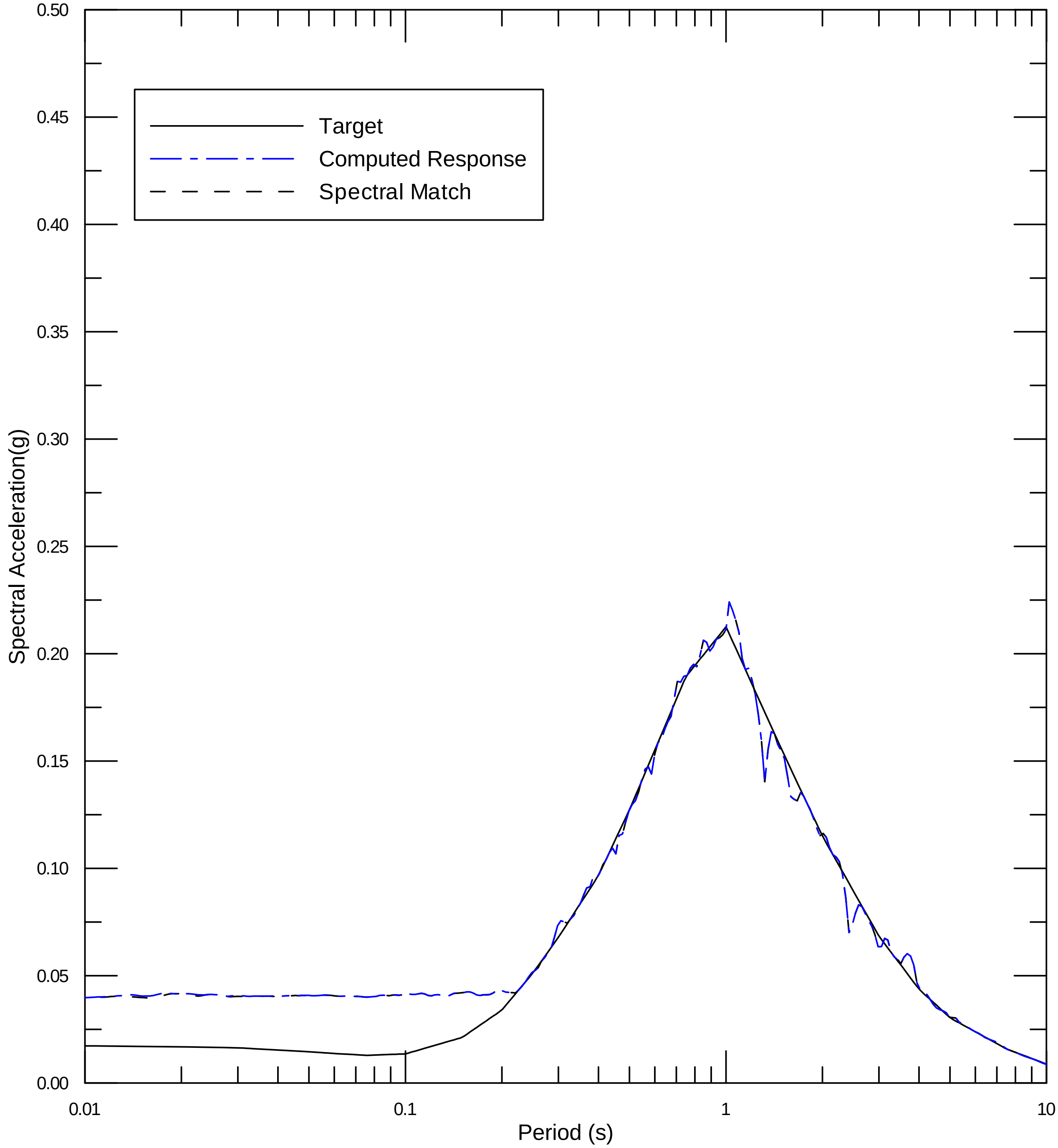

URS

Project No. 26818581

Resolution Copper
Arizona

SPECTRAL MATCH TO HORIZONTAL
5,000-YEAR RETURN PERIOD 1.0 SEC CMS SPECTRUM
1999 KOCAELI - AFYON (000)
FOR FAR WEST 1 SITE

Figure
130

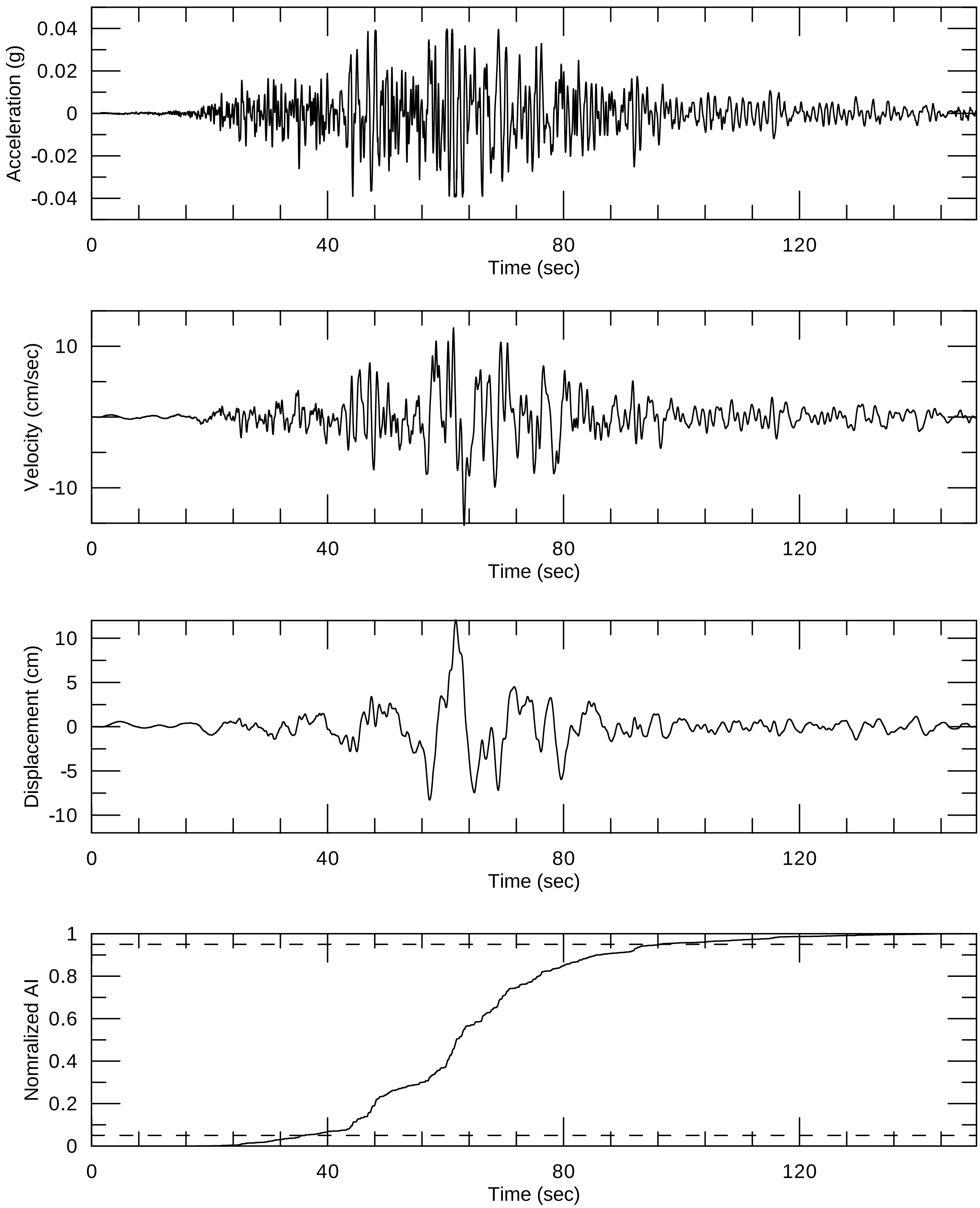

URS	Project No. 26818581 Resolution Copper Arizona	TIME HISTORIES SPECTRALLY MATCHED TO HORIZONTAL 5,000-YEAR RETURN PERIOD 1.0 SEC CMS SPECTRUM 1999 KOCAELI - AFYON (000) FOR FAR WEST 1 SITE	Figure 131